

AIR FORCE INST OF TECH WRIGHT-PATTERSON AFB OH F/G 13/7  
GRAVITATIONAL AGGLOMERATION OF POST-HCDA LMFBR NONSPHERICAL AER--ETC(U)  
DEC 80 R F TUTTLE  
AFIT-CI-80-82D NL

**AER--ETC(U)**

AFIT-CI-80-82D

NL

1.3

2.  $\frac{1}{2} \times \frac{1}{2} = \frac{1}{4}$



AD A106766

UNCLASS

LEVEL II

SECURITY CLASSIFICATION OF THIS PAGE (When Data Entered)

## AFIT-CI - REPORT DOCUMENTATION PAGE

READ INSTRUCTIONS  
BEFORE COMPLETING FORM

1. REPORT NUMBER

80-82D

2. GOVT ACCESSION NO.

AD-A106766

3. RECIPIENT'S CATALOG NUMBER

766

4. TITLE (and Subtitle)

Gravitational Agglomeration of Post-HCDA  
LMFBR Nonspherical Aerosols

5. TYPE OF REPORT &amp; PERIOD COVERED

THESIS/DISSERTATION

6. PERFORMING ORG. REPORT NUMBER

7. AUTHOR(s)

Ronald Forrester Tuttle

8. CONTRACT OR GRANT NUMBER(s)

9 Doctoral thesis

9. PERFORMING ORGANIZATION NAME AND ADDRESS

AFIT STUDENT AT: University of Missouri-Columbia

10. PROGRAM ELEMENT, PROJECT, TASK  
AREA & WORK UNIT NUMBERS

11. CONTROLLING OFFICE NAME AND ADDRESS

AFIT/NR  
WPAFB OH 45433

12. REPORT DATE

Dec 1980

13. NUMBER OF PAGES

248

14. MONITORING AGENCY NAME &amp; ADDRESS (if different from Controlling Office)

12 274

15. SECURITY CLASS. (of this report)

UNCLASS

15a. DECLASSIFICATION/DOWNGRADING  
SCHEDULE

16. DISTRIBUTION STATEMENT (of this Report)

APPROVED FOR PUBLIC RELEASE; DISTRIBUTION UNLIMITED

DTIC  
ELECTE

NOV 6 1981

17. DISTRIBUTION STATEMENT (of the abstract entered in Block 20, if different from Report)

16 OCT 1981

Fredric C. Lynch

18. SUPPLEMENTARY NOTES

APPROVED FOR PUBLIC RELEASE: IAW AFR 190-17

FREDRIC C. LYNCH, Major, USAF  
Director of Public Affairs  
Air Force Institute of Technology (ATC)  
Wright-Patterson AFB, OH 45433

19. KEY WORDS (Continue on reverse side if necessary and identify by block number)

20. ABSTRACT (Continue on reverse side if necessary and identify by block number)

ATTACHED

81 10 27 261

DD FORM 1 JAN 73 1473

EDITION OF 1 NOV 65 IS OBSOLETE

UNCLASS

SECURITY CLASSIFICATION OF THIS PAGE (When Data Entered)

012 200

JH

DTIC FILE COPY

# AGGLOMERATION OF NONSPHERICAL AEROSOLS

Ronald Forrester Tuttle

Dr. S. K. Loyalka

Dissertation Supervisor

## ABSTRACT

This dissertation is a theoretical investigation of collisional dynamics of two particle interactions in a gravitational field. <sup>is neglected.</sup> This research is unique in that it is the first attempt at modeling the hydrodynamic interactions between a nonspherical particle and a spherical particle undergoing gravitational collisions in an LMFBR environment.

~~First~~, basic definitions and expressions are developed for nonspherical particles and related to spherical particles by means of shape factors. Using volume equivalent diameter as the defining length in the gravitational collision kernel, the aerodynamic shape factor,  $\kappa$ , the density correction factor,  $\alpha$ , <sup>alpha</sup> and the gravitational collision shape factor,  $\beta$ , <sup>beta</sup> are used to correct the collision kernel for the case of collisions between aerosol agglomerates. The Navier-Stokes equation in oblate spheroidal coordinates is solved to model a nonspherical particle and then the dynamic equations for two particle motions are developed. A computer program NGCEFF is constructed, the Navier-Stokes equation is solved by the finite difference method, and the dynamical equations are solved by Gear's method. Results are obtained for several

A

cases and are compared with previous work, of atmospheric sciences and LMFBR studies for the spherical cases. It is concluded that the aerosol gravitational collision shape factor can be determined by further theoretical work based on the concepts and methods developed in this dissertation.

Accession For	
NTIS GRA&I	<input checked="checked" type="checkbox"/>
DTIC TAB	<input type="checkbox"/>
Unannounced	<input type="checkbox"/>
Distribution	
Availability Codes	
Dist	Avail and/or Special
A	



## AFIT RESEARCH ASSESSMENT

The purpose of this questionnaire is to ascertain the value and/or contribution of research accomplished by students or faculty of the Air Force Institute of Technology (ATC). It would be greatly appreciated if you would complete the following questionnaire and return it to:

AFIT/NR  
Wright-Patterson AFB OH 45433

RESEARCH TITLE: Gravitational Agglomeration of Post-HCDA LMFBR Nonspherical Aerosols

AUTHOR: Ronald Forrester Tuttle

## RESEARCH ASSESSMENT QUESTIONS:

1. Did this research contribute to a current Air Force project?  
☐ a. YES ☐ b. NO
2. Do you believe this research topic is significant enough that it would have been researched (or contracted) by your organization or another agency if AFIT had not?  
☐ a. YES ☐ b. NO
3. The benefits of AFIT research can often be expressed by the equivalent value that your agency achieved/received by virtue of AFIT performing the research. Can you estimate what this research would have cost if it had been accomplished under contract or if it had been done in-house in terms of manpower and/or dollars?  
☐ a. MAN-YEARS                      ☐ b. \$
4. Often it is not possible to attach equivalent dollar values to research, although the results of the research may, in fact, be important. Whether or not you were able to establish an equivalent value for this research (3. above), what is your estimate of its significance?  
☐ a. HIGHLY SIGNIFICANT ☐ b. SIGNIFICANT ☐ c. SLIGHTLY SIGNIFICANT ☐ d. OF NO SIGNIFICANCE
5. AFIT welcomes any further comments you may have on the above questions, or any additional details concerning the current application, future potential, or other value of this research. Please use the bottom part of this questionnaire for your statement(s).

NAME

GRADE

POSITION

ORGANIZATION

LOCATION

STATEMENT(s):

FOLD DOWN ON OUTSIDE - SEAL WITH TAPE

AFIT/NR  
WRIGHT-PATTERSON AFB OH 45433  
OFFICIAL BUSINESS  
PENALTY FOR PRIVATE USE, \$300



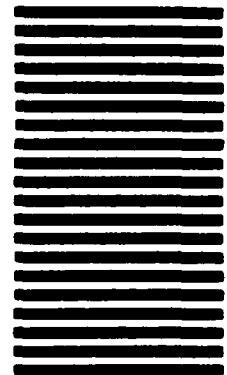
NO POSTAGE  
NECESSARY  
IF MAILED  
IN THE  
UNITED STATES

**BUSINESS REPLY MAIL**

FIRST CLASS PERMIT NO. 73236 WASHINGTON D.C.

POSTAGE WILL BE PAID BY ADDRESSEE

AFIT/ DAA  
Wright-Patterson AFB OH 45433



FOLD IN

# AGGLOMERATION OF NONSPHERICAL AEROSOLS

Ronald Forrester Tuttle

Dr. S. K. Loyalka

Dissertation Supervisor

## ABSTRACT

This dissertation is a theoretical investigation of collisional dynamics of two particle interactions in a gravitational field. This research is unique in that it is the first attempt at modeling the hydrodynamic interactions between a nonspherical particle and a spherical particle undergoing gravitational collisions in an LMFBR environment. First, basic definitions and expressions are developed for nonspherical particles and related to spherical particles by means of shape factors. Using volume equivalent diameter as the defining length in the gravitational collision kernel, the aerodynamic shape factor,  $\kappa$ , the density correction factor,  $\alpha$ , and the gravitational collision shape factor,  $\beta$ , are used to correct the collision kernel for the case of collisions between aerosol agglomerates. The Navier-Stokes equation in oblate spheroidal coordinates is solved to model a nonspherical particle and then the dynamic equations for two particle motions are developed. A computer program NGCEFF is constructed, the Navier-Stokes equation is solved by the finite difference method, and the dynamical equations are solved by Gear's method. Results are obtained for several

cases and are compared with previous work of atmospheric sciences and LMFBR studies for the spherical cases. It is concluded that the aerosol gravitational collision shape factor can be determined by further theoretical work based on the concepts and methods developed in this dissertation.

GRAVITATIONAL AGGLOMERATION  
of  
POST-HCDA LMFBR NONSPHERICAL AEROSOLS

---

A Dissertation  
Presented to  
the Faculty of the Graduate School  
University of Missouri-Columbia

---

In Partial Fulfillment  
of the Requirement for the Degree  
Doctor of Philosophy

---

by  
Ronald Forrester Tuttle  
S. K. Loyalka                      Dissertation Supervisor  
December 1980

## ACKNOWLEDGEMENTS

The author expresses sincere gratitude to those who, through their interest in and constructive criticism of my research, helped complete this phase of my education.

Foremost was my excellent advisor and friend, Dr. S. K. Loyalka. Without his keen insight into the mathematics and physics associated with aerosol science, the topics presented in this dissertation would still be in progress. Equally important was his friendship, exemplified by his unwavering encouragement to complete this research project while also understanding my personal problems which influenced progress.

I also gratefully acknowledge the help of my committee members, Professors M. Q. Jacobs, H. Liu, J. B. Miles, D. G. Retzloff, T. S. Storvick and R. C. Warder. When called upon to help with some aspect of my research, they willingly gave me their valuable time. Certainly the lively discussions have broadened my viewpoint.

As with any similar endeavor, this research would not have been possible without the financial support of various organizations. First, I recognize the significant financial support of the United States Air Force, which sent me back to graduate school through their Air Force Institute of Technology program. Typing of the manuscript was made

possible through a grant from the Nuclear Regulatory Commission. In addition, their financial support of the computer time requirements, without which completion of this research would have been impossible, is gratefully acknowledged. Also, partial travel funds were received from the Missouri Alumni Association through a special graduate school fund.

A great many UMC staff personnel helped in this research project. I am grateful to those of the Campus Computing Center and the Engineering Experiment Station for their special services. I also acknowledge with gratitude the valuable assistance of Pamela A. Loesing, department secretary. Her help in handling all the administrative details associated with my degree was invaluable.

Finally, I would like to thank Mary Jo Adams from Melbourne, Florida, for the expert typing of the final dissertation proof.

This dissertation is dedicated to my two sons, Douglas and Marc.

# TABLE OF CONTENTS

	PAGE
ACKNOWLEDGEMENTS . . . . .	ii
LIST OF FIGURES . . . . .	ix
LIST OF TABLES . . . . .	xi
CHAPTER	
I. INTRODUCTION . . . . .	1
1.1 LMFBR Safety Requirements . . . . .	1
1.2 Dissertation Organization . . . . .	5
II. LMFBR AEROSOLS AND GOVERNING EQUATIONS . . . . .	8
2.1 Morphology and Aerodynamics of LMFBR Aerosols . . . . .	8
2.1.1 Primary Particles . . . . .	8
2.1.2 LMFBR Aggregates . . . . .	9
2.2 Aerosol Behavior Equation . . . . .	15
2.3 Aerosol Particle Coagulation . . . . .	18
2.4 Gravitational Coagulation . . . . .	20
2.5 Problem Statement . . . . .	22
III. REVIEW OF PREVIOUS WORK . . . . .	24
3.0 Introduction . . . . .	24
3.1 Flow Field Approximation . . . . .	25
3.1.1 Steady Flow Past Oblate Spheroids . . . . .	26
3.1.2 Steady Flow Past Spheres . . . . .	31



CHAPTER	PAGE
3.2 The Superposition Model . . . . .	31
3.3 Gravitational Collision Efficiencies for Nonspherical Particles . . . . .	34
IV. MATHEMATICS OF NONSPHERICAL AEROSOL GRAVITATIONAL COAGULATION . . . . .	39
4.0 Introduction . . . . .	39
4.1 Gravitational Coagulation and Shape Factors . . . . .	39
4.2 Coordinates Systems . . . . .	51
4.2.1 Oblate Spheroidal Coordinates . .	51
4.2.2 Circular Cylindrical Coordinates and Transformations . . . . .	54
4.3 Viscous Flow Past Oblate Spheroids . . .	58
4.4 Equations of Aerosol Motion . . . . .	62
4.4.1 Derivation of Dimensional and Nondimensional Equations . . . . .	62
4.4.2 Drag Force Terms: Superposition Method . . . . .	70
V. NUMERICAL METHODS AND COMPUTER CODE DEVELOPMENT . . . . .	73
5.1 Numerical Methods and Analysis . . . . .	73
5.1.1 Solution of the Equations of Motion . . . . .	73

CHAPTER	PAGE
5.1.1.1 Numerical Integration . .	74
5.1.1.2 Determination of Minimum Separation . . . . .	79
5.1.2 Numerical Methods Used to Calculate Velocity Fields . . . .	81
5.1.2.1 Numerical Solution of Stokes Relationships . .	81
5.1.2.2 Interpolation of the Velocity Fields . . . . .	86
5.1.3 Numerical Methods of Solution of the Navier-Stokes Equation . . . .	89
5.1.3.1 Method of Solution and Its Analysis . . . .	95
5.1.3.1.1 Properties of Iterative Matrices . . . .	101
5.2 The NGCEFF Code . . . . .	105
5.2.1 Code Structure . . . . .	107
5.2.1.1 Main Program . . . . .	109
5.2.1.2 Subroutine INITAL . . . .	111
5.2.1.3 Subroutine OBLATE . . . .	112
5.2.1.4 Subroutine SIZE . . . . .	115
5.2.1.5 Subroutine VELCTY . . . .	115

CHAPTER	PAGE
5.2.1.6 Subroutine COLL . . . . .	116
5.2.1.7 Subroutine OUTPUT . . . . .	118
5.2.1.8 Subroutine IDERIV . . . . .	119
5.2.1.9 Subroutine DEFINE . . . . .	120
5.2.1.10 Subroutine DFUN . . . . .	120
5.2.1.11 Subroutine FORSUP . . . . .	121
5.2.1.12 Function Subprograms	
WRH01, WRH02, WZ1, WZ2 . . . . .	121
5.2.1..3 Function Subprograms	
STREAM AND VORTCY . . . . .	122
VI. RESULTS AND DISCUSSIONS . . . . .	123
6.0 Introduction . . . . .	123
6.1 Some Important Numerical Methods	
Results . . . . .	124
6.1.1 Solution to the Navier-Stokes	
Equation . . . . .	124
6.1.2 Solution to the Dynamic Equations	
of Motion and Critical Grazing	
Path . . . . .	128
6.2 Verification of NGCEFF Routines . . . . .	129
6.3 Results from the NGCEFF Code -	
$\beta$ Factor . . . . .	134
VII. CONCLUSIONS AND RECOMMENDATIONS . . . . .	141

CHAPTER	PAGE
7.1 Nonspherical Gravitational Collision	
Efficiencies . . . . .	141
7.2 Collision Shape Factor ( $\beta$ ) . . . . .	143
7.3 Recommendations for Future Work . . . . .	144
7.3.1 Supplementary Dissertations	
Research . . . . .	145
7.3.1.1 Tabulation of Collision	
Shape Factors . . . . .	145
7.3.1.2 Numerical Methods . . . . .	145
7.3.1.3 NGCEFF Code Modification	146
7.3.1.4 Functional	
Representation of the	
Collision Shape Factor . . . . .	146
7.3.2 Additional Research Topics . . . . .	147
7.3.2.1 Synergistic Effects . . . . .	147
7.3.2.2 Coalescent Effects . . . . .	147
7.3.2.3 Knudsen Drag Forces . . . . .	147
7.3.2.4 Other Aerosol Effects . . . . .	148
7.3.2.5 Experimental Data . . . . .	148
REFERENCES . . . . .	149
APPENDIX	
1 Computer Code Listings . . . . .	154
2 Three Function Routines for Spherical	
Particles . . . . .	238

## APPENDIX

## PAGE

3	Kinetic Corrections to Aerosol	
	Gravitational Collisional Efficiency . . . . .	248

## LIST OF FIGURES

FIGURE		PAGE
1.1.1	Simplified Schematic of the Proposed Clinch River Breeder Reactor . . . . .	3
1.1.2	Expansion of Sodium Bubble During HCDA . . .	4
2.1.2.1	Chain Agglomerates . . . . .	11
2.1.2.2	Cluster Agglomerates . . . . .	12
2.1.2.3	Aerosol Particle Density as a Function of Radius <sup>12</sup> . . . . .	14
3.1.1.1	Streamlines for Oblate Spheroids with Axis Ratio 0.2 . . . . .	28
3.1.1.2	Streamlines for Oblate Spheroids with Axis Ratio 0.5 . . . . .	29
3.3.1	Variation of $y_c$ and $y_{min}$ with Sphere Radius, $a_s$ , for 160 micrometers Oblate Spheroid . . . . .	36
3.3.2	Collision Efficiency as a Function of Oblate Spheroid Size, $a_L$ , and Sphere Radius, $a_s$ . . . . .	37
4.2.1.1	Oblate Spheroid Coordinate System . . . . .	53
4.2.2.1	Collision Coordinate System . . . . .	56
5.1.1.3	Determining Minimum Separation Angle $\phi_{min}$ . . . . .	80

FIGURE		PAGE
5.2.1	Flowchart of NGCEFF Program . . . . .	106
A3.1	A Comparison of the Kinetic Corrections with the Experimental Results of Tu and Shaw . . . . .	249

## LIST OF TABLES

TABLE		PAGE
4.4.1.1	Added Mass and Buoyancy Effects . . . . .	65
5.2.1.1	Name and Description of Labeled Commons in NGCEFF . . . . .	108
5.2.1.1.1	Input Variables to NGCEFF Program . . . . .	110
6.2.1	Comparison of Calculated Drag Force Coefficients, Size, and Terminal Velocities for Oblate Spheroids (Axis Ratio = 0.05) as a Function of the Reynolds Number . . . . .	131
6.2.2	Comparison of Calculated Gravitational Collision Efficiencies of Oblate Spheroids (Axis Ratio = 0.999) for Several Cases . . .	135
6.3.1	Oblate Spheroid Values and System Parameters for Collision Results . . . . .	137
6.3.2	Small Particle Values and Parameters for Collision Results . . . . .	138
6.3.3	Gravitational Collision Shape Factor for Oblate Spheroid and Spheres . . . . .	139
A2.1	GEPS Function Capabilities and Limitations .	239
A3.1	Gravitational Collision Efficiency Superposition Method . . . . .	254



## CHAPTER I

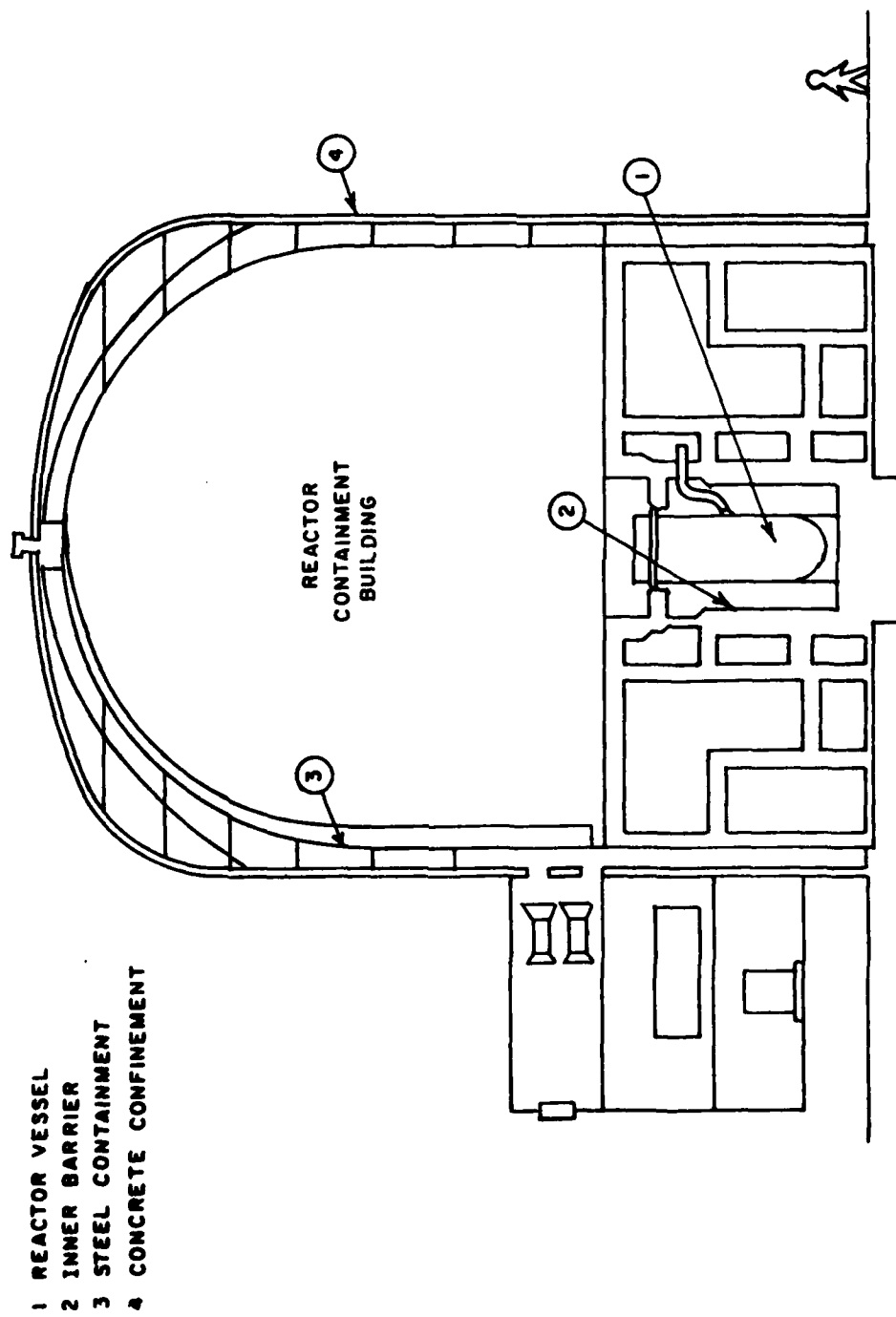
### INTRODUCTION

#### 1.1 LMFBR Safety Requirements

Safety analyses for liquid metal fast breeder reactors (LMFBR) are based on predictions of radioactivity released to the environment under a postulated serious accident condition such as a Hypothetical Core Disruptive Accident (HCDA) which presupposes fuel meltdown and vaporization, and the release of coolant, fuel and structural material into the primary containment. In view of the light water reactor licensing requirements, it is clear that detailed analyses of the consequences of an HCDA will be needed. A critical step in these analyses for LMFBR is the prediction of mass concentration for radioactive material airborne in the containment building at various times after the postulated accident. If this can be accurately calculated, the characteristics of radioactive aerosols outside the containment vessel can be predicted as a function of time. Armed with this information, general population exposure levels downwind of the reactor site can be estimated. Consequently, the development of accurate and physically realistic aerosol behavior models has been the subject of extensive studies.

To help visualize the HCDA environment, Figure 1.1.1 is a schematic of the proposed Clinch River Breeder Reactor (CRBR) containment building. The accident initiating events presently have not been defined. Only the damage mechanisms have been studied<sup>1</sup>. Starting with an energetic power excursion, the active portion of the core is heated to a uniform temperature of 4800°K. The core material expands upward and penetrates the sodium pool as a hemispherical bubble composed of solid fragments, aerosols droplets, vapor, etc. (Figure 1.1.2). The pressure wave created by the bubble damages the reactor vessel, the closure head, and the guard vessel. In most postulated scenarios, the sodium pool burns and creates a log-normal aerosol size distribution with a maximum concentration not exceeding 200 g/m<sup>3</sup>. The aerosol inside the containment building is considered well-mixed with no spatial inhomogeneities for the aerosol.

Thus, following an HCDA, an aerosol mixture of sodium compounds, fuel and core structural materials will begin to plate out on walls, floors, equipment and other components because of various mechanisms. One key mechanism is gravitational coagulation between aerosol particles undergoing simple gravitational settling. This affects the particle size distribution and hence the release of radioactivity to the outside environment.



- 1 REACTOR VESSEL
- 2 INNER BARRIER
- 3 STEEL CONTAINMENT
- 4 CONCRETE CONFINEMENT

Figure 1.1.1.1 Simplified Schematic of the Proposed Clinch River Breeder Reactor

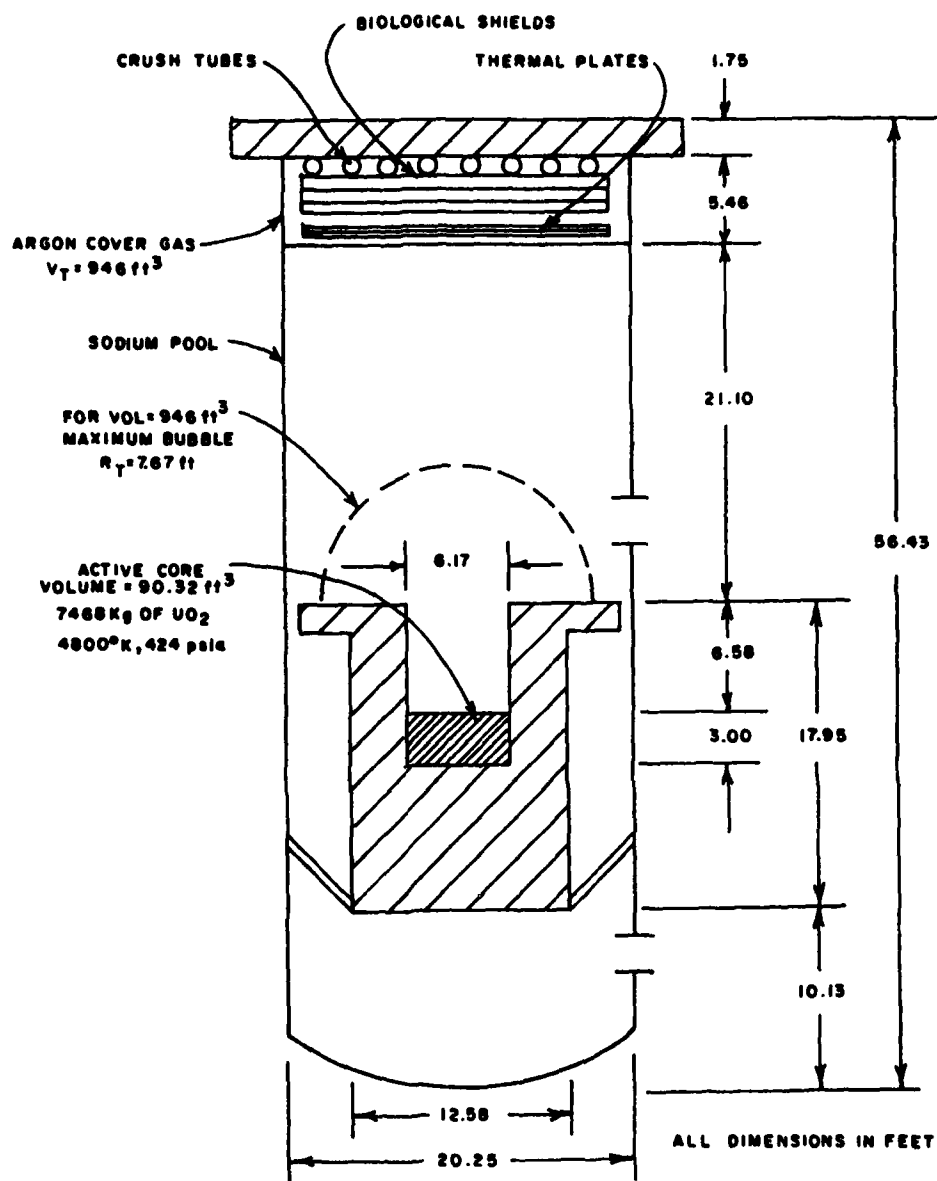


Figure 1.1.2 Expansion of Sodium Bubble During HCDA

Various models have been developed to describe aerosol behavior under postulated accident scenarios. Examples of such models are the HAARM-3 (Heterogeneous Aerosol Agglomeration Revised Model - 3) developed at Battelle Columbus Laboratories<sup>2</sup>, the PARADISEKO-III code at the Karlsruhe Nuclear Research Center<sup>3</sup> and the TRAP code by Brookhaven National Laboratory<sup>4</sup>. These codes attempt to solve the aerosol rate equation, an integro-differential equation describing the rate of change of particle concentration due to the various agglomeration and deposition mechanisms.

## 1.2 Dissertation Organization

This research investigates the hydrodynamic interaction between two LMFBR aerosols falling in a gravitational field. The probability for particle-particle collision, due only to the hydrodynamic and gravitational forces, can be described by defining the gravitational collision efficiency of interacting particles. Determined experimentally or theoretically the collision efficiency is used to estimate the growth of aerosol particles.

The dissertation investigates several ways to improve current theoretical methods for determining the gravitational collision efficiency. Chapter II is a review of LMFBR aerosol characteristics, such as size distribution, chemical composition, shape and density. The aerosol rate equation

is presented and the gravitational collision cross section and efficiency are defined.

Chapter III contains a review of previous work done to estimate the gravitational collision efficiency. Determining the gravitational collision kernel is a fundamental problem of aerosol science which has been extensively investigated by meteorologists because of its importance in the formation and growth of raindrops and hailstones.

Chapter IV derives the equations needed to calculate a generalized gravitational collision kernel. A review of the HAARM-3 code is presented using the expressions derived from this chapter.

Chapter V presents the numerical methods used to solve the equations and the problems associated with various numerical techniques. Code development is examined and options available are explained.

Chapter VI contains the results for the cases studied and their application to current aerosol codes like HAARM-3.

Chapter VII reviews the research project and makes recommendations for future work.

Studies associated with the dissertation topic are presented in the appendices. It includes kinetic corrections to the superposition method for calculating the gravitational collision kernel for spherical particles, a listing of

FORTTRAN function routines for calculating gravitational collision efficiencies, and a discussion of the computer codes used for the dissertation.

## CHAPTER II

### LMFBR AEROSOLS AND GOVERNING EQUATIONS

#### 2.1 Morphology and Aerodynamics of LMFBR Aerosols

Aerosols can be produced by fragmentation during the postulated energetic core disruptive accident and by condensation of vapors during and following the accident. The resulting aerosols can consist of a number of different materials, such as sodium, plutonium, uranium and their oxides, and reactor structural material. Due to the large mass of sodium coolant present, it is reasonable to assume that the bulk of LMFBR aerosols is composed of sodium compounds. Because of this assumption, the majority of investigators have reported the characteristics and behavior of sodium and its compounds, although recently more research into the morphology of plutonium and uranium oxides has been reported.

##### 2.1.1 Primary Particles

Condensation is believed to be more important to the production of LMFBR aerosols than fragmentation<sup>5</sup>. Particles formed by nucleation are of the order of 0.001  $\mu\text{m}$  diameter. Once formed, they grow rapidly by condensation. Although primary particles actually define the starting point for the



agglomeration process, they coagulate so rapidly that it is impractical to describe the aerosol source in terms of the characteristics of primaries. Therefore, the aerosol term is normally characterized by specifying the properties of the LMFBR aggregates.

### 2.1.2 LMFBR Aggregates

It is generally accepted that the agglomerates of sodium oxide, plutonium and uranium oxides are branched chain-like structures composed of spherical, small in diameter (0.01 to 0.45  $\mu\text{m}$ ) primary particles that are distributed log-normally<sup>6-8</sup>. Because of the complex nature of the structures, measurements of these agglomerates are typically concerned with aerodynamic shape factor,  $\kappa$ , and density correction factor,  $\alpha$ , given mathematically by the formulas:

$$\kappa = \frac{V_s}{V_a} \quad (2.1.2.1)$$

$$\alpha = \frac{\rho_a}{\rho_m} \quad (2.1.2.2)$$

where:

$V_s$  ~ Stokes settling velocity

$V_a$  ~ Actual or measured velocity

$\rho_a$  ~ Density of the agglomerate

$\rho_m$  ~ Density of the material.

These quantities are further defined in Chapter IV. The important point is that solid aerosol particles are rarely seen to be spherical, at least so far as those particles are concerned which can be seen in an optical microscope or electron microscope. Figures 2.1.2.1 and 2.1.2.2 typify the general characteristics of chain agglomerates and indicate the problem associated with any mathematical description of the aggregates. Aggregates have been classified into two groups, one appearing to be almost clusters of particles and the second type being long chains. The theoretical problem is to simulate these agglomerates with simple geometric solids which characterize the general behavior of the aerosol.

Jordan and Geiseke<sup>6</sup> measured the aerodynamic shape factor for agglomerates of  $UO_2$  aerosol particles and estimated the approximate range as  $3 \leq \kappa \leq 16$ . Using the work of Kops et al.<sup>9</sup>, Jordan and Geiseke tried to correlate  $\kappa$  with mass equivalent radius of the agglomerate but were unsuccessful. Their conclusion was that  $UO_2$  particles observed in the Millikan thermal cell did not fall into the category of either fluffy ball with constant packing density or straight chain. This conclusion is difficult to support because the statistics of the Millikan analysis is poor compared with that of the Stöber centrifuge method, which was the technique used by Kops. Jordan and Gieseke measured the



(a)



(b)

Figure 2.1.2.1 Chain Agglomerates

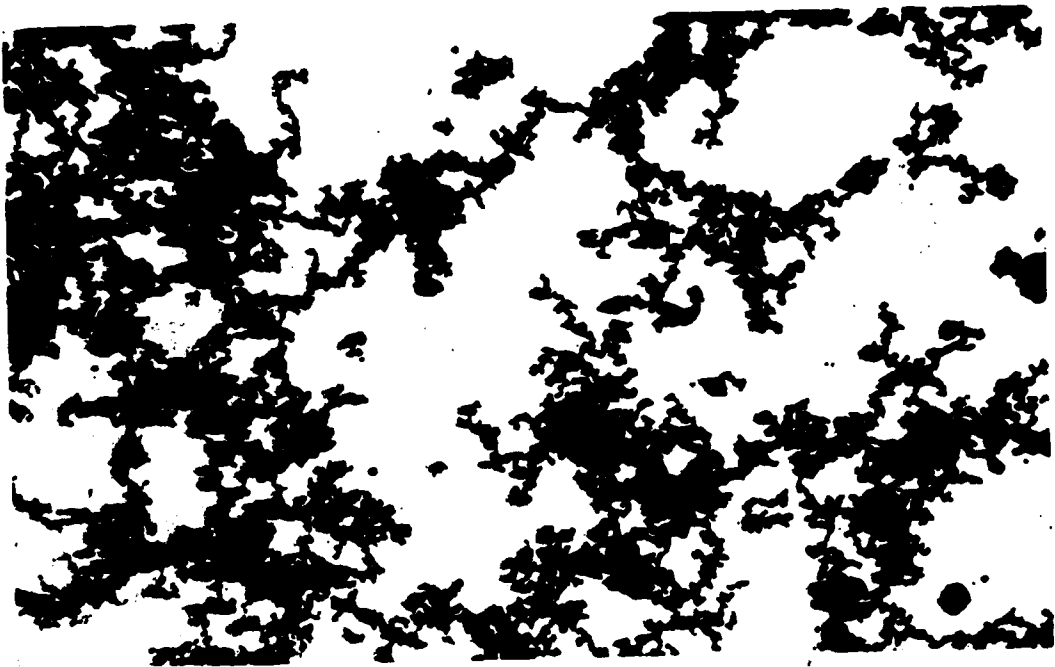


Figure 2.1.2.2 Cluster Agglomerates

characteristics of individual particles in the Millikan cell whereas Kops measured the average properties of agglomerates with the Stöber centrifuge. Kops' work on the aerodynamic diameter of branched chain-like agglomerates was verified by Wegrzyn and Shaw<sup>10</sup> who used a sodium burn chamber to produce the metal oxide instead of the exploding wire technique of Kops. Their results seem consistent with the observed fact that the metal oxide vapors condense to form aggregates.

The most consistent work is that of Wegrzyn and Shaw<sup>8</sup>, Kops et al.<sup>9</sup>, and Van de Vate et al.<sup>11</sup>. These studies indicate that the shape of the metal oxide aerosol is a branched, chain-like agglomerate made up of spherical primary particles. Spiral centrifuge analysis yielded aerodynamics shape factors,  $\kappa$ , between 0.8 and 4. Van de Vate observed that increased humidity for sodium oxide particles would lead to compaction of the fluffy aggregates resulting in an increase aerodynamic diameter and decrease shape factor. None of the researchers reported a shape factor greater than 4 and thus the work of Jordan and Gieseke cannot be verified.

Pertmer<sup>12</sup>, and Pertmer and Loyalka<sup>18</sup> showed that the gravitational collision efficiency is sensitive to the particle density. Pertmer reported Figure 2.1.2.3 showing the relationship between agglomerate radius and density. This result is from Battelle Columbus Laboratories and has not been verified elsewhere. Wegrzyn and Shaw<sup>8</sup> did similar

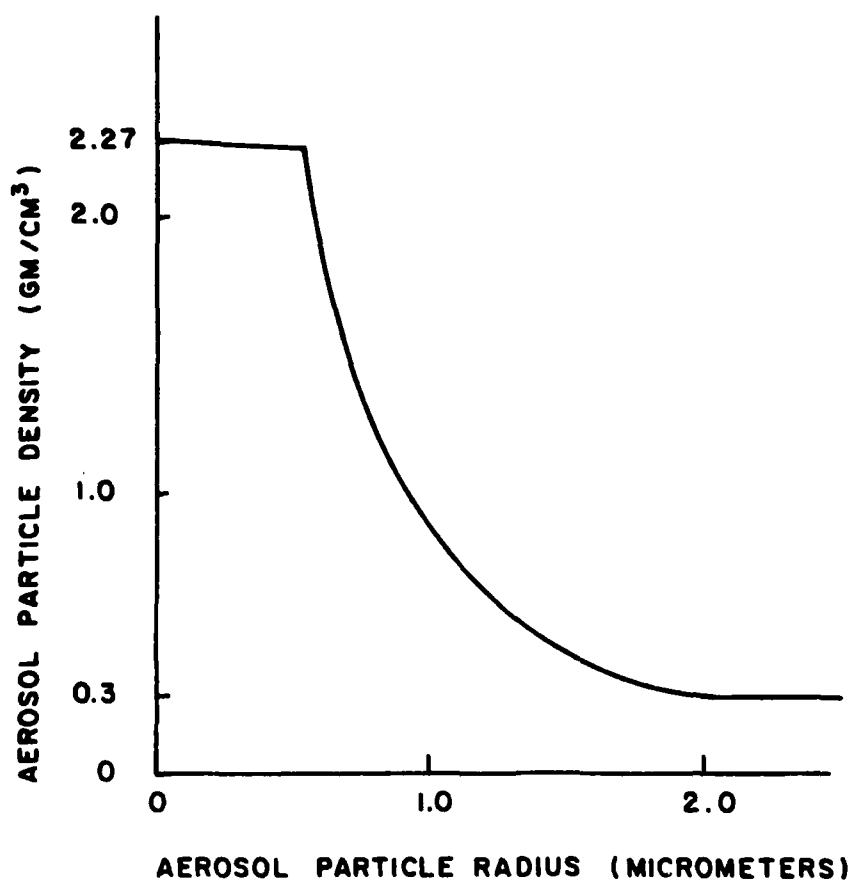


Figure 2.1.2.3 Aerosol Particle Density as  
a Function of Radius<sup>12</sup>

sodium pool fire studies and reported an average agglomerate density ( $\alpha\rho_m$ ) of  $1.32 \text{ g/cm}^3$  for chain-like particles with aerodynamic diameters between  $0.6$  to  $0.7 \text{ }\mu\text{m}$ . If one assumes a primary particle density of  $2.27 \text{ g/cm}^3$  ( $\text{Na}_2\text{O}$ ) then the density factor ( $\alpha$ ) is  $0.58$ . There is evidence<sup>11</sup> that as the agglomerate grows, the density factor decreases as one would predict but a value as low as  $0.13$  (suggested by Figure 2.1.2.3) has not been collaborated. Until new data supports Figure 2.1.2.3, this result will not be used in this research.

## 2.2 Aerosol Behavior Equation

The dynamics of dispersed aerosol systems such as the one following a HCDA is described by the aerosol behavior equation. Derivation of this equation is straightforward and is given by Hidy and Brock<sup>13</sup>, who also discuss its solution.

The number of particles of a given size in the containment atmosphere at any time can be defined in terms of the aerosol density distribution function:

$$n(x,t)dx \sim \text{Number of aerosol particles of size } x \text{ in } dx \text{ at time } t \text{ per unit volume } (\#/ \text{cm}^3).$$

Applying this definition the governing aerosol rate equation is written in the following form:

$$\begin{aligned}
\frac{\partial}{\partial t} n(x,t) &= \frac{1}{2} \int_0^x dx' \phi(x-x',x) n(x-x',t) n(x',t) \\
&\quad - n(x,t) \int_0^\infty dx' \phi(x',x) n(x',t) \\
&\quad - n(x,t) R(x) + S(x,t)
\end{aligned}
\tag{2.2.1}$$

where

$x$  ~ volume of aerosol particle with volume equivalent radius  $r_{1,v}$

$$= \frac{4}{3} \pi r_{1,v}^3 \text{ (cm}^3\text{)}$$

$x'$  ~ volume of aerosol particle with volume equivalent radius  $r_{2,v}$

$$= \frac{4}{3} \pi r_{2,v}^3 \text{ (cm}^3\text{)}$$

$\phi(x',x)$  ~ Normalized collision kernel predicting the probability of collision between two particles of sizes  $x'$  and  $x$  ( $\frac{\text{cm}^3}{\text{sec}}$ )

$R(x)$  ~ Removal rate of particles of size  $x$  due to settling to the containment floor, wall plating, leakage, and so forth (#/sec)



$S(x,t)dx$  ~ Source rate of particles of size  $x$  in  $dx$  at  
time  $t$  per unit volume per unit time  
(#/cm<sup>3</sup>-sec).

The concept of volume equivalent radius is explained in detail in Chapter IV. For our purpose here, it is the radius of a sphere having the same volume as the irregularly shaped particle.

The first integral in Equation 2.2.1 represents the formation rate of particles of size  $x$  due to collisions between particles of size  $x'$  and  $x-x'$ . The integral is multiplied by  $1/2$  so as not to count each collision twice. The second integral represents the disappearance rate of particles in the size range between  $x$  and  $x + dx$  due to collisions with all other particles.

The third term of Equation 1.1 is a removal factor which accounts for a decrease in  $n(x,t)$  resulting from non-collisional losses of particles of size  $x$ . Losses include leakage from the containment building, deposition on internal surfaces due to gravitational settling, thermophoresis, and Brownian diffusion, and mechanical removal by a recirculation cleanup system. The fourth term accounts for all source particles of size  $x$ .

Understanding the nature of the various quantities described in Equation 2.2.1 is of considerable interest. If

should be recognized, however, that this equation is not strictly rigorous, as it omits a number of variables which affect actual aerosol behavior<sup>14</sup>.

To what extent these variables will influence results depend on validation experiments and development of a benchmark code. Work has begun on HAARM-3 code verification procedure<sup>15</sup>.

A benchmark code must describe all phenomenological mechanisms believed to be important in predicting the aerosol density distribution. The resultant code is then to act as a reference against which HAARM-3 and other approximate but more practical codes could be tested. Such a benchmark code, called CRAB, is under development at Battelle Columbus Laboratories<sup>16</sup>.

### 2.3 Aerosol Particle Coagulation

Coagulation is used to describe the process of growth of aerosol particles through collision and their coalescence with one another. Growth of aerosol particles is described by such interaction mechanisms as Brownian coagulation, gravitational coagulation, and turbulent coagulation. Since relatively little is known about the efficiency of coalescence, the coagulation efficiency is assumed equal to the collision efficiency, i.e., the probability of sticking after collision is unity.

The collision kernel in Equation 2.2.1 gives the probability of collision between particles of size  $x, x'$ . The three dominant mechanisms that make up the collision kernel are assumed to be separable and additive. The kernel can be written:

$$\phi(x', x) = B(x', x) + G(x', x) + T(x', x) \quad (2.3.1)$$

where

$B(x', x) \sim$  Brownian coagulation

$G(x', x) \sim$  Gravitational coagulation

$T(x', x) \sim$  Turbulent coagulation.

The validity of the assumption that the three coagulation mechanisms are separative and additive has not been established. Synergistic effects probably exist for certain cases, but before any of these cases can be investigated, each of the three coagulation processes must be accurately defined. The functional form of  $\phi(x', x)$  depends on the dominant mechanism of coagulation and the Knudsen number. Detailed discussions of the expressions for  $\phi(x', x)$  for the different coagulation mechanisms are given in Hidy and Brock<sup>13</sup>. For conciseness only the gravitational coagulation term,  $G(x', x)$ , will be developed here since this is the dominant term in the problem being considered in this dissertation.

## 2.4 Gravitational Coagulation

The gravitational coagulation term,  $G(x',x)$ , of Equation 2.3.1 can be written as:

$$G(x',x) = \sigma_G(r_{1,v},r_{2,v}) |V(x') - V(x)| \quad (2.4.1)$$

where:

$r_{1,v}$  ~ volume equivalent radius of aerosol particle of volume  $x$

$r_{2,v}$  ~ volume equivalent radius of aerosol particle of volume  $x'$

$V(x)$  ~ terminal settling velocity of aerosol particle  $x$

$V(x')$  ~ terminal settling velocity of aerosol particle  $x'$

$\sigma_G(r_{1,v},r_{2,v})$  ~ gravitational collision cross section between particles of radii  $r_1$  and  $r_2$  undergoing gravitational motion.

The gravitational collision cross section defined in Equation 2.4.1 can be written as:

$$\sigma_G(r_{1,v},r_{2,v}) = \pi y_c^2(r_{1,v},r_{2,v}) \quad (2.4.2)$$

$$= \pi R_{12}^2 \epsilon(r_{1,v},r_{2,v}) \quad (2.4.3)$$

where  $y_c(r_{1,v}, r_{2,v})$  is the maximum horizontal separation between the particle of size  $x$  and  $x'$  that would lead to a collision. The term,  $R_{12}$ , is the sum of the particle radii and  $\epsilon$ , the gravitational collision efficiency, is defined by:

$$\epsilon(r_{1,v}, r_{2,v}) = \left( \frac{y_c}{r_{1,v} + r_{2,v}} \right)^2 \quad (2.4.4)$$

The gravitational collision efficiency, defined in Equation 2.4.4 is a nondimensional quantity defining the collision process as a function of the particle equivalent radii and initial horizontal separation. A gravitational efficiency of one means that the center of the smaller particle can lie anywhere in a circle of radius  $r_{1,v} + r_{2,v}$  and there will be a collision between the two particles. If there is hydrodynamic interactions between the two particles, the particles will have horizontal velocity components which will tend to push them apart and cause the gravitational collision efficiency to be less than one. If the efficiency is equal to zero, the smaller aerosol particle would have to be initially positioned directly under the larger aerosol particle if any collision is to occur, and even then there is the possibility that the particles will miss each other. In the actual case, the gravitational collision efficiency will depend on the hydrodynamic interactions which will be a function of such quantities as aerosol particle size, density, and shape and contaminant atmospheric properties.

## 2.5 Problem Statement

The purpose of this research is to investigate the gravitational collision efficiency for post-HCDA LMFBR aerosol particles. As discussed in Section 2.1, agglomerates of sodium oxides, plutonium and uranium oxides are branched chain-like structures. To date collision efficiency calculations are based on the assumption that particles are spherically shaped. Results<sup>17</sup> from a sensitivity analysis of the HAARM-3 Code have shown that this model is sensitive to the gravitational collision efficiency, density correction term, and two particle shape factors designed to correct for the deviation from sphericity of the agglomerates.

The theoretical determination of the gravitational collision efficiency requires solving the full, steady state Navier-Stokes equation of motion. Given the velocity fields and drag coefficients of the particles involved, the superposition method can be used to approximate the actual hydrodynamic interaction between the two particles. Numerical integration methods are then used to solve the first-order, coupled differential equations which describe the particles' trajectories. The critical trajectory which results in a grazing collision gives  $y_c$ . At present, the theoretical work on collisional mechanism and efficiency appears more advanced than the experimental information. This is the state of affairs for the work in this dissertation also.

The contributions of this research may be summarized as follows:

1. Investigation of the nonspherical gravitational collision kernel. To date all aerosol behavior codes have used very simple collision kernels based on the assumption that LMFBR aerosols were spherical in shape. Any correction for nonspherical particles was based on single particle shape factors.

2. Investigation of the slow convergence rate of the Navier-Stokes equation as a function of Reynolds number and axis ratio.

3. Development of a generalized computer code, NGCEFF, written to solve the Navier-Stokes equation, the equations of aerosol motion and to determine the matrix parameters affecting convergence.

4. Development of several function programs using the collision efficiencies determined from the spherical collision efficiency program, GCEFF.

5. Formulation of function routines for nonspherical particles which will facilitate the use of the results of NGCEFF.

6. A preliminary investigation of the effects of slip on collisions efficiency when kinetic corrections are made to the Stokes approximation.

## CHAPTER III

### REVIEW OF PREVIOUS WORK

#### 3.0 Introduction

The preceding chapters introduced the research problem associated with the calculation of the gravitational collision efficiency. Most of the interest in this quantity in the past has been in the atmospheric sciences in conjunction with the prediction of the growth rate of raindrops in the clouds. One notable exception is the recent work of Pertmer and Loyalka<sup>18</sup>, who investigated the gravitational collision efficiency of aerosols formed following an HCDA. In computing the collision kernels, researchers in the atmospheric and nuclear sciences relied on the work of Stokes, Oseen, Stimson and Jeffery, Hocking and others to determine the flow field around a single sphere and the drag forces between the hydrodynamic interacting spheres. Consequently, much is known about the collision efficiencies of two hydrodynamically interacting rigid spheres, while very little is known about the collision efficiencies of nonspherical aerosols.

In this chapter, the previous investigations of the flow field and drag calculations for oblate spheroids, and the collision efficiency for nonspherical aerosols are reviewed. Appropriate references will be made to the contributions of



those researchers who worked with spherical particles but for a detailed review of this body of literature, the reader should consult other references<sup>12,13,14,18</sup>.

### 3.1 Flow Field Approximation

To determine the gravitational collision kernel, the velocity fields and drag forces between two interacting aerosol particles must be known. As stated in previous chapters, an oblate spheroid will be used to model the nonspherical particle.

In principle, the velocities and forces on nonspherical aerosols can be determined by solving the continuity and Navier-Stokes equation of momentum. Since these partial differential equations are nonlinear, closed form solutions are available for only special cases.

The only exact solutions of a two particle problem is that of Stimson and Jeffery<sup>49</sup>, for the Stokes motion of two spheres parallel to their line of centers. The system of bipolar coordinates employed is unique in that it permits one to satisfy simultaneously the boundary conditions on two external spheres.

For the case of a sphere colliding with a nonspherical body, it is not generally possible to find coordinate systems which permit simultaneous satisfaction in all the boundary conditions. Accordingly, numerical schemes must be sought

whereby the boundary value problem may be solved by considering boundary conditions associated with one particle at a time. Even numerical schemes are limited in their ability to predict flow conditions around nonspherical particles. Consequently, nonspherical particles must be chosen which permit investigation of viscous flow around objects of rotational symmetry. An oblate spheroid possesses such rotational symmetry.

### 3.1.1 Steady Flow Past Oblate Spheroids

The problem of calculating numerically the velocity field and drag coefficient for viscous fluid flowing past a single sphere is well documented in the literature. Jensen<sup>20</sup>, using the Stokes stream function and the concept of vorticity, successfully applied the finite difference method to solve the Navier-Stokes equation for flow past a sphere at Reynolds numbers up to 40. Later, Rimon and Cheng<sup>21</sup> obtained the transient uniform flow around a sphere for Reynolds numbers to 1000. However, their results for the surface pressure distribution at steady state conditions are a variance with those of Jensen and of Pearcey and McHugh<sup>22</sup>. Rimon and Lugt<sup>23</sup>, using similar methods as those of Rimon and Cheng, arrived at the steady state solution for flow past oblate spheroids at Reynolds numbers of 10 and 100. They showed that the earlier work of Michael<sup>24</sup> does not

correctly treat the sharp edge of the disk for axis ratios 0.2 and 0.5, where the axis ratio is defined as the minor axis divided by the major axis. However, the works of Rimon and Lugt are also suspect, as discussed by Pruppacher<sup>25</sup> et al., due to inherent difficulties in reaching steady-state conditions by solving the time-dependent Navier-Stokes equation of motion and problems associated with their numerical method of solution, which also plagued their treatment of the spherical case.

For oblate spheroids, the best results are those reported by Pitter et al.<sup>26</sup>, and Masliyah and Epstein<sup>27</sup>. Pitter performed calculations for spheroids of axis ratio 0.05 and 0.2 and Reynolds numbers between 0.1 and 100 while Masliyah and Epstein's results were for axis ratio 0.2 and 0.5 and Reynolds numbers between 1 and 100. Figures 3.1.1.1 and 3.1.1.2 show the influence of axis ratio and Reynolds numbers on the flow around oblate spheroids. The vorticity is generated upstream and is carried by the fluid around the spheroid to considerable distances downstream. It is interesting to note that the streamlines of magnitude 4.0 tend to be less curved with increasing Reynolds number, indicating that the flow becomes undisturbed at a shortened distance from the spheroid as Reynolds number increases. This result correlates with the results that Pitter obtained when he calculated the collision efficiency between an oblate

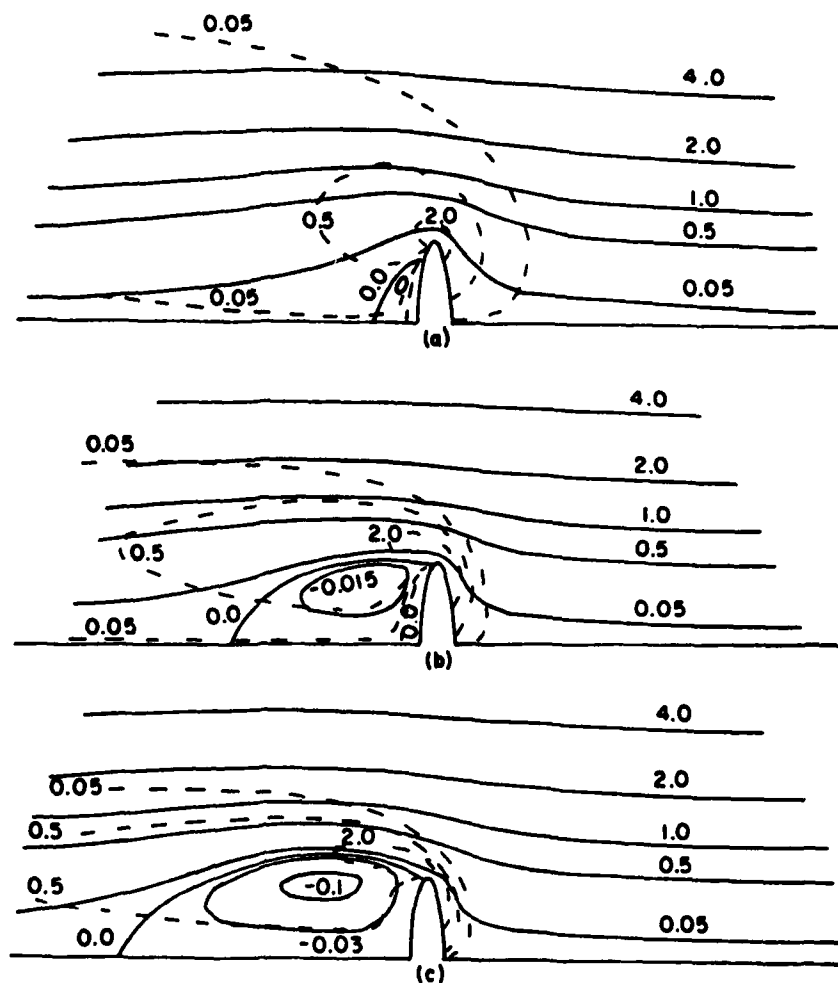


Figure 3.1.1.1 Streamlines for Oblate Spheroids  
with Axis Ratio 0.2 Vorticity Lines Are  
Indicated by Dash Lines Reynolds Number  
(a) 10, (b) 50, (c) 100<sup>27</sup>

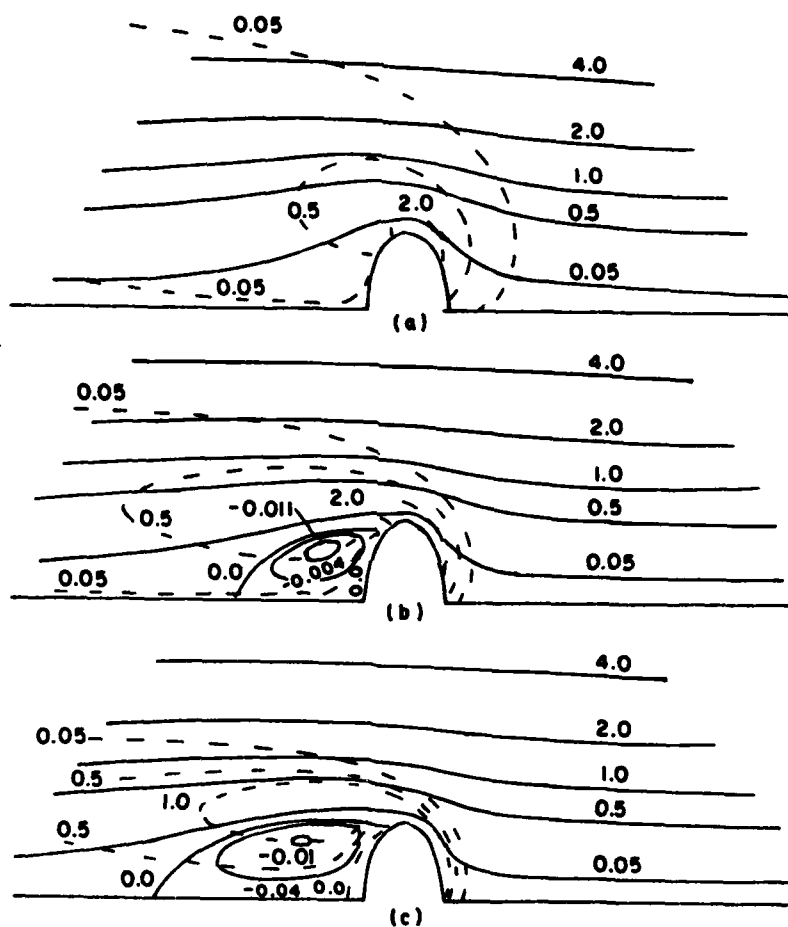


Figure 3.1.1.2 Streamlines for Oblate Spheroids  
with Axis Ratio 0.5 Vorticity Lines Are  
Indicated by Dash Lines Reynolds Number  
(a) 10, (b) 50, (c) 100<sup>27</sup>

spheroid with an axis ratio 0.05 and a colliding sphere and found that collision occurred on the outer edges of the spheroid but not on the interior of the spheroid for higher Reynolds numbers. This surprising result will be discussed later in this chapter.

Equally important were the findings of Pitter for the drag on oblate spheroids. He determined that as the Reynolds number becomes less than one, the drag is approximated better by the Oseen drag expression for oblate spheroids than by way of creeping flow drag expression. This is consistent with the finding of LeClair et al.<sup>28</sup> for spheres, and with the findings of Pruppacher et al.<sup>25</sup> for cylinders. Furthermore for Reynolds numbers less than 0.01 Pitter claims that the drag on a thin oblate spheroid is given accurately by the Oseen drag expression.

Related to these findings of Pitter, is an important result presented by Klett<sup>29</sup> for two particle motion. He found that strong relative motions exist between two particles at very small Reynolds numbers, where according to Stokes theory the viscous forces should prevent this motion. This indicates that the inertia terms of the full Navier-Stokes equation cannot be neglected and possibly why Pertmer and Loyalka<sup>18</sup> found that the Oseen approximation agreed better with the experimental data of Tu and Shaw<sup>48</sup> for cloud droplets than the results of other researchers who

used Stokes' approximation. Another possibility is discussed in Appendix A3, Kinetic Corrections to Aerosol Gravitational Collision Efficiency.

Nevertheless, there is enough doubt about Stokes' approximation for calculations related to the gravitational collision efficiency that any solution should use the full Navier-Stokes equation. This will be discussed further when the so-called superposition method is reviewed.

### 3.1.2 Steady Flow Past Spheres

This topic has been investigated both analytically and numerically. Analytical solutions are limited to Stokes, Oseen and variations of them. For higher Reynolds numbers, empirical and numerical methods must be used. For their research, Masliyah and Epstein<sup>27</sup> showed that an oblate spheroid with an axis ratio 0.999 can be considered to be a sphere for Reynolds numbers 1 to 100. This is one advantage of using oblate spheroids to model nonspherical particles.

### 3.2 The Superposition Model

In order to model the hydrodynamic interaction of two spheres with as much physical realism as possible, Klett<sup>29</sup>, Pertmer and Loyalka<sup>18</sup>, and others used analytical methods, based on Stokes and Oseen equations, which simultaneously satisfied the changing boundary conditions for interacting

spheres. While such analytical treatment is highly desirable for the problem being considered here, the complex geometry associated with the interaction between an oblate spheroid and sphere presently prevents it.

Langmuir<sup>30</sup>, Shafrir and Neiburger<sup>31</sup>, Pearcey and Hill<sup>32</sup>, Shafrir and Gal-Chen<sup>33</sup>, and Pertmer and Loyalka<sup>18</sup> have used the so-called superposition model to compute the collision efficiencies of aerosols. In this model, the motion of each particle is superpositioned onto a fluid velocity field and the drag force is assumed to be taken into account by the velocity difference between the particle's velocity and the fluid velocity field of the second particle superpositioned onto the first particle.

In order to utilize this model, the flow fields of each particle must be defined. Pertmer and Loyalka<sup>18</sup> employed Stokes' approximation to the Navier-Stokes equation to obtain the flow field around one aerosol particle as it falls in isolation. This was one of the options available in their code, GCEFF. They reported that the superposition method and the analytical model using Stokes' approximation gave similar collision efficiencies. This seems to indicate that the superposition method is a good approximation to be used to estimate the drag force terms, if certain conditions are satisfied. These are discussed below.



Pearcey and Hill<sup>32</sup> utilized the Oseen approximation in order to determine the flow field. Shafrir and Neiburger<sup>31</sup>, on the other hand, solved the Navier-Stokes equation to evaluate fluid flow velocities, as did Lin and Lee<sup>34</sup>. A comparison of all of these results is possible but since the resulting equations of motion, necessary to calculate the gravitational collision efficiency, possess the problem of mathematical stiffness, it is difficult to isolate differences due to drag force terms and differential equation integrator routines used by the various investigators.

Pitter and Pruppacher<sup>35</sup> used the superposition method to calculate collision efficiencies between falling ice crystals and raindrops. They developed an extensive argument which justified the use of this method. Basically they found that a reasonable quantity for evaluating the effect of the smaller particle flow field on the larger particle is the mass ratio of the two particles. For interactions investigated by them this quantity never exceeded 0.05 even though the velocity ratio of interacting water drop and ice crystal was as high as 0.8. This is important since, when bodies have similar fall velocities, the results are questionable due to the length of time for interactions to take place. Another important reason to keep the mass ratio small is to prevent tilting of the crystal.

Thus the possibilities available to represent the flow field include Stokes and Oseen approximation and solutions to the full Navier-Stokes equation. As discussed earlier, Stokes' solution for flow around oblate spheroids is questionable. Oseen's solution is also limited to low Reynolds number. It was decided that numerical solutions to the full Navier-Stokes equation offered the greatest capability.

### 3.3 Gravitational Collision Efficiencies for Nonspherical Particles

If the problem of particle deposition of fibrous filters is omitted, then it has been only recently that some attempts to obtain collision efficiencies for nonspherical bodies has appeared in the literature. The most recent is by Pitter and Pruppacher<sup>35</sup> who numerically investigated the hydrodynamic interaction between simple ice plate, modeled as oblate spheroids of axis ratio 0.5 and spherical water drops. The spheroids had semi-major axis lengths between 147 and 404  $\mu\text{m}$  and drops with radii up to 53  $\mu\text{m}$ . As indicated earlier, their investigation revealed the surprising result that water spheres of certain sizes were found which would not collide inside some inner critical trajectory offset, termed  $y_{\min}$ , which is less than the initial offset of the critical grazing trajectory, denoted as  $y_c$ . In other words, if  $y_{\min} = 0$ , the collision domain beneath the spheroid can be pictured

as a circular cylinder with its axis of symmetry of the spheroid. However, when  $y_{\min} > 0$ , the collision domain can be pictured as a circular annulus of radii  $y_{\min}$  and  $y_c$ .

Figure 3.3.1 shows the variation of  $y_c$  and  $y_{\min}$  for an ice plate with a major axis equal to 160  $\mu\text{m}$  for different sphere radii. Figure 3.3.2 displays collision efficiencies of several ice plates interacting with water droplets. The interesting feature of Figure 3.3.2 is the cutoffs at large and small raindrops sizes. The decrease in droplet size, which can collide with increasing ice plate size is due to the inertia of the small droplet moving it across streamlines and larger terminal velocities for larger spheroids. This effect can also be deduced from Figure 3.1.1.1, as can the possibility of having an annular collision domain. Basically a sphere tends to fall at its terminal velocity with respect to the fluid immediately surrounding it, at least this is the case for most collision efficiency models. Also, a sphere's acceleration is proportional to the difference between the velocity the sphere tends to reach and its actual velocity. If for  $y > y_c$  and the water sphere is able to accelerate to the terminal velocity of the oblate spheroid of ice before they collide, the horizontal forces will move the drop around the ice plate before a collision occurs. Naturally the largest  $y$  at which this occurs is called  $y_{\min}$ .

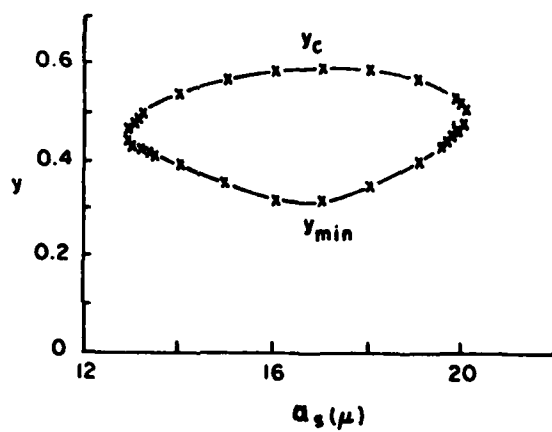


Figure 3.3.1 Variation of  $y_c$  and  $y_{min}$  with  
Sphere Radius,  $a_s$ , for 160 micrometers  
Oblate Spheroid

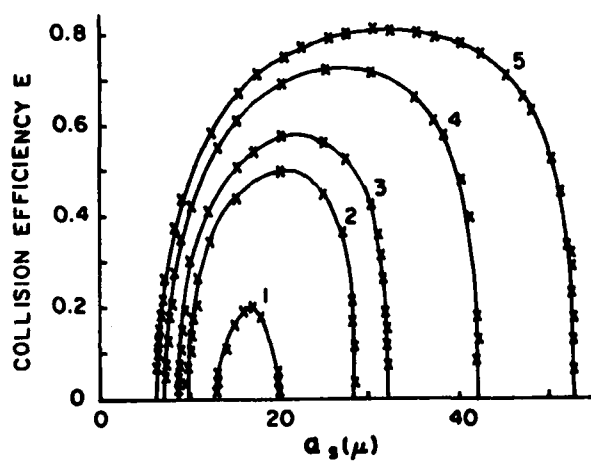


Figure 3.3.2 Collision Efficiency as a Function of Oblate Spheroid Size,  $a_L$ , and Sphere Radius,  $a_s$ .  
 Oblate Spheroid Sizes: (1) 160, (2) 194, (3) 213, (4) 289, (5) 404 micrometers.

The cutoffs at larger water droplets sizes is more difficult to explain. Pitter and Pruppacher gave no explanation for this effect but it may be due to the increased interaction time which would allow the horizontal forces to act longer on the raindrop. Another possibility may be the integration routine used to solve the system of differential equations, which are stiff as showed by Pertmer and Loyalka<sup>18</sup>.

## CHAPTER IV

### MATHEMATICS OF NONSPHERICAL AEROSOL GRAVITATIONAL COAGULATION

#### 4.0 Introduction

The gravitational collision efficiency has been discussed and its importance in the calculation of the aerosol density distribution function has been established by sensitivity analysis<sup>17</sup>. Many researchers feel that the numerical methods necessary to solve the aerosol rate equation are sufficiently well advanced and what really is needed at present are fairly accurate collision kernels for the aerosol rate equation.

In this chapter, the mathematics describing the collision process between an oblate spheroid and a sphere is presented. Where possible, generalized equations are derived which can apply to any nonspherical particle or particles. However, to solve the stated research problem, generalized equations must be abandoned for the detailed, specific equations. It is hoped that the concepts and technique presented can be used for other shaped particles.

#### 4.1 Gravitational Coagulation and Shape Factors

As defined in Chapter 2, Equation 2.4.1, the gravitational collision kernel of two aerosol particles of volume

equivalent radii,  $r_{1,v}$  and  $r_{2,v}$ , is written as:

$$G(x_1, x_2) = \sigma_G(r_{1,v}, r_{2,v}) |V(x_1) - V(x_2)| \quad (4.1.1)$$

or in its expanded form:

$$G(x_1, x_2) = \pi(r_{1,v} + r_{2,v})^2 \epsilon_N(r_{1,v}, r_{2,v}) \cdot |V(x_1) - V(x_2)| \quad (4.1.2)$$

where  $\epsilon_N(r_{1,v}, r_{2,v})$  is the nonspherical gravitational collision efficiency for particles  $x_1$  and  $x_2$  with terminal settling velocities  $V(x_1)$  and  $V(x_2)$ .

Mass equivalent radii are defined by the relationship:

$$r_{i,m} = (3m_i/4\pi\rho_i)^{1/3} \quad i = 1, 2 \quad (4.1.3)$$

where  $m_i$  and  $\rho_i$  are the mass and material density of the  $i^{\text{th}}$  particle. In the case of agglomerates, the actual (measured) agglomerate density  $\rho'_i$ , is related to the material density by:

$$\rho'_i = \alpha_i \rho_i \quad i = 1, 2 \quad (4.1.4)$$

where  $\alpha_i$  is called the density correction factor for the  $i^{\text{th}}$  particle. The volume equivalent radii are then related to the mass equivalent radii by the relationship:



$$r_{i,v} = \alpha_i^{-1/3} r_{i,m} \quad (4.1.5)$$

$$i = 1, 2$$

$$r_{i,v} = f r_{i,m} \quad (4.1.6)$$

where Equation 4.1.6 defines a "shape factor" referred to as the effective diameter factor. For the remainder of this chapter, the notation of the  $i^{\text{th}}$  particle will refer to particle  $x_1$  or  $x_2$ .

There are several other "shape factors" which are quoted in the literature and applied in aerosol codes such as HAARM-3<sup>2</sup>. Since particles encountered in the environment are generally irregular in shape, the diameter assigned to an aerosol particle usually depends on the manner in which it is measured. A fundamental concept, called sphericity, measures the deviation of an individual particle's shape from that characterized by a sphere. It is defined as the ratio of the surface area of a sphere of the same volume as the particle to the actual surface area,  $F$ , of the particle. Mathematically, sphericity,  $\phi$ , is expressed as:

$$\phi = \frac{4\pi(r_v)^2}{F} \quad (4.1.7)$$

where  $r_v$  is the volume equivalent radius of a sphere of the same volume as the original particle.

For investigations of the motion of aerosols the well known Stokes law is often used. Stokes showed that the resistance to the motion of a spherical particle through a viscous fluid will be proportional to the product of the viscosity of the fluid and the velocity and diameter of the particle, provided the fluid medium is infinite in extent and that the inertia forces are negligible compared to the viscous forces. If the shape of a particle is not spherical, the single dimension of diameter will no longer be sufficient to describe the resistance of the fluid to the motion of this particle. An aerodynamic diameter  $d_a$  has been utilized in this case and is defined as the diameter of a spherical particle with unit density,  $\rho_0$ , with the same settling velocity as that measured for a given nonspherical particle. This diameter tends to obscure shape effects rather than explain them, since often neither the shape nor the size of a particle is measured. Mathematically, aerodynamic radius,  $r_{i,a}$  is given by the formula:

$$V_{i,a} = \frac{2}{9} \frac{\rho_0 g}{\mu} \frac{r_{i,a}^2}{D(r_{i,a})} \quad (4.1.8)$$

where  $V_{i,a}$  is the actual (measured) settling velocity for the  $i^{\text{th}}$  particle,  $g$  is the gravitational constant,  $\mu$  is the fluid viscosity, and  $D(r_{i,a})$  is the corrected drag coefficient defined by:

$$D(r_{i,a}) = \psi(r_{i,a}) \frac{Re}{24} \quad (4.1.9)$$

where  $\psi(r_{i,a})$  is the measured drag coefficient and  $Re$  is the Reynolds number. For aerosols, the variable  $D(r_{i,a})$  is approximated by:

$$D(r_{i,a}) = \frac{1.0 + 0.13 Re_{i,a}^{0.85}}{C(r_{i,a})} \quad (4.1.10)$$

where  $C(r_{i,a})$  is the Cunningham-Stokes correction term, applicable when the Knudsen number is not negligible.

Since the aerodynamic radius tends to obscure shape effects, another shape factor based on a ratio of settling velocities has been defined. If the volume equivalent radius and actual agglomerate density, defined by Equations 4.1.5 and 4.1.4, respectively, are used in Stokes law, a settling velocity different from the measured settling velocity would be calculated. In this context, the volume equivalent radius is sometimes called the Stokes radius in order to conform with its use. The Stokes settling velocity,  $V_{i,s}$ , based on the volume equivalent radius is given by:

$$V_{i,s} = \frac{2}{9} \frac{\rho_i g}{\mu} \frac{r_{i,v}^2}{D(r_{i,v})} \quad (4.1.11)$$

where  $D(r_{i,v})$  is the correction drag coefficient for the Stokes radius. At this point the aerodynamic or dynamic shape factor,  $\kappa_i$ , is defined as the ratio of the Stokes settling velocity to the aerodynamic (actual or measured) settling velocity. Thus:

$$\kappa_i = \frac{V_{i,s}}{V_{i,a}} = \frac{\rho_i'}{\rho_o} \left( \frac{r_{i,v}}{r_{i,a}} \right)^2 \frac{D(r_{i,a})}{D(r_{i,v})} \quad (4.1.12)$$

or applying Equation 4.1.10

$$\kappa_i = \frac{\rho_i'}{\rho_o} \left( \frac{r_{i,v}}{r_{i,a}} \right)^2 \frac{C(r_{i,v})}{C(r_{i,a})} \frac{(1 + 0.13 \text{Re}_{i,a}^{0.85})}{(1 + 0.13 \text{Re}_{i,v}^{0.85})} \quad (4.1.13)$$

Equation 4.1.13 points out that the drag correction factor depends on the Reynolds number for the  $i^{\text{th}}$  particle and on the radius used to characterize the particle. In the majority of cases, the approximate shape factor,  $\bar{\kappa}_i$ , defined by:

$$\begin{aligned} \bar{\kappa}_i &= \frac{\rho_i'}{\rho_o} \left( \frac{r_{i,v}}{r_{i,a}} \right)^2 \\ &= \kappa_i \frac{C(r_{i,a})}{C(r_{i,v})} \frac{(1 + 0.13 \text{Re}_{i,v}^{0.85})}{(1 + 0.13 \text{Re}_{i,a}^{0.85})} \end{aligned} \quad (4.1.14)$$

can be used.

Equation 4.1.2 can now be expanded further by substituting the actual (measure) settling velocity, Equation 4.1.8, into it, and by using Equations 4.1.11 and 4.1.12, the entire expression is based on volume equivalent radii. At this point, the drag correction term,  $D(r_{i,v})$ , is approximated by the Cunningham correction factor,  $C_v$ , and the gas mean free path,  $\lambda$ , by the following expression:

$$D(r_{i,v}) = \left(1 + C_v \frac{\lambda}{r_{i,v}}\right)^{-1} \quad (4.1.15)$$

When the density correction factors,  $\alpha_i$ , are used, Equation 4.1.2 finally becomes:

$$\begin{aligned} G(x_1, x_2) = & \pi(r_{1,v} + r_{2,v})^2 \epsilon_N(r_{1,v}, r_{2,v}) \frac{2}{9} \frac{g}{\mu} \frac{\alpha_1 \rho_1}{\kappa_1} \\ & \cdot \left| r_{1,v}^2 \left(1 + C_v \frac{\lambda}{r_{1,v}}\right) - \frac{\alpha_2}{\alpha_1} \frac{\rho_2}{\rho_1} \frac{\kappa_1}{\kappa_2} r_{2,v}^2 \right. \\ & \left. \cdot \left(1 + C_v \frac{\lambda}{r_{2,v}}\right) \right|. \quad (4.1.16) \end{aligned}$$

If a similar expression is derived using mass equivalent radius as the basis for the gravitation collision efficiency, Equation 4.1.16 becomes:

$$\begin{aligned}
G(x_1, x_2) = & \pi(r_{1,m} + r_{2,m})^2 \epsilon_N(r_{1,m}, r_{2,m}) \\
& \cdot \frac{2}{9} \frac{g}{\mu} \frac{\alpha_1^{1/3} \rho_1}{\kappa_1} \left| r_{1,m}^2 \left( 1 + \frac{C_v \lambda \alpha_1^{1/3}}{r_{1,m}} \right) \right. \\
& - \left( \frac{\alpha_2}{\alpha_1} \right)^{1/3} \left( \frac{\rho_2}{\rho_1} \right) \left( \frac{\kappa_1}{\kappa_2} \right) r_{2,m}^2 \\
& \left. \cdot \left( 1 + \frac{C_v \lambda \alpha_2^{1/3}}{r_{2,m}} \right) \right|. \tag{4.1.17}
\end{aligned}$$

The relationship between the gravitational collision efficiency based on mass equivalent radii and volume equivalent radii is:

$$\begin{aligned}
\epsilon_N(r_{1,m}, r_{2,m}) = & \frac{\epsilon_N(r_{1,v}, r_{2,v})}{\alpha_1^{2/3}} \\
& \cdot \frac{(r_{1,m} + (\frac{\alpha_1}{\alpha_2})^{1/3} \cdot r_{2,m})^2}{(r_{1,m} + r_{2,m})^2} \tag{4.1.18}
\end{aligned}$$

Since density correction factors are less than one,  $\epsilon_N(r_{1,m}, r_{2,m}) > \epsilon_N(r_{1,v}, r_{2,v})$  when  $y_c$  (see Equation 2.4.2) is measured or calculated based on the volume or mass equivalent radii of the colliding particles. In fact if  $\alpha_1 = \alpha_2$ , the relationship is simply:

$$\epsilon_N(r_{1,m}, r_{1,m}) = \alpha^{-2/3} \epsilon_N(r_{1,v}, r_{2,v}). \tag{4.1.19}$$

Equations 4.1.16 and 4.1.17 have done little insofar as allowing the gravitational collision kernel to be evaluated since the nonspherical gravitational collisional efficiency,  $\epsilon_N$ , is still unknown. If one assumes that both particles of size  $x_1$  and  $x_2$  are spheres with radii  $r_{1,v}$  and  $r_{2,v}$  and that calculations give a maximum horizontal separation,  $y_{CS}$ , which determines a spherical gravitational collision efficiency,  $\epsilon_S(r_{1,v}, r_{2,v})$ , the  $\epsilon_S$  is written as:

$$\epsilon_S(r_{1,v}, r_{2,v}) = \left( \frac{y_{CS}}{r_{1,v} + r_{2,v}} \right)^2 \quad (4.1.20)$$

However, the nonspherical gravitational collision efficiency,  $\epsilon_N$ , will in general differ from  $\epsilon_S$  because the maximum horizontal separation will be influenced by the geometric projection area and hydrodynamic effects of the nonspherical particles. Equation 4.1.20 is thus written as:

$$\epsilon_N(r_{1,v}, r_{2,v}) = \frac{y_{CN}^2}{(r_{1,v} + r_{2,v})^2} \quad (4.1.21)$$

From Equations 4.1.20 and 4.1.21, the gravitational collision shape factor  $\beta$ , is defined:

$$\epsilon_N(r_{1,v}, r_{2,v}) = \beta \epsilon_S(r_{1,v}, r_{2,v}) \quad (4.1.22)$$

$$\beta = \left( \frac{y_{CN}}{y_{CS}} \right)^2 \quad (4.1.23)$$

Expression 4.1.22 can now be evaluated by using the spherical collision efficiency results of Pertmer<sup>12</sup> and a range of  $\beta$  values for different LMFBR aerosol particles. Before discussing one method to calculate  $\beta$  values, the HAARM-3 expression for the gravitational collision kernel will be reviewed.

Briefly, HAARM-3 expression is derived from Equation 4.1.16 by implicitly assuming:

$$\begin{aligned}\alpha_1 &= \alpha_2 = \alpha \\ \rho_1 &= \rho_2 = \rho \\ \kappa_1 &= \kappa_2 = \kappa\end{aligned}\tag{4.1.24}$$

which reduces this expression to:

$$\begin{aligned}G(x_1, x_2) &= \pi(r_{1,v} + r_{2,v})^2 \epsilon_N(r_{1,v}, r_{2,v}) \frac{2}{9} \frac{g}{\mu} \frac{\alpha\rho}{\kappa} \\ &\cdot \left| r_{1,v}^2 \left(1 + C \frac{\lambda}{r_{1,v}}\right) - r_{2,v}^2 \right. \\ &\cdot \left. \left(1 + C \frac{\lambda}{r_{2,v}}\right) \right|\end{aligned}\tag{4.1.25}$$

or by rearranging terms:

$$\begin{aligned}G(x_1, x_2) &= \frac{2}{9} \frac{\pi g \rho}{\mu} \frac{\alpha \beta}{\kappa} \epsilon_S(r_{1,v}, r_{2,v}) \\ &\cdot [(r_{1,v} + r_{2,v})^3 |r_{1,v} - r_{2,v}| \\ &+ \lambda C (r_{1,v} + r_{2,v})^2 |r_{1,v} - r_{2,v}|].\end{aligned}\tag{4.1.26}$$



A similar expression can be derived for the collision kernel based on mass equivalent radii. This is easily done by using Equation 4.1.17, remembering conditions established by Equation 4.1.24, and using the definition of  $\beta$ , the kernel based on mass equivalent radii becomes:

$$\begin{aligned}
 G(x_1, x_2) = & \frac{2}{9} \frac{\pi g \rho}{\mu} \frac{\alpha^{1/3} \beta}{\chi} \epsilon_S(r_{1,m}, r_{2,m}) \\
 & \cdot [(r_{1,m} + r_{2,m})^3 |r_{1,m} - r_{2,m}| \\
 & + \alpha^{1/3} \lambda C (r_{1,m} + r_{2,m})^2 \\
 & \cdot |r_{1,m} - r_{2,m}|] \quad (4.1.27)
 \end{aligned}$$

At this point it is worthwhile to compare the expression used in the HAARM-3 code<sup>2</sup> and the shape factors used to correct for nonspherical particles. HAARM-3 defines a dynamic shape factor,  $\chi$ , as the square of the ratio of the volume equivalent diameter to the aerodynamic diameter (based on  $\rho'$  instead of  $\rho_0$ ). Also a collision shape factor,  $\gamma$ , is defined as the ratio of the so-called "collision diameter",  $d_c$ , to the volume equivalent diameter,  $d_v$ . It is not clear whether  $d_v$  is based on only one or both particles. The HAARM-3 expression is:

$$\begin{aligned}
G(x_1, x_2) = & \frac{2}{9} \frac{\pi g \rho \alpha^{-1/3} \gamma^2}{\mu \chi} \epsilon_S(r_{1,m}, r_{2,m}) \\
& \cdot [(r_{1,m} + r_{2,m})^3 |r_{1,m} - r_{2,m}| \\
& + \alpha^{1/3} \lambda C(r_{1,m} + r_{2,m})^2 \\
& \cdot |r_{1,m} - r_{2,m}|] \quad (4.1.28)
\end{aligned}$$

The differences between Equations 4.1.27 and 4.1.28 are due to the factor  $\alpha$  and  $\gamma$ . The density correction factor is easily explained by the incorrect assumption that  $\epsilon_S(r_{1,m}, r_{2,m}) = \epsilon_S(r_{1,v}, r_{2,v})$ , when it is correctly given by Equation 4.1.19. The introduction of  $\gamma$  is more serious because  $\gamma$  lacks theoretical basis in view of the defining relationship and the final HAARM-3 expression. It appears that  $\gamma$  is used to represent the same quantity as  $\beta$  but is not clear how  $\gamma$  would be calculated or determined experimentally.

The remainder of this chapter will provide insight into the nature of  $\beta$  for irregularly shaped aerosols by first considering the case of oblate spheroids of different axis ratios. Besides providing a suitable coordinate system, an oblate spheroid of varying axis ratio will provide a general family of possible aerosol shapes by which the collision process can be studied. It is hoped that the methods developed in this research will provide the basis needed to study more complex shapes.

## 4.2 Coordinates Systems

As noted in previous chapters, coordinate systems must be chosen which facilitate the solution of the Navier-Stokes equation. This not only allows the boundary conditions to be specified easily but simplifies the Navier-Stokes equation expressed in the particular coordinate system chosen. Oblate spheroidal coordinates are the natural choice for the translation of any ellipsoid parallel to a principal axis. Also ellipsoids can be varied from a sphere (axis ratio = 1.0) to a circular disk (axis ratio = 0.0) and thus a range of nonspherical particles is available.

Happel and Brenner<sup>36</sup> describe many orthogonal curvilinear coordinate systems associated with bodies of revolution in terms of cylindrical coordinates. Since flow is assumed to be axisymmetrical, cylindrical coordinates offer the advantage that the interaction between nonspherical bodies can be calculated using the velocity fields associated with each particle after being transformed from their respective coordinate system.

### 4.2.1 Oblate Spheroidal Coordinates

Happel and Brenner<sup>36</sup> define the oblate spheroidal coordinate system based on the transformation:

$$z + i\rho = c \sinh(\xi + i\eta) \quad (4.2.1.1)$$

where  $z$  and  $\rho$  are cylindrical coordinates,  $z$  positive in the upstream direction and  $\rho$  positive outward from the axis of symmetry,  $\xi$  and  $\eta$  are oblate spheroidal coordinates,  $c$  is a positive constant, and  $i = \sqrt{-1}$ . The azimuthal coordinate,  $\phi$ , is the same in both systems. Since  $c > 0$ , this leads to the relations:

$$z = c \sinh \xi \cos \eta \quad (4.2.1.2)$$

$$\rho = c \cosh \xi \sin \eta \quad (4.2.1.3)$$

Each coordinate is limited by the ranges:

$$0 \leq \xi \leq \infty, \quad 0 \leq \eta \leq \pi, \quad 0 \leq \phi < 2\pi \quad (4.2.1.4)$$

Referring to Figure 4.2.1.1, surfaces of constant  $\xi$  are oblate spheroids, so the geometry is suited for selecting  $c$  such that  $\xi$  is constant on the surface of the spheroid. By defining the axis ratio  $AR = b/a$ , where  $a$  is the major axis and  $b$  is the minor axis, the following expressions hold:

$$b = c \sinh \xi_0, \quad \eta = 0 \quad (4.2.1.5)$$

$$a = c \cosh \xi_0, \quad \eta = \pi/2 \quad (4.2.1.6)$$

and at the surface of constant  $\xi_0$  it holds that

$$b/a = \tanh \xi_0 = AR \quad (4.2.17)$$

which leads to  $\xi_0$  defined by:

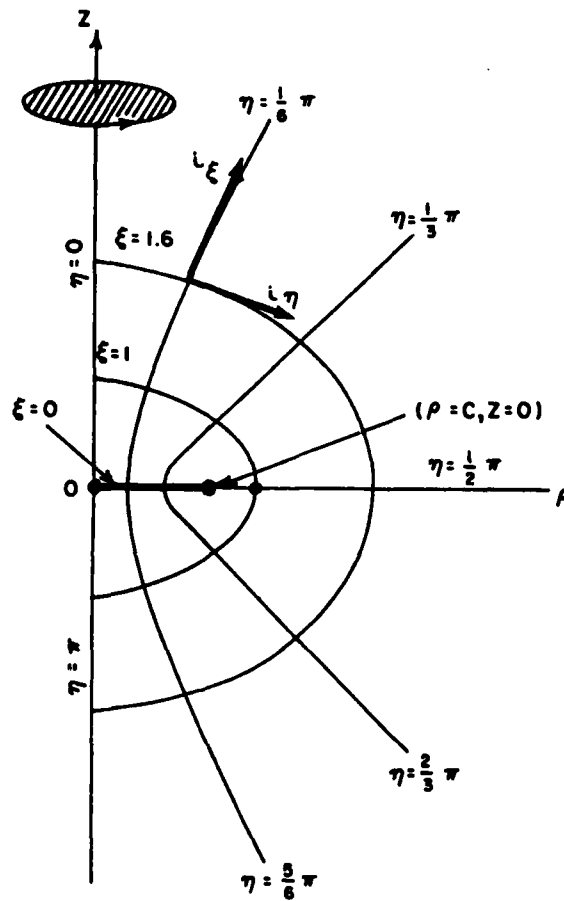


Figure 4.2.1.1 Oblate Spheroid Coordinate System

$$\xi_0 = \frac{1}{2} \log \left( \frac{1 + AR}{1 - AR} \right) \quad (4.2.1.8)$$

Happel and Brenner<sup>36</sup> review the metric coefficients and give the expressions needed to derive the various operators of vector calculus. The most important one for this study is the  $E^2$  operator in oblate spheroidal coordinates given by:

$$E^2 = \frac{(\sinh^2 \xi + \cos^2 \eta)}{c^2} \left[ \frac{\partial^2}{\partial \xi^2} + \frac{\partial^2}{\partial \eta^2} - \tanh \xi \frac{\partial}{\partial \xi} - \cot \eta \frac{\partial}{\partial \eta} \right] \quad (4.2.1.9)$$

where  $c$  is given by Equation 4.2.1.6.

#### 4.2.2 Circular Cylindrical Coordinates and Transformations

Since this coordinates system is widely used in engineering, it will not be reviewed in detail. However, transformation relationships from oblate spheroidal to cylindrical coordinates are needed. From Happel and Brenner<sup>36</sup> it can be shown that the transformation of vector components from oblate spheroidal to cylindrical coordinates is given by:

$$u_z = \frac{u_\xi \cosh \xi \cos \eta - u_\eta \sinh \xi \sin \eta}{(\sinh^2 \xi + \cos^2 \eta)^{1/2}} \quad (4.2.2.1)$$

$$u_\rho = \frac{u_\xi \sinh \xi \sin \eta + u_\eta \cosh \xi \cos \eta}{(\sinh^2 \xi + \cos^2 \eta)^{1/2}} \quad (4.2.2.2)$$

$$u_{\phi} = u_{\phi} \quad (4.2.2.3)$$

where the vector components are:

$$\bar{u}(\rho, \phi, z) = u_{\rho} \hat{i}_{\rho} + u_{\phi} \hat{i}_{\phi} + u_z \hat{i}_z \quad (4.2.2.4)$$

$$\bar{u}(\xi, \phi, \eta) = u_{\xi} \hat{i}_{\xi} + u_{\phi} \hat{i}_{\phi} + u_{\eta} \hat{i}_{\eta} \quad (4.2.2.5)$$

for the cylindrical and oblate spheroidal coordinates, respectively.

Figure 4.2.2.1 represents the collision between an oblate spheroid and a sphere. A sphere is said to have collided with the oblate spheroid when the sphere center was within one sphere radius of the spheroid surface. Due to the geometry of the two particles, the scheme is involved but still only requires two dimensions since the oblate spheroid has rotational symmetry about its minor axis.

The cylindrical coordinates of the curve representing the intersection of the oblate spheroidal surface with the meridional plane is:

$$z_1 \hat{i}_z + \rho_1 \hat{i}_{\rho} = AR \cos \phi \hat{i}_z + \sin \phi \hat{i}_{\rho} \quad (4.2.2.6)$$

where the angle  $\phi$  is the angle which gives the shortest distance between the center of the sphere and the surface of the oblate spheroid. Equation 4.2.2.6 has been nondimensionalized by dividing by the semi-major axis length,  $a$ , of the





oblate spheroid. Referring to Figure 4.2.2.1, the separation distance,  $S$ , is:

$$\begin{aligned} S^2 &= (z_2 - z_1)^2 + (\rho_2 - \rho_1)^2 \\ &= (z_2^2 + \rho_2^2 + AR^2 \cos^2 \phi + \sin^2 \phi \\ &\quad - 2ARz_2 \cos \phi - 2\rho_2 \cos \phi \end{aligned} \quad (4.2.2.7)$$

Since  $S$  is a function of the angle  $\phi$ , the closest distance is achieved when  $dS/d\phi$  is zero. Differentiating and setting the result equal to zero gives:

$$\sin \phi \cos \phi (1 - AR^2) + ARz_2 \sin \phi - \rho_2 \cos \phi = 0 \quad (4.2.2.8)$$

The angle  $\theta$  is easily determined by:

$$\theta = \tan^{-1} \frac{\rho_2}{z_2} \quad (4.2.2.9)$$

so that the angle  $\phi$  can be determined implicitly by the following expressions:

$$f(\phi) = \sin \phi (1 - AR^2) - z_2 (\tan \theta - AR \tan \phi) = 0 \quad (4.2.2.10)$$

$$0^\circ \leq \theta \leq 45^\circ$$

$$f(\phi) = \cos \phi (1 - AR^2) - \rho_2 (\cot \phi - AR \tan \theta) = 0 \quad (4.2.2.11)$$

$$45^\circ \leq \theta \leq 90^\circ.$$

Both equations are stable and converge rapidly to the angle  $\phi$  for a sufficiently good initial estimate is made. In an iteration scheme, the initial guess should be  $\phi = \theta$  and then allow the scheme to converge to an error  $\leq 10^{-14}$  or smaller.

If the Newton-Raphson method of finding the zeros of a function is used, convergence is very fast. Derivatives are:

$$f'(\phi) = \cos\phi(1 - AR^2) + \frac{Z_2 AR}{\cos^2\phi} = 0 \quad (4.2.2.12)$$

$$0^\circ \leq \theta \leq 45^\circ$$

$$f'(\phi) = \sin\phi(1 - AR^2) - \frac{\rho_2}{\sin^2\phi} = 0 \quad (4.2.2.13)$$

$$45^\circ \leq \theta \leq 90^\circ.$$

Again the initial guess should be  $\phi = \theta$ .

#### 4.3 Viscous Flow Past Oblate Spheroids

The steady, axisymmetric incompressible flow around an oblate spheroid is described by the Navier-Stokes equation. This equation is nonlinear, second-order partial differential equation with three unknown quantities, i.e., two velocity components and pressure. Pressure is eliminated by taking the curl twice of the Navier-Stokes equation, and the Stokes stream function, which is related to the velocity, reduces the unknown velocity components to one unknown quantity.

This results in a fourth-order partial differential equation with only the stream function unknown. By introducing vorticity as the curl of velocity, this fourth-order differential equation is split up into two second-order coupled partial differential equations. This procedure is well known and can be found in standard fluid mechanics textbooks.

Using oblate spheroid coordinates and the above procedure, the Navier-Stokes equations can be written as:

$$E^2 \psi = G \quad (4.3.1)$$

$$E^2 G = \frac{\text{Re} \cosh \xi_0 \cosh \xi \sinh \eta}{2(\sinh^2 \xi + \cos^2 \eta)} J_{\xi, \eta} (\psi, F) \quad (4.3.2)$$

where:

$\psi$  ~ Stokes stream functions

$G$  ~ modified vorticity defined by Equation 4.3.3

$F$  ~ modified vorticity defined by Equation 4.3.4

$J_{\xi, \eta}$  ~ Jacobian operator defined by Equation 4.3.6

$\text{Re}$  ~ Reynolds number.

The two modified vorticities are defined in terms of the dimensionless vorticity  $\omega$  as:

$$G = \omega \frac{\cosh \xi \sinh \eta}{\cosh \xi_0} \quad (4.3.3)$$

$$F = \frac{\omega \cosh \xi_0}{\cosh \xi \sinh \eta} \quad (4.3.4)$$

where  $\omega$  is defined in terms of the velocity  $\vec{V}$  by:

$$\vec{\omega} = \text{curl } \vec{V} \quad (4.3.5)$$

the Jacobian operator is simply:

$$J_{\xi, \eta}(\psi, F) = \frac{\partial \psi}{\partial \xi} \frac{\partial F}{\partial \eta} - \frac{\partial \psi}{\partial \eta} \frac{\partial F}{\partial \xi}. \quad (4.3.6)$$

The velocity is related to the stream function and is given in oblate spheroidal coordinates as:

$$u_{\xi} = - \frac{\cosh^2 \xi_0 \frac{\partial \psi}{\partial \eta}}{\cosh \xi \sinh \eta (\sinh^2 \xi + \cos^2 \eta)^{1/2}} \quad (4.3.7)$$

$$u_{\eta} = \frac{\cosh^2 \xi_0 \frac{\partial \psi}{\partial \xi}}{\cosh \xi \sinh \eta (\sinh^2 \xi + \cos^2 \eta)^{1/2}} \quad (4.3.8)$$

$$\vec{V} = u_{\xi} \hat{i}_{\xi} + u_{\eta} \hat{i}_{\eta}. \quad (4.3.9)$$

The following dimensionless quantities were used:

$$\psi = \psi^*/u_{\infty} a^2 \quad (4.3.10)$$

$$\omega = a \omega^*/u_{\infty} \quad (4.3.11)$$

$$\text{Re} = \frac{2 a u_{\infty}}{\nu} \quad (4.3.12)$$

where  $u_\infty$  is the velocity of the undisturbed stream,  $\nu$  is the kinematic viscosity of the fluid,  $\psi^*$  is the dimensional stream function and  $\omega^*$  the dimensional vorticity. The quantity  $a$  is the length of the semi-major axis of the spheroid, and is equal to  $c \cosh \xi_0$ , where  $\xi_0$  is given by Equation 4.2.1.8.

Boundary conditions are based on the Stokes stream function and vorticity. As the partial differential equations are of second order, four boundary conditions are needed to uniquely determine a solution. They are:

$$\begin{aligned} \text{Along the axis of symmetry: } \eta &= 0, \pi \\ \Rightarrow \psi &= 0; \omega = 0 \end{aligned} \quad (4.3.13)$$

$$\begin{aligned} \text{Along the surface of spheroid: } \xi &= \xi_0 \\ \Rightarrow \psi &= 0; \omega = G/\sin \eta \end{aligned} \quad (4.3.14)$$

$$\begin{aligned} \text{At the outer boundary: } \xi &= \xi_b \\ \Rightarrow \psi &= \psi_b; \omega = 0 \end{aligned} \quad (4.3.15)$$

where  $\psi_b = \frac{1}{2} \frac{\sin^2 \xi_b \cosh^2 \xi_b}{\cosh^2 \xi_0}$  and  $\xi_b$  is an outer spheroid shell

where  $u_\xi/u_\infty \leq 0.999$  at  $\eta = 0$ .

The solution to Equations 4.3.1 and 4.3.2 for the case of Stokes flow past an oblate spheroid has been discussed by

Happel and Brenner<sup>36</sup> based on the work of Oberbeck<sup>36</sup>. For cases where  $Re > 0$ , numerical methods must be used and Chapter V will discuss these solutions.

#### 4.4 Equations of Aerosol Motion

##### 4.4.1 Derivation of Dimensional and Nondimensional Equations

The equations of aerosol particle motion are derived by summing the external forces acting on a particle. Typical forces include gravitational, hydrodynamic, electrostatic, thermophoretic and diffusiophoretic. To determine the gravitational collision efficiency in this study, only gravitational and laminar shear forces are considered. The equation of particle motion is:

$$\langle m_i \rangle \frac{d\vec{V}_i}{dt} = [m_i \vec{g}] + F_i \quad (4.4.1.1)$$

where:

$\langle m_i \rangle$  ~ mass the  $i^{\text{th}}$  aerosol particle, allowing for added mass effects

$[m_i \vec{g}]$  ~ gravitational force, allowing for fluid buoyancy effects

$V_i$  ~ velocity of the  $i^{\text{th}}$  aerosol particle

$F_i$  ~ drag force of the  $i^{\text{th}}$  particle.

The added mass effect of the fluid as the particle moves through the fluid cannot always be neglected since the added

mass is a function of the fluid density,  $\rho_f$ , volume of the particles and its shape. This can be expressed as:

$$m_{i,f} = \frac{4}{3}\pi r_{i,v}^3 \rho_f \Delta_A \quad (4.4.1.2)$$

where  $m_{i,f}$  is the added mass to the  $i^{\text{th}}$  particle and  $\Delta_A$  is the added mass coefficient given by<sup>37</sup>:

Oblate ( $AR < 1$ )

$$\Delta_A = \frac{\text{ARcos}^{-1}\text{AR} - (1 - \text{AR}^2)^{1/2}}{\text{AR}^2(1 - \text{AR}^2)^{1/2} - \text{ARcos}^{-1}\text{AR}} \quad (4.4.1.3)$$

Sphere ( $AR = 1$ )

$$\Delta_A = 1/2 \quad (4.4.1.4)$$

The mass of the  $i^{\text{th}}$  aerosol particle becomes:

$$\begin{aligned} \langle m_i \rangle &= m_i + m_{i,f} \\ &= \frac{4}{3}\pi r_{i,v}^3 \rho_i \left(1 + \frac{\rho_f}{\rho_i} \Delta_{A_i}\right) \end{aligned} \quad (4.4.1.5)$$

and the error if the added mass is neglected is:

$$\text{Error} = \left| 1 - \left(1 + \frac{\rho_f}{\rho_i} \Delta_A\right)^{-1} \right| \quad (4.4.1.6)$$

The buoyancy effect is expressed as:

$$[m_i g] = \frac{4}{3}\pi r_{i,v}^3 \rho_i \left(1 - \frac{\rho_f}{\rho_i}\right) \quad (4.4.1.7)$$

and the error introduced in Equation 4.4.1.1 if neglected is:

$$\text{Error} = \left| 1 - \left( 1 - \frac{\rho_f}{\rho_1} \right)^{-1} \right| \quad (4.4.1.8)$$

From Table 4.4.1.1 it is apparent that for spheres, both effects can be neglected since the error is on the order of  $10^{-3}$ . However, as the  $AR \rightarrow 0$ , the strong effect of added mass dictates that this term be retained in Equation 4.4.1.1. Thus there is no justification for neglecting the added mass term and retaining buoyancy term, since buoyancy is only negligible if the added mass is negligible.

Equation 4.4.1.1 can be expanded into six to eight dimensional equations depending on whether relative or absolute position is needed. For this research project, only six equations are used and are written as:

$$* \langle m_1 \rangle \frac{dV_{z1}}{dt} = [m_1 g] + F_{z1} \quad (4.4.1.9)$$

$$* \langle m_1 \rangle \frac{dV_{\rho 1}}{dt} = F_{\rho 1} \quad (4.4.1.10)$$

$$* \langle m_2 \rangle \frac{dV_{z2}}{dt} = [m_2 g] + F_{z2} \quad (4.4.1.11)$$

$$* \langle m_2 \rangle \frac{dV_{\rho 2}}{dt} = F_{\rho 2} \quad (4.4.1.12)$$

$$* \frac{dz}{dt} = V_{z2} - V_{z1} \quad (4.4.1.13)$$



Table 4.4.1.1

Added Mass and Buoyancy Effects<sup>†</sup>

## Added Mass Effect

<u>AR</u>	<u><math>\Delta_A</math></u>	<u>Error</u>
0.001	636	$7.3(10^{-1})$
0.01	63.5	$2.1(10^{-1})$
0.05	12.5	$5.1(10^{-2})$
0.10	6.2	$2.6(10^{-2})$
0.50	1.1	$4.7(10^{-3})$
0.75	0.70	$3.0(10^{-3})$
1.00	0.50	$2.1(10^{-3})$

## Buoyancy Effect

Error $4.3(10^{-3})$ <sup>†</sup>Table Based on Following Densities

$$\rho_f = 1.29(10^{-3})\text{g/cm}^3, \rho_i = 3.0(10^{-1})\text{g/cm}^3$$

$$* \frac{d\rho}{dt} = V\rho_2 - V\rho_1 \quad (4.4.1.14)$$

The asterisk before the equation means that all quantities carry dimensional units whereas if the asterisk appears over individual quantities then only those quantities carry dimensional units. Equations 4.4.1.9 - 4.4.1.14 assume that the oblate spheroid (particle one) has a larger terminal velocity than the sphere (particle two).

The expressions for the mass of the oblate spheroid and sphere are given by Equations 4.4.1.5. The semi-major axis,  $a$ , is related to the volume equivalent radius of the spheroid by:

$$* a = \frac{r_{1,v}}{AR^{1/3}} \quad (4.4.1.15)$$

To render the six equations of motion nondimensional, the nondimensionalizing unit of length is taken as the volume equivalent radius of the oblate spheroid,  $r_{1,v}$ , and the nondimensionalizing unit of velocity is taken as the Stokes terminal velocity of the larger particle,  $V_{\infty 1}$ , where:

$$* V_{\infty 1} = \frac{2}{9} \frac{\rho_1' g r_{1,v}^2}{\mu_f} \left(1 - \frac{\rho_f}{\rho_1'}\right) \quad (4.4.1.16)$$

Again, fluid properties are viscosity,  $\mu_f$ , and density,  $\rho_f$ . Time is nondimensionalized with respect to particle one:

$$* t_1 = \frac{r_{1,v}^*}{V_{\infty 1}^*} \quad (4.4.1.17)$$

Each of the variables in the dimensional equations, Equations 4.4.1.9 - 4.4.1.14, is nondimensionalized as:

$$V_{z1} = V_{z1}^*/V_{\infty 1}^* \quad (4.4.1.18)$$

$$V_{\rho 1} = V_{\rho 1}^*/V_{\infty 1}^* \quad (4.4.1.19)$$

$$V_{z2} = V_{z2}^*/V_{\infty 1}^* \quad (4.4.1.20)$$

$$V_{\rho 2} = V_{\rho 2}^*/V_{\infty 1}^* \quad (4.4.1.21)$$

$$z = z^*/r_{1,v}^* \quad (4.4.1.22)$$

$$\rho = \rho^*/r_{1,v}^* \quad (4.4.1.23)$$

$$t = t^*/t_1^* \quad (4.4.1.24)$$

The force terms are written in the general form as:

$$F_{j1} = F_{j1}^*/6\pi\mu_f^* r_{1,v}^* V_{\infty 1}^* \quad (4.4.1.25)$$

$$F_{j2} = F_{j2}^*/6\pi\mu_f^* r_{2,v}^* V_{\infty 1}^* \quad (4.4.1.26)$$

where  $j = z$  or  $\rho$ , the cylindrical coordinates.

The nondimensional groups and four nondimensional constants are now defined. The first constant,  $r$ , is the ratio of the particle volume equivalent radii,

$$r = r_{2,v}^*/r_{1,v}^* \quad (4.4.1.27)$$

the second,  $\gamma$ , is the ratio of the particle densities,

$$\gamma = \rho_2^*/\rho_1^* \quad (4.4.1.28)$$

the third,  $B$ , is the ratio of the particle buoyancy effects,

$$B = \frac{(1 - \rho_f^*/\rho_2^*)}{(1 - \rho_f^*/\rho_1^*)} \quad (4.4.1.29)$$

and the final constant,  $I$ , is the particle inertial effects due to added mass,

$$I = \frac{1 + (\rho_f^*/\rho_2^*) \Delta_{A_2}}{1 + (\rho_f^*/\rho_1^*) \Delta_{A_1}} \quad (4.4.1.30)$$

so that the first nondimensional group,  $L$ , relates the differences between the particle radii, density, and shape, that is:

$$\begin{aligned} L &= r^4 \gamma^2 B I \\ &= \left( \frac{r_{2,v}^*}{r_{1,v}^*} \right)^4 \left( \frac{\rho_2^*}{\rho_1^*} \right)^2 \left( \frac{1 - \rho_f^*/\rho_2^*}{1 - \rho_f^*/\rho_1^*} \right) \left( \frac{1 + (\rho_f^*/\rho_2^*) \Delta_{A_2}}{1 + (\rho_f^*/\rho_1^*) \Delta_{A_1}} \right) \\ &= \left( \frac{r_{2,v}^*}{r_{1,v}^*} \right)^4 \left( \frac{\rho_2^* - \rho_f^*}{\rho_1^* - \rho_f^*} \right) \left( \frac{\rho_2^* + \rho_f^* \Delta_{A_2}}{\rho_1^* + \rho_f^* \Delta_{A_1}} \right) \quad (4.4.1.31) \end{aligned}$$

The second nondimensional group is the Stokes number,  $Stk$ , and is the ratio of the penetration distance of the small particle to the characteristic radius of the obstacle (projected radius of oblate spheroid for the case being considered). If the smaller particle were injected into motionless fluid with a velocity equal to its Stokes terminal velocity,  $V_{\infty 2}$ , the particle will come to rest after travelling  $z_2$ , its penetration distance. Integration of the equations of motion gives the penetration distance as:

$$* z_2 = \frac{\langle m_2 \rangle}{\pi \mu_f r_{2,v}} V_{\infty 2} \quad (4.4.1.32)$$

and the Stokes number is:

$$Stk = z_2^*/a^* = AR^{1/3} z_2^*/r_{1,v}^*$$

The Stokes number is also given by:

$$Stk = \frac{\bar{V}_{\infty 1}^2}{g^* a^*} r_{\gamma 2B}^4 \frac{(1 + (\rho_f^*/\rho_2^*) \Delta_{A_2})}{(1 - \rho_f^*/\rho_1^*)} \quad (4.4.1.33)$$

Thus the six nondimensional equations, Equation 4.4.1.9 - 4.4.1.14, are now written as:

$$\frac{dV_{z1}}{dt} = AR^{1/3} \frac{L}{Stk} (1 + F_{z1}) \quad (4.4.1.34)$$

$$\frac{dv_{\rho 1}}{dt} = AR^{1/3} \frac{L}{Stk} F_{\rho 1} \quad (4.4.1.35)$$

$$\frac{dv_{z 2}}{dt} = \frac{AR^{1/3}}{T} \frac{L}{Stk} \left( B + \frac{F_{z 2}}{r^2} \right) \quad (4.4.1.36)$$

$$\frac{dv_{\rho 2}}{dt} = \frac{AR^{1/3}}{T} \frac{L}{Stk} \left( \frac{F_{\rho 2}}{\gamma r^2} \right) \quad (4.4.1.37)$$

$$\frac{dz}{dt} = v_{z 2} - v_{z 1} \quad (4.4.1.38)$$

$$\frac{d\rho}{dt} = v_{\rho 2} - v_{\rho 1} \quad (4.4.1.39)$$

#### 4.4.2 Drag Force Terms: Superposition Method

The drag force in Equations 4.4.1.34 - 4.4.1.39 must be known before these equations can be integrated. As previously mentioned, no analytical expressions are available to model the hydrodynamic interaction between an oblate spheroid and a sphere. It is therefore necessary to use the so-called superposition scheme. In this method, the motion of each particle is superpositioned onto a fluid velocity field. For the superposition method, the nondimensional force terms are:

$$F_{j 1} = \left( \frac{C_D Re}{24} \right)_1 (V_{j 1}^* - W_{j 2}^*) / V_{\infty 1}^* \quad (4.4.2.1)$$

$$F_{j 2} = \left( \frac{C_D Re}{24} \right)_2 (V_{j 2}^* - W_{j 1}^*) / V_{\infty 1}^* \quad (4.4.2.2)$$

where  $j = z, \rho$  and  $C_D$  is the drag coefficient for the  $i^{\text{th}}$  particle. The velocities of the particles,  $V_{j1}$  and  $V_{j2}$ , are obtained from integration of the equations of motion. The fluid velocity terms caused by motion of the two particles are  $W_{j1}$  and  $W_{j2}$ . In order to evaluate the nondimensional force terms, the flow fields around the oblate spheroid and sphere must be known. Several possibilities exist which include using Stokes solution, Oseen solution, or a numerical approximation to the full Navier-Stokes equation.

Since the oblate spheroids were assumed to be the collecting particle, it was decided to solve the full steady-state Navier-Stokes equation as described on page 58. The possibility of having Reynolds numbers greater than one is quite likely. On the other hand for very small spheres, the particles being collected, there is some advantage in using an analytical expression for the velocity field. However, if the Reynolds number is large enough to invalidate Stokes solution, the velocity field can be calculated by using an oblate spheroid with an axis ratio 0.999. For Stokes flow, the analytical expression for the velocity field around a sphere in cylindrical coordinate system is:

$$W_{\rho 2} = C \left\{ \frac{3}{4} \frac{r_{2,v} \rho z}{(\rho^2 + z^2)^{3/2}} \left( 1 - \frac{r_{2,v}^2}{(\rho^2 + z^2)} \right) \right\} \quad (4.4.2.3)$$

$$\begin{aligned}
 w_{z2} = C \{ & \frac{3}{4} \frac{r_{2,v} z^2}{(\rho^2 + z^2)^{3/2}} \left( 1 - \frac{r_{2,v}^2}{(\rho^2 + z^2)} \right) \\
 & + \frac{3}{4} \frac{r_{2,v}}{(\rho^2 + z^2)^{1/2}} + \frac{1}{4} \frac{r_{2,v}^3}{(\rho^2 + z^2)^{3/2}} \} \quad (4.4.2.4)
 \end{aligned}$$

where  $C = V_{\infty 2}/V_{\infty 1}$ .

These expressions are valid for  $Re \ll 1$ . For larger Reynolds numbers, it is appropriate to solve the full steady-state Navier-Stokes equation.



## CHAPTER V

### NUMERICAL METHODS AND COMPUTER CODE DEVELOPMENT

#### 5.0 Introduction

In the previous chapters, the Navier-Stokes equation, the equations of aerosol particle motion, and other relationships are derived in order to determine the gravitational collision efficiency. This chapter explains the numerical methods used and analyzes the problems associated with each. These methods are used in the computer code NGCEFF, a code specifically tailored to calculate the gravitational collision shape factor,  $\beta$ , for oblate spheroidal shaped particles.

The last portion of this chapter explains how the code works and various options available. The code is written as a series of subroutines and function routines, thereby allowing for modifications and improvements. This is done so that other nonspherical shaped particles can be substituted without writing a new code from the beginning. Hopefully the comment statements and descriptive variable names will aid in this effort.

#### 5.1 Numerical Methods and Analysis

##### 5.1.1 Solution of the Equations of Motion

### 5.1.1.1 Numerical Integration

The solution of the six nondimensional equations, Equations 4.4.1.34 - 4.4.1.39, require that an accurate numerical scheme be used. The problems involved in integrating a set of equations exhibiting the mathematical property of stiffness are discussed by Gear<sup>38</sup> and also Pertmer<sup>12</sup>, who addressed this question specifically for the problem at hand.

A stiff set of differential equations can be defined as a set of differential equations which have eigenvalues with negative real parts that are widely separated from each other. From Gear<sup>38</sup>, consider the following set of equations:

$$\begin{aligned} u' &= 998u + 1998v \\ v' &= -999u - 1999v \end{aligned} \quad (5.1.1.1.1)$$

This system has two eigenvalues, -1 and -1000, and its solution is:

$$\begin{aligned} u &= 2e^{-t} - e^{-1000t} \\ v &= -e^{-t} + e^{-1000t} \end{aligned} \quad (5.1.1.1.2)$$

Although the terms  $e^{-1000t}$  die away rapidly with increasing time  $t$ , they dominate the solution initially and control the stability and accuracy of the numerical method. Decreasing the step size during integration will help if enough significant digits are available. This significantly increases the time of integration, and if the integration routine is

part of an inner scheme which in turn is part of an outer iteration scheme, then this solution may be impractical. If not enough significant digits are available for the machine being used, then any solution is really meaningless since excessive errors will be introduced by truncation or roundoff procedures in the initial steps.

Gear<sup>38</sup> in his book defines stiff stability and proceeds to determine the existence of stable systems of order up to six. Basically, Gear's method is a modification of an Adams multistep predictor-corrector method. The IMSL<sup>39</sup> subroutine, DGEAR, makes use of Gear's subroutine DIFSUB. A complete discussion of Gear's method can be found in his book, and DGEAR is available from IMSL or many computing centers at universities.

From the numerical calculations of Pertmer<sup>12</sup>, the problem of mathematical stiffness gets increasingly difficult as the particle sizes decrease. His investigation of the variables in the aerosol equations of motion shows that the most rapidly changing variable was a particle's horizontal velocity. This is a reasonable result and certainly one which applies to the present case. Pertmer believes that the stiffness of the aerosol equations of motion is due to large horizontal accelerations of both particles.

Since Gear's method successfully solved the six non-dimensional equations of motion derived by Pertmer, it was

natural to employ this method for the six equations derived in Chapter V. The initial conditions needed to integrate these equations are based on the Stokes terminal velocity and the volume equivalent radius of particle one. It is assumed that the aerosol particles are falling vertically downward with velocities equal to their actual terminal velocities based on their Reynolds numbers. The terminal velocities are:

$$* V_{\infty 1} = \frac{2}{9} \frac{\rho_1}{\mu} g r_{1,v}^2 (1 - \rho/\rho_1) \quad (5.1.1.1.3)$$

$$* V_{\infty a} = Re_a \mu / 2a\rho \quad (5.1.1.1.4)$$

$$* V_{\infty v,1} = Re_{v,1} \mu / 2r_{1,v}\rho \quad (5.1.1.1.5)$$

$$* V_{\infty v,2} = \frac{2}{9} \frac{\rho_2}{\mu} g r_{2,v}^2 (1 - \rho/\rho_2) \quad (5.1.1.1.6)$$

where:

$V_{\infty 1}$  ~ Stokes terminal velocity of particle one based on its volume equivalent radius,  $r_{1,v}$

$V_{\infty a}$  ~ Terminal velocity of particle one based on its semi-major axis length,  $a$

$V_{\infty v,1}$  ~ Terminal velocity of particle one based on its volume equivalent radius,  $r_{1,v}$

$V_{\infty v,2}$  ~ Stokes terminal velocity of particle two based on its volume equivalent radius,  $r_{2,v}$ .

In Chapter IV, the equations of motion were nondimensionalized with respect to  $V_{\infty 1}$  and  $r_{1,v}$ . Assuming the initial vertical separation of the particles is taken to be fifty times the volume equivalent radius of the larger aerosol particle, the initial horizontal velocities are set equal to zero. The initial conditions now become:

$$V_{z1})_0 = V_{\infty a}^*/V_{\infty 1}^*; V_{\infty v,1}^*/V_{\infty 1}^* \quad (5.1.1.1.7)$$

$$V_{z2})_0 = V_{\infty v,2}^*/V_{\infty 1}^* \quad (5.1.1.1.8)$$

$$V_{\rho 1})_0 = 0 \quad (5.1.1.1.9)$$

$$V_{\rho 2})_0 = 0 \quad (5.1.1.1.10)$$

$$z)_0 = 50 \quad (5.1.1.1.11)$$

The initial vertical separation is somewhat arbitrary. It should be large enough so that one aerosol particle has little or no effect on the initial motion of the other aerosol particle but small enough so that integration time is appropriate and worthwhile. Pertmer<sup>12</sup> found that 50 was a satisfactory compromise, as did Pitter and Pruppacher<sup>35</sup> in their investigation.

AD-A106 766

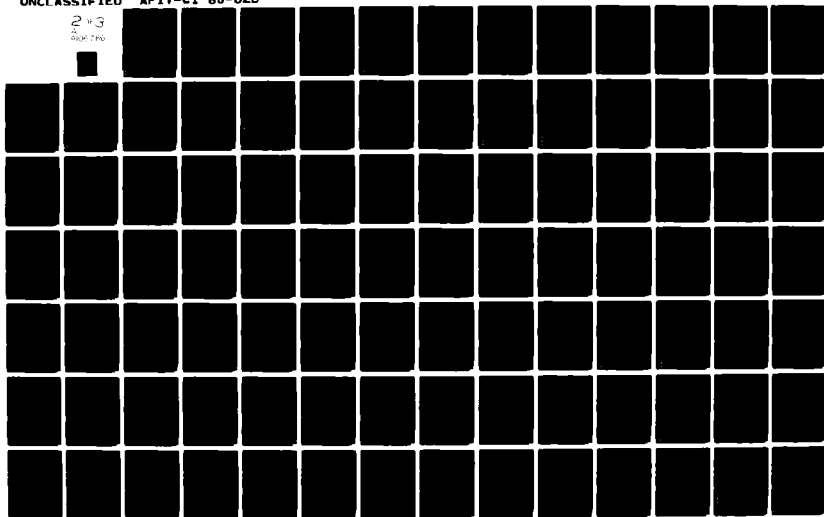
AIR FORCE INST OF TECH WRIGHT-PATTERSON AFB OH  
GRAVITATIONAL AGGLOMERATION OF POST-HCDA LMFBR NONSPHERICAL AER--ETC(U)  
DEC 80 R F TUTTLE  
AFIT-CI-80-82D

F/G 13/7

UNCLASSIFIED

NL

2 13  
0000 710



The aerosol particle initial horizontal separation,  $\rho_0$ , is the parameter which determines the gravitational collision efficiency. From the integration of the six equations of aerosol motion, the critical initial horizontal separations between the two aerosol particles can be determined. From the results of Pitter and Pruppacher<sup>35</sup>, the gravitational collision efficiency must consider the possibility that the collision domain is a circular annulus. Thus the definition needs to be expanded to:

$$\epsilon = \left( \frac{\Sigma \rho_c}{r_{1,v} + r_{2,v}} \right)^2 \quad (5.1.1.1.12)$$

where  $\Sigma \rho_c$  is the sum of collision domains above the particle in question. Pitter and Pruppacher<sup>35</sup> found only one collision domain, which is defined as the difference between the largest and smallest initial horizontal separations which give grazing collisions. Collisions were always assumed to occur if the initial horizontal separation was greater than the smallest and less than the largest critical grazing values.

The possibility of having an annular collision domain presents a problem in any search routine. The bisection method is not suitable since cases can be formulated in which the scheme will fail. Normally detail information is not available, so that any elaborate bisection scheme creates

needless complications. The most prudent scheme is to locate the maximum  $\rho$  for a grazing collision and then decrease  $\rho$  in hopes of finding any "breaks" or discontinuities between the maximum  $\rho$  and  $\rho$  equal to zero.

#### 5.1.1.2 Determination of Minimum Separation

After each step of integration, the oblate spheroid moves closer to the spherical particle. Associated with each step is an angle of separation,  $\phi$ , and the corresponding separation distance,  $S$  (see Figure 4.2.2.1). If a direct or grazing collision occurs, the integration routine will stop. However, if the smaller particle misses the larger, nonspherical particle, the minimum separation does not have to correspond to one of the separation distances calculated for each time step. Figure 5.1.1.3 illustrates what may occur during integration. To estimate the minimum separation distance,  $S_{\min}$ , the minimum separation angle,  $\phi_{\min}$ , is determined by fitting a natural cubic spline to the data points. From the cubic spline function, the angle of minimum particle separation is found by taking the derivative of the spline and setting it equal to zero. Of the two solutions, only one angle will lie between  $\phi_1$  and  $\phi_3$ . To find minimum particle separation, the natural cubic spline calculates it by using  $\phi_{\min}$ . Spline coefficients are determined by using IMSL<sup>39</sup> subroutine ICSICU and interpolation is accomplished using IMSL subroutine ICSEVU.



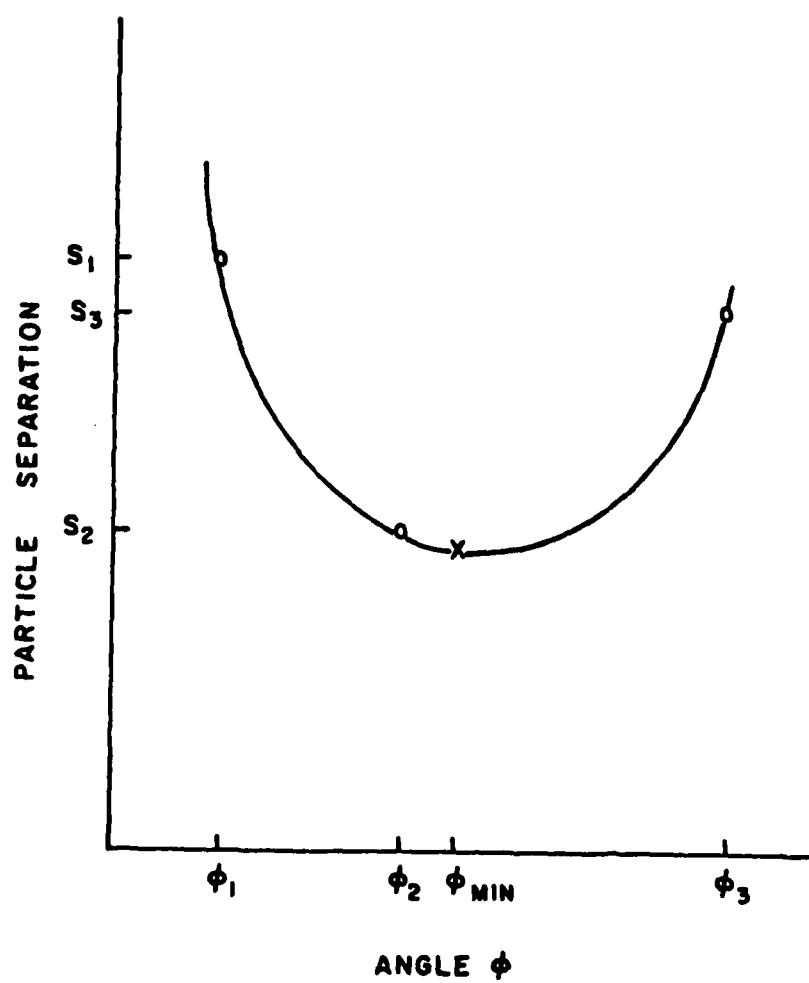


Figure 5.1.1.3 Determining Minimum Separation  
Angle  $\phi_{\min}$

### 5.1.2 Numerical Methods Used to Calculate Velocity Fields

The equations of aerosol motion require that the velocity fields around both particles be known in order to estimate the drag forces (see Equations 4.4.2.1 and 4.4.2.2). The flow field around the smaller particle is obtained from Stokes analytical expression. The flow field around the larger particle, i.e., either the oblate spheroid or its volume equivalent sphere, must be calculated from the solution of the Navier-Stokes equation. The solution of this equation is in terms of the stream function and vorticity. To find the flow fields, Stokes relationships must be used with some appropriate numerical method. By knowing the location of the center of each interacting particle, the velocity field of each can be interpolated at the location of the other particle. Thus two numerical procedures must be used. The first has to do with the solution of Stokes relationships and the second is the interpolation of the velocity fields at the proper locations.

#### 5.1.2.1 Numerical Solution of Stokes Relationships

From Equation 4.2.2.1 and 4.2.2.2, the velocity field in cylindrical coordinates is easily obtained. Determination of oblate spheroidal velocities  $U_{\xi}$  and  $U_{\eta}$  is more difficult. Formally  $U_{\xi}$  and  $U_{\eta}$  are given by the following expressions:

$$U_{\xi} = - \frac{\cosh^2 \xi_0 \partial\psi/\partial\eta}{\cosh\xi \sin\eta (\sinh^2\xi + \cos^2\eta)^{1/2}} \quad (5.1.2.1.1)$$

$$U_{\eta} = \frac{\cosh^2 \xi_0 \partial\psi/\partial\xi}{\cosh\xi \sin\eta (\sinh^2\xi + \cos^2\eta)^{1/2}} \quad (5.1.2.1.2)$$

Previous investigators<sup>27,35</sup> used a finite difference scheme with second order accuracy to compute the velocity at each grid point.

It was decided that piecewise cubic splines offered certain advantages over the finite difference scheme. First, since cubic splines are derived by matching the first and second derivatives (and thus the slope and curvature) at each grid point in order to form a piecewise continuous (smooth) curve, the fitting of the stream function field with cubic splines gives directly the derivatives at each grid point. All that is required to calculate the partial derivatives in Equations 5.1.2.1.1 and 5.1.2.1.2 is to take the derivative of a spline, which is simply the derivative of a polynomial of order 4 or of degree 3 (deBoor<sup>40</sup>).

Since two partial derivatives are required, two sets of splines are formed. One set contains those splines constructed with respect to the coordinate  $\eta$  (holding  $\xi$  constant) and the other set contains those splines constructed with respect to the coordinate  $\xi$  (holding  $\eta$  constant). Splines and their corresponding spline coefficients were computed

using the IMSL<sup>39</sup> routine ICSICU. ICSICU computes the piecewise continuous splines coefficients when given a set of points and arbitrary, but somewhat appropriate, second derivative end conditions. From the IMSL description of ICSICU, define  $f_1''$ ,  $f_2''$ ,  $f_{k-1}''$ , and  $f_k''$  where  $k$  is the number of data points, as the second derivatives of the curve formed by the set of data points. The arbitrary second derivative end conditions are:

$$2f_1'' + q_1 f_2'' = q_2 \quad (5.1.2.1.3)$$

$$q_3 f_{k-1}'' + 2f_k'' = q_4 \quad (5.1.2.1.4)$$

where  $q_i$ ,  $i = 1, \dots, 4$  are the four arbitrary input boundary conditions.

Equations 5.1.2.1.3 and 5.1.2.1.4 point out the second advantage of splines over the finite difference method. Computation of  $U_\xi$  on the axis of symmetry presented Pitter and Pruppacher<sup>35</sup> with a problem because when  $\eta = 0$ , both the  $\sin \eta$  and  $\partial \psi / \partial \eta$  are zero, necessitating the use of L'Hospital's rule. Pitter and Pruppacher found that the use of L'Hospital's rule gave unsatisfactory numerical results. They had to use the adjacent derivatives to estimate  $U_\xi$  at the grid locations that gave the indeterminate results. Spline, however, makes use of the fact that  $\partial \psi / \partial \eta = 0$  at  $\eta = 0$  and  $\pi$  by forcing the spline at the end points to have first derivatives equal to

zero. This is accomplished by setting  $q_1 = q_3 = 1$  and:

$$q_2 = (\psi_2 - \psi_1)/(\Delta\eta)^2 \quad (5.1.2.1.5)$$

$$q_4 = (\psi_k - \psi_{k-1})/(\Delta\eta)^2 \quad (5.1.2.1.6)$$

This results in "shaping" the splines at the end points so that  $U_\xi$  can be determined accurately at the adjacent grid points. To compute  $U_\xi$  at  $\eta = 0$ , L'Hospital's rule can now be applied to Equation 5.1.2.1.1 and the end splines can be differentiated twice to give  $\partial^2\psi/\partial^2\eta$ . This will give good results, but, surprisingly, better results can be obtained by using Gregory-Newton forward and backward extrapolation formula, i.e.:

$$U_\xi)_{\eta=0} = 3(U_{\xi_2} - U_{\xi_3}) + U_{\xi_4} \quad (5.1.2.1.7)$$

$$U_\xi)_{\eta=\pi} = 3(U_{\xi_k} - U_{\xi_{k-1}}) + U_{\xi_{k-2}} \quad (5.1.2.1.8)$$

Calculation of  $U_\eta$  requires a different approach to estimate the end point parameters. First and second derivatives are not necessarily known but because of the no-slip condition imposed at the surface of the oblate spheroid, the value of  $U_\eta)_{\xi=\xi_0}$  is already known, where  $\xi_0$  is the value of

$\xi$  at the surface of the spheroid. It is, therefore, not important to calculate  $U_{\eta}|_{\xi=\xi_0}$  but  $U_{\eta}|_{\xi=\xi_n}$  is needed, where

$\xi_n$  is the value of  $\xi$  at the chosen outer boundary envelope. By specifying the second derivatives at the end points, the correct curvature of adjacent splines can be insured. This is done by setting:

$$q_1 = q_3 = 0 \quad (5.1.2.1.9)$$

$$q_2 = 2(2\psi_1 - 5\psi_2 + 4\psi_3 - \psi_4)/(\Delta\xi)^2 \quad (5.1.2.1.10)$$

$$q_4 = 2(-\psi_{k-3} + 4\psi_{k-2} - 5\psi_{k-1} + 2\psi_k)/(\Delta\xi)^2 \quad (5.1.2.1.11)$$

where second order forward and backward difference expressions are used to estimate second derivatives. Equations 5.1.2.1.10 and 5.1.2.1.11 assume that the angle  $\eta$  is held constant. The opposite was the case for Equations 5.1.2.1.5 - 5.1.2.1.8.

The accuracy of the methods discussed here could be checked since an analytical solution is available for Reynolds number equal to zero. Thus, Oberbeck's solution was used to verify the improvement offered by Equations 5.1.2.1.5 - 5.1.2.1.11 over that offered by a finite difference scheme.

### 5.1.2.2 Interpolation of the Velocity Fields

In order to use the velocity components determined by Equations 4.2.2.1 and 4.2.2.2, the location of the sphere center in oblate spheroidal coordinates must be calculated. This information gives the grid location with the proper indices, which are required in order to select the correct velocity components from the two velocity field arrays.

To determine the angle  $\eta$ , the following relationship is used:

$$\frac{\rho^2}{S^2 (1 - \cos^2 \eta)} - \frac{z^2}{S^2 \cos^2 \eta} = 1 \quad (5.1.2.2.1)$$

where  $z$  and  $\rho$  are the known cylindrical coordinates,  $\eta$  is the unknown oblate spheroidal angle, and  $S$  is semi-major axis length,  $a$ , divided by volume equivalent radius of the spheroid,  $r_{1,v}$ , and the quantity  $\cosh \xi_0$ . The  $\cosh \xi_0$  is the oblate characteristic length specified by Equation 4.2.1.6. Solving for  $\cos^2 \eta$ , the following expression is derived:

$$\cos^2 \eta = \frac{D^2 \pm (D^2 D^2 + 4 S^2 z^2)^{1/2}}{2 S^2} \quad (5.1.2.2.2)$$

where:

$$D^2 = S^2 - (z^2 + \rho^2). \quad (5.1.2.2.3)$$

If the positive sign in Equation 5.1.2.2.2 is selected, the angle  $\eta$  is:

$$\eta = \cos^{-1}(x), \quad z \geq 0 \quad (5.1.2.2.4)$$

$$\eta = \pi - \cos^{-1}(x), \quad z < 0 \quad (5.1.2.2.5)$$

where:

$$x = (\cos^2 \eta)^{1/2}, \quad x \leq 1 \quad (5.1.2.2.6)$$

otherwise:

$$x = 1. \quad (5.1.2.2.7)$$

To calculate  $\xi$  coordinate, remember that:

$$z = S \sinh \xi \cos \eta \quad (5.1.2.2.8)$$

so that  $\xi$  is given by:

$$\xi = \sinh^{-1} \left( \frac{z}{S \cos \eta} \right) \quad (5.1.2.2.9)$$

where  $S = a/r_{i,v} \cosh \xi_0$ .

To determine the indices needed to select the correct velocity components, define:

$$\xi = (j - 1)\Delta\xi + \xi_0, \quad j = 1, 2, \dots, n \quad (5.1.2.2.10)$$

$$\eta = (i - 1)\Delta\eta, \quad i = 1, 2, \dots, m \quad (5.1.2.2.11)$$



where  $\Delta\xi$  and  $\Delta\eta$  are the step sizes for the radial coordinate  $\xi$  and angular coordinate  $\eta$ , and  $n$  and  $m$  are the number of steps.

From Equation 5.1.2.2.9, the index association with radial coordinate  $\xi$  is:

$$J = (\xi - \xi_0)/\Delta\xi + 1 \quad (5.1.2.2.12)$$

and likewise, for angular coordinate  $\eta$ , the index is

$$I = \eta/\Delta\eta + 1 \quad (5.1.2.2.13)$$

where:

$$j \leq J < j + 1 \quad (5.1.2.2.14)$$

$$i \leq I < i + 1 \quad (5.1.2.2.15)$$

To determine the value of the velocity component at location  $(I,J)$ , the four velocity components around this location are properly weighted. From the discussion about Equation 4.4.2.1, the velocity at location  $(I,J)$  is  $w_{j2}$ ,  $j = z, \rho$ . Thus at  $(I,J)$ :

$$\begin{aligned} w_{z2} = & w_1 U_{z_{i,j}} + w_2 U_{z_{i,j+1}} + w_3 U_{z_{i+1,j}} \\ & + w_4 U_{z_{i+1,j+1}} \end{aligned} \quad (5.1.2.2.16)$$

$$\begin{aligned}
 W_{\rho 2} = & w_1^U \rho_{i,j} + w_2^U \rho_{i,j+1} + w_3^U \rho_{i+1,j} \\
 & + w_4^U \rho_{i+1,j+1}
 \end{aligned}
 \tag{5.1.2.2.17}$$

where  $w_i, i=1, \dots, 4$  are the weighting factors defined by the following expressions:

$$w_1 = [i - I + 1][j - J + 1] \tag{5.1.2.2.18}$$

$$w_2 = [i - I + 1][J - j] \tag{5.1.2.2.19}$$

$$w_3 = [I - i][j - J + 1] \tag{5.1.2.2.20}$$

$$w_4 = [I - i][J - j]. \tag{5.1.2.2.21}$$

The results from Equations 5.1.2.2.16 and 5.1.2.2.17 are now used in Equation 4.4.2.1.

### 5.1.3 Numerical Methods of Solution of the Navier-Stokes Equation

As a first step to compute the collision efficiencies of oblate spheroids with spheres, the flow fields around oblate spheroids with different Reynolds numbers and axis ratios are needed. To determine the collision shape factor,  $\beta$ , the flow fields around volume equivalent spheres with different Reynolds numbers are also needed. Since the

Navier-Stokes equation is a second-order, nonlinear partial differential equation, a numerical method of solution is necessary.

Chapter III reviews the literature which reported numerical studies of the flow past oblate spheroids at low and intermediate Reynolds numbers. These studies show that the finite difference method can work but that slow convergence and stability of the iteration method are problems that needed to be analyzed.

Recalling Equations 4.3.1 and 4.3.2 central difference expressions can be used on the  $E^2$  and Jacobian operators at grid locations where the Taylor series expansion is valid. If the difference equations are solved for the value of the stream function  $\psi$  and vorticity  $G$  at the points of expansion, the results are:

$$\begin{aligned} \psi_{i,j}^{k+1} = \frac{1}{h_0} \{ & e_1 \psi_{i,j+1}^k + e_2 \psi_{i,j-1}^k + e_3 \psi_{i+1,j}^k \\ & + e_4 \psi_{i-1,j}^k - f G_{i,j}^k \} \end{aligned} \quad (5.1.3.1)$$

$$i = 2, 3, \dots, m-1$$

$$j = 2, 3, \dots, n-1$$

where:

$$h_0 = 2[(\Delta\xi)^2 + (\Delta\eta)^2]/(\Delta\xi)^2(\Delta\eta)^2 \quad (5.1.3.2)$$

$$e_1 = (1 - \frac{1}{2} \Delta\xi \tanh\xi)/(\Delta\xi)^2 \quad (5.1.3.3)$$

$$e_2 = (1 + \frac{1}{2} \Delta \eta \tanh \xi) / (\Delta \xi)^2 \quad (5.1.3.4)$$

$$e_3 = (1 - \frac{1}{2} \Delta \eta \cot \eta) / (\Delta \eta)^2 \quad (5.1.3.5)$$

$$e_4 = (1 + \frac{1}{2} \Delta \eta \cot \eta) / (\Delta \eta)^2 \quad (5.1.3.6)$$

$$f = (\sinh^2 \xi + \cos^2 \eta) / \cosh^2 \xi_0 \quad (5.1.3.7)$$

and

$\xi$  ~ radial coordinate in oblate spheroidal coordinates

$\eta$  ~ angular coordinate in oblate spheroidal coordinates

$\Delta \xi$  ~ radial coordinate step size

$\Delta \eta$  ~ angular coordinate step size

$j$  ~ index associated with radial coordinate,  $\xi$ , see  
Equation 5.1.2.2.10

$i$  ~ index associated with angular coordinate,  $\eta$ , see  
Equation 5.1.2.2.11

$\xi_0$  ~ value of  $\xi$  that corresponds with the surface of  
the oblate spheroid

$k$  ~ iteration number.

The coefficients  $e_1$ ,  $e_2$ ,  $e_3$ ,  $e_4$ , and  $f$  are evaluated at the grid location  $(i,j)$  being considered. To determine the proper value of  $\xi$  and  $\eta$ , Equations 5.1.2.2.10 and 5.1.2.2.11 are used to generate the vectors and arrays.

The vorticity transport equation, Equation 4.3.2, is more difficult to expand. The problem is caused by trying to use central difference expansions on the Jacobian around a grid point next to the boundary where  $\eta = 0, \pi$ . For example, if one expands the Jacobian using a central difference expression, one of the factors which must be evaluated is:

$$F_{i+1,j}^k - F_{i-1,j}^k \quad (5.1.3.8)$$

where  $F$  is defined by Equation 4.3.4 and is related to  $G$  by:

$$F = \frac{\cosh^2 \xi_0 G}{\cosh^2 \xi \sin^2 \eta} \quad (5.1.3.9)$$

When Expression 5.1.3.8 is evaluated at the adjacent points to  $\eta = 0, \pi$  (i.e.,  $i=2, m-1$ ), the  $\sin$  is zero as well as the vorticity. Application of L'Hospital rule gives poor results. This problem is avoided if a forward difference expansion is used when  $i=2$  and a backward difference expansion is used when  $i=m-1$ . For grid points with  $3 \leq i \leq m-2$ , a central difference expansion can be employed. This procedure results in three iteration formulas:

$$G_{2,j}^{k+1} = \frac{1}{h_1} \{ d_1 G_{2,j-1}^k + d_2 G_{2,j+1}^k + d_3 G_{3,j}^k + d_4 G_{4,j}^k \} \quad j = 2, 3, \dots, n-1 \quad (5.1.3.9)$$

where  $G_{1,j} = 0$  (boundary condition),

$$G_{i,j}^{k+1} = \frac{1}{h_0} \{ d_5 G_{1,j-1}^k + d_6 G_{i,j+1}^k + d_7 G_{i-1,j}^k + d_8 G_{i+1,j}^k \} \quad (5.1.3.10)$$

$$i = 3, 4, \dots, m-2$$

$$j = 2, 3, \dots, n-1$$

$$G_{m-1,j}^{k+1} = \frac{1}{h_2} \{ d_9 G_{m-1,j-1}^k + d_{10} G_{m-1,j+1}^k + d_{11} G_{m-2,j}^k + d_{12} G_{m-3,j}^k \} \quad (5.1.3.11)$$

$$j = 2, 3, \dots, n-1$$

where  $G_{m,j} = 0$  (boundary condition). The coefficients in Equations 5.1.3.9 - 5.1.3.11 are:

$$h_1 = \{ h_0 \frac{\tilde{R}e \cdot 3\psi_{3,j}^k}{\cosh^2 \xi \sin^2 \eta} \} \quad (5.1.3.12)$$

$$h_2 = \{ h_0 + \frac{\tilde{R}e \cdot 3\psi_{3,j}^k}{\cosh^2 \xi \sin^2 \eta} \} \quad (5.1.3.13)$$

$$d_1 = \{ e_2 + \frac{\tilde{R}e \cdot \psi_{3,j}^k}{\cosh^2 (\xi + \Delta \xi) \sin^2 \eta} \} \quad (5.1.3.14)$$

$$d_2 = \{e_1 + \frac{\tilde{Re} \cdot \psi_{3,j}^k}{\cosh^2(\xi + \Delta\xi) \sin^2 \eta}\} \quad (5.1.3.15)$$

$$d_3 = \{e_3 - \frac{\tilde{Re} \cdot 4(\psi_{2,j+1}^k - \psi_{2,j-1}^k)}{\cosh^2 \xi \sin^2(\eta + \Delta\eta)}\} \quad (5.1.3.16)$$

$$d_4 = \{\frac{\tilde{Re} \cdot (\psi_{2,j+1}^k - \psi_{i-1,j}^k)}{\cosh^2 \xi \sin^2(\eta + 2\Delta\eta)}\} \quad (5.1.3.17)$$

$$d_5 = \{e_2 - \frac{\tilde{Re} \cdot (\psi_{i+1,j}^k - \psi_{i-1,j}^k)}{\cosh^2(\xi - \xi\Delta) \sin^2 \eta}\} \quad (5.1.3.18)$$

$$d_6 = \{e_1 + \frac{\tilde{Re} \cdot (\psi_{i+1,j}^k - \psi_{i-1,j}^k)}{\cosh^2(\xi + \Delta\xi) \sin^2 \eta}\} \quad (5.1.3.19)$$

$$d_7 = \{e_4 + \frac{\tilde{Re} \cdot (\psi_{i,j+1}^k - \psi_{i,j-1}^k)}{\cosh^2 \xi \sin^2(\eta - \Delta\eta)}\} \quad (5.1.3.20)$$

$$d_8 = \{e_3 - \frac{\tilde{Re} \cdot (\psi_{i,j+1}^k - \psi_{i,j-1}^k)}{\cosh^2 \xi \sin^2(\eta + \Delta\eta)}\} \quad (5.1.3.21)$$

$$d_9 = \{e_2 + \frac{\tilde{Re} \cdot \psi_{m-2,j}^k}{\cosh^2(\xi - \Delta\xi) \sin^2 \eta}\} \quad (5.1.3.22)$$

$$d_{10} = \{e_1 - \frac{\tilde{Re} \cdot \psi_{m-2,j}^k}{\cosh^2(\xi + \Delta\xi) \sin^2 \eta}\} \quad (5.1.3.23)$$

$$d_{11} = \{e_4 + \frac{\tilde{Re} \cdot 4(\psi_{m-1,j+1}^k - \psi_{m-1,j-1}^k)}{\cosh^2 \xi \sin^2(\eta - \Delta\eta)}\} \quad (5.1.3.24)$$

$$d_{12} = \{- \frac{\tilde{Re} \cdot (\psi_{m-1,j+1}^k - \psi_{m-1,j-1}^k)}{\cosh^2 \xi \sin^2(\eta - 2\Delta\eta)}\} \quad (5.1.3.25)$$

and  $\tilde{Re}$  is the modified Reynolds number defined by:

$$\tilde{Re} = \frac{Re \cosh \xi \sinh \eta}{8(\Delta\xi)(\Delta\eta) \operatorname{sech} \xi_0} \quad (5.1.3.26)$$

Coefficients  $h_0$ ,  $e_1$ ,  $e_2$ ,  $e_3$ , and  $e_4$  were defined earlier.

#### 5.1.3.1 Method of Solution and Its Analysis

Varga<sup>41</sup> discusses the basic iterative methods available to solve matrix equations such as Equations 5.1.3.1 and 5.1.3.9 - 5.1.3.11. Methods include the point Jacobi, Gauss-Seidel, and successive overrelaxation and underrelaxation (SOR) algorithms. The SOR algorithm offers all the advantages of the Gauss-Seidel method plus the advantage of accelerating convergence.

Woo<sup>42</sup> investigated the computational efficiency of the SOR, alternating direction implicit (ADI), and a version of the SOR method called the dominant eigenvalue algorithm (see Orback and Crowe<sup>43</sup>). He applied these methods to the problem of viscous flow around spheres, a problem similar to the one being considered here. He found that the dominant eigenvalue algorithm (DEM) to be 3-4 times faster than SOR



and ADI. Pitter et al.<sup>26</sup>, applied DEM to viscous flow around oblate spheroid and claimed that it helped to accelerate convergence.

The DEM algorithm is based upon the observation that most iterations eventually approach a geometric progression. The iteration procedure continues until the largest eigenvalue of iteration forcing matrix dominates the solution. The dominant eigenvalue can then be used to extrapolate toward the solution before resuming the iteration scheme.

In practice, the dominate eigenvalue is not calculated. The DEM algorithm is applied as follows. Divide the iteration of the loop parameter  $k$  into two half iterations for the index  $j$ , the index associated with the radial component  $\xi$ . The scheme is to use successive substitution with eigenvalue promotion for half of the grid points and no update for the other half of the grid points. For the second half of the  $k^{\text{th}}$  iteration, the updating of field values is reversed. Expressed mathematically, the algorithm is:

$$[\Omega_{ij}^{k+1} = \Omega_{ij}^k + SW_{ij}(\Omega_{ij}^{k+1} - \Omega_{ij}^k)] \quad q = -\ell \quad (5.1.3.1.1)$$

$$[\Omega_{ij}^k = \Omega_{ij}^k] \quad q = \ell \quad (5.1.3.1.2)$$

$$i = 1, 2, 3, \dots, m$$

where  $\ell = -1, 1$  so that when:

$$q = -1 \Rightarrow j = 2, 4, 6, \dots, n-1 \quad (5.1.3.1.3)$$

$$q = 1 \Rightarrow j = 1, 3, 5, \dots, n \quad (5.1.3.1.4)$$

In equation 5.1.3.1.1,  $S$  is the acceleration parameter based on the dominant eigenvalue and  $W_{ij}$  is a matrix of relaxation parameters to be discussed later. The variable  $\Omega_{ij}$  is just a dummy variable representing either  $\psi_{ij}$  or  $G_{ij}$ . The promotion factor  $S$  is related to the dominant eigenvalue  $\lambda_1$  by:

$$S = \frac{\alpha}{1 - |\lambda_1|} \quad (5.1.3.1.5)$$

where  $\alpha$  is a scaling factor so that  $S$  is bounded since in extreme cases,  $|\lambda_1|$  is very close to unity. In practice  $S$  is not applied on every increment of the loop parameter  $k$  but only every 20 increments.

Woo found that a range of 10-15 for  $S$  to give about the same rate of convergence. No justification was given for this range. It appears that it is based on numerical experimentation since no eigenvalues were published by Woo. In general Woo found that stability is not sensitive to the convergence promotion factor  $S$  so long as it is not applied too often. When the convergence promotion factor is not being applied, the factor  $S$  is set equal to one in Equation 5.1.3.1.1.

The use of relaxation parameters is the unique features of any SOR algorithm. The relaxation factors  $W_{ij}$  in Equation 5.1.3.1.1 plays an important role in determining the rate of convergence of the solution. An optimum value usually exists, however for most cases, there exists no theoretical basis for calculating this optimum value, except for the particular case of a square grid system. Varga<sup>41</sup> treats these special cases.

Both Woo<sup>42</sup> and Pitter et al.<sup>26</sup>, used a constant relaxation factor for the stream function, i.e., Equation 4.3.1. They based it on the work of Russell<sup>44</sup>, who studied the solution of the Navier-Stokes equation for flow over flat plates. Russell suggested that the relaxation factor for the stream function equation can be selected as uniform over the entire field. His choice of relaxation factor is based on the number of steps of each independent variable and for the case considered here, is given by:

$$W_{\psi} = \frac{2}{1 + \pi^2(m^{-2} + n^{-2})^{1/2}} \quad (5.1.3.1.6)$$

where  $m$  and  $n$  have been previously defined. Pitter tried to use Equation 5.1.3.1.6 for the case of flow around an oblate spheroid but found by trial and error that using:

$$W_{\pi} = \frac{2}{\sqrt{2} + \pi(m^{-2} + n^{-2})^{1/2}} \quad (5.1.3.1.7)$$

gave better results. Equation 5.1.3.1.7 is used in the current code NGCEFF to start the solution. However, after approximately 20 increments of the loop parameter  $k$ ,  $W_\psi$  is recomputed using the following relationship:

$$W_{\psi_{\text{opt}}} = \frac{2}{1 + (1 - \Xi)^{1/2}} \quad (5.1.3.1.8)$$

where  $\Xi$  is determined as follows: Define the norm of variable  $\psi$  as:

$$|| \cdot ||^{k+1} = \sum_{j=1}^n \sum_{i=1}^m |\psi_{i,j}^{k+1} - \psi_{i,j}^k|. \quad (5.1.3.1.9)$$

Now define  $\Xi$  as:

$$\Xi = \frac{1}{k+1} \sum_{\lambda=1}^{k+1} \frac{|| \cdot ||^{\lambda+1}}{|| \cdot ||^{\lambda}} \quad (5.1.3.1.10)$$

provided  $|| \cdot ||^{\lambda+1} < || \cdot ||^{\lambda}$  and  $|| \cdot ||^{\lambda} \neq 0$ , which indicates convergence. This was found to accelerate convergence of the  $\psi$  field even better than Equation 5.1.3.1.7.

The relaxation of the vorticity field  $G_{ij}$  is much more difficult. Equation 4.3.2 is programmed using Equations 5.1.3.9 - 5.1.3.11, and the DEM iteration procedure explained earlier. However, instead of having a constant relaxation factor for the entire vorticity field, a matrix of relaxation factors,  $W_{ij}$ , is calculated using the relationships developed by Woo<sup>42</sup>. According to Woo, Equation 4.3.2 could be reasonably

relaxed to a numerical solution by the relationship:

$$W_{ij} = \frac{4}{2 + \frac{\sqrt{2} \operatorname{Re} \cosh \xi_0}{\sin \eta \cosh \xi} \left( \left( \frac{\partial \psi}{\partial \eta} \right)^2 + \left( \frac{\partial \psi}{\partial \xi} \right)^2 \right)^2} \quad (5.1.3.1.11)$$

$$i = 2, 3, \dots, m-1$$

$$j = 2, 3, \dots, n-1$$

where  $\operatorname{Re}$  is the Reynolds number,  $\eta$  is the angular coordinate and  $\xi$  is the radial coordinate. These relaxation factors were used but because of severe stability problems associated with the vorticity transport equation, it was necessary to stabilize the vorticity field while the stream function field was allowed to relax. Once the stream function field converged, the vorticity field was allowed to change slowly. Of course this caused the stream function field to change which required, because of stability problems, to slow down the rate of convergence of the vorticity field. Thus the matrix of relaxation factors  $W_{ij}$  were initially multiplied by  $10^{-5}$  and as iteration continued the multiplication factor was raised until it reached one.

This procedure did not always work and in fact, too often the iteration procedure would diverge rapidly regardless of the value of relaxation factors. If sensed in time the divergence could be stopped by multiplying by zero and allowing the stream function field to converge again, and

then allow small changes in the vorticity field. This procedure rarely worked but was tried before stopping the computer code.

#### 5.1.3.1.1 Properties of Iterative Matrices Being Considered

The system of equations generated by Equations 5.1.3.1 and 5.1.3.9 - 5.1.3.11 can be written in the general form:

$$\underline{\underline{A}} \underline{\underline{x}} = \underline{\underline{b}} \quad (5.1.3.1.1.1)$$

or converted into an equivalent form:

$$\underline{\underline{x}} = \underline{\underline{T}} \underline{\underline{x}} + \underline{\underline{c}} \quad (5.1.3.1.1.2)$$

where  $\underline{\underline{A}}$  is the matrix of coefficients,  $\underline{\underline{b}}$  is a column vector of boundary conditions,  $\underline{\underline{x}}$  is a column vector of the unknowns, and matrix  $\underline{\underline{T}}$  and column vector  $\underline{\underline{c}}$  are quantities which depend on which matrix iterative procedure is used, i.e., Jacobi, Gauss-Seidel, SOR, etc.

The solution to Equation 5.1.3.1.1.2 exists and is unique provided  $\underline{\underline{A}}$  is nonsingular. For small systems of equations, its solution can be found easily by computing  $\underline{\underline{A}}^{-1}$  however for large systems of equations, it is neither practical nor computationally efficient to do so.

For the equations considered earlier in this chapter, the number of unknowns and hence the number of equations,  $N_r$ , is:

$$N_r = (m - 2)(n - 2) \quad (5.1.3.1.1.3)$$

which makes  $\underline{\underline{A}}$  and  $\underline{\underline{T}}$   $N_r \times N_r$  matrices.

Matrix  $\underline{\underline{A}}$  in Equation 5.1.3.1.1.1 can be expressed as a matrix sum:

$$\underline{\underline{A}} = \underline{\underline{D}} - \underline{\underline{L}} - \underline{\underline{U}} \quad (5.1.3.1.1.4)$$

where  $\underline{\underline{D}}$ ,  $\underline{\underline{L}}$  and  $\underline{\underline{U}}$  are the diagonal, lower and upper triangular matrices. In matrix notation, the point Jacobi interactive method is expressed as:

$$\underline{\underline{x}}^{k+1} = \underline{\underline{B}} \underline{\underline{x}}^k + \underline{\underline{D}}^{-1} \underline{\underline{b}} \quad (5.1.3.1.1.4)$$

where  $\underline{\underline{B}}$  is the point Jacobi matrix:

$$\underline{\underline{B}} = \underline{\underline{D}}^{-1} (\underline{\underline{L}} + \underline{\underline{U}}) \quad (5.1.3.1.1.5)$$

and  $\underline{\underline{D}}^{-1}$  is the inverse of  $\underline{\underline{D}}$ . Even though the point Jacobi scheme is not used in the code NGCEFF, it plays an important role in the analysis of the other iterative techniques.

The SOR and DEM iterative methods in matrix notation are:

$$\underline{\underline{x}}^{k+1} = \underline{\underline{L}} \underline{\underline{x}}^k + (\underline{\underline{I}} - \underline{\underline{W}} \underline{\underline{D}}^{-1} \underline{\underline{L}}) \underline{\underline{D}}^{-1} \underline{\underline{W}} \underline{\underline{b}} \quad (5.1.3.1.1.6)$$

where  $\underline{\underline{L}}$  is the point successive relaxation matrix given by:

$$\underline{\underline{L}} = (\underline{\underline{I}} - \underline{\underline{W}} \underline{\underline{D}}^{-1} \underline{\underline{L}})^{-1} \{(\underline{\underline{I}} - \underline{\underline{W}}) \underline{\underline{I}} + \underline{\underline{W}} \underline{\underline{D}}^{-1} \underline{\underline{U}}\} \quad (5.1.3.1.1.7)$$

and  $\underline{\underline{W}}$  is either a diagonal matrix corresponding to the relaxation factors multiplied by the DEM factor or a scalar value equal to the relaxation factor multiplied by the DEM factor.

Convergence depends on whether or not the spectral radius,  $\rho(A)$ , is less than one. To each of the iterative methods described, an associated error vector  $\underline{\underline{\epsilon}}^k$ , defined by:

$$\underline{\underline{\epsilon}}^k = \underline{\underline{x}}^k - \underline{\underline{x}} \quad (5.1.3.1.1.8)$$

$$k \geq 0$$

where  $\underline{\underline{x}}$  is the solution vector, is formulated. Equation 5.1.3.1.1.8 can be rewritten as:

$$\underline{\underline{\epsilon}}^k = \underline{\underline{T}}^k \underline{\underline{\epsilon}}^0 \quad (5.1.3.1.1.9)$$

$$k \geq 0$$

where  $\underline{\underline{T}}$  is the matrix  $\underline{\underline{B}}$  or  $\underline{\underline{L}}$ . These iterative matrices tend to converge or, stated another way, given any:

$$\underline{\underline{\epsilon}}^0 > 0$$

then

$$\underline{\underline{\epsilon}}^k \rightarrow 0, \text{ if } \rho(M) < 1. \quad (5.1.3.1.1.10)$$

To calculate the spectral radius of the point successive relaxation matrix is difficult and can be avoided by applying



the following theorem.

Theorem: Let the Jacobi matrix be a non-negative  $n \times n$  matrix with zero diagonal entries, and let  $L$  be the Gauss-Seidel matrix, the special case  $\underline{W} = (W)_{ij} = 1$ . Then, one and only one of the following mutually exclusive relations is valid:

1.  $\rho(B) = \rho(L) = 0$
2.  $0 < \rho(L) < \rho(B) < 1$
3.  $1 = \rho(B) = \rho(L)$
4.  $1 < \rho(B) < \rho(L)$ . (5.1.3.1.1.11)

The above theorem, unfortunately, does not apply when matrix  $\underline{B}$  is not a non-negative matrix. Examples can be formulated where one iterative method is convergent while the other is divergent, when  $\underline{B}$  is not a non-negative matrix. However, if a matrix is not non-negative it can still be convergent if matrix  $\underline{A}$  is strictly or irreducibly diagonally dominant.

Besides requiring,  $\rho(A) < 1$ , a measure of the speed or rate of convergence is the condition number,  $K(A)$ , which is very important in the study of rounding error, also. In other words, when  $K(A)$  is large, small relative errors in  $A$  can lead to large errors in the solution.

Thus, two numbers, the spectral radius and the condition numbers, are computed by the Code NGCEFF and these will be reported in the next chapter.

## 5.2 The NGCEFF Code

The numerical determination of the gravitational collision shape factor  $\beta$  is accomplished by the NGCEFF code, which calculates both the nonspherical and its volume equivalent spherical gravitational collision efficiencies. Figure 5.2.1 is a flowchart of the code. The code first calculates the nonspherical collision efficiency,  $\epsilon_N$ , based on the Reynolds number of the oblate spheroid. The volume equivalent radius, based on the semi-major axis length of the oblate spheroid, is determined and a Reynolds number is guessed for a spherical particle. From the results of solving the Navier-Stokes equation, a comparison is made between the calculated size (radius), based on the guessed Reynolds number, and the actual volume equivalent radius for the sphere. A new Reynolds number is guessed if the size and actual radius disagree. When agreement is achieved, the spherical gravitational collision efficiency,  $\epsilon_S$ , is calculated and then the shape factor  $\beta$ . This procedure is done so as to insure uniformity, i.e., the same assumptions and algorithms are used to determine  $\epsilon_N$  and  $\epsilon_S$ .

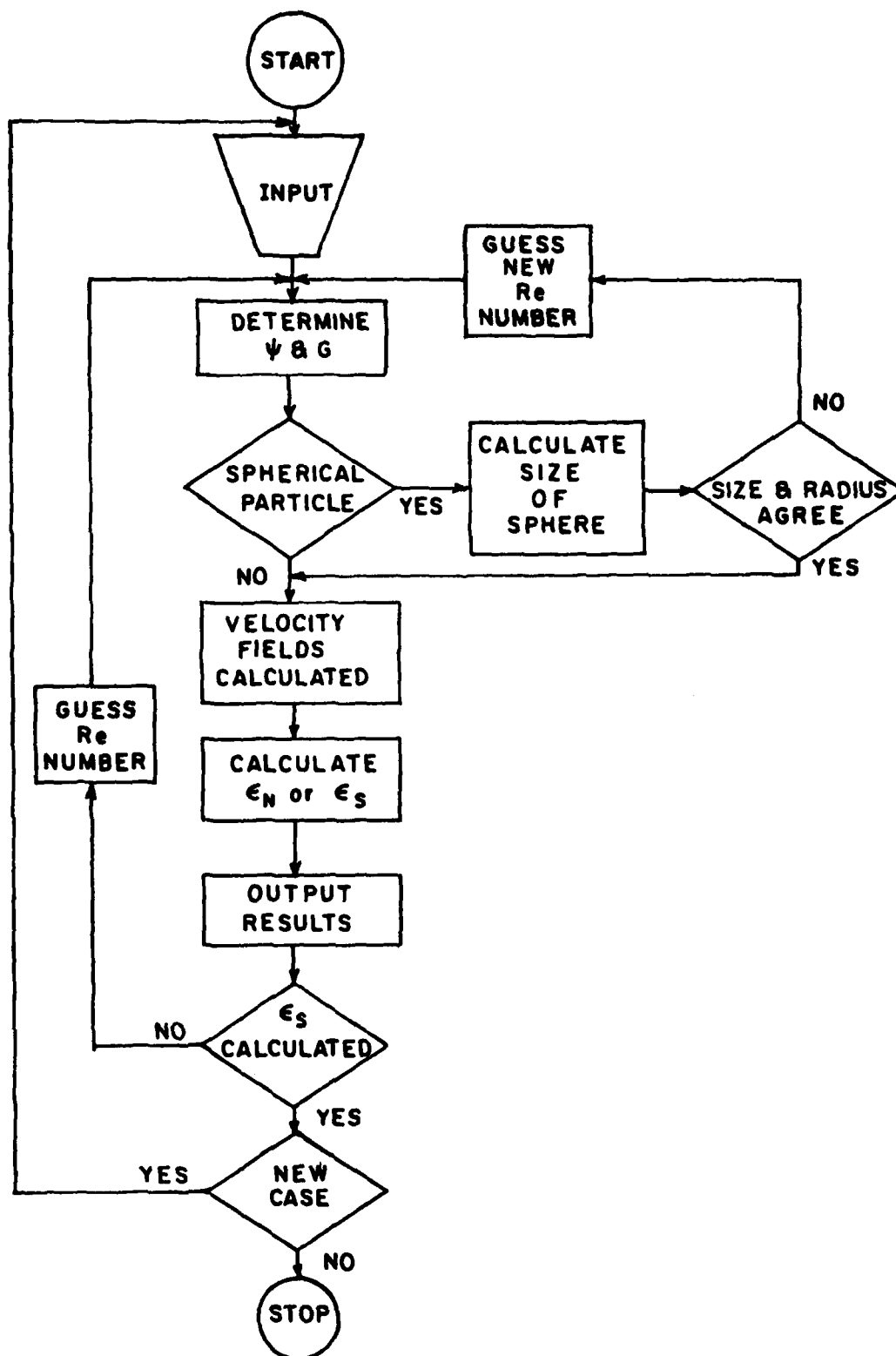


Figure 5.2.1 Flowchart of NGCEFF Program

The NGCEFF code is written in IBM double precision FORTRAN language. The main program controls the logic as depicted in Figure 5.2.1. The listing of the code is given in an appendix. Not listed are subroutines that are part of IMSL<sup>39</sup> and LINPACK<sup>45</sup> subprogram libraries.

Except for IMSL and LINPACK subroutines, this section describes the subroutines and function subprograms of the NGCEFF code.

### 5.2.1 Code Structure

Since numerical solutions to the Navier-Stokes equation requires large arrays, the code uses many common blocks and equivalence statements so that arrays can be used as working or multi-variable arrays. This is accomplished by storing intermediate results that are needed later, on direct access storage devices such as disks. Most of the output and input from disks is done using unformatted I/O statements, which are extremely fast data transfer statements since there is a one-to-one correspondence between internal storage locations (bytes) and external record positions.

Table 5.2.1.1 lists the common blocks and gives a description of the type of variables contained in it. Since many of the subroutines are common to both spheroid and spherical particles, a labeled common block SWITCH is placed in those subroutines and the values of the variables are

Table 5.2.1.1

<u>Name</u>	<u>Description</u>
Blank	Variables common to the entire program
AIR	Properties of the containment atmosphere
VER1	Quantities associated with volume equivalent spheres
AERSL1	Quantities associated with the oblate spheroids
AERSL2	Quantities associated with the smaller aerosols
SWITCH	Variables which depend on the type particle
NAVIER	Parameters needed by subroutine OBLATE
OBLAT\$	Stream function and modified vorticity arrays
WORK	Work arrays and vectors

Name and Description of Labeled Commons in NGCEFF

changed for the type of particle being considered. Labeled common blocks OBLAT\$ and WORK are used to store subscripted variables. With the exception of SWITCH, OBLAT\$ and WORK, the values of the variables in the remaining common blocks do not change once determined for a specific case.

#### 5.2.1.1 Main Program

The MAIN program reads in the values of variables needed to run the code and controls its operation. Before terminating the code, MAIN checks to determine if another case needs to be evaluated. Table 5.2.1.1.1 lists the input variables. Variable GOTO allows the user to consider very similar cases without having to redefine all the input variables. The MAIN program calls subroutine INITAL, OBLATE, SIZE, control parameters. The first, I, identifies the type of large particle being considered and how much information is known about that particle. The second parameter, J, is used to indicate that only the variables associated with the similar particle have been changed. This allows certain subroutines to be skipped. The final parameter, JSTART, is used to generate the initial guess for the stream function and vorticity fields, and then is used to check that the radius, drag coefficient, and Reynolds number all agree for the volume equivalent particle.

Table 5.2.1.1.1

## Input Variables to NGCEFF Program

```

00010 C*****
00020 C
00030 C
00040 C INPUT:  PARAMETER CARD(COLUMNS) FORMAT USAGE
00050 C          MU          1  (1-10 ) G10.0  AIR VISCOSITY
00060 C          RHO        1  (11-20 ) G10.0  AIR DENSITY
00070 C          LAMBDA     1  (21-30 ) G10.0  MEAN FREE PATH OF AIR
00080 C          EPS        1  (31-40 ) G10.0  ERROR CRITERIA FOR ALL
00090 C*****
00100 C          REYN1       2  (1-10 ) G10.0  REYNOLDS NUMBER FOR OBLATE
00110 C          AR1        2  (1-10 ) G10.0  AXIS RATIO OF OBLATE
00120 C          DENS1      2  (11-20 ) G10.0  BULK DENSITY OF OBLATE
00130 C          ALPHA1    2  (21-30 ) G10.0  DENSITY CORRECTION FACTOR
00140 C          DISK       2  (31-40 ) G10.0  SELECT OPTION NEEDED...
00150 C                                     0.0-GENERATE PSI AND G FIELDS
00160 C                                     1.0-READ FIELDS FROM DISK,
00170 C                                     UNIT NUMBER IS FT09F001
00180 C*****
00190 C          DZETA       3  (1-10 ) G10.0  RADIAL STEP SIZE, SPHEROIDAL
00200 C          MP1        3  (11-15 ) I5    NUMBER OF ANGULAR STEPS
00210 C          N         3  (16-20 ) I5    NUMBER OF RADIAL STEPS
00220 C          MATRX     3  (21-25 ) I5    SELECT OPTION NEEDED...
00230 C                                     0-NO MATRIX ANALYSIS
00240 C                                     1-MATRIX ANALYSIS:
00250 C                                     SPECTRAL RADIUS,EIGENVALUES
00260 C                                     AND RECIPROCAL CONDITION
00270 C                                     NUMBER CALCULATED
00280 C          IOUT      3  (26-30 ) I5    SELECT OPTION NEEDED...
00290 C                                     1-OUTPUT RESULTS
00300 C                                     FT08F001 MUST BE DEFINED
00310 C                                     FT09F001 MUST BE DEFINED
00320 C                                     FT10F001 MUST BE DEFINED
00330 C                                     ABOVE DATA SETS USE
00340 C                                     UNFORMATED WRITE & READ
00350 C                                     STATEMENTS
00360 C                                     0-NO OUTPUT NEEDED
00370 C*****
00380 C          R2V         4  (1-10 ) G10.0  VOLUME EQUIVALENT RADIUS OF
00390 C                                     SMALLER PARTICLE.
00400 C          DENS2       4  (11-20 ) G10.0  BULK DENSITY OF SMALLER
00410 C          ALPHA2     4  (21-30 ) G10.0  DENSITY CORRECTION FACTOR OF
00420 C*****
00430 C          GOTO        5  (1-10 ) G10.0  SELECT OPTION...
00440 C                                     1.0-NEW CARDS 1-4 NEEDED.
00450 C                                     2.0-NEW CARDS 2-4 NEEDED.
00460 C                                     3.0-NEW CARDS 3&4 NEEDED
00470 C                                     4.0-ONLY CARD 4 CHANGED
00480 C                                     99.0-STOP CODE.
00490 C
00500 C
00510 C*****

```

### 5.2.1.2 Subroutine INITAL

The subroutine INITAL initializes the parameters necessary to carry out calculations by the subroutine COLL. Not all parameters are determined the first time the subroutine is called, since not all the information is known and therefore subroutine INITAL is called several times as more information is determined. The following is a list of the parameters and their definitions:

GV	- Gravitational constant
PI	- The mathematic constant $\pi$
CLL	- Collision parameter
ERR	- Error criterion for bisection method in COLL
CDTOTL	- Drag coefficient OBLATE
NEQTN	- Number of equations, IMSL subroutine DVOGER
MAXDER	- Maximum order, IMSL subroutine DVOGER
HD	- Initial time step size, IMSL subroutine DVOGER
HDMIN	- Minimum time step size, IMSL subroutine DVOGER
HDMAX	- Maximum time step size, IMSL subroutine DVOGER
MTH	- Integration method, IMSL subroutine DVOGER
GAMMA	- Ratio of smaller particle density to larger particle density
BRHO	- Ratio of particle buoyancy effects
IAR1	- Ratio of inertia effects for oblate spheroid particle



IR1V - Ratio of inertia effects for volume equivalent particle

VINF2 - Stokes terminal velocity for smaller particle

REYN2 - Reynolds number of smaller particle

CDAR1 - Drag coefficient for smaller particle

SEMI - Semi-major axis length for oblate spheroid

R1V - Radius of volume equivalent particle

UNIF - Stokes terminal velocity of larger particle

VINF1 - Actual terminal velocity of oblate spheroid

R - Ratio of volume equivalent radii

STK1 - Stokes number based on oblate spheroid

LYK1 - Interaction number based on oblate spheroid

CDV1 - Drag coefficient of volume equivalent particle

REYNV1 - Reynolds number of volume equivalent particle

VINFV1 - Actual terminal velocity of volume equivalent particle

STKV1 - Stokes number based on volume equivalent particle

LYKV1 - Interaction number based on volume equivalent particle.

#### 5.2.1.3 Subroutine OBLATE

As the name implies, this subprogram solves the Navier-Stokes equation for flow around an oblate spheroid. Since an axis ratio of 0.999 has been shown to approximate a

sphere<sup>27</sup>, this subroutine also gives the solution for spheres. The equations used to find the stream function and modified vorticity fields are given in Section 5.1.3.

To start the iteration scheme, which has been described in the previous chapter, an initial guess is made for the stream function (PSI) and the modified vorticity (G) fields. Two options are available. If no previous solutions are available, then DISK should equal 0 so that subroutine START is called to generate an initial guess by using Oberbeck's solution. If DISK does not equal zero, the subroutine OBLATE assumes that starting (initial guess) values are on a random access device with a file name FT09F001. When convergence is achieved, control is returned to the MAIN program with JSTART equal to 2. Key parameters returned are PSI, G, and the total drag coefficients, CDTOTL.

The pressure drag coefficient  $C_p$  is determined from the relation:

$$C_p = 2 \int_0^{\pi} k \sin \eta \cos \eta \, d\eta \quad (5.2.1.3.1)$$

and the friction drag coefficient  $C_f$  is determined by

$$C_f = \frac{8}{Re} \tanh \xi_0 \int_0^{\pi} G_0 \sin \eta \, d\eta \quad (5.2.1.3.2)$$

where the total drag coefficient CDTOTL is just the sum of the pressure drag and friction drag coefficients. The terms in Equations 5.2.1.3.1 and 5.2.1.3.2 are

$k \sim$  Nondimensional pressure unit

$$= 1 + \frac{8}{Re} \int_{\xi_0}^{\xi_b} \left. \frac{\partial \omega}{\partial \eta} \right|_{\eta=0} d\xi + \frac{4}{Re} \int_0^{\eta} \left[ \frac{\partial \omega}{\partial \xi} + \omega \tanh \xi \right]_{\xi=\xi_0} d\eta \quad (5.2.1.3.3)$$

$G_0 \sim$  Modified vorticity at surface oblate spheroid,  
i.e.,  $\xi = \xi_0$

$\omega \sim$  Vorticity

$Re \sim$  Reynolds number

$\xi_b \sim$  Value of  $\xi$  at the outer envelope.

Equation 5.2.1.3.3 was evaluated by the trapezoidal rule, since higher order integration methods were unstable.

The iteration scheme in subroutine OBLATE for finding the stream and vorticity fields was not as stable as was hoped. It is very sensitive to the relaxation parameters and the initial guess. Thus if the Reynolds number is not approximately equal to 0, the use of subroutine START is not recommended.

#### 5.2.1.4 Subroutine SIZE

This subroutine is used only to determine the correct Reynolds number for the volume equivalent particle. Once the semi-major axis of the spheroid is determined, the volume equivalent radius is known but not the Reynolds number. As an initial guess, Stokes law can be used and then subroutine OBLATE is called. The results of OBLATE allow the radius of a sphere corresponding to the guessed Reynolds number to be calculated. Comparison of this radius with the volume equivalent radius allows the program to adjust the Reynolds number. Subroutine OBLATE is then called again. After three guesses, subroutine SIZE uses ISML subroutines ICSICU and ICSEVU to interpolate the next Reynolds number. This procedure is continued until the absolute difference between the calculated radius and the volume equivalent radius is less than EPS. When this occurs, control JSTART is set equal to four and the two arrays PSI and G are placed on a random access device using file name FT09F001. This is done so that, if the user wants to consider similar cases, the initial guess can be closer to the actual answer than the analytically generated guess.

#### 5.2.1.5 Subroutine VELCTY

Given the discrete values of the stream function in spheroidal coordinates, this subroutine will calculate the

velocity fields in cylindrical coordinates by using Stokes relationships and the transformation expressions listed in Chapter 4. Results are stored on a random access device using file name FT10F001.

#### 5.2.1.6 Subroutine COLL

The COLL subroutine utilizes the results from INITIAL and VELCTY and integrates the six nondimensional equations of aerosol motion (Equations 4.4.1.34 - 4.4.1.39) to determine  $\epsilon_S$  and  $\epsilon_N$ . The velocity fields, which are necessary for estimating drag forces, are read in from a random access device using file name FT10F001. The older IMSL routine DVOGER is the integrator because it offers some advantages over the newer integrator routine DGEAR.

The initial conditions, Equations 5.1.1.7 - 5.1.1.11, are computed and control parameters are initialized. DVOGER is repeatedly called to determine the particles' trajectory for an initial horizontal separation. Integration is continued until a hit or miss occurs between the larger particle and the smaller particle. COLL determines the angle of separation and distance of separation (Equations 4.2.2.10 - 4.2.2.13) for each initial horizontal separation. Whenever a grazing collision occurs, i.e., distance of separation is less than  $10^{-6}$ , the horizontal separation distance is saved.

As indicated in Chapter III, after the maximum critical grazing trajectory is found, it is still necessary to determine the inner critical trajectory offset. Once this is accomplished, the gravitational collision efficiency can be computed.

The search strategy is to start with:

$$\rho)_0 = (a^* + r_{2,v}^*)/r_{1,v}^* \quad (\text{OBLATE}) \quad (5.2.1.6.1)$$

$$\rho)_0 = (r_{1,v}^* + r_{2,v}^*)/r_{1,v}^* \quad (\text{Volume Equivalent Sphere}) \quad (5.2.1.6.2)$$

where  $\rho)_0$  is the nondimensional initial horizontal offset,  $a$  is the semi-major axis length,  $r_{1,v}$  is the large sphere volume equivalent radius, and  $r_{2,v}$  is the volume equivalent radius of the smaller sphere. To continue searching, the new horizontal offset,  $\rho)_0^k$ , is:

$$\rho)_0^k = \rho)_0 \left(1 - \frac{k}{10}\right) \quad (5.2.1.6.3)$$

$$k = 1, 2, \dots, 10$$

until a hit occurs. Once this happens the bisection technique is used to determine the bisection horizontal offset,  $\rho)_b$ , which is:

$$\rho)_b = [\rho)_0^{k+1} + \rho)_0^k]/2 \quad (5.2.1.6.4)$$

The search strategy for the minimum horizontal offset is the same as for the maximum horizontal offset.

The advantages of the DVOGER routine is that it will adjust the time step size internally to meet error criteria and to achieve finer numerical detail of the particle trajectory calculations. In addition, DVOGER has the capability to repeat the last step of integration if for some reason too large of a time step was taken which caused the larger particle to pass through the smaller particle (physically not realistic). When these problems occur, new maximum and minimum step sizes can be given to DVOGER in order to complete the integration. These features are not available in DGEAR.

#### 5.2.1.7 Subroutine OUTPUT

The OUTPUT subroutine summarizes all the input data and the key intermediate and final results. It is called three times by the MAIN program. The routine first prints the values of the input parameters associated with control of the code and those quantities for containment conditions. Later OUTPUT is called to give the nonspherical gravitational collision efficiency  $\epsilon_N$  and particle quantities used to calculate the efficiency. The last time OUTPUT is called results in giving spherical gravitational collision efficiency  $\epsilon_S$  and the collision shape factor  $\beta$ .

### 5.2.1.8 Subroutine IDERIV

Subroutine IDERIV is called twice by subroutine VELCTY to calculate the derivatives of the stream function field (PSI). IDERIV uses the cubic spline coefficients determined by IMSL routine ICSICU. The two derivatives determined by IDERIV are those in Equation 4.3.7 and 4.3.8. Basically IDERIV is the IMSL routine ICSEVU except the derivative of a cubic spline is calculated instead of the IMSL library notebook, the value of the derivative of the spline approximately at the points  $U_i$  is:

$$S'_i = (3C_{j,3}D + 2C_{j,2})D + C_{j,1} \quad (5.2.1.8.1)$$

where:

$S'_i$  ~ Derivatives at the points  $U_i$ ,  $i=1,2,\dots, m$

$C_{j,k}$  ~ Spline coefficients,  $k=1,2,3$ ;  $j=1,2,\dots, nx-1$

$nx$  ~ Number of function values of data point

$m$  ~ Number of interpolating points

and  $D = U_i - X_j$  where the interval is determined by:

$$X_j \leq U_i < X_{j+1}$$

where  $X_j$  are the abscissae data points. If the derivatives are needed only at the original data points, then  $D = 0$  and

$$S'_i = C_{j,1}.$$



#### 5.2.1.9 Subroutine DEFINE

This subroutine loads the proper values into the common block called SWITCH. This allows subroutines like OBLATE, VELCTY and COLL to be used by either the oblate spheroidal particle or its volume equivalent spherical particle. Parameters associated with the oblate spheroid are in common block AERSL1 and those associated with the volume equivalent sphere are in common block VER1. Subroutine DEFINE uses the MAIN control parameter I to correctly load SWITCH.

#### 5.2.1.10 Subroutine DFUN

The subroutine DVOGER requires a user supplied subroutine which contains the differential equations to be integrated. Thus DFUN contains the six nondimensional equations of aerosol particle motion, Equations 4.4.1.34 - 4.4.1.39.

The drag force terms used in the equation are calculated in separate subroutines. Since the explicit drag force terms are not given in DFUN, but are calculated elsewhere, this subroutine is very general and allows modification of the drag force terms in the separate subroutines without affecting DFUN.

The DVOGER subroutine allows the user to provide a separate subroutine to calculate the Jacobian of the equations of motion. This occurs when MTH is equal to 1. Since analytical

expressions are not available for the drag force terms, the Jacobian has to be calculated numerically. This is automatically done by the subroutine DVOGER if MTH is equal to 2. The array associated with the Jacobian is PW(6,6) and can be used as a working array.

Drag forces are called by subroutine FORSUP, which utilizes function subprograms WRHOL, WZ1, WRH02, and WZ2.

#### 5.2.1.11 Subroutine FORSUP

This subroutine is called by subroutine DFUN to calculate the drag forces. Drag forces are determined by using Equations 1.4.2.1 and 4.4.2.2, which is based on the differences between the nondimensional particle velocities  $V_{\rho 1}$ ,  $V_{\rho 2}$ ,  $V_{z1}$ ,  $V_{z2}$ , and the generated nondimensional velocity fields  $W_{\rho 1}$ ,  $W_{\rho 2}$ ,  $W_{z1}$ ,  $W_{z2}$ , which are determined by function subprograms WRH01, WZ1, WRH02, WZ2.

#### 5.2.1.12 Function Subprograms WRH01, WRH02, WZ1, WZ2

These subprograms determine the velocity around the particle at the point in space where the other particle is. The subprograms WRH01 and WZ1 use the results from VELCTY and the interpolating Equations 5.1.2.2.16 and 5.1.2.2.17 to determine  $W_{z1}$  and  $W_{\rho 1}$ , respectively. The weighing factors are determined by the formulas in the same section.

The subprogram WRH02 and WZ2 use Equations 4.4.2.3 and 4.4.2.4 to calculate  $W_{z2}$  and  $W_{\rho 2}$ , respectively.

#### 5.2.1.13 Function Subprograms STREAM and VORTCY

These subprograms are called by subroutine START to calculate the stream function and vorticity fields around oblate spheroids and spheres. Oberbeck's and Stokes solutions are imbedded in them.

## CHAPTER VI

### RESULTS AND DISCUSSIONS

#### 6.0 Introduction

This chapter utilizes the theory developed in Chapter IV and the numerical methods described in Chapter V to calculate values of the gravitational collision efficiency for spherical and nonspherical particles and the collision shape factor  $\beta$ .

The aerosol sizes and densities were determined by reviewing the theoretical analysis of the characteristics of typical LMFBR particles and agglomerates. No attempt was made to model the collisions between raindrops and ice particles per se, a subject of great interest in atmospheric science. Fluid parameters were selected based on predicted HCDA post-accident conditions inside the LMFBR containment.

Some important results presented in this chapter are (1) the instability of the numerical method used to solve the vorticity transport equation and how to deal with this problem, (2) the effect caused by incorrectly determining the separation distance between the spherical and nonspherical particles before collision occurs, and (3) the results of the program NGCEFF, i.e.,  $\epsilon_S$ ,  $\epsilon_N$ ,  $\beta$  and other key quantities are reported.

## 6.1 Some Important Numerical Methods Results

### 6.1.1 Solution to the Navier-Stokes Equation

Recalling Equations 4.3.1 and 4.3.2 and the numerical techniques discussed in Section 5.1.3, solutions to the Navier-Stokes equations were sought, starting with  $Re = 0$  and then increasing it to  $Re = 5$ .

Convergence was fairly rapid when Oberbeck's solution was used as the trial solution and the  $Re = 0$ . This occurs because the vorticity transport equation is reduced to:

$$E^2 G = 0 \quad (6.1.1.1)$$

and therefore the Jacobian operator does not need to be computed. The stream function field converged fairly rapidly (less than 200 iterations), but the vorticity field was more difficult to relax. Relaxation factors in Equation 5.1.3.1.11 were multiplied by 0.001 initially to prevent divergence. Once a stable, non-oscillating field was achieved, the relaxation scaling factor could be increased until it was greater than 0.7.

Although a converged solution was achieved for Oberbeck's solution, the use of this solution for Reynolds numbers greater than zero proved to be impossible. Convergence was more dependent on trying different combinations of scaling factors and  $DEM^{43}$  factors than on the internal logic of

the numerical method. It was decided that further investigations were necessary than reported by other investigators<sup>26,42</sup>.

Before proceeding it is worthwhile to discuss the motivation behind this investigation. In calculating the gravitational collision efficiency the subroutine OBLATE is used to calculate the drag coefficients for both the nonspherical particle and the volume equivalent sphere. Furthermore, the determination of the size of these two particles required an inner and outer iteration scheme. The outer iteration scheme was between the subroutines SIZE and OBLATE to adjust the Reynolds number, which is not known a priori, to the drag coefficient from the solution of the Navier-Stokes equation. When these two quantities are known, the volume equivalent radius of the oblate spheroid can be compared with the one determined from Equation 5.1.1.1.5 and

$$r_{1,v} = \{3\mu^2 C_D Re_{v,1}^2 AR(\rho_1 - \rho) \rho g/32\}^{1/3}. \quad (6.1.1.2)$$

The Reynolds number must be changed until the three quantities ( $Re_{v,1}$ ,  $C_D$ ,  $r_{1,v}$ ) give consistent solutions. The inner iteration procedure is the Navier-Stokes numerical scheme, which typically required between 1500-2000 iterations under the best conditions before convergence was achieved. Thus a numerical method had to be chosen which could be predicted to give convergence without user intervention.

An investigation of the problem proceeded as follows. A review of the stream function and vorticity field lattice values was done for the cases where the stream function  $\psi$  was held constant and vorticity  $\omega$  allowed to vary until convergence or divergence occurred. This procedure was repeated for different values of Reynolds numbers. A similar technique was used for the stream function field, holding the vorticity field constant. Actual convergence was possible when the vorticity field was held constant; however, allowing the vorticity field to change after the stream function field had converged caused divergence, resulting in overflow problems almost immediately if the size of the Reynolds number exceeded 0.001.

At this point the spectral radius and condition number of the vorticity transport matrix was determined for a 20 x 20 matrix ( $n = 6$ ,  $m = 7$ , see Equation 5.1.3.1.1.3). Results are given below:

Re	$\rho(\omega)$	$K(\omega)$	$\rho(\psi)$	$K(\psi)$
0.5	1431	$4 \times 10^{-7}$	4.199	$1.2 \times 10^{-1}$
0.0001	4.48	$1.2 \times 10^{-1}$	4.199	$1.2 \times 10^{-1}$

where the AR = 0.999 and  $\Delta\xi = 1.6$ . The problem of convergence is immediately obvious for Reynolds number greater than 0.001.

Since these matrices do not have spectral radii less than one (see Chapter V) any oscillates in the numerical technique applied will cause problems.

A close review of the voriticity field indicated that the oscillations started near the boundary of the oblate spheroid. The boundary condition at the surface of the spheroid is,

$$\omega = G/\sin\eta, \quad \xi = \xi_0 \quad (6.1.1.3)$$

which is evaluated by means of Equation 4.3.1, and when written in finite difference form becomes

$$G_{i,1} = \frac{\cosh^2 \xi_0}{\sinh^2 \xi_0 + \cos^2 \eta} \frac{\partial^2 \psi}{\partial \xi^2}, \quad \xi = \xi_0. \quad (6.1.1.4)$$

It is the representation of  $\partial^2 \psi / \partial \xi^2$  on the surface of the spheroid which causes oscillations of the vorticity field, which if not controlled by methods used by Woo<sup>42</sup> and Pitter et al.<sup>26</sup>, will lead to divergence. Pitter et al. used the following one-sided finite-difference equation,

$$\frac{\partial^2 \psi_{i,1}}{\partial \xi^2} = \frac{8 \psi_{i,2} - \psi_{i,3}}{2(\Delta \xi)^2}, \quad O(h) \quad (6.1.1.5)$$

which when replaced by the expression;



$$\frac{\partial^2 \psi_{i,1}}{\partial \xi^2} = \frac{-2 \psi_{i,2} + \psi_{i,3}}{(\Delta \xi)^2}, O(h) \quad (6.1.1.6)$$

did not cause oscillates near the boundary. Higher order forward representations were derived by replacing successively more terms in the Taylor series expansions and making use of the fact that  $\psi_{i,1} = 0$  on the boundary. These representations caused more problems by introducing higher order harmonics which could not be damped out by the scaling factors. Thus, Equation 6.1.1.6 is the expression used in NGCEFF.

#### 6.1.2 Solution to the Dynamic Equations of Motion and Critical Grazing Path

The use of Gear's<sup>38</sup> method to solve the six equations of particle motion, Equations 4.4.1.34 - 4.4.1.39, was satisfactory. Remembering that the equations are integrated for the purpose of determining if a direct, grazing, or missed collision occurs, it is necessary to start the integration routine when the particles are at a distance of at least 50 radii from each other. When this was done, it took approximately 200 steps to integrate these equations to get the separation angle and particle-particle separation distance (see Figure 5.1.1.3). Normally fifteen to twenty initial horizontal offset values were needed before the

grazing path was determined from the cubic spline curve fitting technique described in Section 5.1.1.1.2.

One key requirement in solving these six equations of motion is calculation of the forces acting on the particles. Interpolation of the velocity fields must be done correctly or else the forces will be incorrectly applied by the superposition principle. Pitter *et al.*<sup>26</sup> incorrectly programmed Equations 5.1.2.2.1 - 5.1.2.2.2 letting  $c$ , the characteristic length in the spheroid coordinate system, be equal to  $\cosh \xi_0$ , where  $\xi_0$  is the surface of the oblate spheroid. This problem was first determined when his collision trajectory consistently ended up inside the oblate spheroid. Time did not permit modification of his program to check his reported observation of an annular collision domain, but it is suspected that this programming error contributed to his findings.

## 6.2 Verification of NGCEFF Routines

It was important to verify the various routines in the NGCEFF code. Each major subroutine was subjected to extensive testing before merging it with NGCEFF. For example, the subroutines VORTCY and STREAM were developed to generate the vorticity field and stream function values for Oberbeck's solution ( $Re = 0$ ). Verification of these two subroutines was checked by comparing the generated fields with those

from solving the Navier-Stokes equation with the Reynolds number equal to zero. This procedure also verified the output from subroutine OBLATE since the initial fields used by OBLATE were not converged fields.

Subroutine VELCTY was checked by taking the output from OBLATE and STREAM and letting the subroutine VELCTY operate on it to create the velocity fields in oblate spheroidal coordinate system. These results were then compared to the analytical solution available from Oberbeck's solution for Reynolds number equal to zero. This procedure in essence also verified the correctness of the subroutines OBLATE and STREAM.

Subroutine SIZE and OBLATE were merged together to check on the calculated pressure and skin drag coefficient needed for the six equations of motion. The size and terminal velocity of an oblate spheroid is fixed only after the drag coefficients from subroutine OBLATE are numerically calculated. From Pitter et al.<sup>26,35</sup>, Table 6.2.1 shows the comparison between results reported by them to the present research.

Finally, to check the logic of NGCEFF and the integration subroutine COLL, the code was programmed to determine the spherical and nonspherical gravitational collision efficiencies for oblate spheroids with an axis ratio equal to 0.999. If correctly written, the results of efficiency

Table 6.2.1

Comparison of Calculated Drag Force Coefficients, Size, and Terminal Velocities for Oblate Spheroids (Axis Ratio = 0.05) as a Function of the Reynolds Number\*

Re	$C_D$	Semi-Major Axis ( $\mu\text{m}$ )	Terminal Velocity (cm/sec)
0.1	210.1 (207.1)	48.9 (50.6)	1.79 (1.78)
0.5	44.1 (43.5)	86.5 (87.9)	5.14 (5.12)
1.0	23.3 (23.0)	110.1 (113.0)	8.07 (7.97)
2.0	12.9 (12.7)	146.0 (147.0)	12.8 (12.3)
4.0	7.29 (7.28)	193.7 (194.0)	18.9 (18.6)

\*Present Results (Pitter et al.<sup>26,35</sup>)

calculations should be the same and therefore the collision shape factor,  $\beta$ , equal to one. These results also afford a chance to compare their values with those published by Pertmer and Loyalka<sup>18</sup>. For the NGCEFF code operation, the containment atmospheric conditions were taken to be:

$$\rho_f = 1.29 \times 10^{-3} \text{ gm/cm}^3$$

$$\mu_f = 2.0 \times 10^{-4} \text{ gm/cm-sec}$$

corresponding to a temperature of 120°F and pressure of 0 psig for air. The first time the code was run the following system parameter held true:  $AR = 0.999$ ,  $Re_1 = 0.49984$ ,  $CD_1 = 52.261$ , semi-major axis length = 0.002574 cm,  $\rho_1 = 2.27$ ,  $V_{\infty a} = 15.05 \text{ cm/sec}$ ,  $v_{1,m} = 0.002574 \text{ cm}$ . The values of the small particle were:  $r_{2,v} = 0.001 \text{ cm}$ ,  $\rho_2 = 2.27$ ,  $Re_2 = 0.0319$ ,  $V_{\infty v,2} = 2.472 \text{ cm/sec}$ . System parameters were:  $Stk = 2.044$ ,  $L = 2.277$ ,  $I = 1.0$ ,  $\gamma = 1.0$ ,  $\beta = 1.0$ ,  $V_{\infty 1} = 16.38 \text{ cm/sec}$ . Results of NGCEFF were:

	<u>Volume Basis</u>	<u>Mass Basis</u>
$\epsilon_N$	0.7102	0.7102
$\epsilon_S$	0.7099	0.7099

$$\beta = 1.000 \text{ (mass ratio} < 0.059 \text{)}$$

The mass ratio is important to check since values greater than 0.34 will tend to tilt the oblate spheroid. In the present case it is not important since the larger particle is basically a sphere. The definitions and relationships for the parameters listed above are found in Chapters IV and V. It is noted that in general the terminal velocity of the oblate spheroid,  $V_{\infty a}$ , is not equal to the terminal velocity of its volume equivalent sphere,  $V_{\infty v,1}$ , except when  $AR = 0.999$ . Also,  $V_{\infty v,1}$  is not equal to the Stokes terminal velocity,  $V_{\infty 1}$ , based on the oblate spheroid's volume equivalent radius, because the former is calculated using the drag coefficient from the Navier-Stokes equation whereas the latter makes use of Stokes terminal velocity expression ( $Re = 0$ ).

For a similar case as given above but for a different small aerosol particle with a  $r_{2,v} = 0.0015$  cm, the following values were computed by NGCEFF:  $Re_2 = 0.1076$ ,  $V_{\infty v,2} = 5.562$ ,  $Stk = 10.35$ ,  $L = 0.1153$ ,  $I = 1.0$ ,  $\gamma = 1.0$ ,  $\beta = 1.0$ ,  $V_{\infty 1} = 16.38$  cm/sec,

	<u>Volume Basis</u>	<u>Mass Basis</u>
$\epsilon_N$	0.7866	0.7866
$\epsilon_S$	0.7864	0.7864

$\beta = 1.000$  (mass ratio < 0.98).

A third case was run for an oblate spheroid with a semi-major axis length equal to 0.0038 cm. The following values applied:  $AR = 0.999$ ,  $Re_1 = 1.5$ ,  $\rho_1 = 2.27$  g/cc,  $C_{D1} = 19.37$ ,  $V_a^\infty = 30.2$  cm/sec,  $r_{1,m} = 0.003848$  cm,  $r_{2,v} = 0.001$ ,  $\rho_2 = 2.27$  g/cc,  $Re_2 = 0.03189$ ,  $V_2^\infty = 2.47$  cm/sec,  $Stk = 1.106$ ,  $L = 0.004566$ ,  $I = 1.0$ ,  $\gamma = 1.0$ ,  $\beta = 1.0$ ,  $V_1^\infty = 36.58$  cm/sec. The results were

	<u>Volume Basis</u>	<u>Mass Basis</u>
$\epsilon_N$	0.80787	0.80787
$\epsilon_S$	0.80755	0.80755

$\beta = 1.000$  (mass ratio < 0.0176).

Table 6.2.2 summarizes these results and compares them with those reported by Pertmer<sup>12</sup>. Additional cases were available for large particle radius 38.5  $\mu$ m but are not shown since Pertmer's results for particles with radii greater than 30  $\mu$ m are based on densities less than 2.27 g/cc. GCEFF made use of Figure 2.1.2.1 for establishing densities of colliding particles.

### 6.3 Results from the NGCEFF Code - $\beta$ Factors

Collision efficiencies were computed for oblate spheroids of axis ratio 0.05 and Reynolds number 2.5 and spherical particles from 12.9 to 20.2  $\mu$ m in radius. Flow

Table 6.2.2

Comparison of Calculated Gravitational Collision  
Efficiencies for Oblate Spheroids (Axis Ratio = 0.999)  
for Several Cases\*

Radii ( $\mu\text{m}$ )		Ratio ( $r_{2,v}/r_{1,v}$ )	Efficiency	Results
<u><math>r_{1,v}</math></u>	<u><math>r_{2,v}</math></u>		<u>Present</u>	<u>Pertmer<sup>12</sup></u>
25.7				
	10	0.39	0.71	0.66
	15	0.58	0.79	0.73
38.5				
	10	0.26	0.81	0.89**

\*From Table 6.3.1.1, Reference 12.

\*\*Extrapolated Value.



fields around the oblate spheroid and its volume equivalent sphere were taken from previous computations discussed earlier.

In order to compute the collision efficiencies it was necessary to determine the size and terminal velocity of the oblate spheroid. Size and terminal velocity were computed using Equations 5.1.1.1.5 and 6.1.1.2. Excellent agreement was found between the terminal velocities calculated from the present results and the results reported by Pitter *et al.*<sup>26</sup>.

Table 6.3.1 and 6.3.2 lists all the important values and quantities for the case being considered. Asterisks denote input values. The remaining values are determined by NGCEFF. Additionally, the number of radial and angular steps were 49 and 31, respectively, with a radial increment size of 0.1. A collision was scored if the separation distance was less than  $10^{-5}$  cm.

Table 6.3.3 lists the collision efficiencies based on geometric sweepout, i.e.,

$$\epsilon_g = \left( \frac{\Sigma \rho_c}{a + r_{2,v}} \right)^2 \quad (6.3.1)$$

where  $a$  equals semi-major axis length and the remaining terms are defined by Equation 5.1.1.1.12. These were calculated for comparison purposes with those reported by

Table 6.3.1

Oblate Spheroid Values and System Parameters For  
Collision Results

Oblate Spheroid

0.0116	Semi-Major Axis Length (cm)
0.05*	Axis Ratio
2.5*	Reynolds Number
1.0*	Density (g/cc)
0.92*	Density Correction Factor
10.8	Drag Coefficient
19.4	Terminal Velocity (cm/sec)
0.00426	Volume Equivalent Radius (cm)
0.894	Equivalent Reynolds Number
31.03	Equivalent Drag Coefficient
18.9	Equivalent Terminal Velocity (cm/sec)
0.00414	Mass Equivalent Radius (cm)

Collision Parameters

0.847	Stokes Number (Stk)
0.00993	Interaction Number (L)
1.00	Inertia Number (I)
1.09	Ratio of Particle Densities ( $\gamma$ )
1.00	Ratio of Particle Buoyancy Effect ( $\beta$ )
21.8	Stokes Terminal Velocity of Volume Equivalent Sphere

Fluid Parameters

980.6*	Gravitational Constant (cm/sec <sup>2</sup> )
$1.713 \times 10^{-4}$ *	Fluid Viscosity (gm/cm x sec)
$6.500 \times 10^{-6}$ *	Mean Free Path ( $\lambda$ ) of Fluid (cm)
$1.007 \times 10^{-3}$ *	Density of Fluid (g/cc)

DVOGER Initial Values

$1.0 \times 10^{-7}$ *	Initial Time Step (sec)
$1.0 \times 10^{-3}$ *	Maximum Time Step (sec)
$1.0 \times 10^{-12}$ *	Minimum Time Step (sec)

\*Input Values to NGCEFF

Table 6.3.2  
Small Particle Values and Parameters for Collision Results  
( $\rho_2^* = 1.0$ ,  $\rho_2^* = 1.0$ )

$r_{2,v}(\mu m)^*$	Small Particle Values		Particle Parameters		Mass Ratio
	Re	$V_{\infty V,2}(\text{cm/sec})$	Stk	L	
12.9	0.0312	2.17	0.331	0.00981	0.03
13.0	0.0319	2.21	0.342	0.0101	0.03
13.1	0.0326	2.24	0.352	0.0104	0.032
13.2	0.0334	2.28	0.363	0.0108	0.032
13.3	0.0342	2.31	0.374	0.0111	0.033
13.4	0.0349	2.35	0.386	0.0114	0.034
13.5	0.0357	2.38	0.397	0.0118	0.035
14.0	0.0398	2.57	0.460	0.0136	0.039
15.0	0.0490	2.94	0.606	0.0179	0.047
16.0	0.0595	3.34	0.784	0.0232	0.058
17.0	0.0713	3.77	0.999	0.0296	0.069
18.0	0.0847	4.23	1.26	0.0372	0.082
19.0	0.0996	4.71	1.56	0.0462	0.096
19.5	0.108	4.97	1.73	0.0512	0.104
19.6	0.109	5.02	1.77	0.0523	0.106
19.7	0.111	5.07	1.80	0.0533	0.107
19.8	0.113	5.12	1.84	0.0544	0.109
19.9	0.114	5.17	1.88	0.0555	0.111
20.0	0.116	5.22	1.91	0.0567	0.112
20.1	0.118	5.28	1.95	0.0578	0.114
20.2	0.120	5.33	1.99	0.0590	0.116

\*Input Values to NGCEFF

Table 6.3.3

Gravitational Collision Shape Factor for Oblate Spheroid and Spheres  
 Axis Ratio = 0.05  
 Semi-Major Axis = 0.01157 cm

Radius ( $\mu\text{m}$ )	Volume Basis		Mass Basis		BETA Shape Factor	$\epsilon_g$
	NGCEFF	SGCEFF*	NGCEFF	SGCEFF*		
12.9	2.738	0.6429	2.857	0.6705	4.259	0.511
13.0	2.756	0.6446	2.877	0.6725	4.276	0.515
13.1	2.771	0.6478	2.891	0.6759	4.277	0.519
13.2	2.787	0.6541	2.908	0.6824	4.261	0.523
13.3	2.803	0.6552	2.924	0.6834	4.278	0.527
13.4	2.816	0.6573	2.938	0.6856	4.285	0.530
13.5	2.822	0.6614	2.944	0.6898	4.268	0.533
14.0	2.888	0.6746	3.011	0.7034	4.281	0.551
15.0	2.997	0.7005	3.122	0.7298	4.278	0.583
16.0	3.069	0.7217	3.195	0.7513	4.252	0.608
17.0	3.120	0.7386	3.246	0.7684	4.224	0.630
18.0	3.151	0.7549	3.276	0.7843	4.177	0.648
19.0	3.155	0.7656	3.278	0.7955	4.120	0.660
19.5	3.169	0.7724	3.291	0.8023	4.102	0.669
19.6	3.171	0.7738	3.294	0.8037	4.098	0.671
19.7	3.169	0.7751	3.291	0.8050	4.088	0.672
19.8	3.171	0.7761	3.293	0.8059	4.086	0.673
19.9	3.168	0.7773	3.289	0.8072	4.072	0.674
20.0	3.171	0.7783	3.292	0.8082	4.074	0.675
20.1	3.168	0.7791	3.291	0.8089	4.068	0.676
20.2	3.168	0.7800	3.289	0.8098	4.061	0.677

\*Spherical collision efficiency calculated by Code NGCEFF assuming a Volume Equivalent Sphere.

Pitter et al.<sup>26</sup>. This was not possible, however, because the annular collision domain reported by Pitter et al. was not observed in any of the present cases. As discussed in Section 6.1.2, an error in programming may have resulted in the generation of the annular collision domains reported by Pitter et al..

Table 6.3.3 lists the final results. These are significant results since they confirm the belief that it should be possible to theoretically determine nonspherical collision efficiencies and the collision shape factor  $\beta$ . By improving on the methods developed in this research, it will be possible to create tables of shape factors for various nonspherical aerosols.

Finally, developers of aerosol rate codes such as HAARM-3 can now place more confidence on the usage of a collision shape factors. Current practice involves running these codes with different  $\beta$ 's until a fairly good fit to the experimental data is achieved. By using shape factors like those in Table 6.3.4, the testing of these codes is more rigorous and may result in revealing relationships that were being masked by the present "curve fitting" procedures.

## CHAPTER VII

### CONCLUSIONS AND RECOMMENDATIONS

#### 7.1 Nonspherical Gravitational Collision Efficiencies

The results of the nonspherical gravitational collision efficiencies indicate that it is inappropriate to assume that agglomerates collide with the same efficiencies as spherical particles. During the early stages of agglomerate growth, there will be collisions between chain-like particles and spherical particles, and in this case the results from Chapter VI show clearly that the collision shape factor  $\beta$  is necessary to modify the spherical gravitational collision efficiencies. For the case considered in Chapter VI, a  $\beta$  factor equal to 4.0 was determined.

The abrupt cutoffs in collision efficiency reported by Pitter and Pruppacher<sup>35</sup> was not observed from the computational results. As discussed in Chapter VI, the annular collision domain suggested by the results of Pitter and Pruppacher is most likely due to an error in their computer program. Time did not permit a change in their program to determine if different results would be calculated but when NCGEFF was modified to include their expressions for computing the collision separation distance, some of their

results were obtained. However, considerable problems occurred because the separation distances were always being calculated incorrectly, which resulted in the spherical particle inside the oblate spheroid. This same problem was experienced by Pitter and Pruppacher. When the correct expressions were substituted into NCGEFF, this problem disappeared.

The results of the Navier-Stokes solution to the flow around an oblate spheroid showed that the calculations are very sensitive to the difference expression used to model the boundary conditions. Higher order terms [ $> \theta(h)$ ] caused the solution to diverge; the smaller the error associated with the expression was, the greater the divergence observed. This is a numerical problem with the finite difference method, although it was not suspected until after considerable effort had been spent in finding the part of the vorticity field which caused the onset of divergence.

The use of cubic splines to interpolate the velocity fields associated with the oblate spheroid was superior when compared with the finite difference method. The indeterminate form at each boundary was easily calculated by using cubic splines. The calculations were verified for the case where the Reynolds number equals zero by using

Oberbeck's solution. Boundary calculations were further improved by using Gregory-Newton forward and backward extrapolation formula.

## 7.2 Collision Shape Factor ( $\beta$ )

The concept of the collision shape factor is not new but in this dissertation it is rigorously derived from basic definitions. Furthermore, detail information in Chapter IV showed that the gravitational collision efficiency based on mass equivalent radii is not, in general, equal to the gravitational collision efficiency based on volume equivalent radii, and therefore the  $\beta$  factor will be incorrect if the same basis is not used for both the spherical particle and the nonspherical particle.

The calculation of  $\beta$  factors was demonstrated in Chapter VI. These were extremely difficult calculations to do, requiring considerable computer time and hence financial support and commitment in order to complete this research. However, more  $\beta$  factors are necessary if any confidence is to be placed in their usage in such aerosol rate codes like HAARM-3. It is impossible to calculate every  $\beta$  factor needed and therefore results from such programs like GCEFF<sup>12</sup> should be used in conjunction with a set of  $\beta$  factors. Currently aerosol rate codes make use of the concept of a



$\beta$  shape factor and an average  $\beta$  shape factor is established, not from a priori knowledge, but from curve fitting with experimental data.

### 7.3 Recommendations for Future Work

Basic aerosol research is applicable to many scientific fields and technologies. The research reported herein is not only useful to the developers of aerosol rate codes for an HCDA in an LMFBR but equally useful to developers of similar aerosol rate codes for postulated generalized working accidents for light water reactors (LWR), high temperature gas-cooled reactors (HTGR) and gas-cooled fast reactors (GCFR). This research is equally important to researchers of meteorologic phenomena and environmental pollution effects. Thus, basic aerosol research involving collisional mechanisms impacts many areas of science and technology.

In this section, research areas where future work appears worthwhile are outlined. First the areas in which the work of this dissertation can be improved are presented. Then areas not considered by this dissertation that need to be investigated in order to more fully understand the mechanisms and processes that are influencing particle phenomena are highlighted.

### 7.3.1 Supplementary Dissertation Research

#### 7.3.1.1 Tabulation of Collision Shape Factors

It was noted in Chapter VI that the gravitational collision efficiencies for nonspherical and spherical particles radically differ from each other. Two efforts need undertaking. First, collision shape factors for oblate spheroids and spheres for various densities and containment parameters are necessary to determine bounds on this very important shape factor. Completion of this phase would lead to the next effort, which is to calculate the collision shape factors for other nonspherical particles such as prolate spheroids. When completed the upper and lower limits on the collision shape factor,  $\beta$ , would be better defined (on a sound theoretical basis) than it had been before in aerosol science.

#### 7.3.1.2 Numerical Methods

Any effort to tabulate collision shape factors needs to address improved numerical schemes to solve the Navier-Stokes equation and the six linear differential equations of aerosol motion and interaction. The finite element method offers promise in solving the Navier-Stokes equation in both spherical and spheroids coordinate systems. Likewise, additional research of the stiff behavior of the six equations

of aerosol interaction may produce a more efficient integration routine. These areas of research, if successful, will have a significant impact on reducing computational expenses associated with shape factor tabulation.

#### 7.3.1.3 NGCEFF Code Modification

The computer code NGCEFF listed in Appendix 1 to determine the collision shape factor,  $\beta$ , is a very general code. In its present configuration it can determine aerosol particle trajectories, drag forces between particles and velocity fields around oblate spheroids. This information is of scientific interest and should be merged with graphics packages for display and tabulated for future reference. NGCEFF can be modified or expanded as required without a major rewriting to incorporate new information such as kinetic corrections to drag forces.

#### 7.3.1.4 Functional Representation of the Collision Shape Factor

Since the collision shape factor,  $\beta$ , plays an important role in aerosol rate code such as HAARM-3, effort should go into the development of an efficient and accurate functional representation of  $\beta$  after tabulation of its values is accomplished. In the past the data were fit using a natural

cubic spline to interpolate between known values. This may not be the best way to represent  $\beta$ , because of the increase in the number of variables and therefore research is necessary to define the problem and formulate an approximate solution.

### 7.3.2 Additional Research Topics

#### 7.3.2.1 Synergistic Effects

It is stipulated that the three coagulation mechanisms are separative and additive for the collision kernel,  $\phi$ , Equation 2.3.1. Possible synergistic effects of one mechanism on another should be investigated in order to verify this assumption or determine what corrections are necessary to model observed phenomena and its associated theory.

#### 7.3.2.2 Coalescent Effects

One effect that needs thorough investigation is coalescence of particles. This effect must be studied both by the experimentist and theorist and a method for calculating the fraction of particles that coalesce determined.

#### 7.3.2.3 Knudsen Drag Forces

As reported in Appendix 3, Knudsen drag forces can significantly improve the accuracy of the computational method

used to determine the collision efficiency. Considerable more effort is needed in this area even if it is extremely complicated. This research, if successful, would be extremely important to the developers of aerosol rate codes and to the scientific community as a whole.

#### 7.3.2.4 Other Aerosol Effects

Many other aerosol effects must be taken into consideration. Some of these include radiation and electrical charge effects, water vapor (humidity) and thermal gradient effects, and diffusiophoretic, inertial and turbulent deposition effects.

The complete description of the processes affecting an aerosol is extremely complicated. It is important, however, to concentrate on understanding these processes individually and then together before any real confidence can be placed on codes like HAARM-3.

#### 7.3.2.5 Experimental Data

It is important to compare the results of the present research with experimental data. An important consideration here is to study the effects of particle shape on the gravitational collision efficiency and collision shape factor. Aerosol characteristics and fluid parameter of post-HCDA containments need to be included into the design of such experiments.

## REFERENCES

1. Erdman, C.A., et al., "Bubble Behavior in LMFBR Code Disruptive Accidents," University of Virginia, NUREG/CR-0604, 1979.
2. Gieseke, J.A., K.W. Lee and L.D. Reed, "HAARM-3 Users Manual," Battelle Columbus Laboratories, BMI-NUREG-1991, 1978.
3. Jordan, H., and C. Sack, "A Computer Code for Determining the Behavior of Contained Nuclear Aerosols (PARADISEKO-III)," Karlsruhe Nuclear Research Center, KFK 2151, 1975.
4. Lindaner, G.D., and A.J. Castleman, Jr., "The Importance of Gravitational Coagulation on the Settling of High Mass Density Aerosols," Nucl. Sci. Engr., 42, 58, 1970.
5. "Nuclear Aerosols in Reactor Safety," Report by a Group of Experts of the Nuclear Energy Agency on the Safety of Nuclear Installations, A State-of-the-Art Report Published by the Organization for Economic Co-operation and Development, 1979.
6. Jordan, H., and J.A. Gieseke, "Characterization of Agglomerates of  $UO_2$  Aerosol Particles," Battelle Columbus Laboratories, BMI-2009, NUREG/CR-0489, 1978.
7. Zanutelli, W.A., G.D. Miller and E.W. Johnson, "1978 Annual Report: Aerosol Characterization From a Simulated HCDA," Monsanto Research Corporation, MLM-2597, NUREG/CR-0740, 1979.
8. Wegrzyn, J., and D.T. Shaw, "Experimental Investigation of Aerosol Behavior in a Post-LMFBR Accident Reactor Containment Atmosphere," State University of New York at Buffalo, NUREG/CR-0799, 1979.
9. Kops, J., G. Dibbets, L. Hermans and J.F. Van de Vate, "The Aerodynamic Diameter of Branched Chain-like Aggregates," J. Aerosol Sci., 6, 329, 1975.
10. Wegrzyn, J., and D.T. Shaw, "Experimental Investigation of Aerosol Behavior in a Post-LMFBR Accident Reactor Containment Atmosphere," State University of New York at Buffalo, LAPES 78-002, NUREG/CR-0287, 1978.

11. Van de Vate, J.F., W.F. van Leeuwen, A. Plomp and H.C.D. Smit, "Morphology and Aerodynamics of Sodium Oxide Aerosol at Low Relative Humidities," OECD/NEA-CSNI Specialist Meeting Nuclear Aerosols in Reactor Safety, Gatlinburg, Tennessee, 15th - 17th April, 1980.
12. Pertmer, G.A., "Gravitational Agglomeration of Post-HCDA LMFBR Aerosol," Ph.D. Dissertation, University of Missouri, Columbia, Missouri, 1978.
13. Hidy, G.M., and J.R. Brock, "The Dynamics of Aerocolloidal Systems," Pergamon Press, 1970.
14. Loyalka, S.K., "Analysis of Aerosol Particles Undergoing Gravitational Agglomeration," University of Missouri-Columbia, NUREG/CR-0780, 1979.
15. Gieseke, J.A., K.W. Lee, H. Jordan and M.P. Rausch, "HAARM-3 Code Verification Procedure," Battelle Columbus Laboratories, Draft NUREG/CR-BMI-2030/R7, 1979.
16. Jordan, H., B. Vaishnavi and J.A. Gieseke, "The Numerical Method of the Aerosol Behavior Reference Code, CRAB," Battelle Columbus Laboratories, BMI-2016, NUREG/CR-0620, 1979.
17. Lee, K.W., J.A. Gieseke and L.D. Reed, "Sensitivity Analysis of the HAARM-3 Code," NUREG/CR-0527, BMI-2008, 1978.
18. Pertmer, G.A., and S.K. Loyalka, "Gravitational Collision Efficiency of Post Hypothetical Core Disruptive Accident Liquid Metal Fast Breeder Reactor Aerosols: Spherical Particles," Nucl. Technol., 47, 70, 1980.
19. Pruppacher, H.R., and J.D. Klett, "Microphysics of Clouds and Precipitation," D. Reidel Publishing, 1978.
20. Jensen, V.G., "Viscous Flow Round a Sphere at Low Reynolds Numbers ( $<40$ )," Proc. Roy. Soc. A, 249, 346, 1959.
21. Rimon, Y., and S.I. Cheng, "Numerical Solution of a Uniform Flow Over a Sphere at Intermediate Reynolds Numbers," Phys. Fluids, 12, 949, 1969.
22. Pearcey, T., and B. McHugh, "Calculation of Viscous Flow Around Spheres at Low Reynolds Numbers," Phil Mag (7), 46, 783, 1955.

23. Rimon, Y., and H.J. Lugt, "Laminar Flow Past Oblate Spheroids of Various Thicknesses," *Phys. Fluids*, 12, 2465, 1969.
24. Michael, P., "Steady Motion of a Disk in a Viscous Fluid," *Phys. Fluids*, 9, 466, 1966.
25. Pruppacher, H.R., B.P. LeClair and A.E. Hamielec, "Some Relations Between Drag and Flow Pattern of Viscous Flow Past a Sphere and a Cylinder at Low and Intermediate Reynolds Numbers," *J. Fluid Mech.*, 44, 781, 1970.
26. Pitter, R.L., H.R. Pruppacher and A.E. Hamielec, "A Numerical Study of Viscous Flow Past a Thin Oblate Spheroid at Low and Intermediate Reynolds Numbers," *J. Atmos. Sci.*, 30, 125, 1973.
27. Masliyah, J.H., and N. Epstein, "Numerical Study of Steady Flow Past Spheroids," *J. Fluid Mech.*, 44, 493, 1970.
28. LeClair, B.P., A.E. Hamielec and H.R. Pruppacher, "A Numerical Study of the Drag on a Sphere at Low and Intermediate Reynolds Numbers," *J. Atmos. Sci.*, 27, 308, 1970.
29. Klett, J.D., "The Interaction and Motion of Rigid Spheres Falling in a Viscous Fluid At Low Reynolds Numbers," Ph.D. Dissertation, University of California, Los Angeles, 1968.
30. Langmuir, I., "The Production of Rain By a Chain-Reaction in Cumulus Clouds at Temperatures Above Freezing," *J. Meteor.*, 5, 175, 1948.
31. Shafrir, U., and M. Neiburger, "Collision Efficiencies of Two Spheres Falling in A Viscous Medium," *J. Fluid Mech.*, 34, 808, 1963.
32. Pearcey, T., and G.W. Hill, "A Theoretical Estimate of the Collection Efficiencies of Small Droplets," *J. Geophys. Res.*, 68, 4141, 1963.
33. Shafrir, U., and T. Gal-Chen, "A Numerical Study of Collision Efficiencies and Coalescence Parameters for Droplet Pairs With Radii Up to 300 Microns," *J. Atmos. Sci.*, 28, 741, 1971.
34. Lin, C.L., and S.C. Lee, "Collision Efficiency of Water Drops in the Atmosphere," *J. Atmos. Sci.*, 32, 1412, 1975.



35. Pitter, R.L., and H.R. Pruppacher, "A Numerical Investigation of Collision Efficiencies of Simple Ice Plates Colliding With Supercooled Water Drops," J. Atmos. Sci., 31, 551, 1974.
36. Happel, J., and H. Brenner, "Low Reynolds Number Hydrodynamics," Englewood Cliffs, N.J., Prentice Hall, Inc., 1965.
37. Lai, R.Y.S., and L.F. Mockros, "The Stokes-Flow Drag on Prolate and Oblate Spheroid During Axial Translatory Accelerations," J. Fluid Mech., 52, 1, 1972.
38. Gear, C.W., "Numerical Initial Value Problems in Ordinary Differential Equations," Prentice-Hall, 1971.
39. International Mathematical and Statistical Libraries, Inc., 7500 Bellaire, Blvd., Houston, Texas, 77036.
40. deBoor, C., "A Practical Guide to Splines," Springer-Verlog, 1978.
41. Varga, R.S., "Matrix Iterative Analysis," Prentice-Hall, Inc., 1962.
42. Woo, S.W., "Simultaneous Free and Forced Convection Around Submerged Cylinders and Spheres," Ph.D. Dissertation, McMaster University, Hamilton, Canada, 1971.
43. Orback, O., and C.M. Crowe, "Convergence Promotion in the Simulation of Chemical Processes with Recycle-the Dominant Eigenvalue Method," Can. J. Chem. Engr., 49, 509, 1971.
44. Russell, D.B., ARC R&M No. 3331, London, 1962.
45. LINPACK, National Energy Software Center, Argonne National Laboratory, 9700 South Cass Avenue, Argonne, IL 60439.
46. Loyalka, S.K., "A Numerical Method for Solving Integral Equations of Kinetic Theory," IX International Symposium on Rarefied Gas Dynamics, 1974.
47. Tomoeda, M., "A Theoretical and Experimental Study on the Flow of Rarefied Gas Past A Sphere," UTIAS Report No. 216, May, 1977.

48. Tu, K.W., and D.T. Shaw, "Experimental Determination of Interception Collection Efficiencies for Small Cloud Droplets," J. Colloid Interface Sci., 62, 40, 1977.
49. Stimson, M., and G.B. Jeffery, "The Motion of Two Spheres in a Viscous Fluid," Proc. Roy. Soc. A, 111, 110, 1926.

APPENDIX 1  
COMPUTER CODE LISTINGS

The listings of the computer code NCGEFF is contained in this Appendix. The complete descriptions of the code and of code usage can be found in Chapter V.

The code utilizes the following subroutines from the International Mathematical and Statistical Libraries, Inc. (IMSL): ZFALSE, ICSICU, and ICSEVU. The IMSL subroutines are not listed. Calculation of the eigenvalues of the two matrices associated with the vorticity transport equations is done with the LINPACK routines and are available from Argonne Laboratory or IMSL. Subroutine DVOGER has been merged with NCGEFF since it is no longer a current IMSL subroutine. It was utilized in lieu of DGEAR because of certain features not available in DGEAR.

```

MASTER.FORT
00010 C*****
00020 C
00030 C
00040 C INPUT:  PARAMETER CARD(COLUMNS)  FORMAT  USAGE
00050 C          MU      1  (1-10 ) G10.0  AIR VISCOSITY
00060 C          RHO     1  (11-20 ) G10.0  AIR DENSITY
00070 C          LAMBDA 1  (21-30 ) G10.0  MEAN FREE PATH OF AIR
00080 C          EPS     1  (31-40 ) G10.0  ERROR CRITERIA FOR ALL
00090 C*****
00100 C          REYN1    2  (1-10 ) G10.0  REYNOLDS NUMBER FOR OBLATE
00110 C          AR1      2  (1-10 ) G10.0  AXIS RATIO OF OBLATE
00120 C          DENS1    2  (11-20 ) G10.0  BULK DENSITY OF OBLATE
00130 C          ALPHA1  2  (21-30 ) G10.0  DENSITY CORRECTION FACTOR
00140 C          DISK    2  (31-40 ) G10.0  SELECT OPTION NEEDED...
00150 C          0.0-GENERATE PSI AND G FIELDS
00160 C          1.0-READ FIELDS FROM DISK,
00170 C*****
00180 C          DZETA    3  (1-10 ) G10.0  RADIAL STEP SIZE, SPHEROIDAL
00190 C          MP1      3  (11-15 ) 15    NUMBER OF ANGULAR STEPS
00200 C          N        3  (16-20 ) 15    NUMBER OF RADIAL STEPS
00210 C          MATRX   3  (21-25 ) 15    SELECT OPTION NEEDED...
00220 C          0-NO MATRIX ANALYSIS
00230 C          1-MATRIX ANALYSIS:
00240 C          SPECTRAL RADIUS,EIGENVALUES
00250 C          AND RECIPROCAL CONDITION
00260 C          NUMBER CALCULATED
00270 C          IOUT     3  (26-30 ) 15    SELECT OPTION NEEDED...
00280 C          1-OUTPUT INTERMEDIATE RESULTS
00290 C          0-NO OUTPUT NEEDED
00300 C          JDERIV   3  (31-35 ) 15    SELECT VELOCITY OPTION
00310 C          0-SPLINES
00320 C          1-FINITE DIFFERENCE METHOD.
00330 C*****
00340 C          R2V       4  (1-10 ) G10.0  VOLUME EQUIVALENT RADIUS OF
00350 C          SMALLER PARTICLE.

```

```

00360 C      DENS2      4      (11-20 ) G10.0      BULK DENSITY OF SMALLER
00370 C      ALPHA2     4      (21-30 ) G10.0      DENSITY CORRECTION FACTOR OF
00380 C      PATH      4      (31-40 ) G10.0      SELECT TRAJECTORY OPTION...
00390 C                                     0.0-NO OUTPUT NEEDED.
00400 C
00410 C*****
00420 C      GOTO      5      (1-10 ) G10.0      SELECT OPTION...
00430 C      1.0-NEW CARDS 1-4 NEEDED.
00440 C      2.0-NEW CARDS 2-4 NEEDED.
00450 C      3.0-NEW CARDS 3&4 NEEDED
00460 C      4.0-ONLY CARD 4 CHANGED
00470 C      99.0-STOP CODE.
00480 C
00490 C
00500 C*****
00510 C
00520 C      THREE PROGRAM CONTROL PARAMETERS.
00530 C
00540 C      I--TELLS PROGRAM THE TYPE OF LARGE PARTICLE BEING CONSIDERED.
00550 C      J--TELLS PROGRAM IF NEW LARGE PARTICLE OR PROPERTIES INPUTED.
00560 C      JSTART--TELLS SUBROUTINE OBLATE WHETHER OR NOT TO USE INITIAL GUESS.
00570 C
00580 C      IMPLICIT REAL*8(A-H,O-Z)
00590 C      REAL*8 MU,LAMBDA,LYK,LYK1,LYKV1,IAR1,IR1V,INTIA
00600 C      COMMON PI,GV,R,EPS,DISK,BRHO,GAMMA,ERR,CLL,UINF,DENS1,ALPHA1
00610 C      COMMON/AIR/ MU,RHO,LAMBDA
00620 C      COMMON/VER1/R1V,REYN1,CDV1,VINFU1,STKV1,LYKV1,IR1V
00630 C      COMMON/AERSL1/REYN1,AR1,SEMI,CDAR1,VINF1,STK1,LYK1,IAR1
00640 C      COMMON/AERSL2/R2V,DENS2,ALPHA2,VINF2,REYN2
00650 C      COMMON/SWITCH/AR,CDTOTL,AXIS,STK,LYK,INTIA,VINF,RE
00660 C      COMMON/NAVIER/DZETA,MF1,N,NSF,IOUT,MATRX,JDERIV
00670 C      COMMON/COLL$/PATH,YIMAX,SIMAX,YIMIN,SIMIN,IETA,I35,JMAX,JMIN
00680 C      COMMON/OBLAT$/ PSI(100,100),G(100,100)
00690 C      COMMON/WORK/COSH22(100),SINET2(100),COEF1(100),COEF2(100),COEF3(10
00700 C      $),COEF4(100),SVORT(5000),PRESS(5000),VECTOR(5000)

```

```

01060 C
01070 C
01080 C
01090 C
01100 1000 FORMAT(5G10.0)
01110 1001 FORMAT(G10.0,5I5)
01120 END
01130 SUBROUTINE INITIAL(II,JJ)
01140 IMPLICIT REAL*8(A-H,O-Z)
01150 REAL*8 MU,LAMBDA,LYK,LYK1,LYKV1,IAR1,IR1V,INTIA
01160 COMMON PI,GV,R,EPS,DISK,BRHO,GAMMA,ERR,CLL,UINF,DENS1,ALPHA1
01170 COMMON/AIR/ MU,RHO,LAMBDA
01180 COMMON/DVGE$/HD,HDMIN,HDMAX,NEQTN,MAXDER,MTH
01190 COMMON/VER1/R1V,REYN1,CDV1,VINFV1,STKV1,LYKV1,IR1V
01200 COMMON/AERSL1/REYN1,AR1,SEMI,CDAR1,VINF1,STK1,LYK1,IAR1
01210 COMMON/AERSL2/R2V,DENS2,ALPHA2,VINF2,REYN2
01220 COMMON/SWITCH/AR,CDTOTL,AXIS,STK,LYK,INTIA,VINF,RE
01230 COMMON/OBLAT$/ PSI(100,100),G(100,100)
01240 IF(II.NE.0) GO TO 10
01250 IF(JJ.EQ.1) GO TO 2
01260 GV=980.621
01270 PI=3.141592653589793D00
01280 CLL=1.0D-05
01290 ERR=1.0D-02*CLL
01300 CDTOTL=0.0D00
01310 C
01320 C INPUT PARAMETERS FOR IMSL DVOGER
01330 NEQTN=6
01340 MAXDER=6
01350 HDMAX=1.0D-03
01360 HDMIN=HDMAX*1.0D-09
01370 HD=HDMAX*1.0D-04
01380 MTH=2
01390 C
01400 C

```

```

01410 C INITIALIZE THE FLOW FIELDS.
01420 C
01430 DO 1 I=1,100
01440 DO 1 J=1,100
01450 PSI(I,J)=1.0D00
01460 1 G(I,J)=1.0D00
01470 C
01480 IF(AR1.EQ.1.0D00) DELTA1=1.0D00/2.0D00
01490 IF(AR1.EQ.1.0D00) GO TO 2
01500 TEMP1=AR1*DARCOS(AR1)
01510 TEMP2=DSQRT(1.0D00-AR1*AR1)
01520 DELTA1=(TEMP1-TEMP2)/(AR1*AR1*TEMP2-TEMP1)
01530 C
01540 2 GAMMA=DENS2*ALPHA2/(DENS1*ALPHA1)
01550 BRHO=(DENS2*ALPHA2-RHO)/(DENS1*ALPHA1-RHO)*GAMMA)
01560 IAR1=(DENS2*ALPHA2+RHO/2.0D00)/((DENS1*ALPHA1+RHO*DELTA1)*GAMMA)
01570 IR1V=(DENS2*ALPHA2+RHO/2.0D00)/((DENS1*ALPHA1+RHO/2.0D00)*GAMMA)
01580 C
01590 VINF2=2.0D00*DENS2*ALPHA2*GV*R2V*R2V*(1.0D00-RHO/(DENS2*ALPHA2))/
01600 $9.0D00*MU)
01610 REYN2=VINF2*2.0D00*R2V*RHO/MU
01620 IF(JJ.EQ.0) RETURN
01630 GO TO 15
01640 10 IF(II.NE.1) GO TO 20
01650 CDAR1=CDTOTL
01660 SEMI=3.0D00*MU*CDAR1*REYN1*REYN1
01670 TEMP1=AR1**2.0D00/3.0D00)
01680 SEMI=SEMI/(32.0D00*GV*TEMP1*(DENS1*ALPHA1-RHO)*RHO)
01690 SEMI=SEMI**2.0D00/3.0D00)
01700 R1V=SEMI*AR1**2.0D00/3.0D00)
01710 UINF=2.0D00*DENS1*ALPHA1*GV*R1V*R1V*(1.0D00-RHO/(DENS1*ALPHA1))/
01720 $9.0D00*MU)
01730 VINFI=REYN1*MU/(2.0D00*SEMI*RHO)
01740 15 R=R2V/R1V
01750 STK1=UINF1*VINFI*BRHO*(1.0D00+RHO/(DENS2*ALPHA2*2.0D00))*R**4

```

```

01760      STK1=GAMMA*GAMMA/(GV*SEMI*(1.0D00-RHO/(DENS1*ALPHA1)))
01770      LYK1=BRHO*IAK1*GAMMA*GAMMA**4
01780      IF(II.EQ.0) RETURN
01790 C
01800 C*****
01810 C
01820      20 IF(JJ.EQ.1) GO TO 30
01830      CDV1=CDTOTL
01840      REYNV1=USQRT(48.0D00*R1V*RHO*UINF/(MU*CDV1))
01850      VINNV1=REYNV1*MU/(2.0D00*R1V*RHO)
01860      30 STKV1=VINNV1*VINNV1*ERHO*(1.0D00+RHO/(DENS2*ALPHA2*2.0D00))*R**4
01870      STKV1=STKV1*GAMMA*GAMMA/(GV*R1V*(1.0D00-RHO/(DENS1*ALPHA1)))
01880      LYKV1=BRHO*IR1V*GAMMA*GAMMA**4
01890 C
01900 C
01910      RETURN
01920      END
01930      SUBROUTINE START
01940 C
01950 C
01960 C
01970 C
01980 C
01990 C
02000 C
02010 C
02020 C
02030 C
02040 C
02050 C
02060 C
02070 C
02080 C
02090 C
02100 C

```

PROGRAM EDITED 23 APRIL 1980.

THIS PROGRAM CREATES THE STREAM FUNCTION AND MODIFIED VORTICITY FIELD ON OBLATE SPHEROIDAL MERIDIONAL PLANE. OUTPUT OF THIS PROGRAM IS USED FOR INPUT TO SUBROUTINE ORBLATE.

FOR DEFINITION OF MODIFIED VORTICITY, SEE MASLIYAH AND EPSTEIN, J. FLUID MECH(1970), VOL44, PART3, PP495-512.

DEFINE:

PSI(I,J) AS STREAM FUNCTION FIELD

G(I,J) AS MODIFIED VORTICITY FUNCTION FIELD

WHERE I REPRESENTS THE POLAR ANGLE, ETA

WHERE J REPRESENTS THE RADIAL COORDINATES, ZETA



```

02110 C      ETA VARIES FROM 0 TO 180 DEGREES
02120 C      ZETA VARIES FROM ZETA0, THE VALUE OF ZETA AT THE SURFACE OF THE
02130 C      SPHEROID, TO ZETA=ZETA0+N*DZETA, THE VALUE OF ZETA WHERE THE FLOW
02140 C      IS ASSUMED TO BE FREE STREAM FLOW.
02150 C      IMPLICIT REAL*8(A-H,O-Z)
02160 C      REAL*8 MU,LAMBDA,LYK,LYK1,LYKV1,IAR1,IRIV,INTIA
02170 C      COMMON PI,GV,R,EPS,DISK,BRHO,GAMMA,ERR,CLL,UINF,DENS1,ALPHA1
02180 C      COMMON/SWITCH/AR,CDTOTL,AXIS,STK,LYK,INTIA,VINF,RE
02190 C      COMMON/NAVIER/DZETA,MP1,N,NSF,IOUT,MATRX,JDERIV
02200 C      COMMON/OBLAT$/ PSI(100,100),G(100,100)
02210 C
02220 C      DIMENSION LXI(10)
02230 C      INITIALIZATION OF PARAMETERS
02240 C      MP1 IS THE NUMBER OF DIFFERENT ETA CONSIDERED
02250 C      N IS THE NUMBER OF DIFFERENT ZETA CONSIDERED
02260 C      C IS THE CHARACTERISTIC LENGTH OF THE COORDINATE SYSTEM, EQUAL TO
02270 C      1.0/COSH(ZETA0)
02280 C      AR IS THE AXIS RATIO, B/A,
02290 C      R=C*SINH(ZETA0), MINOR AXIS
02300 C      A=C*COSH(ZETA0), MAJOR AXIS,DEFINE A=1.0
02310 C      DZETA IS THE INCREMENT SIZE OF ZETA AND IS DEFINED AS 0.1.
02320 C      DETA IS THE INCREMENT SIZE OF ETA. GIVEN IS RADIAN.
02330 C      DETA=PI/DFLOAT(MP1-1)
02340 C
02350 C
02360 C      NSF=1, STREAM AND VORTICITY FOR SPHERE.
02370 C      NSF=2, STREAM AND VORTICITY FOR SPHEROID.
02380 C      NSF=3, STREAM AND VORTICITY FOR UNIFORM FLOW.
02390 C      NSF=2
02400 C      IF (AR.GE.0.999D00) NSF=1
02410 C
02420 C
02430 C      CALCULATE ZETA0 FROM AXIS RATIO.
02440 C      ZETA0=DLOG((1.0D00+AR)/(1.0D00-AR))/2.0D00
02450 C      CALCULATE COSHO AND OTHER VALUES BASED ON ZETA0.

```

```

02460 COSH0=DCOSH(ZETA0)
02470 COSH02=COSH0*COSH0
02480 SINH0=DSINH(ZETA0)
02490 SINH02=SINH0*SINH0
02500 ARCT0=PI/2.0D0-DATAN(SINH0)
02510 C
02520 C
02530 C
02540 C
02550 MP2D2=(MP1+1)/2
02560 IF(N.EQ.0) N=100
02570 J=0
02580 2 IF(J.GE.N) GO TO 5
02590 J=J+1
02600 ZETA=ZETA0+DZETA*DFLOAT(J-1)
02610 SINHZ=DSINH(ZETA)
02620 SINHZ2=SINHZ*SINHZ
02630 COSHZ=DCOSH(ZETA)
02640 COSHZ2=COSHZ*COSHZ
02650 ARCT=PI/2.0D0-DATAN(SINHZ)
02660 DO 3 I=1,MP1
02670 ETA=PI*(DFLOAT(I-1)/DFLOAT(MP1-1))
02680 IF(I.EQ.MP1) ETA=0.0D0
02690 PSI(I,J)=STREAM(ETA,COSH0,COSH02,SINH0,SINH02,ARCT0,COSHZ,COSHZ2,
02700 $SINHZ,SINHZ2,ARCT,NSF)
02710 G(I,J)=(COSHZ*DSIN(ETA)/COSH0)*VORTCY(ETA,COSH0,COSH02,SINH0,SINH0
02720 $2,ARCT0,COSHZ,COSHZ2,SINHZ,SINHZ2,ARCT,NSF)
02730 3 CONTINUE
02740 C
02750 DETERMINE IF CRITERIA FOR OUTER ENVELOPE IS SATISFIED.
02760 PSINFT=STREAM(PI/2.0D00,0,COSH02,0,0,0,COSH22,0,0,0,3)
02770 RATIO=PSI(MP2D2,J)/PSINFT
02780 IF(RATIO.GT.0.9999D00)GO TO 5
02790 GO TO 2
02800 5 CONTINUE
      N=J

```

```

02810 C
02820 C
02830 C
02840 C
02850 C SET BOUNDARY CONDITION FOR G AT OUTER ENVELOPE OF SYSTEM.
02860 C SET BOUNDARY CONDITION FOR PSI AT SURFACE OF BODY.
02870 C
02880 DO 6 I=1,MF1
02890 G(I,N)=0.0D00
02900 6 PSI(I,1)=0.0D00
02910 C
02920 C OUTPUT RESULTS IF IOUT.NE.0.
02930 C
02940 IF(IOUT.EQ.0) GO TO 13
02950 C
02960 C*****
02970 C
02980 C OUTPUT RESULTS TO UNIT 6 (LINE PRINTER)
02990 C
03000 C*****
03010 C
03020 C
03030 C
03040 WRITE(6,1000)
03050 WRITE(6,1002) RATIO
03060 WRITE(6,1003) MP1,N,DETA,RE,DZETA,EPS,AR
03070 WRITE(6,1001)
03080 JJJ=0
03090 7 JJ=JJJ+1
03100 JJJ=JJJ+9
03110 IF(JJJ.GE.N)JJJ=N
03120 DO 8 J=1,10
03130 JL=JJ-1+J
03140 8 LXI(J)=JL
03150 WRITE(6,1004) (LXI(J),J=1,10)
DO 9 I=1,MF1

```

```

03160      9 WRITE(6,1005) (PSI(I,J),J=JJ,JJJ)
03170      IF(JJJ.LT.N) GO TO 7
03180      C
03190      C
03200      WRITE(6,1006)
03210      JJJ=0
03220      10 JJ=JJJ+1
03230      JJJ=JJ+9
03240      IF(JJJ.GE.N) JJJ=N
03250      DO 11 J=1,10
03260      JL=JJ-1+J
03270      11 LXI(J)=JL
03280      WRITE(6,1004) (LXI(J),J=1,10)
03290      DO 12 I=1,MP1
03300      12 WRITE(6,1005) (G(I,J),J=JJ,JJJ)
03310      IF(JJJ.LT.N) GO TO 10
03320      13 RETURN
03330      1000 FORMAT('1',' OUTPUT FROM SUBROUTINE START. STREAM FUNCTION AN
03340      $D VORTICITY FIELDS CALCULATED USING STOKES OR OBERBECK SOLUTIONS')
03350      1001 FORMAT('0',' STREAM FUNCTION (REYNOLDS NUMBER APPROXIMATELY EQUA
03360      $L TO ZERO)')
03370      1002 FORMAT('0',' RATIO=',G12.4)
03380      1003 FORMAT(' NUMBER OF ANGULAR STEPS=',G12.4,/,
03390      $' NUMBER OF RADIAL POINTS=',G12.4,/,
03400      $' ANGULAR STEP SIZE=',G12.4,/,
03410      $' REYNOLDS NUMBER=',G12.4,/,
03420      $' RADIAL STEP SIZE=',G12.4,/,
03430      $' ERROR CRITERIA FOR CONV.=',G12.4,/,
03440      $' AXIS RATIO=',G12.4,/)
03450      1004 FORMAT('0',6X,I3,9(10X,I3))
03460      1005 FORMAT(' ',10(2X,G11.5))
03470      1006 FORMAT('1',' MODIFIED VORTICITY (REYNOLDS NUMBER APPROXIMATELY E
03480      $QUAL TO ZERO)')
03490      C
03500      C

```

```

03510      END
03520      FUNCTION STREAM(ETA,COSH0,COSH02,SINH0,SINH02,ARCOTO,COSHZ,COSHZ2,
03530      $SINH2,SINH22,ARCT,NSF)
03540      IMPLICIT REAL*8(A-H,O-Z)
03550      REAL*8 NOMIN
03560      C    QUANTITIES ARE NONDIMENSIONAL.
03570      GO TO (10,20,30) , NSF
03580      C
03590      C
03600      C
03610      C    STREAM FUNCTION FOR SPHERE.
03620      10 SINETA=DSIN(ETA)**2
03630      ROOT=DSQRT(SINETA+SINH22)
03640      STREAM=COSH22*SINETA*(1.0D0-3.0D0*(COSH0/ROOT)/2.0D0+((COSH0/ROOT)
03650      $**3)/2.0D0)/(2.0D0*COSH02)
03660      RETURN
03670      C
03680      C
03690      C
03700      C    STREAM FUNCTION FOR OBLATE SPHEROID.
03710      20 RATIO=(SINH02-1.0D0)/COSH02
03720      DENOM=SINH0/COSH02-RATIO*ARCOTO
03730      NOMIN=SINH2/COSH22-RATIO*ARCT
03740      SINETA=DSIN(ETA)**2
03750      STREAM=COSH22*SINETA*(1.0D0-NOMIN/DENOM)/(2.0D0*COSH02)
03760      RETURN
03770      C
03780      C
03790      C
03800      C    STREAM FUNCTION FOR UNIFORM FLOW.
03810      30 SINETA=DSIN(ETA)**2
03820      STREAM=COSH22*SINETA/(2.0*COSH02)
03830      RETURN
03840      END
03850      FUNCTION VORTCY(ETA,COSH0,COSH02,SINH0,SINH02,ARCOTO,COSHZ,COSHZ2,

```

```

03860 $SINH2,SINH2,ARCT,NSF)
03870 IMPLICIT REAL*8(A-H,O-Z)
03880 QUANTITIES ARE NONDIMENSIONAL QUANTITIES.
03890 GO TO (10,20,30),NSF
03900 C
03910 C
03920 C
03930 C VORTICITY FUNCTION FOR A SPHERE.
03940 10 SINET=DSIN(ETA)
03950 SINETA=SINET*SINET
03960 ROOT=DSQRT(SINETA+SINH2)
03970 VORTCY=3.0D0*COSH02*COSH2*SINET/(2.0D0*ROOT**3)
03980 RETURN
03990 C
04000 C
04010 C
04020 C VORTICITY FUNCTION FOR OBLATE SPHEROID.
04030 20 GAMMAZ=2.0D0/COSH02
04040 BZERO=(SINH0-SINH02*ARCT0+ARCT0)/COSH02
04050 VORTCY=COSH0*DSIN(ETA)*SINH2*GAMMAZ/(COSH2*(SINH2+DCOS(ETA)**2)*B
04060 $ZERO)
04070 RETURN
04080 C
04090 C
04100 C
04110 C VORTICITY FUNCTION FOR UNIFORM FLOW
04120 30 VORTCY=0.0D0
04130 RETURN
04140 END
04150 SUBROUTINE OBLATE(JSTART,II)
04160 IMPLICIT REAL*8(A-H,O-Z)
04170 REAL*8 MU,LAMBDA,LYK,LYK1,LYKV1,IAR1,IRIV,INTIA
04180 COMMON PI,GV,R,EPS,DISK,BRHO,GAMMA,ERR,CLL,UINF,DENS1,ALPHA1
04190 COMMON/SWITCH/AR,CDTOTL,AXIS,STK,LYK,INTIA,VINF,RE
04200 COMMON/NAVIER/DZETA,MP1,N,NSF,IOUT,MATRIX,JDERIV

```

```

04210 COMMON/OBLAT$/ PSI(100,100),G(100,100)
04220 COMMON/WORK/COSH2(100),SINET2(100),COEF1(100),COEF2(100),COEF3(10
04230 $),COEF4(100),SVORT(5000),PRESS(5000),VECTOR(5000)
04240 DIMENSION WV(100,100),LXI(10)
04250 EQUIVALENCE (COSH02,COSH2(1)),(WV(1),SVORT(1)),(WV(5001),PRESS(1)
04260 $)
04270 C
04280 C
04290 1 IF(JSTART.NE.1) GO TO 4
04300 CALL DEFINE(II)
04310 IF(DISK.EQ.0.0D00) GO TO 2
04320 REWIND 8
04330 REWIND 9
04340 NDISK=8
04350 IF(II.NE.0) NDISK=9
04360 READ(NDISK) ((PSI(I,J),I=1,MP1),J=1,N)
04370 READ(NDISK) ((G(I,J),I=1,MP1),J=1,N)
04380 GO TO 3
04390 2 CALL START
04400 3 JSTART=2
04410 4 CONTINUE
04420 C*****
04430 C CALCULATE PARAMETERS DEPENDENT ON COORDINATE ZETA.
04440 DZETA2=DZETA*DZETA
04450 ZETA0=LOG((1.0D00+AR)/(1.0D00-AR))/2.0D00
04460 COSH0=DCOSH(ZETA0)
04470 COSH02=COSH0*COSH0
04480 DO 10 J=1,N
04490 ZETA=ZETA0+DFLOAT(J-1)*DZETA
04500 COSH22(J)=DCOSH(ZETA)**2
04510 TEMP=DTANH(ZETA)
04520 COEF1(J)=(1.0D00-DZETA*TEMP/2.0D00)/DZETA2
04530 COEF2(J)=(1.0D00+DZETA*TEMP/2.0D00)/DZETA2
04540 C*****
04550 C

```

```

04550 C
04570 C
04580 C*****
04590 C CALCULATE PARAMETERS DEPENDENT ON COORDINATE ETA.
04600 M=MP1-1
04610 NM1=N-1
04620 DELTA=PI/DFLOAT(MP1-1)
04630 DELTA2=DELTA*DELTA
04640 DO 20 I=2,M
04650 ETA=PI*(DFLOAT(I-1)/DFLOAT(MP1-1))
04660 SINET2(I)=DSIN(ETA)**2
04670 TEMP=DCOTAN(ETA)
04680 COEF3(I)=(1.0D00-DELTA*TEMP/2.0D00)/DELTA2
04690 COEF4(I)=(1.0D00+DELTA*TEMP/2.0D00)/DELTA2
04700 SINET2(1)=0.0D00
04710 SINET2(MP1)=SINET2(1)
04720 C*****
04730 C
04740 C
04750 C GET REMAINING COEFFICIENTS.
04760 C
04770 C
04780 COEF0=(DELTA2*DELTA2)/((DELTA2+DELTA2)*2.0D00)
04790 COEF5=RE/(COSH0*8.0D00*DELTA*DELTA)
04800 C
04810 C
04820 C*****
04830 C SET BOUNDARY CONDITIONS FOR STREAM FUNCTION.
04840 C
04850 C ON AXIS OF SYMMETRY.
04860 DO 30 J=1,N
04870 PSI(1,J)=0.0D00
04880 30 PSI(MP1,J)=0.0D00
04890 C ON SURFACE OF SPHEROID SET BY SUBROUTINE START.
04900 C AT OUTER BOUNDARY SET BY THIS STATEMENT.

```



```

04910      ZETAB=ZETA0+DZETA*DFLOAT(N-1)
04920      COSHZB=DCOSH(ZETAB)**2
04930      DO 35 I=1,MP1
04940          ETA=PI*(DFLOAT(I-1)/DFLOAT(MP1-1))
04950          35 PSI(I,N)=(COSHZB/(2.0D00*COSH02))*DSIN(ETA)**2
04960      C*****
04970      C
04980      C
04990      C*****
05000      C SET BOUNDARY CONDITIONS FOR VORTICITY.
05010      C
05020      C ON AXIS OF SYMMETRY.
05030      DO 40 J=1,N
05040          G(1,J)=0.0D00
05050          40 G(MP1,J)=0.0D00
05060      C AT OUTER BOUNDARY SET BY SUBROUTINE START.
05070      C*****
05080      C
05090      C
05100      C*****
05110      C
05120      C STREAM FIELD RELAXATION PARAMETER.
05130      C
05140          WS=DFLOAT((N*N+MP1*MP1)/(MP1*MP1*N*N))
05150          WS=1.0D00+PI*DSQRT(WS/2.0D00)
05160          WS=0.5D00*DSQRT(2.0D00)/WS
05170      C*****
05180      C BEGIN ITERATION.
05190      C*****
05200      C PARAMETERS FOR ITERATION OF FLOW FIELD, SET OUTSIDE LOOP.
05210      C
05220      C
05230          SAVE1=1.0D00
05240          SAVE2=1.0D00
05250          NCOUNT=0

```

```

05260 NLOOPS=0
05270 SMEGA1=0.0D00
05280 SMEGA2=0.0D00
05290 NSAVE1=0
05300 NSAVE2=0
05310 SNEW1=0.0D00
05320 SNEW2=0.0D00
05330 C*****
05340 C
05350 C VORTICITY FIELD RELAXATION PARAMETERS.
05360 C
05370 WUTERM=1.0D00
05380 42 CONTINUE
05390 DO 45 I=2,M
05400 DO 45 J=2,NM1
05410 TEMP=REXCOSH/(4.0D00*DSQRT(SINET2(I)*COSH2(J)))
05420 S=(PSI(I,J+1)-PSI(I,J-1))*TEMP/DZETA
05430 Q=(PSI(I+1,J)-PSI(I-1,J))*TEMP/DETA
05440 45 WU(I,J)=1.0D00/(1.0D00+DSQRT((S*S+Q*Q)/2.0D00))
05450 C
05460 C*****
05470 IF(IOUT.NE.0) WRITE(6,1002)
05480 C
05490 C INITIALIZE PARAMETERS FOR NEW LOOP.
05500 C
05510 50 BIGG=0.0D00
05520 BIGPSI=0.0D00
05530 SUMPSI=0.0D00
05540 SUNG=0.0D00
05550 IG=0
05560 JG=0
05570 IPSI=0
05580 JPSI=0
05590 NG=0
05600 NPSI=0

```

```

05610 C *****
05620 C ***** BOUNDARY CONDITION AT THE SURFACE OF SPHEROID. VALUES CHANGE WITH
05630 C ***** EACH ITERATION.
05640 C *****
05650 C *****
05660 DO 60 I=1,MPI
05670 G(I,1)=(-2.0D00*PSI(I,2)+PSI(I,3))/DZETA2
05680 G(I,1)=G(I,1)*COSH02/(COSH02-SINET2(I))
05690 60 CONTINUE
05700 C *****
05710 C *****
05720 C ***** BEGIN LOOP.
05730 C *****
05740 C *****
05750 C *****
05760 C *****
05770 DO 100 I=2,M
05780 DO 100 J=2,NM1
05790 C *****
05800 C ***** CALCULATE NEW STREAM FIELD.
05810 C *****
05820 C *****
05830 C *****
05840 STRMF=PSI(I,J+1)*COEF1(J)+PSI(I,J-1)*COEF2(J)+PSI(I+1,J)*COEF3(I)
05850 STRMF=STRMF+PSI(I-1,J)*COEF4(I)
05860 STRMF=COEF0*(STRMF-G(I,J)*(COSH22(J)-SINET2(I))/COSH02)
05870 DIFF=STRMF-PSI(I,J)
05880 C *****
05890 C *****
05900 C ***** DO NOT USE G-S METHOD TO CALCULATE PSI(I,2).
05910 IF(J.EQ.2) DIFF=0.0D00
05920 C *****
05930 C *****
05940 C *****
05950 C ***** CALCULATE NEW VORTICITY FIELD.

```

```

05960 C
05970 C
05980 C
05990 C
06000 C
06010 C
06020 C
06030 C
06040 C
06050 C
06060 C
06070 C
06080 C
06090 C
06100 C
06110 C
06120 C
06130 C
06140 C
06150 C
06160 C
06170 C
06180 C
06190 C
06200 C
06210 C
06220 C
06230 C
06240 C
06250 C
06260 C
06270 C
06280 C
06290 C
06300 C

      C1=COEF5*DSQRT(COSH22(J)*SINET2(I))

      USE FORWARD DIFFERENCE FOR PARTIAL DG/DN AT I=2 ONLY.
      USE BACKWARD DIFFERENCE FOR PARTIAL DG/DN AT I=M ONLY.
      IF(I.EQ.2) GO TO 70
      IF(I.EQ.M) GO TO 71

      FOUR2=1.0D00
      FOURM=1.0D00
      VORT=0.0D00
      COEFX=1.0D00

      ASM=COSH22(J)*SINET2(I-1)/COSH02
      ASP=COSH22(J)*SINET2(I+1)/COSH02
      65 CONTINUE
      A6M=COSH22(J-1)*SINET2(I)/COSH02
      A6P=COSH22(J+1)*SINET2(I)/COSH02

      C4ASM=COEF4(I)+FOURM*C1*(PSI(I,J+1)-PSI(I,J-1))/ASM
      C2A6M=COEF2(J)-C1*(PSI(I+1,J)-PSI(I-1,J))/A6M
      C1A6P=COEF1(J)+C1*(PSI(I+1,J)-PSI(I-1,J))/A6P
      C3ASP=COEF3(I)-FOUR2*C1*(PSI(I,J+1)-PSI(I,J-1))/ASP

      VORT=VORT+G(I-1,J)*C4ASM+G(I,J-1)*C2A6M+G(I,J+1)*C1A6P+G(I+1,J)*C3
      $ASP
      VORT=COEF0*VORT*COEFX
      DIFFG=VORT-G(I,J)
      GO TO 75
      C*****
      70 ASP2=COSH22(J)*SINET2(4)/COSH02

```

```

06310 CIEQ2=C1*(PSI(2,J+1)-PSI(2,J-1))/A5P2
06320 A5M=1.0D00
06330 A5P=COSH22(J)*SINET2(3)/COSH02
06340 COEFX=1.0D00/COEF0-C1*3.0D00*(PSI(2,J+1)-PSI(2,J-1))/(COSH22(J)*SI
06350 $NET2(2)/COSH02)
06360 COEFX=1.0D00/(COEF0*COEFX)
06370 FOUR2=4.0D00
06380 FOURM=0.0D00
06390 VORT=G(4,J)*CIEQ2
06400 GO TO 65
06410 C
06420 71 A5M2=COSH22(J)*SINET2(I-2)/COSH02
06430 CIEQM=C1*(PSI(M,J+1)-PSI(M,J-1))/A5M2
06440 A5P=1.0D00
06450 A5M=COSH22(J)*SINET2(M-1)/COSH02
06460 COEFX=1.0D00/COEF0+C1*3.0D00*(PSI(M-1,J+1)-PSI(M-1,J-1))/(COSH22(J
06470 $)*SINET2(2)/COSH02)
06480 COEFX=1.0D00/(COEF0*COEFX)
06490 FOUR2=0.0D00
06500 FOURM=4.0D00
06510 VORT=-G(M-2,J)*CIEQM
06520 GO TO 65
06530 C
06540 C*****
06550 C
06560 75 CONTINUE
06570 RESDUL=DABS(DIFFG/VORT)
06580 SUMG=SUMG+DABS(DIFFG)
06590 IF(RESDUL.LE.EPS) GO TO 80
06600 NG=NG+1
06610 IF(RESDUL.LE.BIGG) GO TO 80
06620 BIGG=RESDUL
06630 IG=I
06640 JG=J
06650 80 CONTINUE

```

```

06660 RESDUL=DABS(DIFF/STRMF)
06670 SUMPSI=SUMPSI+DABS(DIFF)
06680 IF(RESDUL.LE.EPS) GO TO 90
06690 NPSI=NPSI+1
06700 IF(RESDUL.LE.BIGPSI) GO TO 90
06710 BIGPSI=RESDUL
06720 IPSI=I
06730 JPSI=J
06740 90 CONTINUE
06750 C
06760 C UPDATE STREAM FIELD AND VORTICITY FUNCTION.
06770 C
06780 PSI(I,J)=PSI(I,J)+WS*DIFF
06790 G(I,J)=G(I,J)+WVTERM*WV(I,J)*DIFFG
06800 100 CONTINUE
06810 DO 102 I=2,M
06820 STRMF=PSI(I,3)/4.0D00
06830 DIFF=STRMF-PSI(I,2)
06840 RESDUL=DABS(DIFF/STRMF)
06850 SUMPSI=SUMPSI+DABS(DIFF)
06860 IF(RESDUL.LE.EPS) GO TO 101
06870 NPSI=NPSI+1
06880 IF(RESDUL.LE.BIGPSI) GO TO 101
06890 BIGPSI=RESDUL
06900 IPSI=I
06910 JPSI=2
06920 101 PSI(I,2)=STRMF
06930 102 CONTINUE
06940 C*****
06950 C CONVERGENCE CHECKED AND RELAXATION PARAMETER ADJUSTED, HERE TO 197.
06960 C*****
06970 C
06980 C INCREMENT LOOP PARAMETER.
06990 NCOUNT=NCOUNT+1
07000 NLOOPS=NLOOPS+1

```

AD-A106 766

AIR FORCE INST OF TECH WRIGHT-PATTERSON AFB OH  
GRAVITATIONAL AGGLOMERATION OF POST-HCDA LMFBF NONSPHERICAL AER--ETC(U)  
DEC 80 R F TUTTLE  
AFIT-CI-80-82D

F/G 13/7

UNCLASSIFIED

NL

3-3  
Cochran

END

DATE

FILED

11-81

DTIC

```

07010 C CALCULATE NORM RATIOS OF EACH FIELD.
07020 OMEGA1=SUMG/SAVE1
07030 SAVE1=SUMG
07040 OMEGA2=SUMPSI/SAVE2
07050 SAVE2=SUMPSI
07060 C CALCULATE SUM OF THE NEWEST 25 SUMG AND SUMPSI TERMS.
07070 C USE LATER TO CHECK ON CONVERGENCE.
07080 C
07090 SNEW1=SNEW1+SUMG
07100 SNEW2=SNEW2+SUMPSI
07110 C
07120 IF(IDOUT.EQ.0) GO TO 160
07130 C
07140 WRITE(6,1001)NLOOPS,NPSI,WS,SUMPSI,BIGPSI,IPSI,JPSI,NG,WVTERM,SUMG
07150 $,BIGG,IG,JG
07160 C CHECK FOR CONVERGENCE.
07170 C
07180 160 IF(NG.EQ.0.AND.NPSI.EQ.0) GO TO 200
07190 C
07200 C CALCULATE RELAXATION PARAMETERS EVERY 25 ITERATION.
07210 C
07220 IF(OMEGA1.LE.1.0D00) GO TO 170
07230 IF(NCOUNT.LT.25) GO TO 180
07240 GO TO 175
07250 170 SMEGA1=SMEGA1+OMEGA1
07260 NSAVE1=NSAVE1+1
07270 IF(NCOUNT.LT.25) GO TO 180
07280 175 IF(NSAVE1.EQ.0) NSAVE1=1
07290 OMEGA1=SMEGA1/DFLOAT(NSAVE1)
07300 WVTERM=2.0D00/(1.0D00+DSQRT(1.0D00-OMEGA1))
07310 C
07320 180 CONTINUE
07330 IF(OMEGA2.LE.1.0D00) GO TO 190
07340 IF(NCOUNT.LT.25) GO TO 195
07350 GO TO 193

```



```

07360      190 SMEGA2=SMEGA2+OMEGA2
07370      NSAVE2=NSAVE2+1
07380      IF(NCOUNT,LT.25) GO TO 195
07390      193 NCOUNT=0
07400      IF(NSAVE2.EQ.0) NSAVE2=1
07410      OMEGA2=SMEGA2/DFLOAT(NSAVE2)
07420      WS=2.0D00/(1.0D00+DSQRT(1.0D00-OMEGA2))
07430      195 CONTINUE
07440      IF(NLOOPS,LT.2000) GO TO 196
07450      IF(SOLD1,GT.SNEW1,AND,SOLD2,GT.SNEW2) NLOOPS=1800
07460      IF(NLOOPS.EQ.1800) GO TO 197
07470      WRITE(6,1003) RE,AR,NPSI,NG
07480      JSTART=10
07490      RETURN
07500      196 IF(NCOUNT,NE.0) GO TO 197
07510      SOLD2=SNEW2
07520      SNEW2=0.0D00
07530      SOLD1=SNEW1
07540      SNEW1=0.0D00
07550      GO TO 42
07560      197 GO TO 50
07570      200 CONTINUE
07580      C*****
07590      C
07600      C CALCULATE DRAG COEFFICIENTS.
07610      C
07620      C*****
07630      C SURFACE VORTICITY
07640      C
07650      SVORT(1)=0.0D00
07660      SVORT(MPI)=0.0D00
07670      DO 210 I=2,M
07680      210 SVORT(I)=G(I,1)/DSQRT(SINET2(I))
07690      C
07700      C

```

```

07710 C   FRONTAL STAGNATION PRESSURE
07720 C
07730     PRESS(1)=0.0D00
07740     ND2=N/2
07750     SIN2=DSQRT(SINET2(2))
07760     SIN3=DSQRT(SINET2(3))
07770     DO 220 I=1,ND2
07780     TEMP=(4.0D00*G(2,2*I-1)/SIN2-G(3,2*I-1)/SIN3)/DSQRT(COSH2(2*I-1))
07790     TEMP=TEMP+4.0D00*(4.0D00*G(2,2*I)/SIN2-G(3,2*I)/SIN3)/DSQRT(COSH2
07800     $(2*I))
07810     TEMP=TEMP+(4.0D00*G(2,2*I+1)/SIN2-G(3,2*I+1)/SIN3)/DSQRT(COSH2(2*
07820     $I+1))
07830     220 PRESS(1)=PRESS(1)+TEMP
07840     PRESS(1)=1.0D00+PRESS(1)*4.0D00*COSH0*DZETA/(3.0D00*DETA*RE)
07850 C
07860 C
07870 C   SURFACE PRESSURE DISTRIBUTION.
07880 C
07890     TEMP=0.0D00
07900     TANHZ=DSQRT((COSH2(1)-1.0D00)/COSH2(1))
07910     COSH2=DSQRT(COSH2(2))
07920     COSH3=DSQRT(COSH2(3))
07930     DO 230 I=2,M
07940     SAVE=TEMP
07950     TEMP=(4.0D00*G(1,2)/COSH2-G(1,3)/COSH3-3.0D00*G(1,1)/COSH0)
07960     TEMP=TEMP/DSQRT(SINET2(1))*COSH0/(2.0D00*DZETA)
07970     TEMP=TEMP+SUORT(I)*TANHZ
07980     230 PRESS(I)=PRESS(I-1)+2.0D00*DETA*(SAVE+TEMP)/RE
07990     PRESS(MP1)=PRESS(M)+2.0D00*DETA*TEMP/RE
08000 C
08010 C
08020 C   PRESSURE DRAG COEFFICIENT.
08030 C
08040     CDP=0.0D00
08050     TEMP=0.0D00

```

```

08060      DO 240 I=2,M,2
08070      ETA=PI*(DFLOAT(I-1)/DFLOAT(MP1-1))
08080      SAVE=TEMP
08090      TEMPP=PRESS(I)*DSQRT(SINET2(I))*DCOS(ETA)
08100      TEMP=PRESS(I+1)*DSQRT(SINET2(I+1))*DCOS(ETA+DETA)
08110      240 CDP=CDP+SAVE+4.0D00*TEMPP+TEMP
08120      CDP=2.0D00*CDP*DETA/3.0D00
08130 C
08140 C
08150 C SKIN DRAG COEFFICIENT.
08160 C
08170      CDF=0.0D00
08180      TEMP=0.0D00
08190      DO 250 I=2,M,2
08200      SAVE=TEMP
08210      TEMPP=G(I,1)*DSQRT(SINET2(I))
08220      TEMP=G(I+1,1)*DSQRT(SINET2(I+1))
08230      250 CDF=CDF+SAVE+4.0D00*TEMPP+TEMP
08240      CDF=8.0D00*DETA*TANH2*CDF/(3.0D00*RE)
08250 C
08260 C
08270 C TOTAL DRAG COEFFICIENT.
08280 C
08290      CDTOTL=GDP+CDF
08300 C
08310      IF(II.NE.0) GO TO 500
08320      REWIND 8
08330      WRITE(8) ((PSI(I,J),I=1,MP1),J=1,N)
08340      WRITE(8) ((G(I,J),I=1,MP1),J=1,N)
08350      WRITE(8) CDTOTL,RE,AR
08360      END FILE 8
08370 C
08380      IF(IOUT.EQ.0) RETURN
08390 C
08400 C OUTPUT RESULTS.

```

```

08410 C
08420 WRITE(6,1000) AR,RE,CDP,CDF,CDTOTL
08430 C
08440 WRITE(6,1007)
08450 WRITE(6,1008) MP1,N,DETA,RE,DZETA,EPS,AR
08460 WRITE(6,1009) RE
08470 JJJ=0
08480 7000 JJ=JJJ+1
08490 JJJ=JJ+9
08500 IF(JJJ.GE.N)JJJ=N
08510 DO 8000 J=1,10
08520 JL=JJ-1+J
08530 8000 LXI(J)=JL
08540 WRITE(6,1004) (LXI(J),J=1,10)
08550 DO 9000 I=1,MP1
08560 9000 WRITE(6,1005) (PSI(I,J),J=JJ,JJJ)
08570 IF(JJJ.LT.N) GO TO 7000
08580 C
08590 C
08600 WRITE(6,1006) RE
08610 JJJ=0
08620 10000 JJ=JJJ+1
08630 JJJ=JJ+9
08640 IF(JJJ.GE.N) JJJ=N
08650 DO 11000 J=1,10
08660 JL=JJ-1+J
08670 11000 LXI(J)=JL
08680 WRITE(6,1004) (LXI(J),J=1,10)
08690 DO 12000 I=1,MP1
08700 12000 WRITE(6,1005) (G(I,J),J=JJ,JJJ)
08710 IF(JJJ.LT.N) GO TO 10000
08720 500 RETURN
08730 C
08740 C
08750 1000 FORMAT('0','AXIS RATIO=',G10.3,5X,'REYNOLDS NUMBER=',G10.3,5X,'PRE

```

```

08760 $SSURE DRAG COEF='G12.4,5X,'SKIN DRAG COEF='G12.4,/, ' **TOTAL DR
08770 $AG COEF**='G12.4)
08780 1001 FORMAT(' ',I5,2(I5,3G15.8,'(','I2',' ',I2,''))))
08790 1002 FORMAT(' ',NLOOPS,NPSI,'6X,'WS',10X,'SUMPSI',10X,
08800 $'BIGPSI(I,J)',10X,'NG',4X,'WUTERM',10X,'SUMG',
08810 $10X,'BIGG(I,J)')
08820 1003 FORMAT('0','NO CONVERGENCE ACHIEVED','RE='G10.3,5X,'AR='G10.3,5X
08830 $,'NPSI='I3,5X,'NG='I3)
08840 1004 FORMAT('0','6X,I3,9(10X,I3))
08850 1005 FORMAT(' ',10(2X,G11.5))
08860 1006 FORMAT('1',' MODIFIED VORTICITY (REYNOLDS NUMBER APPROXIMATELY E
08870 $QUAL TO 'G10.3,'))
08880 1007 FORMAT('1',' OUTPUT FROM SUBROUTINE OBLATE. STREAM FUNCTION AN
08890 $D VORTICITY FIELDS CALCULATED USING NAVIER-STOKES EQUATION')
08900 1009 FORMAT('0',' STREAM FUNCTION (REYNOLDS NUMBER APPROXIMATELY EQUA
08910 $L TO 'G10.3,'))
08920 1008 FORMAT(' NUMBER OF ANGULAR STEPS='G12.4,/,
08930 $' NUMBER OF RADIAL POINTS='G12.4,/,
08940 $' ANGULAR STEP SIZE='G12.4,/,
08950 $' REYNOLDS NUMBER='G12.4,/,
08960 $' RADIAL STEP SIZE='G12.4,/,
08970 $' ERROR CRITERIA FOR CONV.='G12.4,/,
08980 $' AXIS RATIO='G12.4,/)
08990 END
09000 SUBROUTINE SIZE(JSTART,II)
09010 IMPLICIT REAL*8(A-H,O-Z)
09020 REAL*8 MU,LAMBDA,LYK,LYK1,LYKV1,IARI,IRIV,INTIA
09030 COMMON PI,GV,R,EFS,DISK,BRHO,GAMMA,ERR,CLL,UINF,DENS1,ALPHA1
09040 COMMON/AIR/ MU,RHO,LAMBDA
09050 COMMON/NAVIER/DZETA,MP1,N,NSF,IOUT,MATRX,JDERIV
09060 COMMON/SWITCH/AR,CDTOIL,AXIS,STK,LYK,INTIA,VINF,RE
09070 COMMON/OBLAT$/ PSI(100,100),G(100,100)
09080 DIMENSION A(20),REYNDS(20),C(19,3),BPAR(4),U(1),S(1)
09090 DIMENSION LXI(10)
09100 IF(JSTART.EQ.2) I=0

```

```

09110 JSTART=3
09120 I=I+1
09130 IF(I.GT.20) GO TO 80
09140 ASEMI=3.0D00*MU*MU*CDTOTL*RE*RE
09150 ASEMI=ASEMI/(32.0D00*GV*(DENS1*ALPHA1-RHO)*RHO)
09160 X=1.0D00/3.0D00
09170 ASEMI=ASEMI**X
09180 IF(IOUT.NE.0) WRITE(6,2000) AR,RE,CDTOTL,ASEMI
09190 DIFF=ASEMI-AXIS
09200 IF(DABS(DIFF/AXIS).LE.EPS*1.0D-02) GO TO 70
09210 C
09220 C
09230 IF(I.GE.3) GO TO 30
09240 IF(I.EQ.2) GO TO 10
09250 A(1)=ASEMI
09260 REYNDS(1)=RE
09270 IF(DIFF.LT.0.0D00) RE=RE+0.2D00*RE
09280 IF(DIFF.GT.0.0D00) RE=RE-0.2D00*RE
09290 RETURN
09300 C
09310 C
09320 C
10 A(2)=ASEMI
REYNDS(2)=RE
IF(A(1).LT.A(2)) GO TO 20
TEMP=A(1)
A(1)=A(2)
A(2)=TEMP
09330 C
09340 C
09350 C
09360 C
09370 C
09380 C
09390 C
TEMP=REYNDS(1)
REYNDS(1)=REYNDS(2)
REYNDS(2)=TEMP
09400 C
09410 C
09420 C
09430 C
09440 C
09450 C
20 RE=(REYNDS(2)-REYNDS(1))/(A(2)-A(1))

```

```

09460 RE=RE*(AXIS-A(1))+REYNDS(1)
09470 RETURN
09480 C
09490 C
09500 C
09510 30 A(I)=ASEMI
09520 REYNDS(I)=RE
09530 J=I
09540 40 IF(A(J-1).LT.A(J)) GO TO 50
09550 TEMP=A(J-1)
09560 A(J-1)=A(J)
09570 A(J)=TEMP
09580 C
09590 TEMP=REYNDS(J-1)
09600 REYNDS(J)=REYNDS(J)
09610 REYNDS(J)=TEMP
09620 C
09630 J=J-1
09640 IF(J.GE.2) GO TO 40
09650 C
09660 C
09670 C
09680 50 DO 60 J=1,4
09690 60 BPAR(J)=0.0D00
09700 C
09710 C
09720 CALL ICSICU(A,REYNDS,I,BPAR,C,19,IER)
09730 U(1)=AXIS
09740 CALL ICSEVU(A,REYNDS,I,C,19,U,S,1,IER)
09750 RE=S(1)
09760 RETURN
09770 C
09780 C
09790 C
09800 70 JSTART=4

```

```

09810      REMIND 9
09820      WRITE(9) ((PSI(I,J),I=1,MP1),J=1,N)
09830      WRITE(9) ((G(I,J),I=1,MP1),J=1,N)
09840      WRITE(9) CDTOTL,RE,AR
09850      IF(IOUT.EQ.0) RETURN
09860      C
09870      WRITE(6,1007)
09880      WRITE(6,1008) MP1,N,DETA,RE,DZETA,EPS,AR
09890      WRITE(6,1009) RE
09900      JJJ=0
09910      JJ=JJJ+1
09920      JJJ=JJ+9
09930      IF(JJJ.GE.N) JJJ=N
09940      DO 8000 J=1,10
09950      JL=JJ-1+J
09960      LXI(J)=JL
09970      WRITE(6,1004) (LXI(J),J=1,10)
09980      DO 9000 I=1,MP1
09990      WRITE(6,1005) (PSI(I,J),J=JJ,JJJ)
10000      IF(JJJ.LT.N) GO TO 7000
10010      C
10020      C
10030      WRITE(6,1006) RE
10040      JJJ=0
10050      JJ=JJJ+1
10060      JJJ=JJ+9
10070      IF(JJJ.GE.N) JJJ=N
10080      DO 11000 J=1,10
10090      JL=JJ-1+J
10100      LXI(J)=JL
10110      WRITE(6,1004) (LXI(J),J=1,10)
10120      DO 12000 I=1,MP1
10130      WRITE(6,1005) (G(I,J),J=JJ,JJJ)
10140      IF(JJJ.LT.N) GO TO 10000
10150      RETURN

```



```

10160 C
10170 C
10180 C
10190 C
10200 C
10210 80 JSTART=2
10220 RETURN
10230 C
10240 1003 FORMAT('0','NO CONVERGENCE ACHIEVED','RE=',G10.3,5X,'AR=',G10.3,5X
10250 $,'NPSI=',I3,5X,'NG=',I3)
10260 1004 FORMAT('0',6X,I3,9(10X,I3))
10270 1005 FORMAT(' ',10(2X,G11.5))
10280 1006 FORMAT('1',' MODIFIED VORTICITY (REYNOLDS NUMBER APPROXIMATELY E
10290 $EQUAL TO ',G11.3,')')
10300 1007 FORMAT('1',' OUTPUT FROM SUBROUTINE OBLATE. STREAM FUNCTION AN
10310 $D VORTICITY FIELDS CALCULATED USING NAVIER-STOKES EQUATION')
10320 1008 FORMAT(' NUMBER OF ANGULAR STEPS=',G12.4,/,
10330 $' NUMBER OF RADIAL POINTS=',G12.4,/,
10340 $' ANGULAR STEP SIZE=',G12.4,/,
10350 $' REYNOLDS NUMBER=',G12.4,/,
10360 $' RADIAL STEP SIZE=',G12.4,/,
10370 $' ERROR CRITERIA FOR CONV.= ',G12.4,/,
10380 $' AXIS RATIO=',G12.4,/)
10390 1009 FORMAT('0',' STREAM FUNCTION (REYNOLDS NUMBER APPROXIMATELY EQUA
10400 $L TO ',G10.3,')')
10410 2000 FORMAT('0','FROM SUBROUTINE SIZE: AR=',G12.5,5X,'RE=',G12.5,5X,
10420 $'CDTOTL=',G12.5,5X,'ASEMI=',G12.5)
10430 END
10440 SUBROUTINE MATRIX(COEF5,NLOOPS)
10450 IMPLICIT REAL*8(A-H,O-Z)
10460 COMMON PI,GV,R,EPS,DISK,BRHO,GAMMA,ERR,CLL,UINF,DENS1,ALPHA1
10470 COMMON/OBLAT$/ PSI(100,100),G(100,100)
10480 COMMON/WORK/COSH22(100),SINET2(100),COEF1(100),COEF2(100),COEF3(10
10490 $0),COEF4(100),SVORT(5000),PRESS(5000),VECTOR(5000)
10500 DIMENSION B(100,100),COEF(20,20),Z(100),IPUT(100)

```

```

10510 EQUIVALENCE (COEF(1),SVORT(1)),(Z(1),PRESS(1))
10520 EQUIVALENCE (COSH02,COSH22(1))
10530 C
10540 C INITIALIZE PARMETERS
10550 NM1=N-1
10560 M=MP1-1
10570 NORDER=(MP1-2)*(N-2)
10580 IF(NLOOPS.EQ.0) ISTOP=0
10590 C
10600 WRITE(6,1000)
10610 C
10620 C BEGIN ANALYSIS OF VORTICITY FIELD MATRIX
10630 L=0
10640 II=2
10650 JJ=2
10660 C SET ALL ELEMENTS OF ROW L IN JACOBI MATRIX
10670 10 DO 20 I=1,MP1
10680 DO 20 J=1,N
10690 20 COEF(I,J)=0.0D00
10700 C GENERATE THE NON-ZERO ENTRIES IN JACOBI ROW L.
10710 C1=COEF5*DSQRT(COSH22(JJ)*SINET2(II))
10720 C
10730 IF(II.EQ.2) GO TO 40
10740 IF(II.EQ.M) GO TO 45
10750 C
10760 A5M=COSH22(JJ)*SINET2(II-1)/COSH02
10770 A5P=COSH22(JJ)*SINET2(II+1)/COSH02
10780 30 CONTINUE
10790 A6M=COSH22(JJ-1)*SINET2(II)/COSH02
10800 A6P=COSH22(JJ+1)*SINET2(II)/COSH02
10810 C
10820 C4A5M=COEF4(II)+C1*(PSI(II,JJ+1)-PSI(II,JJ-1))/A5M
10830 C2A6M=COEF2(JJ)-C1*(PSI(II+1,JJ)-PSI(II-1,JJ))/A6M
10840 C1A6P=COEF1(JJ)+C1*(PSI(II+1,JJ)-PSI(II-1,JJ))/A6P
10850 C3A5P=COEF3(II)-C1*(PSI(II,JJ+1)-PSI(II,JJ-1))/A5P

```

```

10860
10870 C
10880 C
10890
10900
10910
10920
10930
10940
10950 C
10960 C
10970
10980
10990
11000
11010 C
11020
11030
11040
11050
11060
11070
11080
11090
11100
11110
11120
11130
11140
11150
11160
11170
11180
11190
11200

      GO TO 50

40 ASM=COSH22(JJ)*SINET2(2)/COSH02
   ASP=COSH22(JJ)*SINET2(4)/COSH02
      GO TO 30

45 ASM=COSH22(JJ)*SINET2(II-2)/COSH02
   ASP=COSH22(JJ)*SINET2(II)/COSH02
      GO TO 30

50 IF(II-1.GT.1) COEF(II-1,JJ)=C4A5M
   IF(JJ-1.GT.1) COEF(II,JJ-1)=C2A6M
   IF(JJ+1.LT.N) COEF(II,JJ+1)=C1A6P
   IF(II+1.LT.MP1) COEF(II+1,JJ)=C3A5P
      L=L+1
      K=0
      SUM=0.0D00
      LF=0
      DO 60 I=2,M
      DO 60 J=2,NM1
      K=K+1
      B(L,K)=COEF(I,J)
      IF(B(L,K).EQ.0.0D00) GO TO 60
      LF=LF+1
      IF(LF.EQ.1) WRITE(6,2000) B(L,K),L,K
      IF(LF.EQ.2) WRITE(6,2001) B(L,K),L,K
      IF(LF.EQ.3) WRITE(6,2002) B(L,K),L,K
      IF(LF.EQ.4) WRITE(6,2003) B(L,K),L,K
      SUM=SUM+DABS(B(L,K))
      WRITE(6,2004) SUM
      JJ=JJ+1
      IF(JJ.LE.NM1) GO TO 10
      JJ=2
60

```

```

11210      II=II+1
11220      IF(II.LE.M) GO TO 10
11230      C
11240      C
11250      75 CALL DGECC(B,100,NORDER,IPVT,RCOND,Z)
11260      XLARGE=0.0
11270      DO 80 I=1,NORDER
11280      IF(DABS(B(I,I)).GT.XLARGE) XLARGE=DABS(B(I,I))
11290      80 CONTINUE
11300      WRITE(6,2005) XLARGE,RCOND
11310      WRITE(6,2006)
11320      WRITE(6,2007) (B(I,I),I=1,NORDER)
11330      C
11340      C*****
11350      C
11360      IF(ISTOP.EQ.1) RETURN
11370      C
11380      C*****
11390      C
11400      CONTINUE
11410      C ANALYSIS OF STREAM FUNCTION MATRIX
11420      L=0
11430      II=2
11440      JJ=2
11450      WRITE(6,1001)
11460      C
11470      100 DO 110 I=1,MP1
11480      DO 110 J=1,N
11490      110 COEF(I,J)=0.0D00
11500      IF(II-1.GT.1) COEF(II-1,JJ)=COEF4(II)
11510      IF(JJ-1.GT.1) COEF(II,JJ-1)=COEF2(JJ)
11520      IF(JJ+1.LT.N) COEF(II,JJ+1)=COEF1(JJ)
11530      IF(II+1.LT.MP1) COEF(II+1,JJ)=COEF3(II)
11540      C
11550      L=L+1

```

```

11560      K=0
11570      SUM=0.0D00
11580      LF=0
11590      DO 120 I=2,M
11600      DO 120 J=2,NM1
11610      K=K+1
11620      B(L,K)=COEF(I,J)
11630      IF(B(L,K).EQ.0.0D00) GO TO 120
11640      LF=LF+1
11650      IF(LF.EQ.1) WRITE(6,2000) B(L,K),L,K
11660      IF(LF.EQ.2) WRITE(6,2001) B(L,K),L,K
11670      IF(LF.EQ.3) WRITE(6,2002) B(L,K),L,K
11680      IF(LF.EQ.4) WRITE(6,2003) B(L,K),L,K
11690      120 SUM=SUM+DABS(B(L,K))
11700      WRITE(6,2004) SUM
11710      JJ=JJ+1
11720      IF(JJ.LE.NM1) GO TO 100
11730      JJ=2
11740      II=II+1
11750      IF(II.LE.M) GO TO 100
11760      C
11770      C FIND EIGENVALUES AND RECIPROCAL CONDITION NUMBER
11780      ISTOP=1
11790      GO TO 75
11800      C
11810      C
11820      1000 FORMAT('1','VORTICITY FIELD JACOBI MATRIX',/,
11830      $ 'NON-ZERO ELEMENTS',92X,'OFF DIAGONAL SUM')
11840      1001 FORMAT('1','STREAM FIELD JACOBI MATRIX',/,
11850      $ 40X,'NON-ZERO ELEMENTS',52X,'OFF DIAGONAL SUM')
11860      2000 FORMAT('0',G15.8,' (',I2,',',I2,',')')
11870      2001 FORMAT('+',28X,G15.8,' (',I2,',',I2,',')')
11880      2002 FORMAT('+',56X,G15.8,' (',I2,',',I2,',')')
11890      2003 FORMAT('+',84X,G15.8,' (',I2,',',I2,',')')
11900      2004 FORMAT('+',112X,G15.8)

```



```

12260 C
12270 IC=100
12280 BPAR(1)=1.0D00
12290 BPAR(2)=1.0D00
12300 BPAR(3)=1.0D00
12310 BPAR(4)=1.0D00
12320 DO 100 I=1,100
12330 DO 100 J=1,100
12340 100 UETA(I,J)=0.0D00
12350 C
12360 DZETA2=DZETA*DZETA
12370 DELTA=PI/DFLOAT(MP1-1)
12380 DELTA2=DELTA*DELTA
12390 C
12400 C DEVICE 8 CONTAINS THE RESULTS FORM OBLATE.FORT, SOLUTION OF NAVIER-
12410 C STOKES EQUATION FOR AN OBLATE SPHERIOD.
12420 C DEVICE 9 CONTAINS THE RESULTS FORM OBLATE.FORT, SOLUTION OF NAVIER-
12430 C STOKES EQUATION FOR A SPHERE.
12440 REWIND 8
12450 REWIND 9
12460 REWIND 10
12470 REWIND 11
12480 NDISK=8
12490 IF(II.GT.1) NDISK=9
12500 READ(NDISK) ((PSI(I,J),I=1,MP1),J=1,N)
12510 C CALCULATE NEEDED CONSTANTS FOR VELOCITY FIELD.
12520 ZETA0=DLOG((1.0+AR)/(1.0-AR))/2.0
12530 COSH02=DCOSH(ZETA0)**2
12540 C
12550 IF(JDERIV.NE.0) GO TO 300
12560 C
12570 C*****
12580 C
12590 C FROM HERE TO STATEMENT #4 THE ZETA VELOCITY COMPONENTS ARE CALCULATED
12600 C FOR EACH GRID POINT.

```

```

12610 C *****
12620 C *****
12630 C NX=MP1
12640 C ABSCISSAE DATA POINTS NEEDED FOR ICSICU AND IDERIV
12650 C DO 1 I=1,MP1
12660 C 1 X(I)=PI*(DFLOAT(I-1)/DFLOAT(MP1-1))
12670 C
12680 C DO 4 J=1,N
12690 C VALUES NEEDED TO CALCULATE UZETA(I,J).
12700 C ZETA=ZETA0+UZETA*DFLOAT(J-1)
12710 C COSHZ=DCOSH(ZETA)
12720 C SINHZ2=DSINH(ZETA)**2
12730 C
12740 C DO 2 I=1,MP1
12750 C 2 Y(I)=PSI(I,J)
12760 C ESTIMATE END CONDITION PARAMETERS BPAR(I),I=1,4(SUBROUTINE ICSICU).
12770 C USE THE CONDITION WHICH WILL CAUSE THE CUBIC SPLINE TO HAVE FIRST
12780 C DERIVATIVES EQUAL TO ZERO AT EACH END POINT.
12790 C
12800 C LEFT CONDITION.
12810 C
12820 C BPAR(2)=6.0D00*(Y(2)-Y(1))/DETA2
12830 C
12840 C RIGHT CONDITION.
12850 C
12860 C BPAR(4)=-6.0D00*(Y(MP1)-Y(MP1-1))/DETA2
12870 C
12880 C NX=MP1
12890 C IC.GE.NX-1
12900 C GET THE COEFFICIENTS FOR SPLINES.
12910 C CALL ICSICU(X,Y,NX,BPAR,C,IC,IER)
12920 C CALCULATE THE DERIVATIVES OF THE SPLINES AT GRID POINTS, IE, D(PSI)/D
12930 C ETA, ZETA HELD CONSTANT.
12940 C CALL IDERIV(X,Y,NX,C,IC,X,VRZ,NX,IER)
12950 C VELOCITY COMPONENTS OF ZETA ARE DETERMINED.

```



```

12960      MAX=NX-1
12970      DO 3 I=2,MAX
12980      3 UZETA(I,J)=-VRZ(I)*COSH02/(COSH2*DSIN(X(I))*DSQRT(SINH22+DCOS(X(I)
12990      $)**2))
13000 C
13010 C
13020 C VELOCITY COMPONENTS OF ZETA ARE DETERMINED ALONG AXIS OF SYMMETRY.
13030 C USE GREGORY-NEWTON INTERPOLATION FORMULAS.
13040 C
13050 C
13060 C EXTRAPLATE WITH G-N FORWARD FORMULA.
13070 C
13080 C      UZETA(1,J)=3.0D00*(UZETA(2,J)-UZETA(3,J))+UZETA(4,J)
13090 C
13100 C EXTRAPLATE WITH G-N BACKWARD FORMULA.
13110 C
13120 C      UZETA(MP1,J)=3.0D00*(UZETA(MAX,J)-UZETA(MAX-1,J))+UZETA(MAX-2,J)
13130 C
13140 C
13150 C      4 CONTINUE
13160 C *****
13170 C
13180 C DETERMINE UETA VELOCITY COMPONENTS FOR GRID.
13190 C
13200 C *****
13210 C      NX=N
13220 C      MAX=MP1-1
13230 C      DO 5 J=1,N
13240 C      5 X(J)=ZETA0+DZETA*DFLOAT(J-1)
13250 C      DO 8 I=2,MAX
13260 C      DETERMINE VALUES NEEDED LATER FOR UETA(I,J).
13270 C      ETA=PI*(DFLOAT(I-1)/DFLOAT(MP1-1))
13280 C      SINETA=DSIN(ETA)
13290 C      COSETA=DCOS(ETA)**2
13300 C      DO 6 J=1,N

```

```

13310 C      6 Y(J)=PSI(I,J)
13320 C      ESTIMATE END CONDITION PARAMETERS BPAR(I),I=1,4( SUBROUTINE ICSICU ).
13330 C      USE SECOND ORDER FORWARD AND BACKWARD DIFFERENCES EXPRESSIONS TO ESTI
13340 C      MATE SECOND DERIVATIVES FOR STREAM FUNCTION.
13350 C
13360 C      LEFT CONDITION.
13370 C
13380 C      SPP1=(2.0D00*Y(1)-5.0D00*Y(2)+4.0D00*Y(3)-Y(4))/DZETA2
13390 C      BPAR(2)=2.0D00*SPP1
13400 C      BPAR(1)=0.0D00
13410 C
13420 C      RIGHT CONDITION.
13430 C
13440 C      SPPN=(-Y(N-3)+4.0D00*Y(N-2)-5.0D00*Y(N-1)+2.0D00*Y(N))/DZETA2
13450 C      BPAR(4)=2.0D00*SPPN
13460 C      BPAR(3)=0.0D00
13470 C
13480 C      NX=N
13490 C      IC,GE,NX-1
13500 C      DETERMINE COEFFICIENTS FOR SPLINES.
13510 C      CALL ICSICU(X,Y,NX,BPAR,C,IC,IER)
13520 C      CALCULATE THE DERIVATIVES OF PSI WITH RESPECT TO ZETA, ETA HELD CONST
13530 C      ANT.
13540 C      CALL IDERIV(X,Y,NX,C,IC,X,VRZ,NX,IER)
13550 C      DO 7 J=1,N
13560 C      7 UETA(I,J)=VRZ(J)*COSH2/(DCOSH(X(J))*SINETA*DSQRT(DSINH(X(J))**2+C
13570 C      $OSETA))
13580 C      UETA(I,1)=0.0D00
13590 C      8 CONTINUE
13600 C      *****
13610 C
13620 C      USE TRANSFORMATION FROM OBLATE SPHEROID COORDINATES TO CYLINDERICAL
13630 C      COORDINATES.
13640 C
13650 C      *****

```

```

13660      MAX=0
13670      DO 10 J=1,N
13680      ZETA=ZETA0+DZETA*DFLOAT(J-1)
13690      COSHZ=DCOSH(ZETA)
13700      SINHZ=DSINH(ZETA)
13710      SINHZ2=SINHZ*SINHZ
13720      DO 9 I=1,MP1
13730      MAX=MAX+1
13740      ETA=PI*(DFLOAT(I-1)/DFLOAT(MP1-1))
13750      C1=COSHZ*DCOS(ETA)
13760      C2=SINHZ*DSIN(ETA)
13770      DENOM=DSQRT(SINHZ2+(C1/COSHZ)**2)
13780      VZZ(MAX)=(UZETA(I,J)*C1-UETA(I,J)*C2)/DENOM
13790      9 VRZ(MAX)=(UZETA(I,J)*C2+UETA(I,J)*C1)/DENOM
13800      10 CONTINUE
13810      C*****
13820      C
13830      C   OUTPUT RESULTS TO LINE PRINTER IF(IOUT.NE.0)
13840      C   OUTPUT RESULTS FOR USE BY SUBROUTINE COLL, STORAGE DEVICE IS DISK
13850      C*****
13860      C*****
13870      C
13880      IF(IOUT.EQ.0) GO TO 200
13890      WRITE(6,998)
13900      WRITE(6,999) AR,RE,MP1,N,DETA,DZETA
13910      WRITE(6,1001)
13920      JJJ=0
13930      11 JJ=JJJ+1
13940      JJJ=JJJ+9
13950      IF(JJJ.GE.N) JJJ=N
13960      DO 12 J=1,10
13970      JL=JJ-1+J
13980      12 LXI(J)=JL
13990      WRITE(6,1007) (LXI(J),J=1,10)
14000      DO 13 NN=1,MP1

```

```

14010      13 WRITE(6,1006) (VZZ(MP1*(J-1)+NN),J=JJ,JJJ)
14020      IF(JJJ.LT.N) GO TO 11
14030      WRITE(6,1002)
14040      JJJ=0
14050      14 JJ=JJJ+1
14060      JJJ=JJ+9
14070      IF(JJJ.GE.N) JJJ=N
14080      DO 15 J=1,10
14090      JL=JJ-1+J
14100      15 LXI(J)=JL
14110      WRITE(6,1007) (LXI(J),J=1,10)
14120      DO 16 NN=1,MP1
14130      16 WRITE(6,1006) (VRZ(MP1*(J-1)+NN),J=JJ,JJJ)
14140      IF(JJJ.LT.N) GO TO 14
14150      200 NDISK=NDISK+2
14160      WRITE(NDISK) (VZZ(I), I=1,MAX)
14170      WRITE(NDISK) (VRZ(I),I=1,MAX)
14180      ENDFILE NDISK
14190      C
14200      RETURN
14210      C
14220      C*****
14230      C
14240      C USE CENTRAL FINITE DIFFERENCE TECHNIQUE TO CALCULATE VELOCITY
14250      C COMPONENTS. DETERMINE ZETA VELOCITY COMPONENT FIRST.
14260      C
14270      C*****
14280      C
14290      C CALCULATE ANGLE ETA AND SIN(ETA) AND COS(ETA)**2 FOR LATER USE.
14300      C
14310      300 DO 17 I=1,MP1
14320      X(I)=PI*(DFLOAT(I-1)/DFLOAT(MP1-1))
14330      Y(I)=DCOS(X(I))**2
14340      17 X(I)=DSIN(X(I))
14350      C

```

```

14360 C CALCULATE ZETA VELOCITY COMPONENTS.
14370 C
14380 MAX=MP1-1
14390 DO 19 J=1,N
14400 ZETA=ZETA0+DZETA*DFLOAT(J-1)
14410 COSHZ=DCOSH(ZETA)
14420 SINHZ2=DSINH(ZETA)**2
14430 DO 18 I=2,MAX
14440 18 UZETA(I,J)=COSH02*(PSI(I-1,J)-PSI(I+1,J))/(2.0D00*AR*CDSHZ**X(
    $I)*DSQRT(SINH22+Y(I)))
14450 UZETA(1,J)=UZETA(2,J)
14460 UZETA(MP1,J)=UZETA(MAX,J)
14470
14480 19 CONTINUE
14490 C*****
14500 C
14510 C DETERMINE ETA VELOCITY COMPONENT.
14520 C
14530 C*****
14540 C
14550 C CALCULATE COORDINATE ZETA AND COSH(ZETA) AND SINH(ZETA)**2 FOR LATER
14560 C USE.
14570 C
14580 DO 20 J=1,N
14590 X(J)=ZETA0+DZETA*DFLOAT(J-1)
14600 Y(J)=DCOSH(X(J))
14610 20 X(J)=DSINH(X(J))**2
14620 C
14630 C CALCULATE ETA VELOCITY COMPONENTS.
14640 C
14650 MAX=MP1-1
14660 NX=N-1
14670 DO 22 I=2,MAX
14680 ETA=PI*(DFLOAT(I-1)/DFLOAT(MP1-1))
14690 SINETA=DSIN(ETA)
14700 COSETA=DCOS(ETA)**2

```

```

14710      DO 21 J=2,NX
14720      21 UETA(I,J)=COSH02*(PSI(I,J+1)-PSI(I,J-1))/(2.0D00*DZETA*(J)*SINETA
14730      $*DSQRT(X(J)+COSETA))
14740      22 CONTINUE
14750      DO 23 J=1,N
14760      UETA(1,J)=0.0D00
14770      23 UETA(MP1,J)=0.0D00
14780      C*****
14790      C
14800      C USE TRANSFORMATION FROM OBLATE SPHEROID COORDINATES TO CYLINDERICAL
14810      C COORDINATES.
14820      C
14830      C*****
14840      MAX=0
14850      DO 25 J=1,N
14860      ZETA=ZETA0+DZETA*DFLOAT(J-1)
14870      COSHZ=DCOSH(ZETA)
14880      SINHZ=DSINH(ZETA)
14890      SINHZ2=SINHZ*SINHZ
14900      DO 24 I=1,MP1
14910      MAX=MAX+1
14920      ETA=PI*(DFLOAT(I-1)/DFLOAT(MP1-1))
14930      C1=COSHZ*DCOS(ETA)
14940      C2=SINHZ*DSIN(ETA)
14950      DENOM=DSQRT(SINHZ2+(C1/COSHZ)**2)
14960      VZZ(MAX)=(UZETA(I,J)*C1-UETA(I,J)*C2)/DENOM
14970      24 VRZ(MAX)=(UZETA(I,J)*C2+UETA(I,J)*C1)/DENOM
14980      25 CONTINUE
14990      C*****
15000      C
15010      C OUTPUT RESULTS TO LINE PRINTER AND DEVICE STORAGE DESIGNATED BY NDISK
15020      C
15030      C*****
15040      IF(IOUT.EQ.0) GO TO 400
15050      WRITE(6,1005)

```

```

15060 WRITE(6,999) AR,RE,MP1,N,DETA,DZETA
15070 WRITE(6,1001)
15080 JJJ=0
15090 26 JJ=JJJ+1
15100 JJJ=JJ+9
15110 IF(JJJ.GE.N) JJJ=N
15120 DO 27 J=1,10
15130 JL=JJ-1+J
15140 27 LXI(J)=JL
15150 WRITE(6,1007) (LXI(J),J=1,10)
15160 DO 28 NN=1,MP1
15170 28 WRITE(6,1006) (VZZ(MP1*(J-1)+NN),J=JJ,JJJ)
15180 IF(JJJ.LT.N) GO TO 26
15190 WRITE(6,1002)
15200 JJJ=0
15210 29 JJ=JJJ+1
15220 JJJ=JJ+9
15230 IF(JJJ.GE.N) JJJ=N
15240 DO 30 J=1,10
15250 JL=JJ-1+J
15260 30 LXI(J)=JL
15270 WRITE(6,1007) (LXI(J),J=1,10)
15280 DO 31 NN=1,MP1
15290 31 WRITE(6,1006) (VRZ(MP1*(J-1)+NN),J=JJ,JJJ)
15300 IF(JJJ.LT.N) GO TO 29
15310 400 NDISK=NDISK+2
15320 WRITE(NDISK) (VZZ(I), I=1,MAX)
15330 WRITE(NDISK) (VRZ(I), I=1,MAX)
15340 ENDFILE NDISK
15350 RETURN
15360 998 FORMAT('0',' OUTPUT FROM VELOCITY.FORT ROUTINE. VELOCITY COMPO
15370 $MENTS ARE CALCULATED USING CUBIC SPLINES.')
```

999 FORMAT('1',50X,' AXIS RATIO=',G15.8,/,  
\$' REYNOLDS NUMBER=',G15.8,/,  
\$' NUMBER OF ANGULAR STEPS=',10X,I5,/,

```

15410 $' NUMBER OF RADIAL STEPS=',10X,I5,/,
15420 $' ANGULAR STEP SIZE(RADIANS)=' ,G15.8,/,
15430 $' RADIAL STEP SIZE(NONDIMEN)=' ,G15.8)
15440 1000 FORMAT(10G12.4)
15450 1001 FORMAT('1',' Z-COORDINATE VELOCITY COMPONENTS.')
```

VELOCITY COMP

```

15460 1002 FORMAT('1',' R-COORDINATE VELOCITY COMPONENTS.')
```

VELOCITY COMP

```

15470 1005 FORMAT('1',' OUTPUT FROM VELOCITY.FORT ROUTINE.
15480 $ONENTS ARE CALCULATED USING CENTRAL DIFFERENCES')
```

VELOCITY COMP

```

15490 1007 FORMAT('0',6X,I3,9(10X,I3))
15500 1006 FORMAT(' ',10(2X,G11.5))
15510 END
15520 SUBROUTINE IDERIV(X,Y,NX,C,IC,U,S,M,IER)
15530 DIMENSION X(NX),Y(NX),C(IC,3),U(M),S(M)
15540 DOUBLE PRECISION C,D,DD,S,U,X,Y,ZERO
15550 DATA ZERO/0.0D00/
15560 I=1
15570 JER=0
15580 KER=0
15590 C CHECK DIMENSION OF VECTORS U AND S.
15600 IF(M.LE.0) GO TO 9005
15610 NXM1=NX-1
15620 C CHECK DIMENSION OF VECTORS X AND Y.
15630 IF(I.GT.NXM1)GO TO 9006
15640 C EVALUATE DERIVATIVES AT M POINTS.
15650 DO 40 K=1,M
15660 C FIND THE PROPER INTERVAL BY TESTING D.
15670 D=U(K)-X(I)
15680 IF(D)5,25,15
15690 5 IF(I.EQ.1) GO TO 30
15700 I=I-1
15710 D=U(K)-X(I)
15720 IF(D)5,25,20
15730 10 I=I+1
15740 D=DD.
15750 15 IF(I.GE.NX)GO TO 35
```



```

15760 DD=U(K)-X(I+1)
15770 IF(DD.GE.ZERO)GO TO 10
15780 IF(D.EQ.ZERO)GO TO 25
15790 C PERFORM EVALUATION
15800 20 S(K)=(3.0*C(I,3)*D+2.0*C(I,2))*D+C(I,1)
15810 GO TO 40
15820 25 S(K)=C(I,1)
15830 GO TO 40
15840 30 JER=33
15850 GO TO 20
15860 35 IF(DD.GT.ZERO)KER=34
15870 D=U(K)-X(NXM1)
15880 I=NXM1
15890 GO TO 20
15900 40 CONTINUE
15910 IER=MAX0(JER,KER)
15920 9000 CONTINUE
15930 IF(JER.GT.0)CALL UERTST(JER,6HIDERIV)
15940 IF(KER.GT.0)CALL UERTST(KER,6HIDERIV)
15950 RETURN
15960 9005 WRITE(6,1000)
15970 1000 FORMAT('0','ERROR, SUBROUTINE IDERIV, M.LE.0')
15980 RETURN
15990 9006 WRITE(6,1001)
16000 1001 FORMAT('0','ERROR, SUBROUTINE IDERIV, NX.LE.1')
16010 RETURN
16020 END
16030 SUBROUTINE DEFINE(II)
16040 IMPLICIT REAL*8(A-H,O-Z),
16050 REAL*8 MU,LAMBDA,LYK,LYK1,LYKV1,IAR1,IRIV,INTIA
16060 COMMON PI,GV,R,EPS,DISK,BRHO,GAMMA,ERR,CLL,UINF,DENS1,ALPHA1
16070 COMMON/AIR/ MU,RHO,LAMBDA
16080 COMMON/VER1/R1V,REYNV1,CDV1,VINFV1,STKV1,LYKV1,IR1V
16090 COMMON/AERSL1/REYN1,AR1,SEMI,CDAR1,VINF1,STK1,LYK1,IAR1
16100 COMMON/AERSL2/R2V,DENS2,ALPHA2,VINF2,REYN2

```

```

16110 COMMON/SWITCH/AR,CDTOTL,AXIS,STK,LYK,INTIA,VINF,RE
16120 COMMON/NAVIER/DZETA,MP1,N,NSF,IOUT,MATRX,JDERIV
16130 COMMON/OBLAT$/ PSI(100,100),G(100,100)
16140 IF(II.GE.2) GO TO 10
16150 RE=REYN1
16160 AR=AR1
16170 IF(II.EQ.0) RETURN
16180 AXIS=SEMI
16190 STK=STK1
16200 LYK=LYK1
16210 VINF=VINF1
16220 INTIA=IAR1
16230 CDTOTL=CDAR1
16240 RETURN
16250 10 IF(II.EQ.3) GO TO 20
16260 AR=0.999D00
16270 AXIS=RIV
16280 C*****
16290 C GUESS RE FOR VOLUME EQUIVALENT SPHERE TO START ITERATION PROCEDURE.
16300 VINFV1=2.0D00*DENS1*ALPHA1*GV*RIV*RIV*(1.0D00-RHO/(DENS1*ALPHA1))/
16310 $(9.0D00*MU)
16320 RE=VINFV1*2.0D00*RIV*RHO/MU
16330 C
16340 C USE OSEEN'S SOLUTION TO PREDICT RE NUMBER. FIND IT USING G-N METHOD.
16350 C
16360 FRIV=32.0D00*GV*(DENS1*ALPHA1-RHO)*RHO*RIV**3
16370 FRIV=FRIV/(3.0D00*MU*MU)
16380 12 DELTA=24.0D00*RE+9.0D00*RE*RE/2.0D00-FRIV
16390 DELTA=DELTA/(24.0D00+9.0D00*RE)
16400 IF(DABS(DELTA).LT.0.0001D00) GO TO 14
16410 RE=RE-DELTA
16420 GO TO 12
16430 14 IF(DISK.EQ.0.0D00) GO TO 15
16440 C CHECK TO SEE IF DISK VALUE IS BETTER GUESS.
16450 REWIND 9

```

```

16460 READ(9) ((PSI(I,J),I=1,MP1),J=1,N)
16470 READ(9) ((G(I,J),I=1,MP1),J=1,N)
16480 READ(9) CDTOTL,REDISK,AR
16490 ASEMI=3.0D00*MU*MU*CDTOTL*REDISK*REDISK
16500 ASEMI=ASEMI/(32.0D00*GV*(DENS1*ALPHA1-RHO)*RHO)
16510 X=1.0D00/3.0D00
16520 ASEMI=ASEMI**X
16530 DIFF=ASEMI-AXIS
16540 IF(DABS(DIFF/AXIS).LE.EPS) RE=REDISK
16550 C*****
16560 15 RETURN
16570 20 STA=STKV1
16580 LYK=LYKV1
16590 AXIS=R1V
16600 AR=0.999D00
16610 VINP=VINPV1
16620 INTIA=IR1V
16630 RE=REYNV1
16640 CDTOTL=CDV1
16650 RETURN
16660 END
16670 SUBROUTINE OUTPUT(II)
16680 IMPLICIT REAL*8 (A-H,O-Z)
16690 REAL*8 MU,LAMBDA,LYK,LYK1,LYKV1,IAR1,IR1V,INTIA
16700 REAL*8 NGCEFF
16710 COMMON PI,GV,R,EPS,DISK,BRHO,GAMMA,ERR,CLL,UINF,DENS1,ALPHA1
16720 COMMON/AIR/ MU,RHO,LAMBDA
16730 COMMON/COLL$/PATH,YIMAX,SIMAX,YIMIN,SIMIN,IETA,I35,JMAX,JMIN
16740 COMMON/DVOGE$/HD,HDMIN,HDMAX,NEQTN,MAXDER,MTH
16750 COMMON/VER1/R1V,REYNV1,CDV1,VINPV1,STKV1,LYKV1,IR1V
16760 COMMON/AERSL1/REYN1,ARI,SEMI,CDARI,VINF1,STK1,LYK1,IAR1
16770 COMMON/AERSL2/R2V,DENS2,ALPHA2,VINF2,REYN2
16780 COMMON/NAVIER/DZETA,MP1,N,NSF,IOUT,MATRX,JDERIV
16790 COMMON/WORK/COSH22(100),SINET2(100),COEF1(100),COEF2(100),COEF3(10
16800 $0),COEF4(100),SVORT(5000),PRESS(5000),VECTOR(5000)

```

```

16810 C
16820
16830
16840
16850 C
16860
16870
16880
16890
16900 C
16910
16920
16930
16940
16950
16960
16970
16980
16990
17000
17010
17020
17030
17040
17050
17060
17070
17080
17090
17100
17110
17120
17130
17140
17150

      DIMENSION TD(1000),VIZ(1000),V1RHO(1000),V2Z(1000),V2RHO(1000),
      $ZD(1000),RHOD(1000),RD(1000),SEP(1000),PHI(1000),THETA(1000),SEPAR
      $(1000)
      EQUIVALENCE (TD(1),SVORT(1)),(VIZ(1),SVORT(1001)),
      $(V1RHO(1),SVORT(2001)),(V2Z(1),SVORT(3001)),
      $(V2RHO(1),SVORT(4001)),(ZD(1),PRESS(1)),(RHOD(1),PRESS(1001)),
      $(RD(1),PRESS(2001)),(SEP(1),PRESS(3001)),(PHI(1),PRESS(4001))

      IF(II.NE.0) GO TO 1
      WRITE(6,20)
      WRITE(6,21)
      WRITE(6,22)
      WRITE(6,100)
      WRITE(6,101) GV
      WRITE(6,102) MU
      WRITE(6,103) LAMBDA
      WRITE(6,104) RHO
      WRITE(6,105) MP1
      WRITE(6,106) N
      WRITE(6,107) DZETA
      WRITE(6,601)
      WRITE(6,602)
      WRITE(6,603) AR1
      WRITE(6,604) REYN1
      WRITE(6,605) DENS1
      WRITE(6,606) ALPHA1
      WRITE(6,700)
      WRITE(6,701) R2V
      WRITE(6,702) DENS2
      WRITE(6,703) ALPHA2
      WRITE(6,300)
      WRITE(6,301) HD
      WRITE(6,302) HDMAX

```

```

17160      WRITE(6,303) HDMIN
17170      WRITE(6,400)
17180      WRITE(6,401) EPS
17190      WRITE(6,402) CLL
17200      WRITE(6,500)
17210      IF(DISK.EQ.0.0D00) WRITE(6,501)
17220      IF(DISK.NE.0.0D00) WRITE(6,502)
17230      IF(MATRX.EQ.0) WRITE(6,503)
17240      IF(MATRX.NE.0) WRITE(6,504)
17250      IF(IOUT.EQ.0) WRITE(6,505)
17260      IF(IOUT.NE.0) WRITE(6,506)
17270      IF(PATH.EQ.0.0) WRITE(6,507)
17280      IF(PATH.NE.0.0) WRITE(6,508)
17290      RETURN
17300 C
17310 C RESULTS FOR SPHEROID PRINTED IF II.EQ.1
17320 C
17330 C
17340 C IF I35.NE.0 THAN DVOGER DID NOT WORK.
17350 C
17360 C
17370      1 IF(II.NE.1) GO TO 2
17380      WRITE(6,600)
17390      WRITE(6,601)
17400      WRITE(6,602)
17410      WRITE(6,603) AR1
17420      WRITE(6,604) REYN1
17430      WRITE(6,605) DEN1
17440      WRITE(6,606) ALPHA1
17450      WRITE(6,607) SEMI
17460      WRITE(6,608) CDAR1
17470      WRITE(6,609) VIN1
17480      WRITE(6,700)
17490      WRITE(6,701) R2V
17500      WRITE(6,702) DEN2

```

```

17510 WRITE(6,703) ALPHA2
17520 WRITE(6,704) REYN2
17530 WRITE(6,705) VINP2
17540 WRITE(6,800)
17550 WRITE(6,801) STK1
17560 WRITE(6,802) LYK1
17570 WRITE(6,803) IAR1
17580 WRITE(6,804) GAMMA
17590 WRITE(6,805) BRHO
17600 WRITE(6,806) UINF
17610 *****
17620 C *****
17630 IF(I35.NE.0) GO TO 9
17640 IF(IETA.NE.0) GO TO 4
17650 C
17660 DOMAIN=1.0D00
17670 IF(YIMIN.NE.0.0D00) DOMAIN=2.0D00
17680 NGCEFF=((YIMAX-YIMIN)/(R1V+R2V))**2
17690 ERROR=DABS(SIMAX*100.0D00/CLL)
17700 ERROR=ERROR+DABS(SIMIN*100.0D00/CLL)
17710 *****
17720 WRITE(6,900)
17730 WRITE(6,901) NGCEFF
17740 PGCEFF=NGCEFF*((R1V+R2V)/(SEMI+R2V))**2
17750 WRITE(6,904) PGCEFF
17760 WRITE(6,902) ERROR
17770 WRITE(6,903) DOMAIN
17780 IF(PATH.NE.0.0D00) GO TO 5
17790 RETURN
17800 C
17810 2 CONTINUE
17820 WRITE(6,1000)
17830 WRITE(6,601)
17840 WRITE(6,1001)
17850 WRITE(6,1002) R1V

```

```

17860      WRITE(6,605) DENS1
17870      WRITE(6,606) ALPHA1
17880      WRITE(6,1003) REYNV1
17890      WRITE(6,1004) CDV1
17900      WRITE(6,1005) VINNV1
17910      WRITE(6,700)
17920      WRITE(6,701) R2V
17930      WRITE(6,702) DENS2
17940      WRITE(6,703) ALPHA2
17950      WRITE(6,704) REYN2
17960      WRITE(6,705) VINNF2
17970      WRITE(6,800)
17980      WRITE(6,1101) STKV1
17990      WRITE(6,1102) LYKV1
18000      WRITE(6,1103) IR1V
18010      WRITE(6,804) GAMMA
18020      WRITE(6,805) BRHO
18030      WRITE(6,806) UINF
18040      C*****
18050      C
18060      IF(I35.NE.0) GO TO 9
18070      IF(IETA.NE.0) GO TO 4
18080      C
18090      DOMAIN=1.0D00
18100      IF(YIMIN.NE.0.0D00) DOMAIN=2.0D00
18110      SGCEFF=(YIMAX-YIMIN)/(R1V+R2V)**2
18120      ERROR=DABS(S1MAX*100.0D00/CLL)
18130      ERROR=ERROR+DABS(S1MIN*100.0D00/CLL)
18140      C*****
18150      WRITE(6,900)
18160      WRITE(6,1201) SGCEFF
18170      WRITE(6,902) ERROR
18180      WRITE(6,903) DOMAIN
18190      IF(PATH.NE.0.0D00) GO TO 5
18200      3 WRITE(6,2000)

```

```

18210 WRITE(6,2001)
18220 WRITE(6,603) AR1
18230 WRITE(6,607) SEMI
18240 WRITE(6,605) DENS1
18250 WRITE(6,606) ALPHA1
18260 WRITE(6,2006) R2V
18270 WRITE(6,702) DENS2
18280 WRITE(6,703) ALPHA2
18290 WRITE(6,3000)
18300 WRITE(6,3001) NGCEFF
18310 WRITE(6,3002) SGCEFF
18320 WRITE(6,4000)
18330 C
18340 C
18350 R1M=R1V*ALPHA1**((1.0D00/3.0D00)
18360 R2M=R2V*ALPHA2**((1.0D00/3.0D00)
18370 TEMP=(R1M+R2M*(ALPHA1/ALPHA2)**((1.0D00/3.0D00)))**2
18380 TEMP=TEMP/(R1M+R2M)**2
18390 TEMP=TEMP/ALPHA1**((2.0D00/3.0D00)
18400 NGCEFF=NGCEFF*TEMP
18410 SGCEFF=SGCEFF*TEMP
18420 BETA=NGCEFF/SGCEFF
18430 RATIO=(DENS2/DENS1)*(R2M/R1M)**3
18440 C
18450 C
18460 WRITE(6,4001) R1M
18470 WRITE(6,4002) R2M
18480 WRITE(6,3001) NGCEFF
18490 WRITE(6,3002) SGCEFF
18500 WRITE(6,5000)
18510 WRITE(6,5001) BETA
18520 WRITE(6,5002) RATIO
18530 RETURN
18540 C
18550 4 WRITE(6,6000)

```



```

18560      RETURN
18570      5 WRITE(6,7000) YIMAX
18580      WRITE(6,7001)
18590      DO 6 I=1,JMIN
18600      6 WRITE(6,7002) TD(I),V1Z(I),V2Z(I),V1RHO(I),V2RHO(I),ZD(I),RHOD(I),
18610      $RD(I),SEP(I),PHI(I)
18620      IF(YIMIN.EQ.0.0D00) GO TO 8
18630      WRITE(6,7003) YIMIN
18640      WRITE(6,7001)
18650      JMINF1=JMIN+1
18660      DO 7 I=JMINF1,JMAX
18670      7 WRITE(6,7002) TD(I),V1Z(I),V2Z(I),V1RHO(I),V2RHO(I),ZD(I),RHOD(I),
18680      $RD(I),SEP(I),PHI(I)
18690      8 IF(II.GT.2) GO TO 3
18700      RETURN
18710      9 WRITE(6,8000)
18720      RETURN
18730      20 FORMAT('1','*****NGCEFF CODE RESULTS*****')
18740      21 FORMAT('0',5X,'RESULTS IN THREE SECTIONS',//,
18750      $6X,'SECTION 1: COLLISION EFFICIENCY, SPHEROID AND SMALL PARTICLE'
18760      $,//,6X,'SECTION 2: COLLISION EFFICIENCY, SPHERE AND SMALL PARTICL
18770      $E',//,6X,'SECTION 3: COLLISION SHAPE FACTOR, BETA',//
18780      $1X,'INPUT CONSTRAINTS AND PARAMETERS',//,
18790      $1X,'DRAG FORCE COMPUTED BY MEANS OF SUPERPOSITION METHOD')
18800      22 FORMAT('0','DVOGER ROUTINE USES STIFF METHOD, JACOBIAN CALCULATED
18810      1 INTERNALLY')
18820      100 FORMAT('0','FLUID PARAMETERS')
18830      101 FORMAT('0',1PD15.8,5X,'G : GRAVITATIONAL CONSTANT (CM/SEC**2)')
18840      102 FORMAT('0',1PD15.8,5X,'MU : FLUID VISCOSITY (GM/CM*SEC)')
18850      103 FORMAT('0',1PD15.8,5X,'LAMBDA : FLUID MEAN FREE PATH (CM)')
18860      104 FORMAT('0',1PD15.8,5X,'RHO : FLUID DENSITY (GM/CM**3)')
18870      105 FORMAT('0',10X,15.5X,'MPI, NUMBER OF ANGULAR STEPS')
18880      106 FORMAT('0',10X,15.5X,'N, NUMBER OF RADIAL STEPS')
18890      107 FORMAT('0',1PD15.8,5X,'DZETA, RADIAL STEP SIZE')
18900      300 FORMAT('0','DVOGER ROUTINE INITIAL VALUES')

```

```

18910 301 FORMAT('0',1PD15.8,5X,'HD : TIME STEP (SEC)')
18920 302 FORMAT('0',1PD15.8,5X,'HDMAX : MAX TIME STEP (SEC)')
18930 303 FORMAT('0',1PD15.8,5X,'HDMIN : MIN TIME STEP (SEC)')
18940 400 FORMAT('0','ERROR PARAMETERS')
18950 401 FORMAT('0',1PD15.8,5X,'EPS : ERROR CRITERION')
18960 402 FORMAT('0',1PD15.8,5X,'CLL : COLLISION PARAMETER')
18970 500 FORMAT('0','OPTIONS SELECTED')
18980 501 FORMAT('0',5X,'DISK : PSI AND G FIELDS GENERATED FROM OBERBECKS SO
18990 $LUTION')
19000 502 FORMAT('0',5X,'DISK : PREVIOUS CASE PSI AND G FIELDS USED')
19010 503 FORMAT('0',5X,'MATRIX : NO MATRIX ANALYSIS DONE')
19020 504 FORMAT('0',5X,'MATRIX : MATRIX ANALYSIS REQUESTED')
19030 505 FORMAT('0',5X,'IOUT : NO OUTPUT OF INTERMEDIATE RESULTS')
19040 506 FORMAT('0',5X,'IOUT : OUTPUT ALL INTERMEDIATE RESULTS')
19050 507 FORMAT('0',5X,'PATH : NO TRAJECTORY DATA REQUESTED')
19060 508 FORMAT('0',5X,'PATH : TRAJECTORY DATA FROM SUBROUTINE COLL REQUEST
19070 $ED')
19080 600 FORMAT('1',' SECTION 1: COLLISION EFFICIENCY, OBLATE SPHEROID AND
19090 $ SMALL PARTICLE')
19100 601 FORMAT('0',' AEROSOL PARTICLE PARAMETERS')
19110 602 FORMAT('0',' ***OBLATE SPHEROID')
19120 603 FORMAT('0',1PD15.8,5X,'AR, AXIS RATIO')
19130 604 FORMAT('0',1PD15.8,5X,'REYN1, REYNOLDS NUMBER')
19140 605 FORMAT('0',1PD15.8,5X,'DENS1, BULK DENSITY (G/CM**3)')
19150 606 FORMAT('0',1PD15.8,5X,'ALPHA1, DENSITY CORRECTION FACTOR')
19160 607 FORMAT('0',1PD15.8,5X,'SEMI, SEMI-MAJOR AXIS LENGTH (CM)')
19170 608 FORMAT('0',1PD15.8,5X,'CDAR1, DRAG COEFFICIENT')
19180 609 FORMAT('0',1PD15.8,5X,'VINFI, TERMINAL VELOCITY (CM/SEC)')
19190 700 FORMAT('0',' ***SMALL PARTICLE (SPHERE)')
19200 701 FORMAT('0',1PD15.8,5X,'R2V, RADIUS (CM)')
19210 702 FORMAT('0',1PD15.8,5X,'DENS2, BULK DENSITY (G/CM**3)')
19220 703 FORMAT('0',1PD15.8,5X,'ALPHA2, DENSITY CORRECTION FACTOR')
19230 704 FORMAT('0',1PD15.8,5X,'REYN2, REYNOLDS NUMBER')
19240 705 FORMAT('0',1PD15.8,5X,'VINFI2, STOKES TERMINAL VELOCITY (CM/SEC)')
19250 800 FORMAT('0',' SYSTEM PARAMETERS')

```

```

19260 801 FORMAT('0','1PD15.8,5X','STK1', STOKES NUMBER')
19270 802 FORMAT('0','1PD15.8,5X','LYK1', INTERACTION NUMBER')
19280 803 FORMAT('0','1PD15.8,5X','IAR1', INERTIA NUMBER')
19290 804 FORMAT('0','1PD15.8,5X','GAMMA', RATIO OF PARTICLE DENSITIES')
19300 805 FORMAT('0','1PD15.8,5X','BRHO', RATIO OF PARTICLE BUOYANCY EFFECTS')
19310 806 FORMAT('0','1PD15.8,5X','UINF', STOKES TERMINAL VELOCITY OF VOLUME EQ
19320 $UIVALENT SPHERICAL PARTICLE')
19330 900 FORMAT('0',' GRAVITATIONAL COLLISION PARAMETERS (RESULTS)')
19340 901 FORMAT('0','1PD15.8,5X','NGCEFF', NONSPHERICAL GRAVITATIONAL COLLISIO
19350 $N EFFICIENCY (BASED ON VOLUME)')
19360 902 FORMAT('0','1PD15.8,5X','ERROR', ESTIMATED ERROR (Z)')
19370 903 FORMAT('0','1PD15.8,5X','DOMAIN', TYPE OF COLLISION DOMAIN')
19380 904 FORMAT('0','1PD15.8,5X','PGCEFF', NONSPHERICAL GRAVITATIONAL COLLISIO
19390 $N EFFICIENCY (BASED ON GEOMETRIC SWEEPOUT)')
19400 1000 FORMAT('1',' SECTION 2: COLLISION EFFICIENCY, VOLUME EQUIVALENT S
19410 $PHERE AND SMALL PARTICLE')
19420 1001 FORMAT('0',' *****VOLUME EQUIVALENT SPHERE')
19430 1002 FORMAT('0','1PD15.8,5X','R1V', VOLUME EQUIVALENT RADIUS (CM)')
19440 1003 FORMAT('0','1PD15.8,5X','REYNV1', REYNOLDS NUMBER')
19450 1004 FORMAT('0','1PD15.8,5X','CDV1', DRAG COEFFICIENT')
19460 1005 FORMAT('0','1PD15.8,5X','VINPV1', TERMINAL VELOCITY (CM/SEC)')
19470 1101 FORMAT('0','1PD15.8,5X','STKV1', STOKES NUMBER')
19480 1102 FORMAT('0','1PD15.8,5X','LYKV1', INTERACTION NUMBER')
19490 1103 FORMAT('0','1PD15.8,5X','IR1V', INERTIA NUMBER')
19500 1201 FORMAT('0','1PD15.8,5X','SGCEFF', SPHERICAL GRAVITATIONAL COLLISION E
19510 $FFICIENCY (VOLUME)')
19520 2000 FORMAT('1',' SECTION 3: GRAVITATIONAL COLLISION SHAPE FACTOR, BET
19530 $A')
19540 2001 FORMAT('0',' *****PARTICLE PARAMETERS')
19550 2006 FORMAT('0','1PD15.8,5X','R2V', VOLUME EQUIVALENT RADIUS OF SMALL PART
19560 $ICLE')
19570 3000 FORMAT('0',' *****VOLUME AS BASIS')
19580 3001 FORMAT('0','1PD15.8,5X','NGCEFF')
19590 3002 FORMAT('0','1PD15.8,5X','SGCEFF')
19600 4000 FORMAT('0',' *****MASS AS BASIS')

```

```

19610 4001 FORMAT('0',1PD15.8,5X,'R1M, MASS EQUIVALENT RADIUS OF OBLATE SPHER
19620 $OID')
19630 4002 FORMAT('0',1PD15.8,5X,'R2M, MASS EQUIVALENT RADIUS OF SMALLER PART
19640 $ICLE')
19650 5000 FORMAT('0', ' *****SHAPE FACTOR*****')
19660 5001 FORMAT('0',1PD15.8,5X,'BETA, COLLISION SHAPE FACTOR')
19670 5002 FORMAT('0',1PD15.8,5X,'RATIO, MASS RATIO(SHOULD NOT EXCEED 0.34)')
19680 6000 FORMAT('0', 'ETA LESS THAN 1.0D-06')
19690 7000 FORMAT('1', 'INTEGRATION RESULTS FOR GRAZING TRAJECTORY, YIMAX=',1P
19700 $D15.8)
19710 7001 FORMAT('0',5X,'T',10X,'V1Z',9X,'V2Z',8X,'VIRHO',7X,'V2RHO',9X,'Z',
19720 $10X,'RHO',10X,'R',9X,'SEP',9X,'PHI')
19730 7002 FORMAT(' ',10(1PD11.4,1X))
19740 7003 FORMAT('1', 'INTEGRATION RESULTS FOR GRAZING TRAJECTORY, YIMIN=',1P
19750 $D15.8)
19760 8000 FORMAT('0', ' THE REQUESTED ERROR IS SMALLER THAN CAN BE HANDLED BY
19770 $ SUBROUTINE DVOGER')
19780 END
19790 SUBROUTINE COLL(II)
19800 IMPLICIT REAL*8(A-H,O-Z)
19810 EXTERNAL DFUN
19820 EXTERNAL ANGLE
19830 REAL*8 MU,LAMBDA,LYK,LYK1,LYKV1,IAR1,IR1V,INTIA
19840 COMMON PI,GU,R,EPS,DISK,BRHO,GAMMA,ERR,CLL,UINF,DENS1,ALPHA1
19850 COMMON/AIR/ MU,RHO,LAMBDA
19860 COMMON/COLL$/PATH,YIMAX,SIMAX,YIMIN,SIMIN,IETA,I35,JMAX,JMIN
19870 COMMON/DVOGE$/HD,HDMIN,HDMAX,NEQTN,MAXDER,MTH
19880 COMMON/ANGLE$/ZDIST,RDIST
19890 COMMON/VER1/R1V,REYNV1,CDU1,VINFV1,STKV1,LYKV1,IR1V
19900 COMMON/AERSL2/R2V,DENS2,ALPHA2,VINF2,REYN2
19910 COMMON/SWITCH/AR,CDTOTL,AXIS,STK,LYK,INTIA,VINF,RE
19920 COMMON/NAVIER/DZETA,MF1,N,NSF,IOUT,MATRX,JDERIV
19930 COMMON/OBLAT$/ W1Z(100,100),W1RHO(100,100)
19940 COMMON/WORK/COSH22(100),SINET2(100),COEF1(100),COEF2(100),COEF3(10
19950 $0),COEF4(100),SVORT(5000),PRESS(5000),VECTOR(5000)

```

```

19960 C
19970 DIMENSION TD(1000),V1Z(1000),V1RHO(1000),V2Z(1000),V2RHO(1000),
19980 $ZD(1000),RHOD(1000),RD(1000),SEP(1000),PHI(1000),THETA(1000),SEPAR
19990 $(1000)
20000 DIMENSION Y(8,6),YMAX(6),ERROR(6),WK(130),COEF(1000,3),BPAR(4),ANS
20010 $(1),QU(1)
20020 C
20030 EQUIVALENCE (Y(1),COSH2(1)),(YMAX(1),COSH2(49)),
20040 $(ERROR(1),COSH2(55)),(BPAR(1),COSH2(61)),(WK(1),SINET2(1)),
20050 $(WK(101),COEF1(1)),(COEF(1),VECTOR(2001)),(COEF(1001),VECTOR(3001)
20060 $),(COEF(2001),VECTOR(4001))
20070 EQUIVALENCE (TD(1),SVORT(1)),(V1Z(1),SVORT(1001)),
20080 $(V1RHO(1),SVORT(2001)),(V2Z(1),SVORT(3001)),
20090 $(V2RHO(1),SVORT(4001)),(ZD(1),PRESS(1)),(RHOD(1),PRESS(1001)),
20100 $(RD(1),PRESS(2001)),(SEP(1),PRESS(3001)),(PHI(1),PRESS(4001))
20110 EQUIVALENCE (THETA(1),VECTOR(1)),(SEPAR(1),VECTOR(1001))
20120 JMAX=0
20130 JMIN=0
20140 YIMAX=0.0D00
20150 YIMIN=0.0D00
20160 SIMAX=0.0D00
20170 SIMIN=0.0D00
20180 CUT=1.0D00
20190 FIND =1.0D00
20200 IC=1000
20210 C
20220 C READ VELOCITY FIELDS FOR SPHEROID OR VOLUME EQUIVALENT SPHERE
20230 C
20240 REWIND 10
20250 REWIND 11
20260 NDISK=10
20270 IF(I1.GT.1) NDISK=11
20280 MAX=MP1*N
20290 READ(NDISK) (SVORT(I),I=1,MAX)
20300 READ(NDISK) (PRESS(I),I=1,MAX)

```

```

20310 C      MAX=0
20320      DO 1 J=1,N
20330      DO 1 I=1,MP1
20340      MAX=MAX+1
20350      WIZ(I,J)=SVORT(MAX)
20360      1 WIRHO(1,J)=PRESS(MAX)
20370 C      DEFINE PARAMETERS IN COMMON BLOCK SWITCH.
20380 C      CALL DEFINE(II)
20390 C
20400 C      BEGIN ITERATION
20410 C
20420 C      DEFINE INITIAL OFFSET YI.
20430 C
20440 C      2 YI=(AXIS+R2V)+0.01D00*(AXIS+R2V)
20450      YI=CUT*YI
20460 C
20470 C      3 IETA=0.0D00
20480      KK=2
20490      ICOUNT=0
20500      HALF=1.0D00
20510 C
20520 C      1001 IF(ICOUNT.GE.25) GO TO 900
20530      J=JMIN+1
20540      JCOMP=0
20550      JSAVE=0
20560      JIND=1
20570      JSTAR=0
20580      I35=0
20590      SAVE=90.0D00
20600      T=0.0D00
20610 C
20620 C      H=(HD*UINF/R1V)*HALF
20630      HMAX=(HDMAX*UINF/R1V)*HALF
20640      HMIN=(HDMIN*UINF/R1V)*HALF
20650

```



```

21010 C      DETERMINE SEPARATION ANGLE AND DISTANCE
21020 C      IF LARGE PARTICLE IS A SPHERE, THETAJ IS CORRECT. OTHERWISE PHI IS.
21030 C      MUST MAKE NONDIMENSIONAL WITH RESPECT TO AXIS SINCE ANGLE DERIVED
21040 C      THAT WAY FOR CALCULATING RD(J).
21050      RDIST=DSQRT(ZD(J)*ZD(J)+RHOD(J)*RHOD(J))
21060      THETAJ=DARCOS(ZD(J)/RDIST)
21070      ZDIST=ZD(J)/AXIS
21080      RDIST=RHOD(J)/AXIS
21090      XL=0.0D00
21100      XR=PI/2.0D00
21110      IF(THETAJ.GT.PI/2.0D00) XL=PI/2.0D00
21120      IF(THETAJ.GT.PI/2.0D00) XR=PI
21130      ITMAX=200
21140      CALL ZFALSE(ANGLE,EPS,8,XL,XR,PHI(J),ITMAX,IERZ)
21150      IF(IERZ.EQ.129.OR.IERZ.EQ.130) WRITE(6,2009) THETAJ,RDIST,ZDIST,IE
21160      $RZ,ITMAX
21170      RD(J)=AXIS*DSQRT(ZD(J)*ZD(J)/AXIS**2+RHOD(J)*RHOD(J)/AXIS**2+
21180      $AR*AR*DCOS(PHI(J))**2+DSIN(PHI(J))**2-
21190      $2.0D00*AR*ZD(J)*DCOS(PHI(J))/AXIS-
21200      $2.0D00*RHOD(J)*DSIN(PHI(J))/AXIS)
21210 C
21220      SEP(J)=RD(J)-R2V
21230      THETAJ=THETAJ*180.0D00/PI
21240      PHI(J)=180.0D00*PHI(J)/PI
21250      COM=DABS(SAVE-(90.0D00-THETAJ))
21260      IF(IOUT.NE.0) WRITE(6,2007) THETAJ,PHI(J),SEP(J)
21270      IF(COM.GE.10.0D00) GO TO 500
21280      IF(SEP(J).GT.(R2V+0.01D00*R2V)) GO TO 5
21290      HMAX=100.0D00*(1.5)/DABS(Y(1,1))
21300      HMIN=1.0D-06*HMAX
21310      H=1.0D-03*HMAX
21320      5 HSAVE=H
21330 C
21340      IF(J.EQ.JMIN+1) GO TO 10
21350      IF(SEP(J).GT.SEP(J-1).AND.JIND.EQ.1) GO TO 600

```



```

21360 IF(JSAVE,NE,0) GO TO 10
21370 IF(SEP(J).GT,SEP(J-1).AND,JIND,EQ,0) JSAVE=J
21380 IF(JSAVE,NE,0) JCOMP=JSAVE+5
21390 10 IF(J,EQ,JCOMP) GO TO 700
21400 IF(SEP(J).LT,0.0D00.AND,KK,EQ,2) GO TO 800
21410 IF(SEP(J).LT,0.0D00.AND,KK,NE,2) GO TO 801
21420 SAVE=90.0D00-THETAJ
21430 J=J+1
21440 IF(IOUT,NE,0) WRITE(6,2008) J,T,(Y(1,IJ),IJ=1,6),H,HMIN,HMAX
21450 1000 CALL DVGGER(DFUN,Y,T,NEGTN,MTH,MAXDER,JSTAR,H,HMIN,HMAX,EPS,YMAX,
21460 1ERROR,WK,IER)
21470 IF(IER,EQ,35) GO TO 900
21480 JSTAR=1
21490 GO TO 999
21500 C
21510 C
21520 C STEPSIZE HALVING
21530 500 H=HSAVE/2.0D00
21540 HMAX=H
21550 HMIN=HMIN/2.0D00
21560 IF(IOUT,NE,0) WRITE(6,2001)
21570 JSTAR=-1
21580 GO TO 1000
21590 C
21600 C CHANGE STEPSIZE BY A FACTOR OF 10, PARTICLES NEAR MINIMUM SEPARATION
21610 C
21620 600 H=HSAVE*0.1D00
21630 HMAX=H
21640 HMIN=HMIN*0.1D00
21650 JIND=0
21660 IF(IOUT,NE,0) WRITE(6,2002)
21670 JSTAR=-1
21680 GO TO 1000
21690 C
21700 C CUBIC SPLINE INTERPOLATION TO FIND MINIMUM SEPARATION

```

```

21710 C      700 DO 710 I=1,4
21720      710 BPAR(I)=0.0D00
21730      DO 701 KKK=1,J
21740      L=J-KKK+1
21750      THETA(KKK)=90.0D00-PHI(L)
21760      701 SEPAR(KKK)=SEP(L)
21770      CALL ICSICU(THETA,SEPAR,J,BPAR,COEF,IC,IERR)
21780      LSAVE=J-JSAVE+1
21790      LS1=LSAVE+1
21800      LS2=LSAVE+2
21810      IF(IOUT.NE.0) WRITE(6,2003) THETA(LSAVE),THETA(LS2)
21820 C      DETERMINE MINIMUM THETA AND MINIMUM SEPARATION
21830      F1=DSQRT(DABS(4.*COEF(LSAVE,2)**2-12.*COEF(LSAVE,3)*COEF(LSAVE,1)
21840      1))
21850      F2=(-2.*COEF(LSAVE,2)-F1)/(6.*COEF(LSAVE,3))
21860      F3=(-2.*COEF(LSAVE,2)+F1)/(6.*COEF(LSAVE,3))
21870      F4=DSQRT(DABS(4.*COEF(LS1,2)**2-12.*COEF(LS1,3)*COEF(LS1,1)))
21880      F5=(-2.*COEF(LS1,2)-F4)/(6.*COEF(LS1,3))
21890      F6=(-2.*COEF(LS1,2)+F4)/(6.*COEF(LS1,3))
21900      ZMAX1=THETA(LS1)-THETA(LSAVE)
21910      ZMAX2=THETA(LS2)-THETA(LS1)
21920 C
21930 C
21940 C
21950 C
21960      IF(F2.LE.ZMAX1.AND.F2.GE.0.) DEGM=F2+THETA(LSAVE)
21970      IF(F3.LE.ZMAX1.AND.F3.GE.0.) DEGM=F3+THETA(LSAVE)
21980      IF(F5.LE.ZMAX2.AND.F5.GE.0.) DEGM=F5+THETA(LS1)
21990      IF(F6.LE.ZMAX2.AND.F6.GE.0.) DEGM=F6+THETA(LS1)
22000      M=1
22010      QU(1)=DEGM
22020      CALL ICSEVU(THETA,SEPAR,J,COEF,IC,QU,ANS,M,IERR)
22030      IF(IOUT.NE.0) WRITE(6,2004) QU(1),ANS(1)
22040 C      INTERPOLATION TO FIND CRITICAL YI
22050      ICOUNT=ICOUNT+1

```

```

22060 IF(FIND.EQ.-1.0D00) GO TO 1010
22070 IF(KK.EQ.0) GO TO 810
22080 SR=ANS(1)-CLL
22090 IF(DABS(SR).LT.ERR) GO TO 870
22100 IF(SR.LT.0.0D00) GO TO 800
22110 IF(KK.EQ.1) GO TO 802
22120 YR=YI
22130 YL=0.0D00
22140 IF(KK.EQ.3) YL=YLSAVE
22150 KK=0
22160 YI=(YR+YL)/2.0D00
22170 GO TO 1001
22180 803 YI=YR+YR/1000.0D00
22190 KK=3
22200 YLSAVE=YL
22210 GO TO 1001
22220 800 IF(FIND.EQ.-1.0D00) GO TO 1020
22230 YR=2.0D00*YI
22240 YL=YI
22250 YI=YR
22260 KK=1
22270 IF(IOUT.NE.0) WRITE(6,2005)
22280 GO TO 1001
22290 802 IF(SEP(J).LT.0.0D00.AND.DABS(YR-YI).LE.1.0D-08) GO TO 803
22300 YI=(YR+YL)/2.0D00
22310 KK=0
22320 GO TO 1001
22330 C
22340 801 IF(FIND.EQ.-1.0D00) GO TO 1030
22350 IF(IOUT.NE.0) WRITE(6,2006)
22360 YL=YI
22370 GO TO 802
22380 810 S1=ANS(1)-CLL
22390 IF(DABS(S1).LT.ERR) GO TO 872
22400 COMP=S1*SR

```

```

22410 IF(COMP.GT.0.0D00) GO TO 850
22420 YL=YI
22430 GO TO 860
22440 850 YR=YI
22450 EPSCHK=(YI/(R1V+R2V))*2
22460 IF(EPSCHK.LE.0.000001) GO TO 880
22470 SR=S1
22480 860 YI=(YR+YL)/2.0D00
22490 GO TO 1001
22500 870 S1=SR
22510 872 IF(FIND.EQ.-1.0D00) GO TO 875
22520 JMIN=J
22530 YIMAX=YI
22540 S1MAX=S1
22550 IF(AR.GE.0.999D00) RETURN
22560 FIND=-1.0D00
22570 YR=YIMAX
22580 YL=0.0D00
22590 YI=(YR+YL)/2.0D00
22600 GO TO 3
22610 875 JMAX=J
22620 YIMIN=YI
22630 S1MIN=S1
22640 RETURN
22650 880 IETA=1
22660 IF(AR.GE.0.999D00) GO TO 905
22670 C*****
22680 C
22690 C SEARCH LOGIC FOR YIMAX, SPHEROIDS ONLY.
22700 CUT=0.9D00*CUT
22710 IF(CUT.LE.0.500D00) GO TO 905
22720 GO TO 2
22730 C
22740 C*****
22750 905 RETURN

```

```

22760      900 I35=1.
22770      IF(HALF.LE.0.0624D00) RETURN
22780      HALF=HALF/2.0D00
22790      GO TO 1001
22800 *****
22810 C *****
22820 C SEARCH LOGIC FOR YIMIN
22830      1010 S1=ANS(1)-CLL
22840      ICOUNT=ICOUNT+1
22850      IF(DABS(S1).LT.ERR) GO TO 872
22860      IF(S1.GT.0.0D00) GO TO 1800
22870      IF(KK.EQ.0) GO TO 1030
22880      1020 YR=YI
22890      YL=0.0D00
22900      YI=(YR+YL)/2.0D00
22910      EPSCHK=(YI/(R1V+R2V))*2
22920      IF(EPSCHK.LE.0.000001D00) RETURN
22930      ICOUNT=ICOUNT+1
22940      GO TO 1001
22950      1030 YR=YI
22960      YI=(YR+YL)/2.0D00
22970      ICOUNT=ICOUNT+1
22980      GO TO 1001
22990      1800 YL=YI
23000      YR=YR
23010      YI=(YR+YL)/2.0D00
23020      KK=0
23030      GO TO 1001
23040 C *****
23050 C *****
23060      2000 FORMAT('0','V1Z=',G10.3,5X,'V2Z=',G10.3,5X,'V1RHD=',
23070      $G10.3,5X,'V2RHD=',G10.3,5X,'ZI=',G10.3,5X,'RHOI=',G10.3)
23080      2001 FORMAT(' ','H X 0.5')
23090      2002 FORMAT(' ','H X 0.1')
23100      2003 FORMAT(' ','MINIMUM SEPARATION BETWEEN ',1PD15.8,2X,'DEGREES AND

```

```

23110      1,'1PD15.8,2X,'DEGREES')
23120      2004 FORMAT(' ','CUBIC SPLINE INTERPOLATION MIN THETA ',
23130      1PD15.8,5X,'MIN SEP ',1PD15.8)
23140      2005 FORMAT(' ','INITIAL YI TOO SMALL, YI DOUBLED')
23150      2006 FORMAT(' ','SEPARATION LESS THAN 0., NEW YI CALCULATED')
23160      2007 FORMAT(' ','THETAJ=',G12.4,5X,'PHI(J)=',G12.4,5X,'SEP(J)=',G12.4)
23170      2008 FORMAT('0','J=',I5,3X,'I=',G9.3,3X,'V1Z=',G15.8,3X,'V2Z=',G15.8,3X
23180      $,'V1RHO=',G15.8,3X,'V2RHO=',G15.8,3X,'ZD=',G15.8,3X,'RHO=',G15.
23190      $8,3X,'H=',G15.8,3X,'HMIN=',G15.8,3X,'HMAX=',G15.8)
23200      2009 FORMAT('0','FROM SUBROUTINE COLL, ERROR OCCURRED SEEKING ANGLE PHI
23210      $',/, ' THETAJ=',G12.4,5X,'RDIIST=',G12.4,5X,'ZDIST=',G12.4,5X,'IER='
23220      $,I5,5X,'ITMAX=',I5)
23230      END
23240      SUBROUTINE DVOGER(DFUN,Y,T,N,MTH,MAXDER,JSTART,H,HMIN,HMAX,EPS,
23250      *      YMAX,ERROR,WK,IER)
23260      C
23270      DIMENSION      Y(8,N),YMAX(N),ERROR(N),WK(10,1),
23280      1      C(8),COEF(7,2,3)
23290      DOUBLE PRECISION
23300      1      ENQ2,ENQ3,HMAX,HMIN,HNEW,HOLD,TOLD,YMAX,
23310      2      ERROR,RACUM,WK,XK,ZERO,HALF,ONE,ONEP
23320      DATA
23330      *      1.D0,1.0000000000001D0,0/
23340      C
23350      C
23360      C
23370      C
23380      DATA
23390      *      COEF/2.,4.5,7.333,10.42,13.7,17.15,1.,
23400      *      2.0,12.0,24.0,37.89,53.33,70.08,87.97,
23410      *      3.0,6.0,9.167,12.5,15.98,1.0,1.0,
23420      *      12.0,24.0,37.89,53.33,70.08,87.97,1.0,
23430      *      1.,1.0,5.0,16.67,0.04133,0.008267,1.0,
23440      *      1.0,1.0,2.0,1.0,.3157,.07407,.0139/
23450      IER=0
      JER=0

```

COEFF CONTAINS THE COEFFICIENTS  
USED IN SELECTING THE STEP SIZE AND  
THE ORDER. THESE CONSTANTS NEED ONLY  
BE ACCURATE TO A FEW DIGITS.

```

23460 N4 = N*N
23470 IF(MTH.EQ.0) N4=0
23480 N1=N*10+N4
23490 N2 = N1 + 1
23500 N3 = N
23510 N5 = N1 + N
23520 N6 = N5 + 1
23530 N7=N6+N+N
23540 N8=N7+N
23550 N9=N8+N
23560 N10=N8-1
23570 IND1=N4+1
23580 IND2=N4+2
23590 IND9=N4+9
23600 IND10=N4+10
23610 IRET = 1
23620 KFLAG = 1

```

CHECK MAXDER. IF MTH=0, MAXDER MUST  
BE LESS THAN 7. MAXDER MUST BE LESS  
THAN 6, OTHERWISE.

```

MXDER=MAXDER
IF(MTH.EQ.0) GO TO 5
IF(MAXDER.LE.6) GO TO 10
JER=68
MXDER=6
GO TO 10
5 IF(MAXDER.LE.7) GO TO 10
JER=68
MXDER=7
10 IF (JSTART .LE. 0) GO TO 35

```

TAKE A STEP CONTINUING FROM THE LAST  
STEP. SAVE INFORMATION FOR A POSSIBLE  
RESTART AND CHECK H FOR A POSSIBLE  
USER CHANGE. HNEW IS THE PREVIOUS  
STEP SIZE AND IO IS THE CURRENT ORDER

```

23630 C
23640 C
23650 C
23660
23670
23680
23690
23700
23710
23720
23730
23740
23750
23760 C
23770 C
23780 C
23790 C
23800 C

```

```

23810 15 DO 20 I = 1,N
23820     DO 20 J = 1,K
23830         WK(N4+J,I)=Y(J,I)
23840     20 CONTINUE
23850     HOLD = HNEW
23860     IF (H .EQ. HOLD) GO TO 30
23870     25 RACUM = H/HOLD
23880     IRET1 = 1
23890     GO TO 375
23900     30 IOOLD = IO
23910     TOLD = T
23920     RACUM = ONE
23930     IF (JSTART .GT. 0) GO TO 135
23940     GO TO 50
23950     35 IF (JSTART .EQ. -1) GO TO 45
23960 C
23970 C
23980     IO = 1
23990     CALL DFUN(Y,T,N,WK(N2,1),WK,0)
24000     DO 40 I = 1,N
24010         N11 = N1 + I
24020         Y(2,I)=WK(N11,1)*H
24030     40 CONTINUE
24040     HNEW = H
24050     K = 2
24060     GO TO 15
24070 C
24080 C
24090     45 IF (IO .EQ. IOOLD) JSTART = 1
24100     T = TOLD
24110     IO = IOOLD
24120     K = IO + 1
24130     GO TO 25
24140 C
24150 C

```

FIRST CALL, THE ORDER IS SET TO 1 AND  
THE INITIAL DERIVATIVES CALCULATED.

REPEAT LAST STEP. RESTORE THE SAVED  
INFORMATION.

SET ALL COEFFICIENTS DETERMINED BY  
THE ORDER AND THE METHOD TYPE.



```

24160      50 IF (MTH .EQ. 0) GO TO 55
24170      GO TO (95,100,105,110,115,120),I0
24180      55 GO TO (60,65,70,75,80,85,90),I0
24190      60 C(1) = -ONE
24200      GO TO 125
24210      65 C(1)=-HALF
24220      C(3)=-HALF
24230      GO TO 125
24240      70 C(1) = -0.4166666666666667D0
24250      C(3) = -0.75D0
24260      C(4) = -0.1666666666666667D0
24270      GO TO 125
24280      75 C(1) = -0.375D0
24290      C(3) = -0.9166666666666667D0
24300      C(4) = -0.3333333333333333D0
24310      C(5) = -0.0416666666666667D0
24320      GO TO 125
24330      80 C(1) = -0.3486111111111111D0
24340      C(3) = -1.0416666666666667D0
24350      C(4) = -0.4861111111111111D0
24360      C(5) = -0.1041666666666667D0
24370      C(6) = -0.008333333333333333D0
24380      GO TO 125
24390      85 C(1) = -0.3298611111111111D0
24400      C(3) = -1.1416666666666667D0
24410      C(4) = -0.625D0
24420      C(5) = -0.1770833333333333D0
24430      C(6) = -0.025D0
24440      C(7) = -0.001388888888888889D0
24450      GO TO 125
24460      90 C(1) = -0.3155919312169312D0
24470      C(3) = -1.225D0
24480      C(4) = -0.7518518518518519D0
24490      C(5) = -0.2552083333333333D0
24500      C(6) = -0.0486111111111111D0

```

```

24510 C(7) = -.4861111111111111D-2
24520 C(8) = -.1984126984126984D-3
24530 GO TO 125
24540 95 C(1)=-ONE
24550 GO TO 125
24560 100 C(1) = -0.6666666666666667D0
24570 C(3) = -0.3333333333333333D0
24580 GO TO 125
24590 105 C(1) = -0.54545455
24600 C(3) = C(1)
24610 C(4) = -0.090909091
24620 GO TO 125
24630 110 C(1) = -0.48D0
24640 C(3) = -0.7D0
24650 C(4) = -0.2D0
24660 C(5) = -0.02D0
24670 GO TO 125
24680 115 C(1) = -0.437956204379562D0
24690 C(3) = -0.8211678832116788D0
24700 C(4) = -0.3102189781021898D0
24710 C(5) = -0.05474452554744526D0
24720 C(6) = -0.0036496350364963504D0
24730 GO TO 125
24740 120 C(1) = -0.4081632653061225D0
24750 C(3) = -0.9206349206349206D0
24760 C(4) = -0.4166666666666667D0
24770 C(5) = -0.0992063492063492D0
24780 C(6) = -0.0119047619047619D0
24790 C(7) = -0.000566893424036282D0
24800 C
24810 C
24820 C
24830 C
24840 C
24850 C

```

IF THE JACOBIAN MUST BE RE-CALCULATED  
 BECAUSE OF AN ORDER CHANGE, SET  
 IWEVAL POSITIVE AND REPEAT THE INTE-  
 GRATION STEP IF IT HAS NOT YET BEEN  
 DONE(IRET=1) OR SKIP TO A FINAL SCAL-  
 ING IF IT HAS BEEN COMPLETED(IRET=2).

E IS USED FOR COMPARISON OF ERRORS IN  
THE CURRENT ORDER. EUP IS USED TO  
INCREASE THE ORDER, EDWN IS USED TO  
DECREASE THE ORDER.

```

24860 C
24870 C
24880 C
24890 C
24900
24910
24920
24930
24940
24950
24960
24970
24980
24990
25000
25010
25020
25030
25040 C
25050 C
25060 C
25070 C
25080
25090
25100
25110
25120
25130
25140
25150 C
25160 C
25170 C
25180 C
25190 C
25200 C

125 K = IO+1
    IDOUB = K
    MTYP = (4 - MTH)/2
    ENQ2 = HALF/(IO + 1)
    ENQ3 = HALF/(IO + 2)
    ENQ1 = HALF/(IO)
    PEP SH = EPS
    EUP = (COEF(IO,MTYP,2)*PEPSH)**2
    E = (COEF(IO,MTYP,1)*PEPSH)**2
    EDWN = (COEF(IO,MTYP,3)*PEPSH)**2
    IF (EDWN .EQ. 0) GO TO 390
    BND = EPS*ENQ3/N
130 IWEVAL = MTH
    GO TO (135,340), IRET

```

COMPUTE THE PREDICTED Y VALUES BY  
EFFECTIVELY MULTIPLYING THE SAVED  
INFORMATION BY THE PASCAL TRIANGLE  
MATRIX.

```

135 T = T + H
    DO 140 J = 2,K
        DO 140 J1 = J,K
            J2 = K - J1 + J - 1
            DO 140 I = 1,N
                Y(J2,I) = Y(J2,I) + Y(J2+1,I)
140 CONTINUE

```

TAKE UP TO 3 CORRECTOR ITERATIONS.  
CONVERGENCE IS TESTED BY REQUIRING  
CHANGES TO BE LESS THAN BND.  
THE SUMS OF THE CORRECTIONS ARE  
ACCUMULATED IN THE ARRAY ERROR(I). IT  
IS EQUAL TO THE K-TH DERIVATIVE OF Y

```

25210 C      MULTIPLIED BY H**K/(FACTORIAL(K-1) *
25220 C      (C(K)), ERROR(I) IS THEREFORE PRO-
25230 C      PORTIONAL TO THE ACTUAL ERRORS IN THE
25240 C      LOWEST POWER OF H PRESENT. (H**K)
25250 C
25260 C      DO 145 I = 1,N
25270 C          ERROR(I) = ZERO
25280 C      145 CONTINUE
25290 C      DO 220 L = 1,3
25300 C          CALL DFUN(Y,T,N,WK(N2,1),WK,0)
25310 C
25320 C      IF THERE HAS BEEN A CHANGE OF ORDER
25330 C      OR THERE HAS BEEN TROUBLE WITH CON-
25340 C      VERGENCE, THE JACOBIAN IS RE-EVALU-
25350 C      ATED PRIOR TO STARTING THE CORRECTOR
25360 C      ITERATION IN THE CASE OF STIFF
25370 C      METHODS. IWEVAL IS THEN SET TO -1 AS
25380 C      AN INDICATOR THAT IT HAS BEEN DONE.
25390 C
25400 C      IF (IWEVAL .LT. 1) GO TO 185
25410 C      IF (MTH .EQ. 2) GO TO 165
25420 C      CALL DFUN(Y,T,N3,WK,WK,1)
25430 C      R = C(1)*H
25440 C      DO 150 I = 1,N4
25450 C          WK(I,1)=WK(I,1)*R
25460 C      150 CONTINUE
25470 C      N11 = N3 + 1
25480 C      N12 = N*N11 - N3
25490 C      DO 160 I = 1,N12,N11
25500 C          WK(I,1)=WK(I,1)+ONE
25510 C      160 CONTINUE
25520 C      IWEVAL = -1
25530 C      IF(N.EQ.1) GO TO 185
25540 C
25550 C      LU DECOMPOSE JACOBIAN
25560 C      CALL LUDATF(WK,WK,N,N3,NDIG,D1,D2,WK(N7,1),WK(N8,1),WK(N9,1),
25570 C      KER)
25580 C      IF (KER) 185,185,225
25590 C      DO 170 I = 1,N
25600 C

```

```

25560      WK(IND9,I)=Y(1,I)
25570      CONTINUE
25580      DO 180 J = 1,N
25590      R=EPS*DMAX1(EPS,DABS(WK(IND9,J)))
25600      Y(1,J) = Y(1,J) + R
25610      D = C(1)*H/R
25620      CALL DFUN(Y,T,N,WK(N6,1),WK,O)
25630      DO 175 I = 1,N
25640      N11 = I + (J-1)*N3
25650      N12 = N5 + I
25660      N13 = N1 + I
25670      WK(N11,1)=(WK(N12,1)-WK(N13,1))*D
25680      CONTINUE
25690      Y(1,J)=WK(IND9,J)
25700      CONTINUE
25710      GO TO 155
25720      IF (MTH,NE, O) GO TO 195
25730      DO 190 I = 1,N
25740      N11 = N1 + I
25750      WK(IND9,I)=Y(2,I)-WK(N11,1)*H
25760      CONTINUE
25770      GO TO 210
25780      DO 200 I = 1,N
25790      N11 = N5 + I
25800      N12 = N1 + I
25810      WK(N11,1)=Y(2,I)-WK(N12,1)*H
25820      CONTINUE
25830      IF(N.GT,1) GO TO 202
25840      WK(N8,1) = WK(N6,1) / WK(1,1)
25850      GO TO 203
25860      CALL LUELMF(WK,WK(N6,1),WK(N7,1),N,N3,WK(N8,1))
25870      DO 205 I=1,N
25880      WK(IND9,I)=WK(N10+I,1)
25890      CONTINUE
25900      NT = N

```

```

25910 DO 215 I = 1,N
25920   Y(1,I)=Y(1,I)+C(1)*WK(IND9,I)
25930   Y(2,I)=Y(2,I)-WK(IND9,I)
25940   ERROR(I)=ERROR(I)+WK(IND9,I)
25950   IF (DABS(WK(IND9,I)).LE. (END*YMAX(I))) NT=NT-1
25960   CONTINUE
25970   IF (NT .LE. 0) GO TO 245
25980   CONTINUE
25990 C
26000 C
26010 C
26020 C
26030 C
26040 C
26050 C
26060 C
26070 C
26080 C
26090 C
26100   T = T - H
26110   IF ((DABS(H) .LE. (DABS(HMIN)*ONEP)) .AND. ((IWEAL - MYP) .LT.
26120     * -1)) GO TO 230
26130   IF ((MTH .EQ. 0) .OR. (IWEAL .NE. 0)) RACUM = RACUM*0.25
26140   IWEAL = MTH
26150   IRET1 = 2
26160   GO TO 375
26170   230 KFLAG = -3
26180   235 DO 240 I = 1,N
26190     DO 240 J = 1,K
26200       Y(J,I)=WK(N4+J,I)
26210     CONTINUE
26220     H = HOLD
26230     IO = IOOLD
26240     JSTART = IO
26250     GO TO 395
26260 C

```

THE CORRECTOR FAILED TO CONVERGE IN 3 ITERATIONS. VARIOUS POSSIBILITIES ARE CHECKED. IF H IS EQUAL TO HMIN AND THIS IS THE ADAMS METHOD OR A STIFF METHOD IN WHICH THE JACOBIAN HAS ALREADY BEEN RE-EVALUATED, A NO CONVERGENCE EXIT IS TAKEN. OTHERWISE THE JACOBIAN IS RE-EVALUATED AND/OR THE STEP IS REDUCED TO TRY TO OBTAIN CONVERGENCE.

THE CORRECTOR CONVERGED AND CONTROL

```

26260 C
26270 C
26280 C
26290 C
26300 C
26310 C
26320 C
26330 C
26340 C
26350 C
26360 C
26370 C
26380 C
26390 C
26400 C
26410 C
26420 C
26430 C
26440 C
26450 C
26460 C
26470 C
26480 C
26490 C
26500 C
26510
26520
26530
26540
26550
26560
26570
26580
26590
26600

IS PASSED TO STATEMENT 260 IF THE
ERROR TEST IS PASSED, AND TO 270
OTHERWISE.
IF THE STEP IS O.K. IT IS ACCEPTED.
IF IDOUB HAS BEEN REDUCED TO ONE,
A TEST IS MADE TO SEE IF THE STEP CAN
BE INCREASED AT ONE LOWER, THE
CURRENT, OR ONE HIGHER ORDER. A STEP
CHANGE IS ONLY MADE IF THE STEP CAN
BE INCREASED BY AT LEAST 1.1#H. IF NO
CHANGE IS POSSIBLE, IDOUB IS SET TO
10 TO PREVENT FURTHER TESTING FOR THE
NEXT TEN STEPS.
IF A CHANGE IS POSSIBLE, IT IS MADE
AND IDOUB IS SET TO 10 + 1 TO PREVENT
FURTHER TESTING FOR THAT NUMBER OF
STEPS. IF THE ERROR WAS TOO LARGE,
THE OPTIMUM STEP SIZE FOR THIS OR
SOME LOWER ORDER IS COMPUTED, AND THE
STEP RETRIED. IF IT SHOULD FAIL TWICE
MORE IT IS AN INDICATION THAT THE
DERIVATIVES THAT HAVE ACCUMULATED IN
THE Y ARRAY HAVE ERRORS OF THE WRONG
ORDER, SO THE FIRST DERIVATIVES ARE
RECOMPUTED AND THE ORDER IS SET TO 1.

245 D = ZERO
DO 250 I = 1,N
  D = D + (ERROR(I)/YMAX(I))**2
250 CONTINUE
IWEVAL = 0
IF (D .GT. E) GO TO 270
IF (K .LT. 3) GO TO 260
DO 255 J = 3,K
  DO 255 I = 1,N
    Y(J,I) = Y(J,I) + C(J)*ERROR(I)

```

```

26610 255 CONTINUE
26620 260 KFLAG = +1
26630 HNEW = H
26640 IF (IDOUT .LE. 1) GO TO 275
26650 IDOUT = IDOUT - 1
26660 IF (IDOUT .GT. 1) GO TO 350
26670 DO 265 I = 1,N
26680 WK(IND10,I)=ERROR(I)
26690 265 CONTINUE
26700 GO TO 350
26710 KFLAG = KFLAG - 2
26720 IF (DABS(H) .LE. (DABS(HMIN)*ONEP)) GO TO 370
26730 T = TOLD
26740 IF (KFLAG .LE. -5) GO TO 360
26750 PR2 = (D/E)**ENQ2*1.2
26760 PR3 = 1.E+20
26770 IF ((IO .GE. MXDER) .OR. (KFLAG .LE. -1)) GO TO 285
26780 D = ZERO
26790 DO 280 I = 1,N
26800 D=D+((ERROR(I)-WK(IND10,I))/YMAX(I))**2
26810 280 CONTINUE
26820 PR3 = (D/EUP)**ENQ3*1.4
26830 PR1 = 1.E+20
26840 IF (IO .LE. 1) GO TO 295
26850 D = ZERO
26860 DO 290 I = 1,N
26870 D = D + (Y(K,I)/YMAX(I))**2
26880 290 CONTINUE
26890 PR1 = (D/EDWN)**ENQ1*1.3
26900 295 CONTINUE
26910 IF (PR2 .LE. PR3) GO TO 325
26920 IF (PR3 .LT. PR1) GO TO 330
26930 300 R = 1.0/AMAX1(PR1,1.E-4)
26940 NEWI = IO - 1
26950 305 IDOUT = 10

```



```

26960 IF ((KFLAG.EQ. 1) .AND. (R .LT. (1.1))) GO TO 350
26970 IF (NEWI .LE. IO) GO TO 315
26980 XK = ONE / K
26990 DO 310 I = 1,N
27000   Y(NEWI+1,I) = ERROR(I)*C(K)*XK
27010 CONTINUE
27020 315 K = NEWI + 1
27030 IF (KFLAG.EQ. 1) GO TO 335
27040 RACUM = RACUM*R
27050 IRET1 = 3
27060 GO TO 375
27070 320 IF (NEWI.EQ. IO) GO TO 135
27080 IO = NEWI
27090 GO TO 50
27100 325 IF (PR2 .GT. PR1) GO TO 300
27110 NEWI = IO
27120 R = 1.0/AMAX1(PR2,1.E-4)
27130 GO TO 305
27140 330 R = 1.0/AMAX1(PR3,1.E-4)
27150 NEWI = IO + 1
27160 GO TO 305
27170 335 IRET = 2
27180 R = DMIN1(R,DABS(HMAX/H))
27190 H = H*R
27200 HNEW = H
27210 IF (IO.EQ. NEWI) GO TO 340
27220 IO = NEWI
27230 GO TO 50
27240 340 R1 = ONE
27250 DO 345 J = 2,K
27260   R1 = R1*R
27270   DO 345 I = 1,N
27280     Y(J,I) = Y(J,I)*R1
27290 345 CONTINUE
27300 IDOUB = K

```

```

27310 350 DO 355 I = 1,N
27320     YMAX(I) = DMAX1(YMAX(I),DABS(Y(1,I)))
27330 355 CONTINUE
27340     JSTART = IO
27350     GO TO 395
27360 360 IF (IO .EQ. 1) GO TO 390
27370     CALL DFUN(Y,T,N,WK(N2,1),WK,0)
27380     R = H/HOLD
27390     DO 365 I = 1,N
27400         Y(1,I)=WK(IND1,I)
27410         N11 = N1 + I
27420         WK(IND2,I)=HOLD*WK(N11,1)
27430         Y(2,I)=WK(IND2,I)*R
27440 365 CONTINUE
27450     IO = 1
27460     KFLAG = 1
27470     GO TO 50
27480 370 KFLAG = -1
27490     HNEW = H
27500     JSTART = IO
27510     GO TO 400
27520 C
27530 C
27540 375 RACUM = DMAX1(DABS(HMIN/HOLD),RACUM)
27550     RACUM = DMIN1(RACUM,DABS(HMAX/HOLD))
27560     R1 = ONE
27570     DO 380 J = 2,K
27580         R1 = R1*RACUM
27590         DO 380 I = 1,N
27600             Y(J,I)=WK(N4+J,I)*R1
27610 380 CONTINUE
27620     H = HOLD*RACUM
27630     DO 385 I = 1,N
27640         Y(1,I)=WK(IND1,I)
27650 385 CONTINUE

```

SCALE ALL VARIABLES CONNECTED WITH  
H AND RETURN TO THE CALLING SECTION

```

27660 IDOUB = K
27670 GO TO (30,135,320),IRET1
27680 390 KFLAG = -4
27690 GO TO 235
27700 395 IF(KFLAG.EQ.1) GO TO 9000
27710 400 IER=32-KFLAG
27720 9000 CONTINUE
27730 IF(JER.NE.0) CALL UERTST(JER,6HDOGER)
27740 IF(IER.GT.33) IER = IER - 1
27750 IF(IER.NE.0) CALL UERTST(IER,6HDOGER)
27760 9005 RETURN
27770 END
27780 SUBROUTINE DFUN(YP,TP,M,DY,PW,IND)
27790 IMPLICIT REAL*8(A-H,O-Z)
27800 REAL*8 MU,LAMBDA,LYK,LYK1,LYKV1,IAR1,IRIV,INTIA
27810 COMMON PI,GV,R,EPS,DISK,BRHO,GAMMA,ERR,CIL,UINF,DENS1,ALPHA1
27820 COMMON/SWITCH/AR,CDTOTL,AXIS,STK,LYK,INTIA,VINF,RE
27830 DIMENSION YP(8,6),PW(6,6),DY(6)
27840 C
27850 CALL FORSUP(F1Z,F1RHO,F2Z,F2RHO,YP)
27860 C
27870 TEMP=AR*(1.0D00/3.0D00)
27880 TEMP=TEMP*LYK/STK
27890 TEMP1=TEMP/INTIA
27900 DY(1)=TEMP*(1.0D00-F1Z)
27910 DY(2)=TEMP1*(BRHO-F2Z/(R*R))
27920 DY(3)=-TEMP*(F1RHO)
27930 DY(4)=-TEMP1*(F2RHO/(GAMMA*R*R))
27940 DY(5)=YP(1,2)-YP(1,1)
27950 DY(6)=YP(1,4)-YP(1,3)
27960 C
27970 RETURN
27980 END
27990 REAL FUNCTION ANGLE*8(PHI)
28000 IMPLICIT REAL*8(A-H,O-Z)

```

```

28010 COMMON/ANGLE$/ZDIST,RDIST
28020 COMMON/SWITCH/AR,CDTOTL,AXIS,STK,LYK,INTIA,VINF,RE
28030 ANGLE=DSIN(PHI)*DCOS(PHI)*(1.0D00-AR*AR)+AR*ZDIST*DSIN(PHI)-RDIST*
28040 $DCOS(PHI)
28050 RETURN
28060 END
28070 SUBROUTINE FORSUP(F1Z,F1RHO,F2Z,F2RHO,YP)
28080 IMPLICIT REAL*8(A-H,O-Z)
28090 REAL*8 MU,LAMEDA,LYK,LYK1,LYKV1,IAR1,IR1V,INTIA
28100 COMMON PI,GV,R,EPS,DISK,BRHO,GAMMA,ERR,CLL,UINF,DENS1,ALPHA1
28110 COMMON/VER1/R1V,REYNV1,CDV1,VINFV1,STKV1,LYKV1,IR1V
28120 COMMON/AERSL1/REYN1,ARI,SEMI,CDAR1,VINF1,STK1,LYK1,IAR1
28130 COMMON/AERSL2/R2V,DENS2,ALPHA2,VINF2,REYN2
28140 COMMON/SWITCH/AR,CDTOTL,AXIS,STK,LYK,INTIA,VINF,RE
28150 COMMON/NAVIER/DZETA,MP1,N,NSF,IOUT,MATRX,JDERIV
28160 COMMON/OBLAT$/ W1Z(100,100),W1RHO(100,100)
28170 C
28180 DIMENSION YP(8,6)
28190 C
28200 GO TO 100
28210 1 F1Z=YP(1,1)-W2Z
28220 F1RHO=YP(1,3)-W2RHO
28230 C
28240 GO TO 200
28250 C
28260 2 WU1Z=(VINF/UINF)*WU1Z
28270 WU1RHO=(VINF/UINF)*WU1RHO
28280 F2Z=YP(1,2)-WU1Z
28290 F2RHO=YP(1,4)-WU1RHO
28300 C
28310 C MULTIPLY BY DRAG COEFFICIENTS.
28320 C
28330 F1Z=CDTOTL*RE*F1Z/24.0D00
28340 F1RHO=CDTOTL*RE*F1RHO/24.0D00
28350 F2Z=1.0D00*F2Z

```

```

28360      F2RHO=1.0D00*F2RHO
28370      RETURN
28380      C*****
28390      C
28400      C
28410      C*****
28420      C VELOCITY FIELDS AROUND SMALL SPHERE.
28430      C*****
28440      C
28450      100 RD=DSQRT(YP(1,5)**2+YP(1,6)**2)
28460      WZZ=(VINP2/UINF)*((3.0D00*RY(1,5)**2)/(4.0D00*RD**3))*(1.0D00-R
28470      **2/RD**2)+3.0D00*R/(RD**4.0D00)+R**3/(4.0D00*RD**3))
28480      C
28490      W2RHO=(VINP2/UINF)*(((3.0D00*RY(1,5)*YP(1,6))/(4.0D00*RD**3))*
28500      *(1.0D00-R**2/RD**2))
28510      C
28520      GO TO 1
28530      C*****
28540      C
28550      C
28560      C
28570      C*****
28580      C COMPUTE VELOCITY AROUND SPHEROID OR VOLUME EQUIVALENT SPHERE.
28590      C*****
28600      C
28610      C DETERMINE ZETA AND ETA FROM Z AND RHO.
28620      200 ZETA0=DLOG((1.0D00+AR)/(1.0D00-AR))/2.0D00
28630      COSH0=DCOSH(ZETA0)
28640      SFCTOR=AXIS/(R1V*COSH0)
28650      C
28660      R1=DSQRT(YP(1,5)**2+(YP(1,6)-SFCTOR)**2)
28670      R2=DSQRT(YP(1,5)**2+(YP(1,6)+SFCTOR)**2)
28680      SINETA=(R2-R1)/(2.0D00*SFCTOR)
28690      ETA=DARSIN(SINETA)
28700      C

```

```

28710      COSETA=DCOS(ETA)
28720 C
28730      IF(YP(1,5).LT.0.0D00) ETA=PI-ETA
28740 C      USE COSHZ IF ANGLE IS APPROACHING 90 DEGREES
28750      IF(ETA*180.0D00/PI.GT.80.0D00) GO TO 210
28760      201 SINHZ=YP(1,5)/(SFCTOR*COSETA)
28770      202 ZETA=DLOG(SINHZ+DSORT(SINHZ**2+1.0D00))
28780 C      CALCULATE INDICES AND WEIGHTING FACTORS FOR INTERPOLATION
28790 C      OF VELOCITY FIELDS FOR LARGE PARTICLE.
28800      CAPJP1=(ZETA-ZETA0)/DZETA+1.0D00
28810 C
28820      IF(CAPJP1.LE.1.0D00) GO TO 220
28830      IF(CAPJP1.GT.DFLOAT(N-2)) GO TO 230
28840 C
28850      CAPIP1=ETA*DFLOAT(MP1-1)/PI+1.0D00
28860      IF(IOUT.NE.0) WRITE(6,1999) ZETA,CAPJP1,ETA,CAPIP1
28870 C
28880      J=CAPJP1
28890      JP1=J+1
28900      I=CAPIP1
28910      IP1=I+1
28920 C
28930      WJP1=CAPJP1-DFLOAT(J)
28940      WIP1=CAPIP1-DFLOAT(I)
28950      WJ=1.0D00-WJP1
28960      WI=1.0D00-WIP1
28970 C
28980      IF(I.EQ.1) GO TO 240
28990 C
29000      WV1Z=WJP1*WIP1*W1Z(IP1,JP1)+WJ*WI*W1Z(I,J)+
29010      $WJP1*WI*W1Z(I,JP1)+WJ*WIP1*W1Z(IP1,J) +1.0D00
29020 C
29030      203 WV1RHO=WJP1*WIP1*W1RHO(IP1,JP1)+WJ*WI*W1RHO(I,J)+
29040      $WJP1*WI*W1RHO(I,JP1)+WJ*WIP1*W1RHO(IP1,J)
29050 C

```

```

29060      GO TO 2
29070      210 COSHZ=YP(1,6)/(SFCIOR*DSIN(ETA))
29080      IF(COSHZ.LT.1.0D00) GO TO 201
29090      SINHZ=DSQRT(COSHZ*COSHZ-1.0D00)
29100      GO TO 202
29110      C
29120      C
29130      220 WV1Z=1.0D00
29140      WV1RHO=0.0D00
29150      IF(IOUT.NE.0) WRITE(6,2000)
29160      GO TO 2
29170      C
29180      C
29190      230 WV1Z=0.0D00
29200      WV1RHO=0.0D00
29210      IF(IOUT.NE.0) WRITE(6,2001) YP(1,5),YP(1,6)
29220      GO TO 2
29230      C
29240      C
29250      240 WV1Z=WJP1*WV1Z(I,JP1)+WJ*WV1Z(I,J)+1.0D00
29260      IF(IOUT.NE.0) WRITE(6,2002)
29270      GO TO 203
29280      C
29290      C
29300      1999 FORMAT('0','ZETA=',1PD15.8,5X,'CAPJP1=',1PD15.8,5X,'ETA=',
29310      $1PD15.8,5X,'CAPIP1=',1PD15.8)
29320      2000 FORMAT(' ','**COMPUTED VELOCITY AT POINT INSIDE SPHEROID**')
29330      2001 FORMAT(' ','**COMPUTED VELOCITY OUTSIDE SPHEROID VELOCITY FIELD**'
29340      $,5X,'DELTA Z=',G15.8,5X,'DELTA RHO=',G15.8)
29350      2002 FORMAT(' ','**COMPUTED VELOCITY AT ETA=0.0 DEGREES**')
29360      END

```

## APPENDIX 2

### THREE FUNCTION ROUTINES FOR SPHERICAL PARTICLES

Computer listings of three FORTRAN IV function subprograms are included in this appendix. The spherical gravitational collision efficiency,  $\epsilon_S$ , for particles with constant densities of  $0.30 \text{ g/cm}^3$ ,  $1.00 \text{ g/cm}^3$  or  $2.27 \text{ g/cm}^3$  can be generated by using these subprograms in conjunction with two IMSL double precision routines, ICSICU and ICSEVU. The A2.1 summarizes the key parameter associated with these routines.

All values of  $\epsilon_S$  were determined by means of the GCEFF code<sup>12</sup> and associated programs called SPLFIT<sup>12</sup> and GPROC. GPROC was a temporarily created TSO executive program written by the author to handle the data from GCEFF and SPLFIT and to create the necessary DATA statement for the GEPS routines. Since it made use of UMC installation depended commands, it was not included in this dissertation. The author wishes to express his appreciation to Mr. Takoshi Enomoto for his assistance in running GCEFF, SPLFIT, and GPROC.



Table A2.1  
GEPS FUNCTION CAPABILITIES AND LIMITATIONS

CALL NAME(Arguments)	Density g/cm <sup>3</sup>	Large Particle Radius, cm*	Small Particle Radius, †cm
GEPS1(A1,A2)	2.27	$10^{-4} \leq A1 \leq 10^{-2}$	A2
GEPS2(A1,A2)	1.00	$10^{-4} \leq A1 \leq 10^{-2}$	A2
GEPS3(A1,A2)	0.30	$10^{-4} \leq A1 \leq 10^{-2}$	A2

\*When the ratio of the smaller particle to the larger particle is less than 0.1 or greater than 0.9, or the large particle radius is less than  $10^{-4}$  cm or greater than  $10^{-2}$  cm, Fuchs expression is used by the GEPS routines. Fuchs expression is:

$$\epsilon_S = 1.50 \left( \frac{A2}{A1 + A2} \right)^2$$

A2 is determined by (A)(A1) where A is  $A2/A1$  and is bound as:

$$0.1 \leq A \leq 0.9.$$

```

C      ** FUNCTION GEPS DATA **
C      FLNCTION GEPS1(A1,A2)
C      ** FUNCTION GEPS DATA **
C      DENSITY = 2.27 G/CM3
C      SEPTEMBER 15.1520
C
C      FUNCTION GEPS1(A1,A2)
C      IMPLICIT REAL*8(A-H,O-Z)
C      DIMENSION AINT(1),AINT(1),S(1),BFAR(4),C(8,3),Y(8),ANSL(9)
C      DIMENSION COEF(S,7,3),AC(9),AID(8),EPSC(S,8)
C      DIMENSION COEF1(3),CCEF2(63),CCEF3(63),WEPSP(72)
C      EQUIVALENCE (COEF(1,1,1),CCEF1(1)),
C      *(COEF(1,1,2),CCEF2(1)),*(CCEF(1,1,3),CCEF3(1)),
C      *(EPSP(1,1),WEPSP(1))
C      DATA COEF1/-3.47187720D+03,-2.42683521C+03,-1.96222729D+03,
C      *-1.77408667D+03,-1.66C78557D+03,-1.52629160D+03,-1.39078247C 03,
C      *-1.24574219D+03,-1.12426147D+03,-2.544C63580D+03,-1.69709448D+03,
C      *-1.23607056D+03,-8.94590234D+02,-6.61581934D+02,-5.48374512D+02,
C      *-5.62822558D+02,-6.63885458D+02,-7.81215820D+02,1.27326004D+02,
C      *-1.1353760D+02,1.05147729D+03,1.329C9253D+03,1.45965845D+03,
C      *-1.46C93521D+03,1.33952881D+03,1.112C7275D+03,7.93098145D+02,
C      *-2.0C859033D+03,2.21441187D+03,1.55754224D+03,1.68103247D+03,
C      *-1.485691382D+03,1.35792310D+03,1.42483911D+03,1.53036621D+03,
C      *-7.13346710D+01,-5.52512665D+01,-5.57437134D+01,-8.69822388D+01,
C      *-4.02346457D+01,1.77C46539D+02,5.08577393D+02,1.84960327D+01,
C      *-9.03933105D+01,9.15216522D+01,5.27170715D+01,7.69161682D+01,
C      *-7.56343384D+01,7.00122375D+01,2.46555164D+01,-3.54866180D+01,
C      *-3.21067810D+01,-1.11730C22D+01,-1.79305692D+01,-1.75707550D+01,
C      *-1.68025360D+01,-1.7C546158D+01,-1.71252289D+01,-1.44682589D+01/
C      DATA COEF2/ 0.0 , 0.0 , 0.0 , 0.0 , 0.0 , 0.0 , 0.0 , 0.0 ,
C      * 0.0 , 0.0 , 0.0 , 0.0 , 0.0 , 0.0 , 0.0 , 0.0 , 0.0 , 0.0 ,
C      * 1.81539200D+06, 2.19774100D+06, 2.31948300D+06, 1.82435100D+06,
C      * 2.06589500D+06, 1.45464200D+06, 2.49701700D+06, 2.44504300D+06,
C      * 2.79254500D+06, 2.83970300D+06, 2.57614375D+05, 2.02333600D+06,
C      * 1.57358400D+06, 1.7348C500D+06, 2.25042500D+06, 1.74626400D+06,
C      * 1.14207200D+06, 1.18548700D+06, 2.05727400D+06, 2.29101400D+06,
C      * 1.72509100D+06, 1.63660C00D+06, 1.64949400D+06, 1.67898100D+06,
C      * 1.42719800D+06, 6.36105375D+04, 3.48059562C+05, 7.43611875D+04,
C      * 1.46117815D+05, 1.49008125D+05, 1.42913625D+05, 1.37673000D+05,
C      * 1.08380187D+05, 5.26692266D+04, 3.04386537D+05, 1.28749102D+05,
C      * 5.82568867D+04, 6.4657383D+04, 6.00239453D+04, 5.66036836D+04,
C      * 5.63647344D+04, 5.32567656D+04, 2.35112852D+04, 3.23548633D+04,
C      * 1.20695352D+04, 7.51373047D+03, 5.56342969D+03, 5.88003125D+03,
C      * 9.744332C3D+03, 1.00002578D+04, 5.62802344D+03, 3.93439380D+03/

```

```

DATA COEF2, 1.93290291D+09, 1.52029286D+05, 1.51282662D+09,
* 1.83145062D+09, 2.03753574D+09, 2.03753574D+09, 1.72491571D+09,
* 1.21220147D+09, 7.14678528D+08, 4.69235200D+08, 6.45462528D+08,
* 6.82874368D+08, 3.51228160D+07, 5.00501504D+08, 5.80972288D+08,
* 2.23396240D+08, 4.28421632D+08, 5.55595616D+08, 1.38846950D+09,
* 1.32734413D+09, 1.60444745D+09, 1.38257011D+09, 1.15711846D+09,
* 1.07006157D+09, 1.12809558D+09, 1.25575174D+09, 1.23940430D+09,
* 4.08560856D+08, 2.86475504D+08, 6.82666456D+08, 6.81534464D+08,
* 6.24699648D+08, 5.93178112D+08, 5.95722456D+08, 5.95787008D+08,
* 4.58176256D+08, 6.46663040D+07, 6.11557440D+07, 2.21096800D+07,
* 3.51346080D+07, 3.48386720D+07, 3.32562240D+07, 2.23396320D+07,
* 2.69394860D+07, 4.85965700D+06, 5.61236320D+07, 5.15740800D+06,
* 1.09684360D+07, 1.24421940D+07, 1.16506630D+07, 1.10580030D+07,
* 1.10608320D+07, 1.04507580D+07, 4.57428000D+06, 3.59498500D+06,
* 1.34105900D+06, 8.34858537D+05, 1.10704800D+06, 1.09778100D+06,
* 1.08270300D+06, 1.11114000D+06, 1.07647000D+06, 4.37154875D+05,
DATA WEP2,
* 4.12597656D-02, 6.44683838D-02, 8.13140669D-02, 9.40294729D-02,
* 1.02600058D-01, 1.07026100D-01, 1.09597200D-01, 1.10244751D-01,
* 1.05597208D-01, 1.16446018D-02, 2.69165039D-02, 4.08639908D-02,
* 5.15564655D-02, 6.03220463D-02, 6.62167536D-02, 7.01680779D-02,
* 7.23841900D-02, 7.31744766D-02, 6.18004799D-03, 1.57067857D-02,
* 3.77664566D-02, 5.78295165D-02, 7.55745240D-02, 8.62603784D-02,
* 6.64038467D-02, 7.88271427D-02, 6.91371560D-02, 3.59999985D-02,
* 1.57199860D-01, 3.86695537D-01, 5.20117044D-01, 5.89457333D-01,
* 6.15129232D-01, 6.05022665D-01, 5.54381311D-01, 4.37379122D-01,
* 1.28843486D-01, 5.79536564D-01, 7.53496885D-01, 8.27273726D-01,
* 8.62333953D-01, 8.76847506D-01, 8.76847506D-01, 8.66987884D-01,
* 8.70173335D-01, 7.17641890D-01, 5.10193324D-01, 9.55105364D-01,
* 5.71519232D-01, 9.78532917D-01, 5.82922673D-01, 9.86677945D-01,
* 5.54818747D-01, 1.04417856D+00, 5.20177577D-01, 5.77393627D-01,
* 9.89468813D-01, 5.94540519D-01, 5.97255325D-01, 9.58657703D-01,
* 1.00088501D+00, 1.00574585D+00, 1.03577614D+00, 1.00449085D+00,
* 1.00103760D+00, 1.00057656D+00, 1.00091553D+00, 1.00382710D+00,
* 1.00673771D+00, 1.00564832D+00, 1.01255989D+00, 1.01547050D+00,
DATA AD, C.100000, 0.200000, C.300000, C.400000,
* C.500000, 0.600000, C.700000, C.800000, 0.900000,
DATA AID,
* 1.00000000D-04, 5.00000000D-04, 5.55555531D-04, 2.00000009D-03,
* 3.00000003D-03, 4.55555585D-03, 6.555559928D-03, 1.00000016D-02,
IF(A1.LT.C.00010) GC IC 40
IF(A1.GT.C.01000) GC IC 40
AINT(1)=A1
AINT(1)=A2/A1
IF(AINT(1).LT.0.10) GC IC 40
IF(AINT(1).GT.0.90) GC IC 40

```

```

00000410
00000420
00000430
00000440
00000450
00000460
00000470
00000480
00000490
00000500
00000510
00000520
00000530
00000540
00000550
00000560
00000570
00000580
00000590
00000600
00000610
00000620
00000630
00000640
00000650
00000660
00000670
00000680
00000690
00000700
00000710
00000720
00000730
00000740
00000750
00000760
00000770
00000780
00000790
00000800
00000810
00000820
00000830
00000840
00000850
00000860

```

```

00000870
00000880
00000890
00000900
00000910
00000920
00000930
00000931
00000950
00000960
00000970
00000980
00000990
00001000
00001001
00001020
00001030
00001040
00001050

C0 30 I=1.9
C0 20 J=1.8
C0 10 K=1.7
C(K,1)=CDEF(I,K,1)
C(K,2)=CDEF(I,K,2)
C(K,3)=CDEF(I,K,3)
10 CCNTINUE
Y(J)=DLOG(EPSD(I,J))
20 CCNTINUE
CALL ICSEVU(AID,Y,8,C,8,A1INT,S,1,IER)
ANSL(I)=S(1)
30 CCNTINUE
CALL ICSICU(AD,ANSL,9,BPAR,C,8,IER)
CALL ICSEVU(AC,ANSL,9,C,8,A1INT,S,1,IER)
GEPSI=DEXF(S(1))
RETURN
40 GEPSI=1.50*(A2**2/(A1+A2)**2)
RETURN
END

```

[illegible]

```

* 1.54589491D+09. 1.25810330D+C9. 1.10251379D+C9. 1.0493722D+09. 00000430
* 1.0116575ED+C9. 5.61247232D+C8. 3.90934554D+C9. 2.78658611D+09. 00000440
* 1.90035814D+09. 1.11565773D+C9. 6.45734312D+C8. 4.10497024D+C8. 00000450
* 4.55268160D+08. 6.314606CED+C8. 7.4575584D+C8. 6.45347584D+C8. 00000460
* 5.12445952D+08. 7.136C7168D+C8. 2.59250816D+C8. 3.23432960D+C7. 00000470
* 1.18546480D+C8. 2.98647840C+C7. 1.72365CE8D+C8. 3.16340736D+C8. 00000480
* 5.3732752D+C8. 6.66603CC8D+C8. 6.65581952D+C8. 5.92416256D+C8. 00000490
* 3.828631C4D+08. 3.17152024D+C8. 3.656C5120D+C8. 4.57151232D+C8. 00000500
* 5.35044352D+C8. 5.45433856D+C8. 4.60581900D+C6. 1.72345056D+C8. 00000510
* 1.51580720D+08. 1.22139648D+C8. 1.11528544D+C8. 1.16641904D+C8. 00000520
* 1.27586240D+08. 1.02636128D+C8. 2.2C814432D+C8. 4.96463360D+C7. 00000530
* 1.56279360D+07. 2.18293760D+C7. 1.72847040D+C7. 1.55616740D+07. 00000540
* 1.62C77140D+07. 1.61E57110D+C7. 3.00E28400D+06. 5.01106500D+C6. 00000550
* 1.499056C0D+06. 4.28C27300D+C6. 3.844E5300D+C6. 3.04091500D+06. 00000560
* 2.742920C0D+06. 2.853547C0D+C6. 3.016C5200D+C6. 1.94701200D+06. 00000570
DATA WPSD,
* 4.12597656D-02. 6.44683838C-02. 8.13140869D-02. 5.40284729D-02. 00000580
* 1.02600059D-01. 1.07C261C0D-01. 1.055972C6D-01. 1.10244751D-01. 00000590
* 1.095972C6D-01. 1.17502213C-02. 2.73993015D-02. 4.16574478D-02. 00000610
* 5.31158447D-02. 6.1E272522D-02. 7.772C557D-02. 7.14674592D-02. 00000620
* 3.38263862D-02. 7.47680664D-02. 7.854C4444D-03. 2.20336914D-02. 00000630
* 3.52478623D-02. 4.61578369C-02. 5.4417EC55D-02. 6.03220463D-02. 00000640
* 6.35734268D-02. 6.58353502D-02. 6.571412C9D-02. 1.75310671D-03. 00000650
* 1.47525221D-02. 3.99804711D-02. 7.85642930D-02. 1.17200911D-01. 00000660
* 1.36C84616D-01. 1.31132066D-01. 1.09112799D-01. 8.84249210D-02. 00000670
* 7.81431794D-04. 5.55450550C-02. 2.54537470D-01. 3.96444857D-01. 00000680
* 4.75682318D-01. 5.07555486C-01. 5.00224845D-01. 4.52975690D-01. 00000690
* 3.63310814D-01. 1.41358376C-01. 8.87C53234D-01. 7.62050986D-01. 00000700
* 8.35845053D-01. 8.71597250D-01. 8.873C9C15D-01. 8.54250512D-01. 00000710
* 9.01E56482D-01. 5.77303147D-01. 5.76775108C-01. 8.53063762D-01. 00000720
* 9.24398243D-01. 5.51E29741D-01. 5.64133680C-01. 5.71248507D-01. 00000730
* 5.78502757D-01. 5.94910C61D-01. 1.0E528C13D+00. 8.56734118D-01. 00000740
* 9.68213260D-01. 9.84405756D-01. 9.91E34114C-01. 9.53844926C-01. 00000750
* 9.569201C9D-01. 1.0C065613C+00. 0.300C0C0. 0.4CC0C0C. 00000760
DATA AD, C.1CC0000. 0.2CC0000. 0.300C0C0. 0.4CC0C0C.
* 0.500000C. 0.6000000. 0.70CC0C00. 0.8CC0C000. 0.9CC00000. 00000780
DATA AID,
* 1.00000005D-04. 5.0CC00C62D-04. 5.555555531D-04. 2.00000009D-03. 00000790
* 3.00000003D-03. 4.5555555856D-03. 6.5555555280-03. 1.00000016D-02. 00000810
IF(A1.LT.C.00010) GU IC 40
IF(A1.GT.C.01C00) GU TO 40
A1INT(1)=A1
AINT(1)=A2/A1
IF(AINT(1).LT.0.1C) GD TC 40
IF(AINT(1).GT.0.90) GC TC 40
CO 30 I=1.9

```

```

DO 20 J=1.8
DO 10 K=1.7
C(K,1)=CDEF(I,K,1)
C(K,2)=CDEF(I,K,2)
C(K,3)=CDEF(I,K,3)
10 CCNTINUE
Y(J)=DLOG(EPDS(I,J))
20 CCNTINUE
CALL ICSEVU(A10,Y,8,C,8,AINT,S,1,IER)
ANSL(I)=S(1)
30 CCNTINUE
CALL ICSEVU(AC,ANSL,9,BPAR,C,8,IER)
CALL ICSEVU(AC,ANSL,9,C,8,AINT,S,1,IER)
GEPS2=DEXF(S(1))
RETURN
40 GEPS2=1.5C*(A2**2/(A1+A2)**2)
RETURN
END
00000890
00000900
00000910
00000920
00000930
00000940
00000950
00000960
00000970
00000980
00000990
00001000
00001010
00001020
00001030
00001040
00001050
00001060

```





```

* 1.73573811D+C9. 1.56825558D+C9. 1.40425088D+C9. 1.29770726D+C9. 00000430
* 1.20585728D+C9. 1.13400050D+C9. 1.62323279D+C9. 2.3585101D+C9. 00000440
* 1.57373555D+C9. 1.57444710D+C9. 1.43323244D+C9. 1.29003085D+C9. 00000450
* 1.19674406D+C9. 1.13120000D+C9. 1.09353249D+C9. 4.24033280D+C8. 00000460
* 1.16533312D+C8. 5.70098560D+C7. 8.85459520D+C7. 5.45952000D+C7. 00000470
* 5.38501600D+C7. 5.28564320D+C7. 1.01621440D+C8. 1.49687584D+C8. 00000480
* 5.50448384D+C8. 5.24245280D+C7. 1.03883440D+C8. 1.45572056D+C8. 00000490
* 1.46457664D+C8. 1.39564552D+C8. 1.30878432D+C8. 1.06974556D+C8. 00000500
* 3.44426080D+C7. 2.35782800D+C6. 6.27873240D+C7. 2.09842880D+C7. 00000510
* 6.65171200D+C7. 1.07353056D+C8. 1.10493216D+C8. 1.03822952D+C8. 00000520
* 8.61734720D+C7. 5.45424560D+C7. 1.35325000D+C8. 1.28678320D+C8. 00000530
* 6.40391680D+C7. 4.40903100D+C6. 1.88066800D+C7. 2.49424640D+C7. 00000540
* 2.07550720D+C7. 7.00216600D+C6. 1.05844580D+C7. 2.59117600D+C7. 00000550
* 3.33584480D+C7. 2.52556560D+C7. 1.34206540D+C7. 8.37670500D+C6. 00000560
* 6.65280500D+C6. 7.52337200D+C6. 1.00400220D+C7. 1.33637180D+C7. 00000570
DATA WEPST/
* 4.12597656D-02. 6.44683838D-02. 8.12140669D-02. 5.40284729D-02. 00000580
* 1.02600058D-01. 1.07026100D-01. 1.09557206D-01. 1.10244751D-01. 00000590
* 1.05972060D-01. 1.21774613D-02. 2.76423057D-02. 4.19569612D-02. 00000600
* 5.36693270D-02. 6.20126724D-02. 6.81138135D-02. 7.21216202D-02. 00000610
* 7.45012760D-02. 7.55712986D-02. 8.94236555D-03. 2.34323144D-02. 00000620
* 3.71051431D-02. 4.33871102D-02. 5.68361431D-02. 6.28667474D-02. 00000630
* 6.68454766D-02. 6.91371560D-02. 6.57505828D-03. 5.95999528D-03. 00000640
* 1.62936152D-02. 3.12296914D-02. 4.21071202D-02. 5.02302647D-02. 00000650
* 5.8221377D-02. 5.52475523D-02. 2.51442343D-02. 3.78614068D-02. 00000660
* 1.433200159D-03. 1.18297487D-02. 2.51442343D-02. 3.78614068D-02. 00000670
* 4.83065881D-02. 5.30420120D-02. 5.88323027D-02. 6.01422936D-02. 00000680
* 6.39425516D-02. 6.33881427D-02. 1.30265676D-02. 2.57501721D-01. 00000690
* 1.46451550D-01. 2.17671454D-01. 2.54691005D-01. 2.57501721D-01. 00000700
* 2.36470520D-01. 2.27373260D-01. 5.95115082D-03. 1.35163069D-01. 00000710
* 3.64562690D-01. 5.13710260D-01. 5.96508092D-01. 6.39077485D-01. 00000720
* 6.54885252D-01. 6.63332603D-01. 7.41544450D-01. 1.90273046D-01. 00000730
* 5.76571584D-01. 7.56254435D-01. 8.35105836D-01. 8.75276500D-01. 00000740
* 5.98266375D-01. 5.18319541D-01. 9.22082148D-01. 1.17671013D+C0. 00000750
DATA AD/ C.100000. 0.200000. C.400000. 0.800000. C.90000000/
* 0.500000. 0.600000. C.700000. 0.800000. C.90000000/ 00000760
DATA AID/ 00000770
* 1.000000. 5.000000. 5.000000. 5.000000. 5.000000. 5.000000. 5.000000. 5.000000. 00000780
* 2.000000. 4.000000. 4.000000. 4.000000. 4.000000. 4.000000. 4.000000. 4.000000. 00000790
IF(AI.LT.C.00010) GO TO 40 00000800
IF(AI.GT.C.01000) GO TO 40 00000810
AIINT(1)=AI 00000820
AIINT(1)=A2/A1 00000830
IF(AIINT(1).LT.C.10) GC TC 40 00000840
IF(AIINT(1).GT.C.90) GC TC 40 00000850
DC 30 I=1.9 00000860
00000870
00000880

```

APPENDIX 3  
KINETIC CORRECTIONS TO AEROSOL  
GRAVITATIONAL COLLISIONAL EFFICIENCY

Sensitivity analyses have shown that the gravitational collision efficiency influences post-hypothetical core disruptive accidents aerosol behavior in LMFBR containment in important ways<sup>17</sup>. It was noted by Pertmer and Loyalka<sup>18</sup> that the assumptions used in computing two body drag forces influences the calculated collisional efficiency strongly. In fact, the Stokes and Oseen approximations to drag forces can lead to results for collisional efficiency that are different from each other by orders of magnitude. In their work it was also noted that the use of Oseen drag forces provided results that agreed well with some available experimental data for large particles (radius  $\geq 30 \mu\text{m}$ ). For small particles (radius  $\leq 30 \mu\text{m}$ ) one would generally expect Stokes to provide better agreement with experimental data, but Pertmer and Loyalka found that Stokes' results differed from experimental data by about two orders of magnitude. Curiously, the Oseen results showed less deviations from experimental data (at most, one order of magnitude; see Figure A3.1).

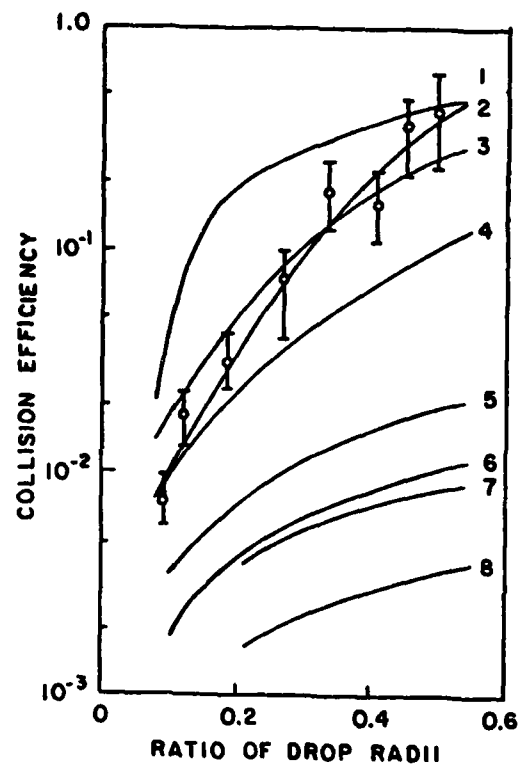


Figure A3.1 A comparison of the kinetic corrections with the experimental results of Tu and Shaw. Here, 1: present work; 2: experimental results; 3: direct interception; 4: Pertmer and Loyalka; 5,6: David and Sartor (slip and no slip); 7,8: Hocking and Jonas (slip and no slip).

This circumstance led to a reexamination of the Stokes' results. The inadequacy of the Stokes' drag forces for small particles and small separations between otherwise large particles was discussed in Chapter III. An acceptable analysis of the forces between small particles ( $\leq 1 \mu$ ) or large Knudsen numbers ( $kn \geq 0.1$ ) requires some type of kinetic corrections, i.e., requires that the Knudsen drag forces on the two spherical particles be obtained by solving the relevant boundary value problem in the framework of the kinetic theory of gases. Pertmer and Loyalka<sup>18</sup> worked out the mathematics necessary for the general case of two spherical particles and the details can be found in References 12 and 46.

Basically, the Knudsen drag forces are determined by solving the relevant boundary value problem for particles interacting in a monatomic simple gas. This is a difficult problem and research is currently underway to obtain expressions for such forces. Meanwhile, useful results can be obtained by using recently determined<sup>46,47</sup> velocity profiles for a sphere moving in a rarefied gas and the method of superposition. The work of Lee and Loyalka provides numerical results for velocity profiles for all  $kn$  by the use of the BGK model. Tomoeda also considered the BGK model and obtained results for  $kn < .1$  by using a technique due to Sone. For  $kn < .1$ , the results of Lee and Loyalka are in agreement with those of Tomoeda. Using the superposition principle,

Knudsen and Stokes drag forces can now be approximated so that the six nondimensional, linear first-order differential equations of motion can be solved to calculate the collisional efficiencies for spherical particles. Pertmer's<sup>12</sup> code, GCEFF, incorporated all necessary features except for the Knudsen velocity profiles. It was therefore decided to derive an approximation to Knudsen velocity profiles which were asymptotically matched to Stokes at a few mean free paths from a sphere, and to incorporate the results into GCEFF.

A convenient representation of the velocity profiles for  $kn \ll 1$  can be obtained by using Tomoeda's results. If we consider spheres of sufficiently large size such that  $kn \ll 1$ , then to a good degree of approximation, we can write:

$$\begin{aligned} \frac{U_{i,r}}{\cos\phi} = & \frac{3}{2} \left(\frac{a_i}{r}\right) \left\{ 1 - \frac{1}{3} \left(\frac{a_i}{r}\right) - \frac{\lambda}{a_i} \right. \\ & \cdot \left[ 1.0161 - \frac{1}{2} \left(\frac{\lambda}{a_i}\right) - \left(\frac{a_i}{r}\right)^2 \right. \\ & \cdot \left. \left. (1.0161 - \underline{0.072488}) \right] \right\} \\ & + f(T_1, T_2, T_3) \end{aligned} \quad (A3.1)$$

$$\begin{aligned} \frac{U_{i,\phi}}{\sin\phi} = & - \frac{3}{4} \left(\frac{a_i}{r}\right) \left\{ 1.0 - (1.0161 - \frac{1}{2} \left[\frac{\lambda}{a_i}\right]) \frac{\lambda}{a_i} \right. \\ & + \left( \frac{1}{3} - (1.0161 - 0.32644 \left[\frac{\lambda}{a_i}\right]) \frac{\lambda}{a_i} \right. \\ & \cdot \left. \left. \left(\frac{a_i}{r}\right)^2 \right\} + f'(T_0, T_1, T_2, T_3) \end{aligned} \quad (A3.2)$$

and

$$\begin{aligned}
 f(T_1, T_2, T_3) = & 3.0 \left( \frac{\lambda}{a_i} \right)^2 \left\{ -0.653551 T_1 \left( \frac{r-a_i}{\lambda} \right) \right. \\
 & + 1.471319 T_2 \left( \frac{r-a_i}{\lambda} \right) \\
 & \left. - 1.117159 T_3 \left( \frac{r-a_i}{\lambda} \right) \right\} \quad (A3.3)
 \end{aligned}$$

$$\begin{aligned}
 f'(T_0, T_1, T_2, T_3) = & \frac{3}{2} \left( \frac{\lambda}{a_i} \right)^2 \left\{ -0.653551 T_0 \left( \frac{r-a_i}{\lambda} \right) \right. \\
 & + 1.471319 T_1 \left( \frac{r-a_i}{\lambda} \right) \\
 & \left. - 1.117159 T_2 \left( \frac{r-a_i}{\lambda} \right) \right\} \\
 & - \frac{3}{2} \left( \frac{\lambda}{a_i} \right)^2 \left\{ -1.01618 T_1 \left( \frac{r-a_i}{\lambda} \right) \right. \\
 & + 4.517256 T_2 \left( \frac{r-a_i}{\lambda} \right) \\
 & \left. - 2.504171 T_3 \left( \frac{r-a_i}{\lambda} \right) \right\} \quad (A3.4)
 \end{aligned}$$

where

$$\begin{aligned}
 a_i &= \tilde{a}_i / \tilde{a}_1 \\
 r &= \tilde{r} / \tilde{a}_1 \\
 \lambda &= \tilde{\lambda} / \tilde{a}_1 \\
 \phi &= \tan^{-1} \tilde{y} / \tilde{x} \quad (A3.5)
 \end{aligned}$$

and these quantities are defined as:

$\tilde{a}_i \sim$  aerosol particle of radius  $a_i$ ,  $i = 1, 2$

$\tilde{r} \sim$  radial distance from center of particle

$\tilde{\lambda} \sim$  mean free path for containment gas

$\tilde{y} \sim$  Cartesian coordinate distance from center of particle,  $\tilde{y} = \tilde{r} \Rightarrow \sin\phi = \pm 1$

$\tilde{x} \sim$  Cartesian coordinate distance from center of particle,  $\tilde{x} = \tilde{r} \Rightarrow \sin\phi = 0$

$T_N(\arg) \sim$  Abramowitz Functions<sup>46</sup>

In Table A3.1 the calculated collisional efficiencies for larger particles radius  $\tilde{a}_1 = 0.1$  to  $30 \mu\text{m}$ , and the particle radii ratio  $a = \tilde{a}_2/\tilde{a}_1 = 0.10$  to  $0.90$  is compared with Stokes' superposition results from Pertmer. Considerable discrepancy is noted for ratios  $< 0.40$  and for collisions between all size particles  $< 5 \mu\text{m}$ . Note that Stokes' results always lead to collisional efficiencies that are too low, and hence use (in aerosol behavior codes) of collisional efficiencies based on Stokes drag forces will lead to very conservative predictions of radioactive release.

Referencing the work of Tu and Shaw,<sup>48</sup> the modified GCEFF code was programmed to calculate the collisional efficiencies between drops of E. Coli and water, the same experimental parameter used in the work of Tu and Shaw. Thus

$$\rho_1 = 1.004 \text{ g/cm}^3$$

$$\rho_2 = 1.0 \text{ g/cm}^3$$

Table A3.1  
Gravitational Collision Efficiency Superposition Method\*

$$\rho = 2.27 \text{ g/cm}^3$$

$\frac{a_1 a_2}{a_1 + a_2}$	0.10	0.20	0.30	0.40	0.50	0.60	0.70	0.80	0.90
0.1									
0.5	$2.19 \times 10^{-1}$ $9.28 \times 10^{-2}$	$3.29 \times 10^{-1}$ $1.15 \times 10^{-1}$	$4.46 \times 10^{-1}$ $1.29 \times 10^{-1}$	$5.45 \times 10^{-1}$ $1.34 \times 10^{-1}$	$6.25 \times 10^{-1}$ $1.34 \times 10^{-1}$	$6.92 \times 10^{-1}$ $1.34 \times 10^{-1}$	$7.45 \times 10^{-1}$ $1.32 \times 10^{-1}$	$7.89 \times 10^{-1}$ $1.29 \times 10^{-1}$	$8.24 \times 10^{-1}$ $1.23 \times 10^{-1}$
1.0	$1.05 \times 10^{-1}$ $3.73 \times 10^{-2}$	$2.38 \times 10^{-1}$ $5.40 \times 10^{-2}$	$3.57 \times 10^{-1}$ $6.44 \times 10^{-2}$	$4.56 \times 10^{-1}$ $7.16 \times 10^{-2}$	$5.36 \times 10^{-1}$ $7.47 \times 10^{-2}$	$6.04 \times 10^{-1}$ $7.69 \times 10^{-2}$	$6.58 \times 10^{-1}$ $7.69 \times 10^{-2}$	$7.03 \times 10^{-1}$ $7.63 \times 10^{-2}$	$7.41 \times 10^{-1}$ $7.47 \times 10^{-2}$
3.0	$8.02 \times 10^{-1}$ $1.23 \times 10^{-2}$	$2.05 \times 10^{-1}$ $2.23 \times 10^{-2}$	$3.15 \times 10^{-1}$ $3.02 \times 10^{-2}$	$4.09 \times 10^{-1}$ $3.62 \times 10^{-2}$	$4.86 \times 10^{-1}$ $4.00 \times 10^{-2}$	$5.51 \times 10^{-1}$ $4.28 \times 10^{-2}$	$6.05 \times 10^{-1}$ $4.49 \times 10^{-2}$	$6.51 \times 10^{-1}$ $4.53 \times 10^{-2}$	$6.90 \times 10^{-1}$ $4.55 \times 10^{-2}$
5.0	$7.58 \times 10^{-1}$ $8.42 \times 10^{-3}$	$1.89 \times 10^{-1}$ $1.67 \times 10^{-2}$	$2.90 \times 10^{-1}$ $2.33 \times 10^{-2}$	$3.76 \times 10^{-1}$ $2.80 \times 10^{-2}$	$4.53 \times 10^{-1}$ $3.12 \times 10^{-2}$	$5.19 \times 10^{-1}$ $3.37 \times 10^{-2}$	$5.79 \times 10^{-1}$ $3.58 \times 10^{-2}$	$6.31 \times 10^{-1}$ $3.77 \times 10^{-2}$	$6.77 \times 10^{-1}$ $3.93 \times 10^{-2}$
10.0	$3.72 \times 10^{-2}$ $5.08 \times 10^{-3}$	$9.68 \times 10^{-2}$ $8.24 \times 10^{-3}$	$1.67 \times 10^{-1}$ $9.82 \times 10^{-3}$	$2.50 \times 10^{-1}$ $1.07 \times 10^{-2}$	$3.33 \times 10^{-1}$ $1.39 \times 10^{-2}$	$4.08 \times 10^{-1}$ $1.71 \times 10^{-2}$	$4.72 \times 10^{-1}$ $1.75 \times 10^{-2}$	$5.30 \times 10^{-1}$ $1.34 \times 10^{-2}$	$5.97 \times 10^{-1}$ $2.11 \times 10^{-2}$
15.0	$1.35 \times 10^{-2}$ $3.18 \times 10^{-3}$	$7.14 \times 10^{-2}$ $1.06 \times 10^{-2}$	$2.28 \times 10^{-1}$ $1.28 \times 10^{-2}$	$3.70 \times 10^{-1}$ $2.49 \times 10^{-2}$	$4.70 \times 10^{-1}$ $3.21 \times 10^{-2}$	$5.42 \times 10^{-1}$ $3.46 \times 10^{-2}$	$5.80 \times 10^{-1}$ $3.26 \times 10^{-2}$	$5.94 \times 10^{-1}$ $2.48 \times 10^{-2}$	$5.88 \times 10^{-1}$ $7.70 \times 10^{-2}$
20.0	$6.95 \times 10^{-3}$ $3.01 \times 10^{-3}$	$1.86 \times 10^{-1}$ $1.72 \times 10^{-2}$	$4.27 \times 10^{-1}$ $3.95 \times 10^{-2}$	$5.72 \times 10^{-1}$ $5.22 \times 10^{-2}$	$6.55 \times 10^{-1}$ $5.86 \times 10^{-2}$	$7.01 \times 10^{-1}$ $6.09 \times 10^{-2}$	$7.21 \times 10^{-1}$ $5.95 \times 10^{-2}$	$7.16 \times 10^{-1}$ $5.32 \times 10^{-2}$	$6.73 \times 10^{-1}$ $3.54 \times 10^{-2}$
30.0	$1.02 \times 10^{-1}$ $1.28 \times 10^{-1}$	$5.42 \times 10^{-1}$ $5.48 \times 10^{-1}$	$7.26 \times 10^{-1}$ $7.20 \times 10^{-1}$	$8.12 \times 10^{-1}$ $7.99 \times 10^{-1}$	$8.57 \times 10^{-1}$ $8.36 \times 10^{-1}$	$8.77 \times 10^{-1}$ $8.15 \times 10^{-1}$	$8.83 \times 10^{-1}$ $8.45 \times 10^{-1}$	$8.74 \times 10^{-1}$ $8.13 \times 10^{-1}$	$8.29 \times 10^{-1}$ $7.08 \times 10^{-1}$

\*Upper Value: Stokes with Kinetic Corrections,  
Lower Value: Stokes Only



$$\rho_f = 1.007 \times 10^{-3} \text{ g/cm}^3$$

$$\tilde{\lambda} = 7.37 \times 10^{-6} \text{ cm}$$

$$\mu_f = 1.713 \times 10^{-4} \text{ poise}$$

where  $\rho_1$  is the density of E. Coli droplets and  $\rho_2$  is the density of water droplets,  $\rho_f$  is the density of air,  $\tilde{\lambda}$  is the mean free path of air, and  $\mu$  is its viscosity. The present results together with the experimental data and several other theoretical results are given in Figure A3.1. It is noted that the present results describe the experimental data well for  $\geq 0.4$ , but for  $\leq 0.40$  the present results do not agree with experimental data. There is a dearth of clear experimental data in this regime and therefore it is not clear if the disagreement is due to inadequacies of the superposition method or the experimental data or both. The present work, however, emphasizes the improvement offered by modeling the effects of slip and this justifies further experimental work and still more improved theoretical calculations.

## VITA

Ronald Forrester Tuttle was born in Boston, Massachusetts on December 5, 1944, the second of three sons of Jay F. and Helen C. Tuttle.

He graduated from Phoenixville Area High School, Phoenixville, Pennsylvania in June of 1963. His first year of college was at the University of North Carolina, Chapel Hill, North Carolina, where he was an honor Student in Chemistry.

His interest, however, was in engineering and this, plus the fact that his parents moved from Pennsylvania to Missouri in 1963, induced him to enroll in the Chemical Engineering Program at the University of Missouri(UMC), Columbia, Missouri. In January 1968 he graduated with a B.S. from UMC and was commissioned a Second Lieutenant, United States Air Force (USAF). Upon graduation, he was a member of Alpha Chi Sigma, honorary in Chemistry, Pi Mu Epsilon, Honorary in Mathematics, Arnold Air Society, professional organization for USAF cadets, and American Nuclear Society, professional organization for engineers and scientists.

In January 1968 he was granted an educational delay from the USAF so that he could enroll in the graduate Nuclear Engineering Program at UMC. He was supported by a National Science Foundation Traineeship grant for his work on his

thesis topic, "Neutron Activation Analysis of Airborne Particulate Matter". He received the M.S. degree in January of 1970.

From February of 1970 to June of 1977 he served on active duty with the USAF and was stationed at McChord Air Force Base, Tacoma, Washington, and Wright-Patterson Air Force Base, Dayton, Ohio. While on active duty he served as the 62nd Military Airlift Wing Nuclear Safety Officer, Foreign Technology Division military analyst for Chemical and Biological Warfare, and Aeronautical Systems Division program manager for chemical agent detectors.

In June of 1977 he was accepted into the Ph.D. program of the Air Force Institute of Technology and was sent to UMC to pursue a Ph.D. in Nuclear Engineering. He received the Ph.D. in December of 1980.

He is presently serving with the USAF Technical Applications Center, Patrick Air Force Base, Florida.

**DAT**  
**ILM**